Manufacture of electrospun scaffolds for investigating behavioural responses of hypothalamic stem cells to topological cues.

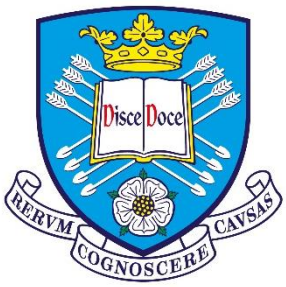

The University Of Sheffield.

Selina Natalie Beal

Thesis presented for the degree of PhD

University of Sheffield

Departments of The School of Clinical Dentistry and Biomedical sciences

Supervisors: Dr Ilida Ortega, Prof Paul Hatton, Prof Marysia Placzek

March 2020

Abstract

A novel stem cell population known as alpha-tanycytes was recently identified in the hypothalamus of the brain of vertebrates. Characterisation of this stem cell population is limited and in general stem cells have historically been difficult to study *in vitro* due to spontaneous differentiation over time. Synthetic culture systems, including 3D environments, have been utilised to study many cell types including for research into the mechanical cues that control stem cell behaviour, highlighting the importance of these cues for stem cell fate decisions. *In vivo,* tanycytes have previously been reported to be organised in a polarised manner and therefore fibre alignment is hypothesised to support the maintenance of tanycytes *in vitro*. The primary aim of this project was therefore to design and manufacture a synthetic 3D scaffold in which to study tanycytes behavioural responses to fibre orientation during *ex vivo* culture.

This project first considered the production of scaffolds using electrospinning methodologies, altering fibre orientation with a rotating collector. Cell behaviour was analysed via the morphology of the neurosphere cultures and immunohistochemistry to label markers associated with certain cell types. An additional tanycyte marker, NrCAM that co-labels with a well-established tanycyte marker Nestin, was identified. Investigation of the established free-floating neurosphere assay showed that while tanycytes are successfully maintained this is not 100% efficient as spontaneous differentiation still occurred. The manufacture of random and aligned scaffolds was optimised using 15 wt% PC12 Poly(Caprolactone) in HFIP and scaffolds were produced at The Electrospinning Company and at The Dental School. Tanycyte derived neurospheres were shown to respond to mechanical cues, such as fibre organisation, both by morphology as on random scaffolds neurospheres were circular but were elongated on aligned fibres, and marker expression. Aligned scaffolds manufactured at The Electrospinning Company, while unable to prevent spontaneous differentiation, was able to maintain tanycytes better than other scaffolds. It was concluded that 3D scaffolds with different topological environments have significant potential as tools for expanding current knowledge of tanycyte biology.

Conferences and Publications

Whilst undertaking my PhD I have attended the following conferences to support my research and have published the following paper:

Attended conferences

BiTEG conference, York, England.

Presentations at the following conferences

S.N. Beal *et al*. (2016). The Design and Fabrication of Synthetic 3D Niche Environments for the Modification of Stem Cell Behaviour In Vitro. Poster presented at MBB-BMS retreat, Derbyshire, England.

S.N. Beal *et al*. (2016). The Design and Fabrication of Synthetic 3D Niche Environments for the Modification of Stem Cell Behaviour *In Vitro*. Poster presented at TERMIS EU conference, Uppsala, Sweden.

S.N. Beal *et al*. (2016). The Manufacture of Synthetic Three Dimensional Scaffolds designed to influence in vitro stem cell behaviour. Poster presented at BiTEG Conference, Durham, England.

S.N. Beal *et al*. (2017). Utilising electrospinning to produce scaffolds with random or aligned fibres. Poster and pitch presented at Mede Conference, Bradford, England.

S.N. Beal *et al*. (2017). The manufacture of 3D electrospun scaffolds with complex features. Oral presentation at UKSB Conference, Loughborough, England.

S.N. Beal *et al*. (2017). The manufacture of 3D electrospun scaffolds with complex features. Poster presented at PPE/Mede Conference, Bradford, England.

S.N. Beal *et al*. (2017). Electrospinning may be employed to manufacture complex 3D scaffolds for regenerative medicine. Poster presented at ESB Conference, Athens, Greece.

S.N. Beal *et al*. (2017). The manufacture of complex 3d scaffolds by Electrospinning for regenerative medicine. Poster and pitch presented at BiTEG Conference, Leeds, England.

S.N. Beal *et al*. (2018). The manufacture of complex 3d scaffolds by electrospinning for regenerative medicine. Poster and pitch presented at Mede Conference, Sheffield, England.

S.N. Beal *et al*. (2018). Manufacture of electrospun scaffolds for investigating behavioural responses of hypothalamic stem cells to topological cues. Oral presented at The School of Clinical Dentistry, Sheffield, England.

S.N. Beal *et al*. (2018). Comparison of Methods to Characterise Orientation in Electrospun Scaffolds. Oral presented at UKSB conference, Bath, England.

S.N. Beal *et al*. (2018). Comparing methods to reliably and reproducibly characterise fibre orientation. Poster presented at TCES conference, Keele, England.

S.N. Beal *et al*. (2018). Analysing microtopography in electrospun scaffolds: a comparative study of fibre alignment analysis. Poster presented at ESB conference, Maastricht, The Netherlands.

Publication

Thomas E. Paterson, **Selina N. Beal**, *et al.* Selective laser melting–enabled electrospinning: Introducing complexity within electrospun membranes. *Journal of Engineering in Medicine.* (2017). 231. 565-574.

> Included is the analysis of average fibre diameters of random scaffold, scaffold 1 large microfeature, scaffold 2 and scaffold 3 (Section 6.3.2).

Papers in preparation

Selina N. Beal, *et al.* Alpha-tanycytes respond to fibre orientation and aligned fibres are an important cue for maintaining the tanycyte population. (2019).

Supervision

Throughout my research I supervised a laboratory based project via the Think Ahead Student Undergraduate Research Experience scheme, (TA SURE), a scheme that provides an opportunity for PhD students to design a project, gain funding and source undergraduate students to supervise throughout the research. Work undertaken by the respective student, Nicholas Cooper, is shown in section 6.6.2.

I also collaborated with the Mathematics and Statistics Department at the University of Sheffield for the utilisation of an undergraduate mathematical student to work on my project, working with SEM images and the relevant data I collected in order to identify a rigorous method required for analysing orientation. However, due to personal circumstance of this undergraduate student this project was not completed, but should be considered for future research.

Acknowledgements

I thank my supervisors Dr Ilida Ortega, Prof. Paul Hatton and Prof. Marysia Placzek for their support and guidance. In particular I thank Dr Ilida Ortega and Prof Paul Hatton for their support in the new field of scaffold production by electrospinning and Prof Marysia Placzek for her support in developing new skills in working with brain tissue and my development of the required knowledge of the hypothalamus region.

With thanks to the additional support provided in the laboratories of both The School of Clinical Dentistry and Biomedical Sciences including the support technicians and other laboratory members. Your support has been important for maintaining morale during the project.

I very much appreciate the collaboration and support of the Electrospinning Company for supporting my research and the opportunity of a placement at their facility. Special thanks to Charlotte Worthy at the Lambda facility for supporting the trial of the Phenom SEM software which has allowed me to improve the analysis methods and processes within my project. Finally thanks to Dr Sebastian Spain for GCP analysis assistance. Thanks to Nicholas Cooper for his hard work during his placements which contributed to electrospun scaffold manufacture optimisation.

Finally, I wish to thank my family for their continued support throughout my education, but especially through this specific research project. There help not only financially but also with constant encouragement has been essential in maintaining progress towards finalising this thesis.

Contents

List of Figures and Tables

Abbreviations

AFM- Atomic force microscopy

ARC- Arcuate nucleus

ASC- Adult stem cell

BBB- Blood-Brain-barrier

bFGF- basic fibroblast growth factor

BMP- Human bone morphogenetic proteins

BSA- Bovine serum albumin

CAM- Cell adhesion molecule

$CHCl_3$- Chloroform

c-Myc- MYC proto-oncogene

CSF- Cerebral spinal fluid

DA- Dopaminergic

DAPI- 4',6-Diamidino-2-phenylindole dihydrochloride

DCM- Dichloromethane

DMF- Dimethylformamide

DMSO- Dimethyl sulfoxide

DS- Dental School

ECM- Extracellular matrix

EFG- Epidermal growth factor

EGF- Epidermal growth factor

ESCs- Embryonic stem cells

FA- Focal Adhesions

FAK- Focal adhesion kinase

GAG - Glycosaminoglycans

GFAP- Glial fibrillary acidic protein

GHRH- Growth hormone-releasing hormone

GMP- Good manufacturing practice

GSC- Germ line stem cell

HFIP- Hexafluoroisopropanol

HFIP- Hexafluroisopropanol

HFSCs- Hair follicle stem cells

HINGS- Heat inactivated goat serum

ICM- Inner cell mass

IPSCs- Induced pluripotent stem cells

JAK- Janus kinase

Klf4- Kruppel like factor 4

MAP2- Microtubule-associated protein 2

ME- Median eminence

MSCs- Melanocyte stem cells

NPY- Neuropeptide Y

NSC – Nerve stem cells

NSS- Neurosphere stock solution

NWS-Neurosphere working solution

OCT- Optimal cutting temperature

Oct4- Octamer-binding transcription factor 4

P3- Passage 3 (represents passage number)

PBS- Phosphate-buffered saline

PCL- Polycaprolactone

PDL- Poly-D-Lysine

PFA- Paraformaldehyde

PH3- Phosphorylated histone H3

PLGA- Polylactice-co-glycolic acid

PU- Polyurethane

PVN- Paraventricular nucleus

SC- Stem cell

SEM-Scanning electron microscopy

SGZ- Subgranular zone

Shh- Sonic hedgehog

SLM- Selective lazer melting

Sox2- Sex determining region Y-box 2

SSCs- Somatic stem cells

STAT- Signal Transducer and Activator of Transcription

SVZ- Subventricular zone

TCP- Tissue culture plastic

TEC- The Electrospinning Company

TGFβ- Transforming growth factor beta

VMN- Ventromedial nucleus

TH- tyrosine hydroxylase

THF- Tetrahydrofuran

TIMPs- Tissue inhibitors of metalloproteinases

Tuj1- neuron-specific class III β-tubulin

VEGF- vascular endothelial growth factors

A-R- Antigen Retrieval

NSPC- Neural stem/progenitor cell

Definitions

Differentiation- The genetic and morphological changes a cell undertakes to change into a different cell type.

Durotaxis- cell migration in response to different mechanical properties of the ECM.

Embryonic stem cells- The group of cells that make up the inner cell mass of the developing embryo, which are pluripotent.

Mechanobiology- the process of cells detecting and responding to mechanical cues.

Mechanotransduction signalling- the signalling which occurs in response to the mechanical environment.

Micoenvironment- A small space of a larger structure which has its own conditions different from the larger conditions for a specific purpose.

Multipotent- The ability to differentiate into more than one cell lineage. E.g. SSCs

Pluripotent- The ability to differentiate into all cell lineages of the three germ layers of embryogenesis. E.g. ESCs

Quiescent- Inactive or very low activity (i.e. dormant).

Somatic/adult stem cells- The cells which develop from ESCs, through development, with limitation on their ability to differentiate into different cell lineages. They are maintained within the adult for homeostasis and repair.

Totipotent- The ability of a single cell to produce a new organism. Therefore, has the capability to differentiate into all the cell types required for this organism, along with the supporting structures required for growth and an essential features is the ability to organise these cells into the infant organism. E.g. The fertilised egg.

Unipotent- The ability to differentiate into one cell lineage. E.g. Progenitor cells.

Induced pluripotent stem cells- A somatic cell which has been reprogrammed to a pluripotent state.

Free-floating culture- Neurospheres cultured in suspension with NWS, (Section 4.1.3).

Differentiation culture- Neurospheres cultured on TCP treated with PDL and fibronectin with differentiation media, (Section 4.1.3).

Chapter 1: Introduction

The hypothalamus is an evolutionarily-ancient and highly conserved part of the brain located in the ventral region surrounding the third ventricle. It has many important functions related to body homeostasis including temperature regulation, hunger and stress responses [1]. Scientists have discovered that the hypothalamus contains a stem cell population and, while there are still some uncertainties regarding which populations are stem/progenitor cells, cells termed alpha-tanycytes are acknowledged to have stem-like properties [2]. To date this population is not well understood, particularly in terms of the characterisation of their function *in vivo*. Fully understanding the stem/progenitor population of the hypothalamus is important as insights could assist greatly with understanding how disorders and diseases linked with the hypothalamus occur and potentially provide provision towards new treatments. Current studies have included the characterisation of these cells *in vivo* as well as their characterisation after *ex vivo* culture, (as free-floating neurospheres), a system designed to assay stem cell characteristics in a simplified environment. One key aim of long-term research is to find conditions in which tanycyte stem cells can be cultured *ex vivo* in an environment that promotes their self-renewal and limits their differentiation so as to expand this stem cell population. However, current 'non-differentiating' culture conditions for many stem cells do not efficiently maintain the stem population and spontaneous differentiation occurs [2,3]; tanycytes are expected to behave similarly. Therefore, there is a need to improve the culture environment to better understand and optimise the conditions that maintain the tanycyte stem cell population.

A wide range of substrates including electrospun scaffolds have been used for 3D culture of cells for many stem cell types. However, currently no study has deployed such scaffolds for the culture of alpha-tanycytes. The concept underpinning the use of scaffolds is that they contribute to the development of a more physiological environment, providing morphological and mechanical cues such as stiffness that influence cell behaviour including stem cell fate decisions. Given that tanycytes are highly organised and polarised *in vivo*, I hypothesised that aligned fibres would aid in replicating this morphology *in vitro* and so maintain tanycytes in a self-renewing, non-differentiating programme. Therefore, this thesis aims to manufacture electrospun

scaffolds with both random and aligned topologies and investigate the impact of these different topologies on tanycyte derived neurospheres.

Before considering the goals of this thesis in more detail, the following chapter will review the published literature related to the current understanding of the impact of biochemical, cell interaction and mechanical cues (including topological ones), on a range of stem cell populations' behaviour. Then I will consider the current understanding of the tanycyte neuronal stem/progenitor population. This information will add considerably to applications of scaffolds in stem cell research, and inform the further development of experimental substrates.

Chapter 2: Literature review

In this Chapter I aim:

- to review stem cell categories and the cues that influence their behaviour;
- to review which population of cells in the hypothalamus is stem-like;
- to review the tanycyte population found within the hypothalamus in terms of organisation and function;
- to review potential scaffolds that could be utilised to develop an *ex vivo* system to further the study of tanycytes by characterising responses to mechanical properties and potentially aiding in improving the maintenance of tanycytes in *ex vivo* culture.

2.1 Stem cells

Stem cells (SC) are a unique cell type with the dual ability to differentiate into other specialised cells, or to self-renew and maintain their own SC population. They are capable of these behaviours due to their un-programmed state (differentiated cells with a specific organ or tissue function are said to be programmed) and their ability to divide in different manners giving either progeny that will maintain a SC character or differentiate. In the vertebrate system there are different categories of SCs, each with slightly reduced differentiation abilities, a characteristic known as potency [4–7].

2.1.1 Stem cells are categorised based on their differentiation abilities

Stem cells found within mammals can be characterised into four classes as shown in Figure 2.1.1 A; overall these indicate changes in potency in SC capabilities through development into adulthood. Importantly, some stem cell populations are maintained into adulthood.

The first class of SC is known as the totipotent SC and these cells are capable of producing all cell types. In mammals the zygote (fertilised oocyte) is the totipotent cell and it is believed that the cells from the first four divisions retain these abilities [6,8,9]. The zygote therefore can produce all

cell types found within the mammal along with the other cell types required to support the developing embryo. Impressively the totipotent cell has all of the information required to produce and organise all cells required to form an organism. This information is preserved throughout development to be contained within the germ cells [9–11].

Following the totipotent SC in development is the pluripotent SC. This can still produce most, if

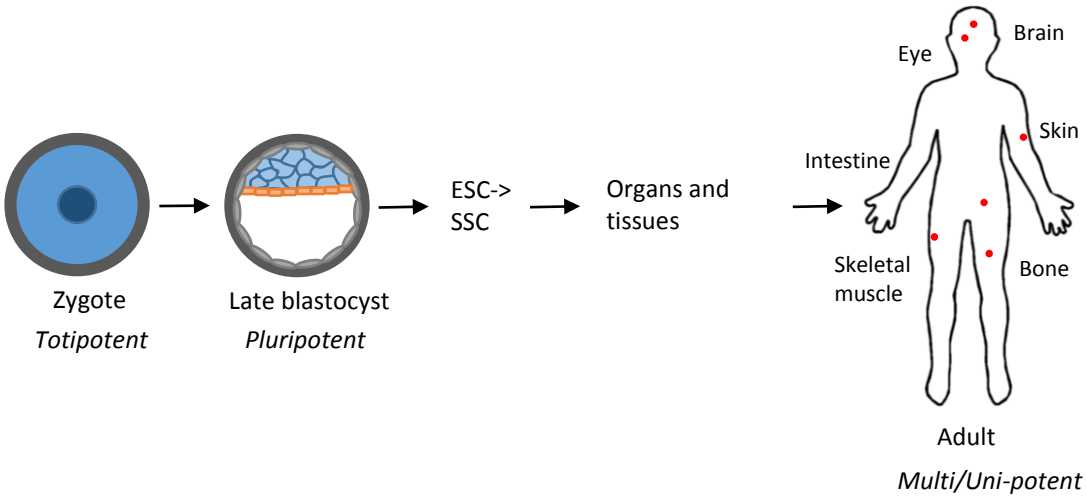

Figure 2.1.1 A: The progression of stem cells through development. The cell with the greatest abilities is the fertilised egg (zygote) which is totipotent. Pluripotent stem cells are known as ESCs and are found in the epiblast of the ICM. During development ESC disappear once the three germ layers have been produced leaving behind SSC from which the organs and tissues are derived. SSC can either be multipotent (can produce cells of several lineages) or unipotent (can only produce one lineage). The human diagram highlights some known human SSC populations. Adapted from (Condic 2014).

not all, cell types of the mammalian embryo and gives rise to the three germ layers which are known as endoderm, mesoderm and ectoderm [6,12,13], but are incapable of producing supporting structures, i.e. placental types [6]. In mammals, pluripotent SCs are found in the embryo as a group of cells known as the inner cell mass (ICM), also known as embryonic stem cells (ESCs) after isolation [6,14]. The ICM consists of several populations of pluripotent SCs. One subset will give rise to primitive endoderm, while a second subset will give rise to the epiblast from which the embryo itself will arise [8,15].

During mammalian embryonic development, ICM cells begin to give rise to a restricted replacement as they differentiate into tissues and organs, known as the somatic stem cell (SSC). SSCs then give rise to organs and tissues in the later stages of development [16]. The majority of differentiation occurs during embryogenesis in mammals with a small population of SCs being maintained into adulthood; these SSC are also known as adult stem cells (ASC). ASCs are

required for maintaining organ homeostasis and repairing damage [17,18]. ASCs have more restrictive differentiation capabilities and are either multipotent (give rise to several cell lineages) such as within the hematopoietic system [14], or unipotent (give rise to one cell lineage) such as the testis [14].

A final stem cell population are known as induced pluripotent stem cells (IPSCs). These stem cells are experimentally created. IPSCs show all key features of pluripotency but are derived from differentiated (somatic) cell types which have been 'reprogrammed'. This process is possible due to the research that has identified differentiation pathways through the stages of potency and has discovered key genes that are essential to the pluripotent state. Markers of the pluripotent state include telomerase, Octamer-binding transcription factor 4 (Oct4) and NANOG, the expression of which are all reduced as cells begin to differentiate [6,19]. Therefore by introducing key genes such as the combination of Sex determining region Y-box 2 (Sox2), Oct4 , Kruppel like factor 4 (Klf4) and MYC proto-oncogene (c-Myc), somatic cells can be reprogramed to a pluripotent state[21–23]. Papers which discuss the changes in expression profiles between SC populations and progenitor cells include [5,6,19,20].

SC populations have very important roles in development and in the case of the ASCs for survival, for example through their ability to provide new cells to repair damage. Therefore the maintenance of SC populations, and/or regulation of their differentiation, via progenitor production is highly controlled. In the following section I will discuss research undertaken to understand the cues involved in this control alongside how these influences change between different stem cell populations.

2.1.2 Stem cell control

ASC populations reside within a unique microenvironment, known as a niche, which typically comprises of a number of stem cells alongside differentiated cells. Even ASCs that are found as isolated cells, for instance the satellite SCs of skeletal muscle, exist in highly specialised

microenvironments. The idea of SCs residing in a niche was first hypothesised by Schofield [24] but was not proven until the identification and characterisation of the germ line stem cell (GSC) niche in *Drosophila melanogaster* [25–27].

The niche has several functions including protecting the ASCs from external influences, such as signalling molecules and non-niche cells which may aberrantly alter the behaviour of the ASC. The niche is supportive of the complex balance between the maintenance of the ASC population and the production of progenitor cells as required [18,28–30]. The importance of the niche environment in the control of self-renewal and fate determination was first demonstrated through analyses of hair follicle SCs (HFSCs in the hair follicle niche); it was shown that HFSCs act very differently when they are removed from their niche and cultured *ex vivo*[16]. The loss of the delicate balance of SC control (i.e. self-renewal versus differentiation) that occurs when SCs are cultured *ex vivo* is now recognised in many other stem cell populations, highlighting the importance of the niche environment [16,22,23]. Given the importance of being able to culture SCs *in vitro* in a system where self-renewal vs differentiation can be regulated with the same precision as *in vivo*, there is a need to develop improved *ex vivo* culture conditions for these cell types, either to maintain the SC population or to specify and control differentiation. In order to achieve this control culture it is important to first understanding SC biology *in vivo*. Current understanding of the cues and the tools utilised to make these conclusions will be reviewed in the following sections.

SC populations are influenced by biochemical signals, cell to cell interactions and mechanical cues including the morphology of their surroundings. One factor alone is unlikely to be able to force a stem cell down a cell fate path without the assistance of other cues [13]. In other words, it is the combination of factors within the niche which ultimately leads to the fate decisions of the SC. An overview of the influences acting upon some characterised ASC populations is displayed in Table 2.1.2 A [7,30–33]. This table shows that many ASC populations have been well characterised for the biochemical and cell interaction cues involved in their behaviour.

*Table 2.1.2 A: Niche microenvironments overview. Adapted from [18,29] with input from other papers stated for each stem cell population . The cells which are derived from the SCs are identified by *. # denotes cells which promote SC maintenance while ^ are cell which promote differentiation. The estimated sizes of the niche environment should be considered with caution.*

Organ	Organism	SCs [number of SCs found in the niche]	Activity	Name of niche	Niche components	Purpose	Important signals	References
Skin	Mouse	Hair follicle-HFSC and MCSC [many]	Constant	Bulge; [34,35]	$K6^+$ bulge*#, dermal papilla^, adipocyte precursor cells, subcutaneous fat, dermal fibroblasts	Differentiate to produce a new hair; repair from wounding in the epidermis	Wnt activation and BMP inhibition both stabilising β-catenin^, TGFß	[7,16,20,28,29,36,37] Diagram- [28,29]
	Mouse	Interfollicular epidermis progenitors [unknown]	Constant	Basal layer of epidermis	Dermis	Maintaining homeostasis in the epidermis	Wnt, Notch	[20,28] Diagram- [28]
Intestine	Mouse	Intestinal Stem Cells (ISCs) [4-6]	Constant with some slow cycling SCs	Crypt; [38]	Paneth cells*^, fibroblasts	Replace the small intestine epithelium	Wnt#, Notch, BMP	[7,18,29] Diagram- [18,29]
Skeletal Muscle	Mouse	Satellite stem cells [1]	Low activity	SC found under the basal lamina on myofibres	Myofibre		Wnt, Notch, HGF, CXCL12	[7,14,17,18,29,39] Diagram- [7]
Haematopoietic system	Mouse	Haematopoietic stem cells (HSC) [1]	Constant	Bone marrow but are exceptionally mobile SCs	Osteoblasts^, osteoclasts#, bone marrow, vasculature, osteoblast progenitors#, adipocytes, mesenchymal cells and non-myelinating schwann cells, nestin+ MSCs#	Replenish myeloid and lymphoid lineages	CXCL12, SCF, Tpo, SHH, Ang1	[7,18,29] Diagram-[29]
Brain	Mouse	Inconclusive-astrocyte populations	Low activity	Subventricular zone (SVZ), Subgranular zone (SGZ),	Ependymal cells, vasculature	SVZ- mature interneurons for the olafactory bulb	EGF, bFGF, SHH, Notch, Wnt, TGFa, VEGF;	[7,18,29,40–44] Diagram- [7]

		suggested [many]		hypothalamus [2]		SGZ- new granular neuron's that contribute to the hippocampus		
Germ line	*Drosophila melanogaster*	Germline stem cells and somatic cyst stem cells [2-3 male and 7-12 female]	Constant	Apical tip of the testis [27]	Hub cells	Asymmetric division to maintain the SC population and a cell that will undergo the differentiation process	Upd->JAK-STAT; BMP like molecules DPP and GBB (in females Notch is also involved)	[18,29] Diagram - [27]

Biochemical cues

Research into different niche systems has highlighted signalling pathways that commonly play roles in the balancing act of SC fate. While the same pathways are frequently found to be involved in many SC populations control they can be performing different purposes in different niches. Consequently it is important to fully characterise and understand each stem cell population in order to identify these differences in the control of different systems. For example WNT signalling promotes self-renewal of haematopoietic stem cells, while for neural stem cells (NSCs) WNTs block maintenance of the SC population and promote differentiation into neurons and astrocytes [45]. Notch signalling, which governs binary cell fate decisions (where there are two possible fates), has been shown to play a role in the decision of neural stem/progenitor cells (NSPC) to either renew or commit to differentiate. Other signalling pathways that govern SCs include transforming growth factor beta (TGFβ), Janus kinase (JAK)/ Signal transducer and activator of transcription (STAT) and Epidermal growth factor (EGF). Many of these signals are extrinsic (made by other cells) and interact with SCs that have the appropriate receptor/signal transduction machinery [14]. For example, EGF is produced by the male GSC niche component cyst cells to promote differentiation of EGF-responsive GSCs [29]. Alternatively, these signals can be intrinsic and so made by and act upon the SC itself, for instance in the case of HFSC [29,46]. Reviews by Fuchs and Chiba among others discuss how these signalling pathways are utilised in different niche systems [13,17,19,45,47]. Generally the biochemical signalling involved in stem cell control are increasingly well understood for characterised stem cell populations.

Cell interactions

Another aspect involved in SC fate decisions is the interactions a SC makes with other cells including other SCs, progenitor and differentiated cells of the niche. These interactions are made by surface adhesion proteins, including cadherins [13]. In *Drosophila*, the anchoring of GSCs to their niche is known to involve E-cadherin and its partner Armadillo (β-catenin in vertebrates)

which together form adherens junctions linked to the internal cytoskeleton. Without these junctions the niche fails to maintain a GSC population as loss of interaction with non-stem cell progeny leads to its differentiation [17]. It has been shown that cellular density is also of importance when there is a higher cell density, SCs are more likely to maintain a SC fate which is likely due to the proximity of SC-produced soluble molecules [13].

The impact of cell to cell contacts, and therefore proximity to biochemical factors released by the neighbouring cells, is important in several systems. In the *Drosophila* germ line the hub cells secrete Upd (a ligand) which activates the JAK-STAT signalling pathway in SCs to maintain the SC population [26]. When this interaction is lost the SCs begin spermatogonia (differentiation) [17], likely a combination of the loss of interaction and the loss of the ligand. These examples not only show the importance of the interactions a cell makes but also the cross over between different types of signals working together.

Mechanotransductive Cues

Before considering mechanical cues, and how these may affect SCs behaviour, it is important to first consider the extracellular matrix (ECM), a structural component found in all tissues and organs [7,14]. In mammals the ECM includes the interstitial matrix, the intercellular space between cells of connective tissue and typically is composed of fibrillary collagen I and III [14] with elastin and fibronectin, all of which form a '3D amorphous gel' [48]. Additionally, the ECM is found as basement membrane (BM), a sheet-like structure surrounding connective tissue with epithelial/endothelial cells attached to it typically composed of laminins, type IV collagen and fibronectin for tensile strength to produce a more dense structure [14,48,49]. Kular 2014 provides an overview of ECM components and their purposes which will briefly be discussed here [48]. The ECM has a basic composition of macromolecules, polysaccharide and water however each tissue has its own unique ECM composition.

The two main macromolecules found in the ECM are fibrous proteins (which are divided into two groups, structural and non-structural) and proteoglycans. Firstly, the structural components of fibrous proteins include collagen (which provides tensile strength) and elastin (provides the ability to recover from stretching such as in the skin dermis). Different tissues have different collagen types dominantly present; for instance, type II collagen is typically found in cartilage, type III collagen is found in blood vessels, type IV collagen is the main component of BM while collagen I is found in most tissues. Collagen is produced by fibroblasts, endothelial and epithelial cells[48]. The second group of ECM proteins are non-structural components which include fibronectin, laminin and tenascin[48]. Fibronectin is linked to cell migration and wound healing while laminins are involved in cell adhesion via integrins and linked to processes including differentiation. Tenascins are found within the interstitial matrix where load bearing is required and also found in skin and within the brain. Tenascins are important for mechanical activity[48].

Polysaccharides consist of a chain of carbohydrate molecules while glycosaminoglycans (GAG) are long unbranched polysaccharides. A proteoglycan consists of a core protein with one or many covalently attached GAG chains. Proteoglycans are hydrophilic and therefore function to hydrate while also withstanding compressive forces[50,51]. ECM proteins have binding sides for cell adhesion and growth factors and proteoglycans are also involved in binding growth factors. Examples of proteoglycans include Heparan sulphate proteoglycans (HSPGs) such as Perlecan, found in the BM, which binds fibroblast growth factors (FGFs) and vascular endothelial growth factors (VEGF). Both growth factors act in angiogenic processes and so are found in blood vessels [48,51]. Chondroitin Sulphate proteoglycan (CSPGs) such as aggrecan binds TGFs [51]. The presence of growth factors within the ECM provides sustained signalling to cells that adhere to the ECM and lead to changes in signalling pathways and gene transcription [7,48,50,52,53]. These signalling molecules can be arranged so that different areas have different concentrations producing concentration gradients of the factors meaning cells are exposed to specific levels

dependent upon their position in the niche [52]. This highlights the link between the biochemical and mechanical cues and shows that many cues are not fully independent.

The ECM is produced during tissue development but is dynamic and therefore constantly changing both due to enzymatic and non-enzyme activity [7,50]. Matrix metalloproteinases (MMPs) are enzymes which function to alter the ECM's composition but are held under control by tissue inhibitors of metalloproteinases (TIMPs) which inhibit MMP activity [50]. There are long term effects of altering the ECM properties via MMPs. For example in a defined brain stem cell niche, the sub-ventricular zone (SVZ), NSCs require ECM remodelling for differentiation and migration to the extent that in the absence of MMPs differentiation is inhibited [52]. This is potentially an important point to consider for the development of a synthetic environment, as should the natural niche have an important remodelling stage the absence of this change in the synthetic version is likely to have important effects which may be beneficial or could be a block to reaching the desired outcome [54].

Mechanotransductive cues impact on cell behaviour

Now that the components of the ECM have been described I will describe the impact of the ECM on cell behaviour.

Mechanobiology describes the process through which cells identify and respond to mechanical stimuli leading to mechanotransduction signalling and hence a downstream change to signalling pathways (including MAPK and Wnt) [7,33,55]. The main link is by focal adhesions (FAs) found mainly in cells when they are stationary (although migrating cells produce dynamic adhesions[48]). A focal adhesion consists of integrins, transmembrane proteins, binding the ECM via their extracellular domains along with other proteins such as Kindlin and Talin. An example of a cell-ECM interaction is the interaction of muscle satellite cells with the basal lamina via α7β1 integrin [7]. As previously stated it is via FAs that cells sense and respond to mechanical properties. This can be achieved as cells change levels of ECM production[48], in turn affecting the cytoskeleton[7,14,56,57] and changing the contractile forces exerted on the cell [13,48]. Through their association with

kinases and phosphatases, such as focal adhesion kinase (FAK), FAs also impact on cell signalling pathways in a manner that alters gene expression [14,52,53,58]. Cells responding to changes in the mechanics of the ECM can also lead to cell migration (a process known as durotaxis), a key aspect of differentiation [33]. Further research into the specific pathways for different conditions for different cell types is ongoing.

In terms of SCs, the ECM is an integral part of the niche environment which is important for SC regulation and is produced by the structural cells of the niche [17,48,59]. In general, evidence shows that when SCs maintain their interactions with the ECM they maintain SC-like characteristics, whereas the loss of interaction with the basement membrane results in differentiation. This can be seen both in experiments with human epidermal cells and GSC [56]. The interaction of the SCs with the ECM indicates how ECM properties have the opportunity to influence SC behaviour.

This experimental support for the impact of mechanical properties on fate decisions of ASCs has been found only relatively recently [33,60]; research in this field is now growing rapidly but there are still many unknown aspects of these types of cues. Reviews of the mechanical features have been published [13,14,32,52] and their effects on SCs will be considered in this section. Methods currently used to study the mechanism of how cells respond differently to mechanical cues include microarrays, atomic force microscopy (AFM), cytocompression and culture on substrates of varying mechanical properties to study cell responses [33,57,61,62]. These substrates are produced utilising methods such as lithography [30,57,63], hydrogels [62,64,65] and thermal imprinting [66] along with arrays which can direct cell fate [67–70]. An alternative method utilised in synthetic environments is fibrous scaffolds. Fibrous scaffolds can be manufactured by a variety of methods (which will be discussed further in Section 2.3) and is the technique used by several groups to produce environments to provide a representative environment for SC populations as the scaffolds are replicative of the fibrous nature of the ECM [71–76].

I will now consider some examples of particular substrates that indicate how mechanical properties impact on SC behaviours. Engler examined substrates of particular stiffness

(measured by the elastic modulus known as the Young's Modulus) and demonstrated that substrate stiffness can affect SC fate [30,33,77,78]. Subsequent studies have indicated that SCs can behave appropriately on scaffolds with the same stiffness as found in the *in vivo* niche. For instance, the SVZ of the brain has a stiffness of 0.5-1 KPa *in vivo*, and when cultured *ex vivo* on substrates of the same stiffness neurogenesis peaks[39,64] (Table 2.1.2 B). This is hypothesised to be due to the fact that stiffness alters cell attachment to the surface leading to changes in cell spreading and exerting different contractile forces that affect cytoskeleton tensile stress and hence gene expression and downstream fate decisions [32,33,57]. However, the mechanism of how the stiffness of the substrate affects fate decisions is not well-understood [31].

Table 2.1.2 B: The effect of substrate stiffness on the fate decisions of SCs. Shown is how different SC populations response on different substrate stiffness. Mesenchymal stem cells (MSC), Neural stem cells (NSC) and embryonic stem cells (ESC). References are included for each study.

SC type	**Soft (<10 KPa)**	**Medium (10-30 KPa)**	**Hard (>30 KPa)**
Muscle satellite SCs		Self-renewal (12Kpa)[79]	
MSCs	Neuroblasts (0.1-1Kpa)[31]	Chrondrocytes (20-25Kpa)[31]	Osteoblasts (30-45Kpa)[31]
NSCs	Proliferation (0.1Kpa)[39] Neural (0.1-0.5Kpa)[39] Glia (1-10 Kpa)[39]		
ESCs	Astrocytes (0.01-0.03 KPa Neurons (0.5-1 KPa)[64]		

Dimensions are also important to cell fate decisions, for instance culturing chondrocytes in a 2D culture, where the cells have flat morphology fibroblasts are produced while in 3D culture when the morphology of cells are spherical they remain as chondrocytes [7,32]. For ESCs, differentiation into neurons and glia occurred at higher levels in 3D (hydrogel) culture versus 2D culture, tested with a variety of coatings such as fibronectin [64].

Another feature of the ECM, or a culture substrate which cells have been shown to respond to, is the morphology which refers to the top surface arrangement of an area including surface roughness, diameter, porosity, and organisation of features [52]. Cells have been shown to detect

slight changes in the environment, including alignment, and respond to these geometric cues [80,81]. It is thought that these changes are due to differing interactions with cell surface protein (integrins) that cause changes in the cytoskeleton, but the exact mechanisms are unclear. Cells form interactions with the surface and if these interactions are altered so is SC fate. The molecular clutch concept has been recently utilised to understand and therefore predict how cells respond to the mechanical properties of a substrate [82]. Micropatterning experiments have begun to show this by looking at changes at a single cell level. Influencing factors have been investigated including density, shape of the contacts and the pattern of the contacts [14,32]. Micropatterning experiments have also been utilised to show that changing cell-surface interactions affects cell shape which in turn impacts upon fate decisions; for example, flattened hMSCs follow a osteogenesis lineage pathways while rounded hMSCs produce adipocytes [13].

Diameter and the alignment of fibres, topology cues, have both been shown to lead to changes in cell shape and fate [30,53,72,83–85]. Experiments with MSCs showed that on gratings (grooves on the culture surface manufactured using, for example, lithography [57]), cells elongated, aligned and showed neuronal markers (Tuj1 and MAP2) without retinoic acid, whereas without grating these markers were only seen with exposure to retinoic acid therefore showing the importance of mechanical cues on stem cell behaviour [86]. This paper also highlighted the impact of fibre diameter, showing thinner grating (350 nm versus 1 μm and 10 μm width) produced more marker expression for neuronal markers [86]. Experiments with human MSCs investigating both stiffness and diameter of grating showed that the nanotopography greatly impacted on the cytoskeleton, with FAs also changing in density on grating versus no grating[57]. Fibrous scaffolds produced by electrospinning are another scaffold used widely for studying cell responses to diameter and orientation. Fibre diameter has been shown to impact on the differentiation of NSCs with thinner fibre diameters (283 nm) promoting higher levels of oligodendrocyte differentiation, while larger diameter fibres (749 nm) promoted neuronal differentiation and the largest diameter of this study (1452 nm) showed less cell viability but with some neuronal differentiation [72]. A study to develop new methods for peripheral nerve repair utilising neuronal

cells with Schwann cells showed that on thicker fibres (13.5 µm) more neuronal differentiation was observed when compared to the thinner fibres (2.4 and 3.7 µm) [87], showing that different fibre diameters appear to influence different cell types in different ways. The study, which used neuronal cells with Schwann cells also showed that aligned fibres were influential in improving neurite outgrowth alignment [87]. Other studies have shown that aligned fibres influence cell behaviour such as with annulus fibrosus stem cells (AFSC) where on aligned substrates, compared to random substrates, cells were more organised and produced higher levels and more organised collagen-1 alongside, impacting on differentiation [71]. Generally fibre alignment appears to influence cells to also organise in a more aligned orientation.

It is important to acknowledge that, like many other complex phenomena, the influencing factors are not fully independent. Therefore a change to a factor such as alignment has been shown to also affect the tensile modulus [88]. This means any identified changes in behaviour could be due to the change in alignment, change in tensile modulus or the combination of both. While some papers do characterise several mechanical properties, including stiffness, such as [83,89,90] other papers only characterised fibre properties and do not state properties such as stiffness [71,72,87,91]. In order to develop a complete understanding of the influence of the range of mechanical cues on different cell types it is important that whenever possible scaffolds are characterised for as many of these properties as possible, to allow for more comparisons between different studies.

Another aspect of current research I noted when reviewing papers utilising fibrous scaffolds was that many of these do not provide sufficient detail in their methods for how they have collected and handled data to characterise fibre diameter or alignment. Therefore the reporting of methods for the characterisation of these features requires further consideration as without this detail methods cannot be repeated or easily compared to other papers. The reporting of these methods can be difficult, particularly for orientation, as it is a complex feature mathematically [89,92,93]. Examples such as [71,73,75,83,87,94–96] have provided some detail of their methods for

characterising either fibre diameter or orientation, in many cases reporting the use of ImageJ but without specific detail. There was a few that provided no method for the characterisation of fibre diameters [70,72,90,91,97]. Other papers including [89,95] did provide detailed methods for their characterisation of fibres.

The studies discussed show good progress towards understanding how mechanical forces impact upon stem cells, ranging from ESCs to ASC populations particularly highlighting the important impact these properties have on the behaviour of stem cell populations. These substrates utilised for this study of mechanical cues as a laboratory tool are also providing culture systems to better culture these cell by utilising tailored mechanical properties to affect cell biology and therefore maintain 'stemness' or to control the direction of differentiation towards a cell lineage. From this there is also great potential for these systems to develop into medical devices [30,98]. An example of such medical treatment devices include research published by the MacNeil/Claeyssens/Ortega team in which they produced a smart construct containing synthetic and well-defined limbal stem cell microenvironments by combining electrospinning and additive manufacturing techniques for the study of limbal stem cell behaviour[75]; these devices have now been tested *in vivo* [99] and a simpler version of the microfabricated device has now been used in a clinical trial with humans showing its potential to be utilised to treat corneal disease (unpublished work, manuscript in preparation).

While a number of SC populations have now been studied for their responses to mechanical and other cues, some key SC populations have yet to be fully characterised including brain adult stem populations. The brain is a highly sophisticated organ where several aspects of its biology are still not fully understood. I will now review what is known about the SC populations of the brain highlighting areas that require further attention and how the substrates described in this section could be utilised to address these gaps in knowledge.

2.2 The brain contains a number of ASC populations

Since the 1960's it has been known that the adult brain is not a quiescent organ but does produce new neurons post-embryogenesis. However, it was only in the last 20 years that the brain ASC populations, termed neural stem cells (NSCs), were identified [40,100,101]. Two well characterised NSC population reside in the forebrain, one in the subventricular zone (SVZ) located around the lateral ventricles and the second in the subgranular zone (SGZ) of the dentate gyrus in the hippocampus[100,102], (Figure 2.2 A).

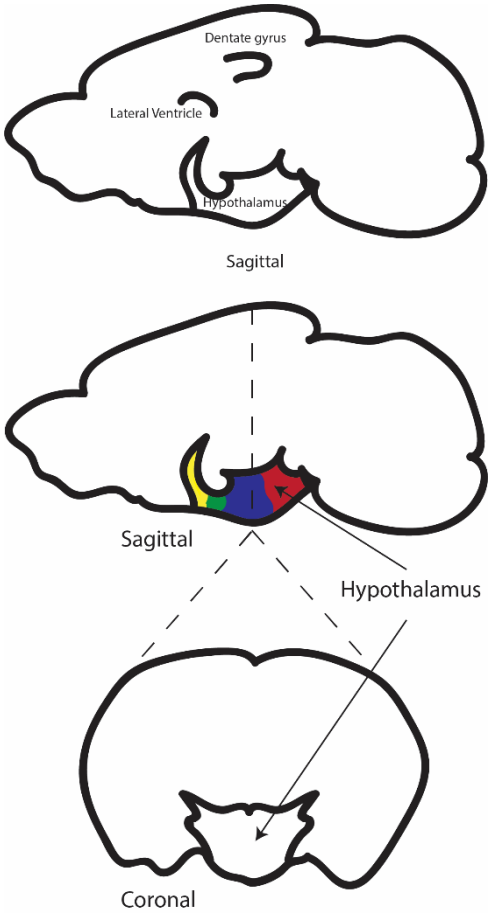

Figure 2.2 A: A sagittal view of the mouse brain. Indicated are the general location of the three NSC population. The SVZ population is located in the later ventricle while the SGZ population is located in the dentate gyrus of the hippocampus. Finally the hypothalamus if located ventrally of these two populations. In a sagittal view the hypothalamus can be segregated into four areas, preoptic (yellow), anterior (green), tuberal (blue) and posterior (red). A coronal view of the tuberal region is also shown. Based on sections on the Mouse Brian Atlas.

In both cases the NSC population is an astrocyte subset derived from radial glia [40,101,103,104] that is positive for GFAP (glial fibrillary acidic protein) and Sox2[105,106]. The SVZ NSC population produces progenitor cells which give rise to neuroblasts that migrate to the olfactory bulb, via the rostral migratory stream, where they differentiate into mature interneurons [40,42,43]. This population has been shown to be heterogenic within the three walls of the SVZ, this heterogeneity having important impacts upon the differentiation of the newborn cell that is

destined for the olfactory bulb[102]. SVZ NSCs also give rise to oligodendrocytes and astrocytes alongside the olfactory bulb interneurons[107]. The second well-characterised NSC population of the brain is located in the subgranular zone (SGZ) of the hippocampus, where NSC produce new granular neurons, the rate of which has been shown to be influence by stress [100]. These new neurons then contribute to the hippocampus and are involved in memory and learning[104]. There is also heterogeneity found within this NSC population[108]. Research is ongoing to fully understand the mechanism of proliferation that maintain the SC population and promote its differentiation within each of these regions. Finally, in more recent work, researchers have also identified a NSC population within the hypothalamus, Figure 2.2 A [109–111]. This project will focus on this novel NSC population found in the adult brain as it is a less well characterised population within a region of great importance to survival, as will be discussed further in Section 2.2.1.

2.2.1 The hypothalamus functions to maintain body homeostasis

Before considering the stem/progenitor population of the hypothalamus firstly I will discuss its functions and why it is such an important region of the brain. The hypothalamus is one of the smallest and evolutionarily-oldest regions of the brain, which is highly conserved particularly between vertebrates[1,112]. The hypothalamus is an integrating node, comparing inputs from the body and other parts of the CNS. Inputs are then compared to optimal 'set points'. The hypothalamus then co-ordinates how similar the detected level are from the 'set point' and if they are different, effects feedback signals to return to the set point. The hypothalamus is therefore essential to individual survival and procreation as this process maintains body homeostasis and basic life functions. In combination with this the hypothalamus is highly sophisticated meaning these 'set points' are continually evaluated to respond to changes in the environment, which is known as allostasis[1,113].

The hypothalamus is located ventrally within the forebrain, superior to the pituitary gland and posterior to the optic chiasm[112,113]. Understanding of how the hypothalamus develops and its

functional processes has lagged behind other brain regions due to its complex structure. Unlike other regions of the CNS, such as the cortex or cerebellum, its neurons are not arranged in a simple columnar structure[112,113]. However it is now known that the hypothalamus develops from the anterior neural tube with WNT and Sonic hedgehog (Shh) being important signalling components[1]. Further development and patterning involves careful signalling of Shh, BMP7 (bone morphogenetic protein) and Nodal that promote patterning, growth and differentiation [114]. A recent study has provided additional understanding of early hypothalamic development [115]. An FGF10+ progenitor population was identified which gives rise to much of the basal hypothalamus, but additionally, a subset appear to be maintained as an Fgf10+ stem-like cell [115]. Currently, little is known about the manner in which a hypothalamic stem cell is established, nor the control cues required for hypothalamic NSPC maintenance and differentiation.

The adult hypothalamus can be divided into four regions when viewed sagittally (Figure 2.2 A). The most rostral region is the preoptic (involved in thermoregulation and reproduction), then moving caudally is the anterior hypothalamus (circadian rhythm and neurosecretory functions) followed by the tuberal hypothalamus (energy balance, stress and mediation of autonomic and neuroendocrine responses). The tuberal region also contains the median eminence (ME) and pituitary stalk which project from the ventral surface. The ME and pituitary are critical for hypothalamic function as this is the region where crosstalk between the brain and the body occurs. This can occur as the blood-brain-barrier (BBB) which normally protects the brain from external influences, is absent in the ME [116]. Neurons within the arcuate nucleus (ARC) and paraventricular nucleus (PVN) interact with this region to lead to hormone release, as neurosecretory axonal ending are located at the pituitary, to the body via the capillaries found at the ME. The hypothalamus is also involved in endocrine signalling via the mechanisms previously outlined. The final region is the posterior hypothalamus including the mammillary bodies (arousal and stress)[112,113].

The hypothalamus is built in a bilaterally symmetrical manner around each side of the third ventricle (Figure 2.2.1 A)[1]. This project will focus on the tuberal hypothalamus. Components of the tuberal hypothalamus include specialised radial glial like cells termed tanycytes, the cerebral spinal fluid (CSF) in the third ventricle, blood vessels within the median eminence, oligodendrocytes and astrocytic cells in the parenchyma alongside progenitor cells that will give rise to cells in the ARC nucleus and the ventromedial nucleus (VMN). Now I will consider these tuberal hypothalamic cell types and review evidence for which of these populations has stem-like characteristics, and may derive from the FGf10+ embryonic NSPC population.

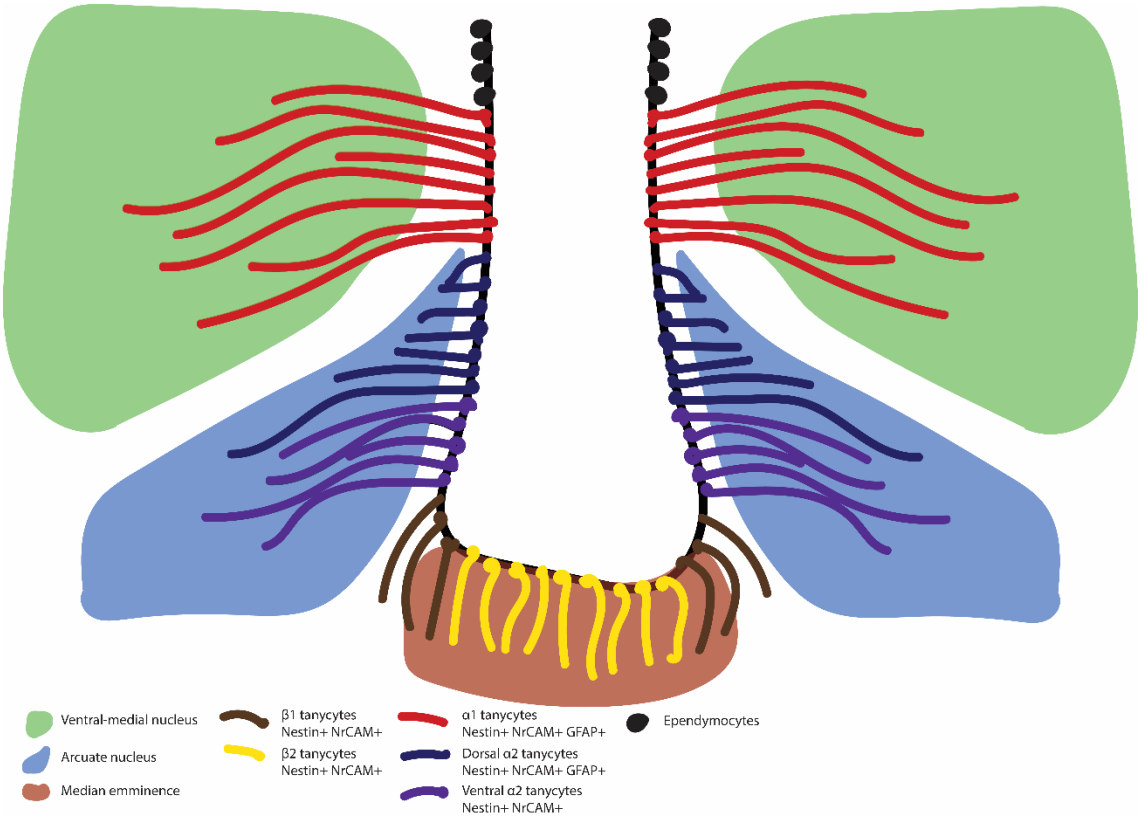

Figure 2.2.1 A: Diagram of the tanycytes lining the third ventricle. A sagittal view of the hypothalamus showing the structure of the hypothalamus is mirrored on each side of the third ventricle. The median eminence (brown) lines ventrally with ß-tanycytes processes feeding into this structure, both ß1 and ß2. Lining the sides of the third ventricle is the arcuate and ventromedial nuclei. α2 tanycytes processes feed into the arcuate nucleus whereas α1 tanycytes feed into the ventromedial nuclei. Based on information from Robins 2013, Elizondo-Vega 2015 and Mullier 2010.

Cell types found in the tuberal hypothalamus

Oligodendrocytes are located within and surrounding the ARC and WMN nuclei [117]. These cells function to insulate neurons by the myelination of axons and recently have been shown to provide trophic support to long axons [117].

Astrocytes are the most abundant glia cell type[118,119] and elsewhere in the brain are involved in cognitive function by modulating synaptic plasticity; the impairment of astrocyte function leads to problems with memory and sleep. Astrocytes of the hypothalamus are involved in the process of maintaining homeostasis by sensing nutrients and acting to metabolise and store glucose, the main source of energy within the brain. The expression of hormone receptors, including receptors for leptin, shows that astrocytes are also involved in endocrine signalling within the hypothalamus[119,120]. Astrocytes are located throughout much of the hypothalamus, including the ARC and VMN nuclei[119]. However, they are involved in re-enforcing the blood-brain-barrier (BBB) and so are absent from the median eminence [121]. In the SVZ and SGZ, the stem populations are astrocytic. This gave rise to the idea that the astrocytes within the hypothalamus might be potential candidate for the hypothalamic stem population [122,123]. Studies have shown proliferation of astrocytes within the parenchyma that also label with the NSC marker, Sox2 [124,125]. However, as discussed below, other studies have suggested the hypothalamus does not have an astrocytic stem population but that a different population is the stem population.

The ARC and VMN both contain mature neuronal populations. These include dopaminergic (DA) and Growth hormone-releasing hormone (GHRH) neurons that reside within the ARC and Neuropeptide Y + (NPY) neurons that reside within both the ARC and VMN. The ARC mainly functions in energy balance and fertility [116]. These functional nuclei work together to sense information from the body and cause the relevant response required to maintain body homeostasis.

Tanycytes are found lining the third ventricle of the central hypothalamus [113,126] and are largely absent from the anterior and posterior hypothalamus. Their cell bodies line the ventricular wall of the third ventricle whilst their single basal process extends into the surrounding parenchyma. Therefore these cells have apico-basal polarity [127]. Dorsal to the tanycytes are ependymocytes, an ependymal cell which lack a basal process[2,128]. The hypothalamic tanycyte population can be subdivided into several different sub-populations, based upon their location within the wall of

the third ventricle and the expression of certain markers. Broadly there are two categories, firstly alpha (α)-tanycytes which line the sides of the ventricle and extend a process into the surrounding nuclei and secondly beta (β)-tanycytes that line the ventral-most part of the third ventricle wall and extend their processes into the median eminence, Figure 2.2.1 A. These two categories are then further subdivided into β1 and β2 subtypes; β1 tanycytes lines the infundibular recess while β2 tanycytes line the medial ventral wall. Further sub-divisions include α1, dorsal α2 and ventral α2. α1 tanycytes are positioned adjacent to the VMN, ventral to these are dorsal α2 tanycytes, ventral α2 then reside next to the β-tanycytes. Both α2 populations interact with the ARC nuclei [2]. Tanycytes have similar morphology to embryonic radial glia, which are the NSPC in the developing CNS, and therefore tanycytes were hypothesised to be the NSPC within the adult hypothalamus. Research into identifying the hypothalamic NSPC of the hypothalamus have considered β-tanycytes and α-tanycytes or more specifically dorsal α2-tanycytes [2,128]. This cell population is now broadly considered to be the hypothalamic stem/progenitor population, with some continuing discussion over which sub-category of tanycyte cell has the most potency. I will now consider the research into identifying this population in terms of their stem/progenitor characteristics along with the other purposes of tanycytes for the hypothalamus' functions to maintain homeostasis.

2.2.2 Tanycytes

In order to identify the hypothalamic stem population researchers employed several experimental techniques to identify which cell population is able to maintain its own population and differentiate into other cell types, the two key features of a stem cell [129,130]. Experiments showed that the neurogenic activity is associated with the tuberal hypothalamus and specifically cells that line the third ventricle, not cells within the parenchyma [2]. The first evidence that tanycytes are the NSCP of the hypothalamus comes through the labelling of this population with the accepted NSC markers Nestin and Sox2 [2]. The previously discussed Sox2+ cells found within

the parenchyma (astrocytes) as now thought to be progenitors of the tanycytes [122]. Other evidence comes from studies on the *in vitro* culture of these cell types, via the neurosphere assay. In 1992 Reynolds and Weiss developed this culture method for NSCs. This assay allows for the culture of NSC in 3D spherical suspension, termed neurospheres, Figure 2.2.2 A, that can then be passaged to examine self-renewal, or differentiated to test potency. Experiments have confirmed that the tanycytes that line the third ventricle of the hypothalamus can produce neurospheres [131]. Isolation of the sub-populations of tanycytes have showed that α-tanycytes produce more neurospheres for more passages than β-tanycytes [2]. Neurospheres cultured via the neurosphere assay can be isolated and then cultured on flat surfaced, treated with PDL and fibronectin under differentiation conditions to differentiate into neurons, astrocytes and oligodendrocytes. Neurospheres derived from the tuberal hypothalamus have been shown to differentiate into these three cell types when cultured under these conditions *ex vivo* [2,132].

Additional support that tanycytes are the hypothalamic NSPC came through lineage tracing studies, using GLAST-CreERT2 reporter mice, which labels α-tanycytes. Analysis of these mice showed that α-tanycytes can give rise to more α-tanycytes or to β-tanycytes and neuronal/astrocyte lineages *in vivo* [2]. In addition, α-tanycytes proliferate in response to FGF signalling and tanycytes lining the third ventricle express FGF-10 and FGF-18[132] further providing results towards this population being the NSPC population. A prevailing view is that α-tanycytes are the adult SC of the hypothalamus, capable of self-renewal and multipotency [133] giving rise to other tanycytes subsets including β-tanycytes, that show progenitor properties [122,134,135]. Studies have shown that β-tanycytes are more prolific with faster BrdU incorporation than α-tanycytes and this is aligned with the view that β-tanycytes are progenitors as they are more prolific than the stem population [125]. More research is required to fully understand all the cell populations in further detail and the purpose that each has in providing new cell types.

Alongside their ability as stem/progenitor cells tanycytes are also involved in other processes such as transporting certain molecules across the median eminence into the ventricle and the

functional nuclei; these functions mean that tanycytes have been termed 'gatekeepers' [136]. Such molecules include leptin which is involved in feeding responses [116,122,134]. Part of this function of transporting molecules across the median eminence is the tight junctions found within tanycytes which modulates the transport of molecules across the median eminence [136,137]. Tight junction proteins include Zonula occludens-1 (ZO-1) which have been identified around tanycytes cell body lining the third ventricle [127,137]. The tight junctions also contribute to the apico-basal polarity of tanycytes [127,138].

Therefore tanycytes are of great interest as they are functioning in both the short and long term to ensure 'allostasis'; the ability of the brain to build new cells in response to new physiological requirements. In the short term they are part of the hypothalamus' process to sense molecules, compare them to the 'set point' and review whether the 'set point' requires adjustment. Then in the longer term their stem/progenitor capabilities are involved in providing new mature cells to surrounding nuclei to adapt to current requirements.

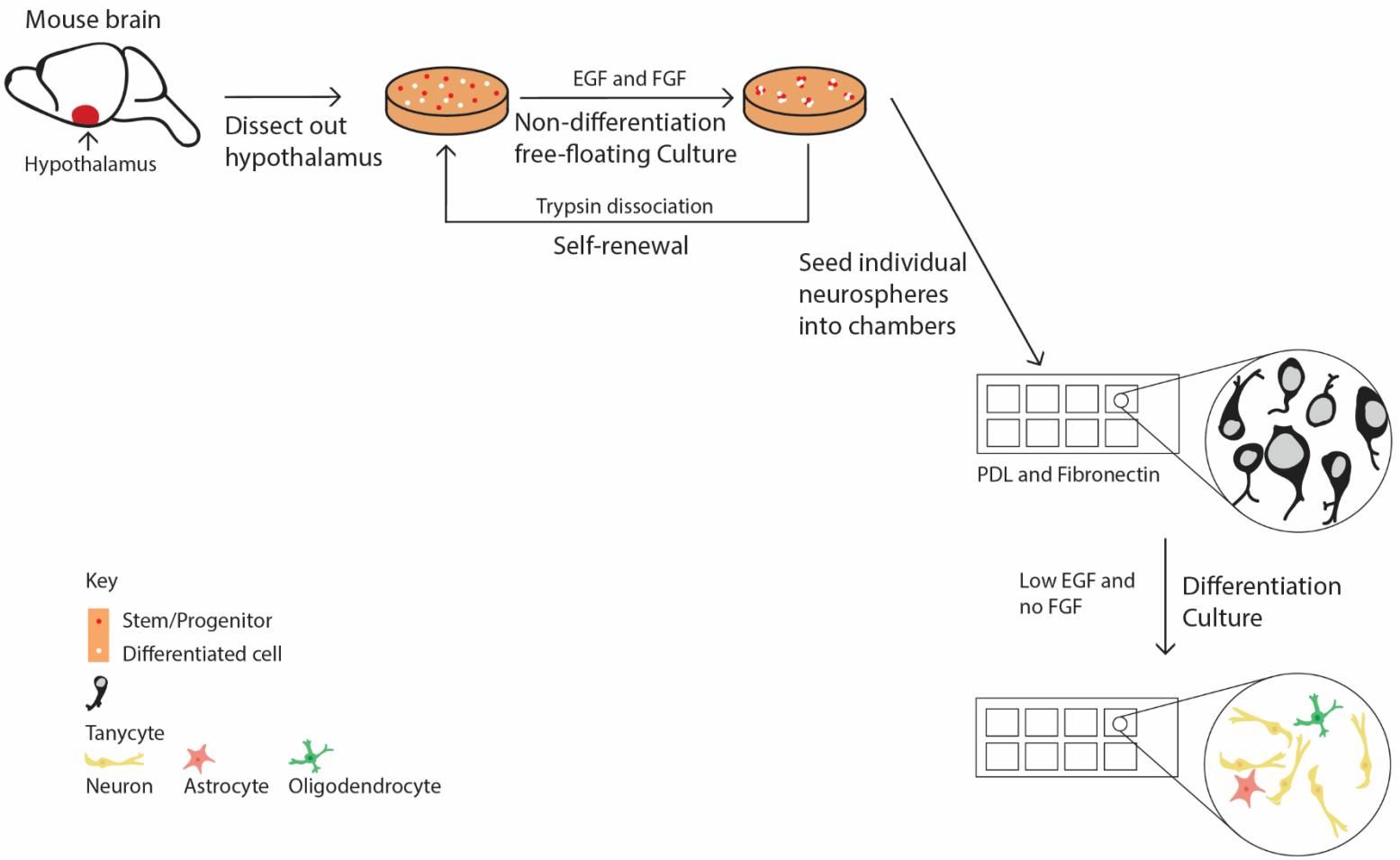

Figure 2.2.2 A: Diagram of the culture of tanycyte neural stem/progenitor population. Tanycytes are isolated from the hypothalamic region and cultured as 3D spheres via the free-floating neurosphere assay. Under these conditions tanycytes self-renew and maintain a tanycyte culture when cultured with EGF and FGF. These neurospheres can then be isolated and cultured on a surface treated with PDL and fibronectin to differentiation into neurons, astrocytes and oligodendrocytes with no FGF and lower levels of EGF.

2.2.3 Limitations in tanycytes knowledge/key questions

Given that the hypothalamic NSC is a relatively recently-discovered population, there are still many unanswered questions regarding its control. Thus there is a lack of knowledge of the cues that control its behaviour (self-renewal vs differentiation) *in vivo* within their niche. One way of better characterising the hypothalamic NSC is through the use of an *ex vivo* culture system, the neurosphere assay, in which tanycytes are seeded at clonal density, cultured to neurospheres and repeatedly passaged. However, it is well documented that for many stem cell types, *ex vivo* culture is not 100% efficient and differentiation and genetic instability occurs[22]. Therefore it is suspected that this will also be the case for tanycyte-derived neurospheres when they are cultured, even when culturing them under 'non-differentiating' conditions (EGF, FGF). Here I will firstly study tanycytes under standard free floating conditions, to ask if this culture system is able to efficiently maintain tanycytes. Should this culture prove to be inefficient topological substrates will be utilised to study responses to mechanical cues, alongside identifying whether these cues can better support the *ex vivo* culture of tanycytes. The long-term aim is to develop a culture system that allows for the continued study of this cell population in which tanycytes are being maintained in an environment that closely replicates their *in vivo* environment.

2.2.4 Preliminary study identified hypothalamic tanycytes respond to fibre orientation

Preliminary data undertaken by Dr Iain Stewart of the Placzek group, along with a summer student David Furley, showed that culturing neurospheres on aligned scaffolds showed different morphology to neurospheres culture on random scaffolds. The two substrates also impacted on marker expression (Figure 2.2.4 A). Therefore as stem-cell like tanycytes appeared to show responses to fibre orientation in this pilot study, the focus of my project was to examine this more carefully and address the impact of aligned versus randomly orientated fibres on the behaviour of hypothalamic neural stem/progenitor cells, tanycytes.

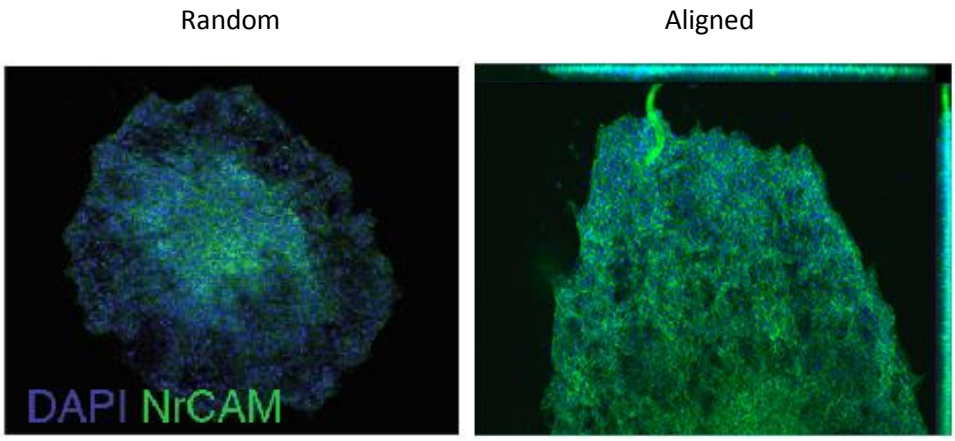

Figure 2.2.4 A: Preliminary data of neurospheres cultured on PCL scaffold. Sigma PCL 10 wt% in DCM/DMF. Initial study showed that neurospheres responded differently to random and aligned fibres morphologically and in the expression of markers including NrCAM. Unpublished.

This initial work, along with the knowledge that tanycytes show highly organised structures *in vivo* being tightly packed and elongated with apico-basal polarity, and the review of current literature showing many stem cell populations response to fibre orientation by becoming organised concludes that this project will specifically focus on the impact of fibre orientation of tanycyte behavioural responses.

2.3 Scaffolds

As discussed in respect to stem cells being influenced by mechanical properties, electrospun scaffolds are one type of substrate utilised to study how stem cells respond to a variety of these types of properties. Due to the use of electrospinning in the initial study, and its ability to alter fibre orientations, this method will be utilised to further study tanycytes responses to biomechanical cues. The process of electrospinning will now be considered further.

2.3.1 Electrospinning

Electrospinning is a process by which an electric field is used to produce fibres from a solution of polymer in organic solvent [73,139]. Electrospinning can be utilised to produced fine fibres in the micron to nanometre range [140]. Polymers can be used to generate a fibrous scaffold by several other methods including melt blowing, phase separation, self-assembly and template

synthesis [139]. Electrospinning is favourable as nanofibres are produced with high surface area and high porosity for cell interaction which is fibrillary similar to the ECM [4,140]. However the process is slow and comes with difficulties of the solvent drying before fibres are deposited and the requirement of an electric field.

Historically Formhals created the original method in two patents [141,142]. The general process of electrospinning is explained in Figure 2.3.1 A.

There are several parameters that affect the morphology of the fibres including the voltage, distance between the needle and the collector, the flow rate, the voltage, temperature, humidity and the solution parameters of the polymer to solvent ratio [88,143,144]. Properties such as diameter are affected when altering these parameters [88,145]. The morphology of the scaffold produced can be altered dependent upon the collector. A flat collect produces a scaffold in which the fibres are randomly orientated (Figure 2.3.1 A (a)). Metallic templates can be used to produce complex 3D features, by attaching the template to the flat plate [76]. However several different collectors produce aligned fibres, including collecting fibres onto a rotating drum (Figure 2.3.1 A (b)) or onto a flat surface with conductive material in regular intervals where the fibres then lay at 90° [143].

There are different polymer routes possible in attempting to generate a synthetic niche. Firstly, adapting a natural component of the ECM, such as chitosan, to alter the chemistry or degradation properties which can result in issues with repeatability and safety despite improving other properties [4]. Other natural polymer examples include collagen and gelatin. Synthetic alternatives are polyurethane (PU), poly(ε-caprolactone) (PCL) or poly(lactic-co-glycolic acid) (PLGA) [140]. A commonly used biodegradable polymer is PLGA [75,143]. This project will utilise the slowly degrading polymer PCL which is also biocompatible [146]. As PCL is a commonly used polymer for electrospinning it was also a good candidate as it was known that the polymer was capable of being electrospun. PCL's slow degradation rate is another reason to choose this polymer as this project is developing an *in vitro* culture system the ability of this polymer to not

be compromised for long periods of time is very important. Finally PCL was utilised in the preliminary study and therefore I wanted to maintain the polymer to ensure that was not a potential factor should I observe different cell responses.

2.3.2 Rational for this laboratory tools development

Electrospun 3D scaffolds show great promise as advanced environments for investigation of cultured cells, but they have not been applied to date in tanycyte culture. In this research programme, that includes the manufacture, characterisation, and evaluation of cell responses to 3D polymer scaffolds, it is important to first establish some parameters to inform their design. Features that are likely to be important in this study based on published research using other cell types include polymer selection, fibre diameter, orientation, mechanical properties, and *in vitro* biocompatibility. It is important to seek to maintain as many properties and features as possible while seeking to alter the one parameter (e.g. fibre orientation) being investigated. Here the focus was primarily on the influence of fibre orientation because of the review of *in vivo* tanycyte structure (Section 2.2.1) along with previous reports of effects on cells reviewed in the literature review (Section 2.1.2). Orientation is a remarkably complex concept, and has been extensively studied (Section 2.1.2) but there is a lack of clarity in the reporting of methods to characterise this feature. Part of this research will focus on developing a reliable and detailed method to represent the level of alignment within fibrous scaffolds allowing for this to be linked to changes in cell behaviour.

This literature review has identified a gap in the current knowledge for the understanding of tanycyte behavioural responses in general but also including mechanobiological cues. The use of substrates such as electrospun scaffolds have been used to study the responses of other stem cell population to features such as orientation and therefore could also be utilised to study tanycyte responses. There is also the potential that current culture conditions are not 100% efficient for the maintenance of tanycytes, which is required for the characterisation for this

stem cell population. These substrates may also be utilised as a novel culture system to improve the *ex vivo* culture of tanycytes.

Chapter 3: Hypothesis, aims, and objectives

Stem cell populations are of great importance in cell biology and regenerative medicine research and understanding their normal *in vivo* behaviour may hold great promise for understanding both the healthy body and disease or ageing. Of the stem cell populations that are currently being studied, the hypothalamic alpha-tanycyte stem/progenitor cell population has not been well characterised, but is of great interest. This is due to the importance of the hypothalamus in regulating homeostasis and due to the potential of its resident stem cell population's involvement in mediating allostasis – the ability of the body to alter its hard-wired cells, to anticipate or respond to new physiological conditions over life, (e.g. adolesence, pregnancy).

Unfortunately, it is known that stem cells are difficult to maintain in a stem cell state *in vitro* using routine methods, as even in standard self-renewing condition they spontaneously differentiate. It is highly likely that tanycytes, when cultured *ex vivo,* will behave in the same manner. Therefore the ability to maintain this stem cell population while reducing spontaneous differentiation *in vitro* would be an important development in the longer-term aim of characterising this population.

This work will consider a scaffold environment that can support the maintenance of the stem-like cell in tanycyte-derived neurospheres, specifically investigating the impact of fibre orientation. *In vivo*, tanycytes are organised in a specific manner. They form the ventricular layer of the third ventricle, an epithelial-like lining in which cells are apico-basally organised: specifically their cell body lines the ventricle wall and their single long process extends into the parenchyma. I hypothesise that aligned fibres will encourage the cells to organise in a similar manner to that found *in vivo*, and that alignment along the fibres will maintain stem-like tanycytes and reduce spontaneous differentiation, Figure 3 A. Consequently, the aim of my research was to design and manufacture a range of reproducible synthetic scaffolds via electrospinning, altering fibre organisation to evaluate the behaviour of hypothalamic neurospheres, (containing hypothalamic neural stem/progenitor cells), when cultured on these different scaffolds.

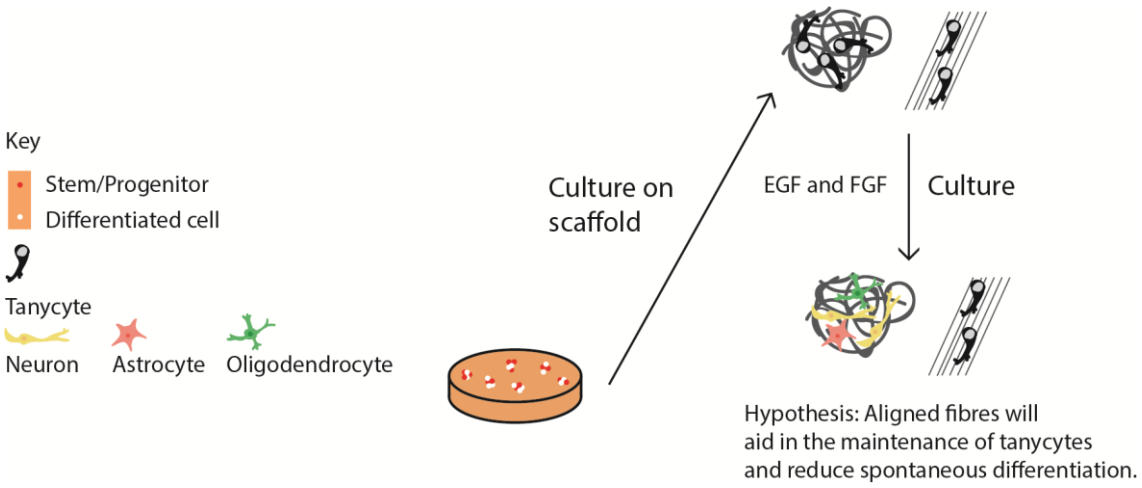

Figure 3 A: The hypothesis of this research is that on aligned scaffold tanycytes will be maintained while differentiation will occur on random fibres.

The specific objectives were:

- to identify the central hypothalamus through coronal sectioning of the mouse brain labelling key cell populations by immunohistochemistry, investigating expression of NrCAM;
- to isolate and culture hypothalamic tanycytes as neurospheres;
- to confirm that hypothalamic tanycytes self-renew and differentiate *ex vivo;*
- to investigate the established *ex vivo* free-floating culture method with non-differentiation conditions for tanycyte derived neurospheres, for its impact on the self-renewal and differentiation levels of this population by immunohistochemistry;
- to investigate how passaging and culturing under non-differentiation conditions impacts on differentiation;
- to electrospin scaffolds with random fibre orientations;
- to investigate a range of metallic templates and the impact of these structures on the fibre topology;
- to characterise the scaffolds in terms of fibre diameter and orientation, including optimisation of this method;

- to alter the electrospinning method to align fibres, thereby producing aligned scaffolds;
- to characterise the random and aligned scaffolds in terms of mechanical properties, specifically stiffness;
- to characterise P3 neurospheres under free-floating 'non-differentiation' culture conditions;
- to investigate whether neurospheres could be cultured on electrospun PCL scaffolds with both random and aligned topologies;
- to investigate the morphology of neurospheres cultured on random and aligned scaffolds;
- to investigate the expression of markers of tanycytes and differentiating neurons on neurospheres cultured on both random and aligned scaffold.

Chapter 4: Materials and methods

4.1 Tanycyte experiments

4.1.1 Solutions

Table 4.1.1 A shows the source and product number of the items required for tanycytes culture.

Table 4.1.1 A: Items required for tanycytes culture.

Item name	**Acronym**	**Source**	**Product number**
4',6-Diamidino-2-phenylindole dihydrochloride	DAPI	Sigma	32670
B27 supplement		Life Technologies	17504-044
Basic fibroblast growth factor (10µg)	bFGF	Life Technologies	13256029
Bovine serum albumin 7.5%	BSA	Gibco	15260-037
Disodium phosphate	Na_2HPO_4	BDH	102494C
DMEM:F12		GIBCO	21331
DNAse		Sigma	D4527
Epidermal growth factor (10µg)	EGF	Life Technologies	PHG0314
Ethanol		Fisher Scientific	E/0665DF/17
Fluroshield with DAPI/without DAPI		Sigma	F6057/F6182
Hanks' balanced salt solution	HBSS	ThermoFisher	88284
HEPES 1M		GIBCO	15630106
Insulin-like growth factor 1	IGF-1	Sigma	I8779-50UG
L-glutamine	L-Glu	GIBCO	25030024
Monosodium phosphate	NaH_2PO_4	BDH	102454R
N2 supplement		GIBCO	17502-048
Paraformaldehyde	PFA	Sigma-aldrich	P6148
Penicillin/Streptomycin	Pen/strep	GIBCO	15140122
Phosphate-buffered saline	PBS	Sigma-aldrich	1002381421

Progesterone		Sigma	P7556
Putrescine		Sigma	P5780
Selenite		Sigma	S5261
Sodium hydroxide		VWR	28244.262
Sucrose		Sigma	50389
Transferrin		Sigma	T0665
Triton X		Sigma	T8787
TrypLE solution		Gibco	12604-013
Trypsin inhibitor		Sigma	T6522-25MG
Tween 20		Sigma	P9416

Following is a list of methods to make required solutions:

- 0.2M phosphate buffer - 35.61 g of Na2HPO4•2H2O and 27.6 g of NaH2PO4•H2O separately in H2O adjusting both to 1 L. For 1 Litre of phosphate buffer mix 770 mL of disodium phosphate (Na_2HPO_4) and 230 mL of monosodium phosphate (NaH_2PO_4), pH to 7.3.
- bFGF (basic fibroblast growth factor) (10 µg 13256029 Life Technologies) - 0.1% Bovine Serum Albumin (BSA) in PBS with 1973.3 µl tissue culture phosphate-buffered saline (PBS), 26.7 µl 7.5% BSA solution, filter sterilize. Add 10 µg growth factor to the 1 ml of collected solution and store in aliquots at -80°C. (20µl of stock added to 10 ml NWS = working concentration of 0.02 µg/ml or 20 ng/ml).
- Differentiation media- 48 ml DMEM;F12, 1 ml B27, 0.5 ml N2, 0.5 ml L-glutamine with 1 µl bFGF/ml.
- Dissociation solution- 48 ml DMEM:F12 (21331; GIBCO) plus 2 ml 7.5% BSA solution. Stored at 4°C.

- DNAse solution (1 mg/ml) - 4.3 ml $Ca2^{+}$/$Mg2^{+}$ free HBSS filter sterilise to collect 3.7 ml. Add 3.7 mg DNAse 1 (D4527-10KU Sigma). Store at -20°C. 50 µl of 1 mg/ml into 1 ml of trypsin + inhibitor = 50 µg/ml working concentration.
- EGF (epidermal growth factor) (10 µg PHG0314 Life Technologies) - 0.1% BSA in PBS with 1973.3 µl tissue culture PBS, 26.7 µl 7.5% BSA solution, Filter sterilize. Add 10 µg mitogen to 1 ml of collected solution and store in aliquots at -80°C. (20 µl of stock added to 10 ml NWS = working concentration of 0.02 µg/ml or 20 ng/ml).
- Freezing medium - 2.7 ml of NWS and 0.3 ml Dimethyl sulfoxide (DMSO).
- N2I – 10 ml DMEM/F12 (21331; GIBCO) containing transferrin (100 mg) (T0665; Sigma). Add the following 10 ul progesterone (P7556; Sigma), 10 ul selenite (S5261; Sigma), 100 ul putrescine (P5780; Sigma), 50 ug IGF-1 (I8779-50UG Sigma). Final concentrations: transferrin 1 mM, progesterone 2 uM, selenite 3 uM, putrescine 10 mM, IGF-1 5 ug/ml.
- Neurosphere stock solution (NSS) – 48 ml DMEM:F12 (21331; GIBCO) with 5 ml pen/strep (15140122: GIBCO). Additions include 500 µl L-glutamine (25030024; GIBCO), 500 µl N2I, 25 µl heparin Final Conc: 5 µg/ml (H3149; Sigma), 1 ml B27 (17504-044; Life Technologies). Store at 4°C can be used for several weeks/months.
- Neurosphere working solution (NWS) – 10 ml NSS with 20 µl bFGF and 10 µl EGF. Store at 4°C use within a week.
- PFA (4% paraformaldehyde fix) – 10 ml of MilliQ water with a few drops of sodium hydroxide. In the fume hood add 1 g paraformaldehyde, allow to dissolve at 65°C stirring at intervals. Filter sterilise using a 0.45 micron filter (Sartorius Stedium biotech 16555-K) to remove any particles. Add 0.2 M phosphate buffer to a final volume of 25 ml. pH to 7.4-7.7. Store at 4°C and use within 24 hours.
- Trypsin inhibitor solution - Step 1: Make 60 ml staining medium: 52.8 ml L-15, 6 ml tissue culture water (sigma), 600 µl pen/strep, 600 µl 1M HEPES, 2.4 ml 7.5% BSA solution (300mg BSA fraction V), Filter sterilize, store at 4°C. Step 2: To 50ml of filter sterilised

staining medium add 7 mg trypsin inhibitor (T6522-25MG Sigma). Filter sterilize, store at 4°C.

- PBS^{2+}- PBS with 1 or 5% Heat inactivated goat serum (HINGS) and 0.1% Triton X.
- Citric buffer – 10 mM citric acid, 0.05% Tween 20 at pH 6. 2.10 g citric acid monohydrate into 1,000 ml distilled water mix to dissolve pH to 6.0. Add 0.5 ml Tween 20 and mix well. Store at 4°C.

4.1.2 Mice

All Mice were wild type C57/BL6J strain (with some wild type/NrCAM null heterozygous adults used for sectioning of the central hypothalamus) adults within the age range of 60-90 days old, both males and females were utilised for both tanycytes isolation to form neurosphere culture and for sectioning through the *in vivo* hypothalamus. Wild type mice were culled by anaesthetic (Isoflo-Isoflurine >3 minutes) with claw reflex tested to ensure death followed by the breaking of the neck. With thanks to Alex Moore and Dr Andy Furley for providing and assisting with tissue isolation.

4.1.3 Neurosphere cell culture

Neurospheres can be cultured through the neurosphere assay as free-floating neurospheres, differentiated on slides or cultured on scaffold, Figure 4.1.3 A shows this overview.

Cell isolation

The brain was dissected out of the skull and the hypothalamus isolated and minced to dissociate cells with the aim to collect alpha-tanycyte cells, the proposed NSPC (Neural stem progenitor population) of the hypothalamus [2]. The hypothalamus cells were treated with protease TrypLE (Life Technologies), to digest proteins, and DNAase (to digest any DNA fragments that are toxic to cells). These P0 cells were then cultured in an ultra-low adhesion 24 well plate (Corning Costar 3473) at 37°C and 5% CO2 to produce neurospheres. When culturing with NWS, as stated in

Section 4.1.1, this is considered culturing under free-floating non-differentiation culture conditions. All neurospheres were cultured under these conditions unless specifically stated.

Cell passage

Once neurospheres have been cultured for ~5-7 days, under free-floating conditions in non-differentiation conditions (NWS), they will have reached a size (above ~500 µm) where oxygen and nutrients cannot reach the centre of the sphere leading to high levels of apoptosis. Therefore the culture was passaged. For each 24 well plate being passaged, 15 ml of NWS was required. A new plate was set up with 400 µl NWS per well and equilibrated to 37°C in the incubator. The remaining NWS, 500 µl TrypLE and 1 ml DS1 were equilibrated to 37°C in a water bath. All wells where neurospheres were in a good condition (not loo large and have not combined to form a large mass) were combined in one 15 ml tube and centrifuged to remove media. The cells were then incubated with 500 µl TrypLE (Life Technologies) for 10 minutes in a 37°C water bath to remove cell-cell interactions. Trypsin inhibitor was added at equal volume (do not warm) with 40 µl DNAse and the solution titrated to dissociate cells. The suspension was then centrifuged to remove solution and re-suspended in 1 ml DS1 and 25 µl DNAse, triturating for 90 seconds. Centrifugation removes the solution and the pellet re-suspended in 500 µl NWS. A haemocytometer (10 µl added) was used to calculate the number of cells in the solution and then the volume of cell suspension required to have a cell concentration of 10,000 cells/ml was identified. During this process the other cells were kept in the water bath. The volume required was then added to the new 24 well plate which contains the 400 µl of NWS warmed. From P1 cells onwards the cultures were fed every two/three days with 100 µl of pre-warmed NWS.

Freezing down cells

Unrequired cells can be frozen down and stored at -80°C, for use at a later time. The cells were cultured (once passaged) overnight in a T25 flask in 4ml NWS. The culture was centrifuged to remove the supernatant and the cells were then re-suspended in the freezing medium, gently

mixing the neurospheres. This solution was aliquoted into 1 ml cryovials and transferred to styrofoam (to slow down the freezing process) and stored at -80°C.

Re-establishing frozen stocks

2.5 ml DS1 and 4 ml NWS were equilibrated to 37°C in a water bath, for one cryovial. The neurospheres were removed from the cryovial and combined quickly with DS1. Then centrifuged to remove the supernatant and the cells were re-suspended with 4 ml NWS and cultured in T25 culture for 5-7 days. Then passaged and cultured in ultra-low adhesion 24 well plates as stated above. Alternatively, cells can be cultured straight in a 24 ultra-low adhesion well plate and then passaged after 5-7 days. Cell were re-suspended in 1 ml NWS and 41 µl added to each well.

Differentiation

Eight chamber slides (Lab/TEK 177445 C7182) were incubated at room temperature in tissue culture hood for 60 minutes with 125 µl Poly-D-Lysine (PDL 150 ug/ml P12024) into each chamber. PDL was removed by tipping onto tissue paper and chambers were gently washes three times with tissue culture water. Per chamber, 85 µl of Fibronectin (100 ug/ml Invitrogen 33010018) was incubated for 4 hours in tissue culture hood. Removed by tipping onto tissue paper and washed gently twice with differentiation medium. Differentiation medium, as stated in Section 2.1.1, (250 µl per chamber), was equilibrated at 37°C for culture under differentiation conditions. Under a microscope one neurosphere was add to each well and cultured for required length time e.g. 8-14 days. Wells were fed every 2-3 days with 125 µl of differentiation media. When the culture time was complete, media was removed and washed with PBS before fixing with 4% PFA for 60 minutes 30 minutes. Slides were then labelled with antibodies firstly removing the chambers to provide a slide which were blocked for 60 minutes using 0.1% HINGS and 0.1% Triton X before incubating overnight with primary antibody at 4 °C, 200-300 µl per slide, and covered with strips of parafilm to ensure even coverage of whole slide. All steps are completed within a humid environment. Slides were washed with PBS before incubating for 60

minutes at room temperature with secondary antibody, again 200-300 µl per slide, and covered with strips of parafilm. Slides were then washed with PBS and then coversliped with fluroshield with DAPI. Slides were then imaged on Apotome. Sections of neurospheres or the whole mount neurospheres were imaged as Z-stacks, whilst for the neurospheres on scaffolds snap images were taken.

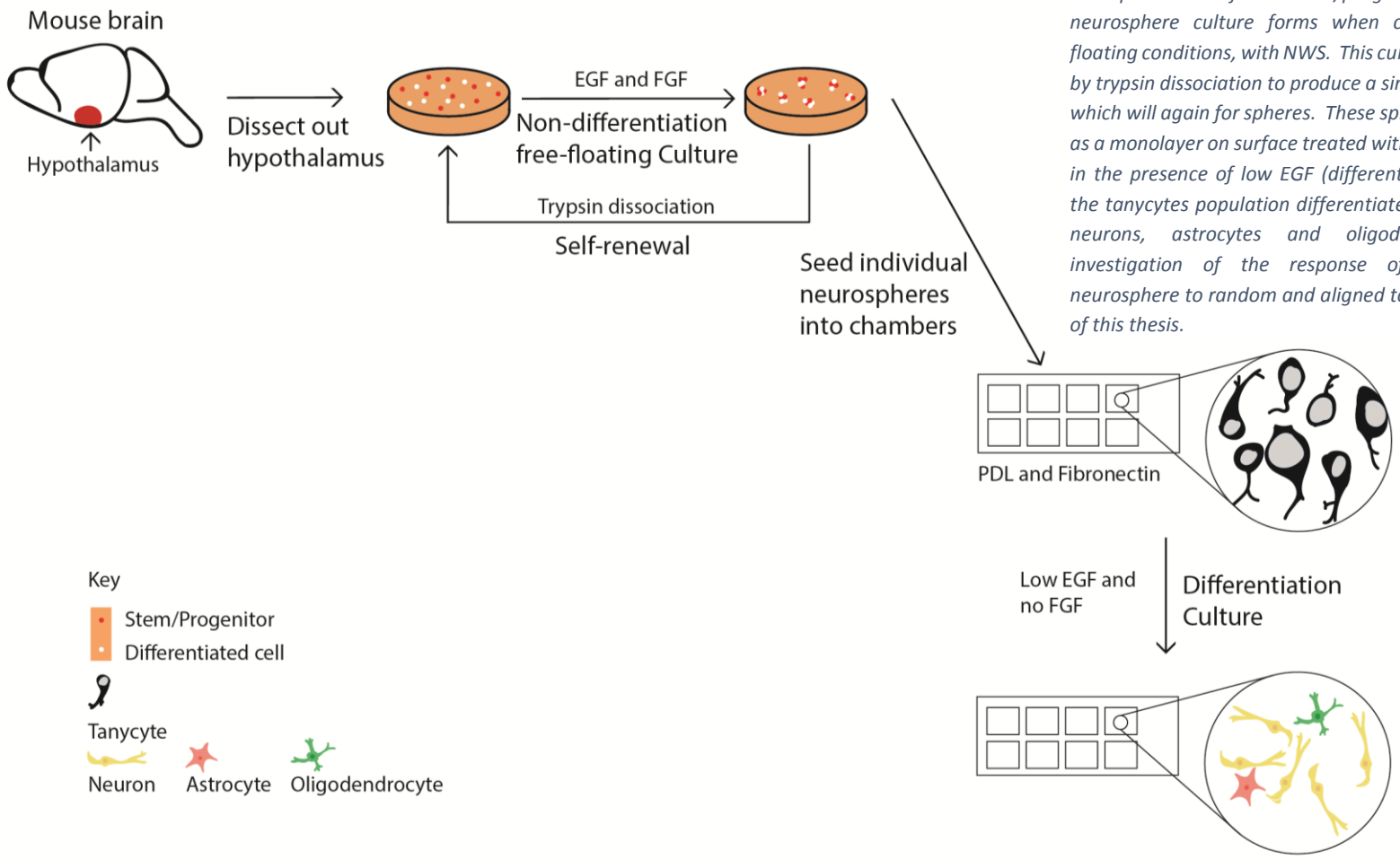

Figure 4.1.3 A: Neurosphere culture protocols. Hypothalamus was isolated out of the mouse brain and minced to produce a single cell culture. Over time due to the presence of a stem/progenitor population a neurosphere culture forms when cultured under free-floating conditions, with NWS. This culture can be passaged by trypsin dissociation to produce a single cell culture again which will again for spheres. These spheres can be cultured as a monolayer on surface treated with PDL and fibronectin in the presence of low EGF (differentiation media) where the tanycytes population differentiates into cells including neurons, astrocytes and oligodendrocytes. The investigation of the response of tanycyte derived neurosphere to random and aligned topologies is the focus of this thesis.

4.1.4 Sectioning

Neurospheres

When the neurospheres were ready to be processed the media was removed from the wells and the neurospheres were combined into one well to be fixed in 4% PFA for 90 minutes. The fix was removed and the neurospheres washed in PBS before being stored overnight in 1 ml 30% sucrose at 4°C. Protocol optimisation showed these steps should be performed under a microscope to monitor the neurospheres.

Using a pipette, the neurospheres were forced to the bottom of the wells and the sucrose removed. The neurospheres were then placed onto a chuck in OCT (optimal cutting temperature) which can be stored at 20°C overnight. The sample was then sectioned, on a cryostat, with 15 µm serial sections collected onto slides. The slides were dried so the tissue fixed to the slide and then was washed with PBS. Block (1% HINGS and 0.1% Triton X) for 60 minutes before incubating overnight with primary antibody at 4°C in a humid environment. Samples were washed with PBS before incubation at room temperature with secondary antibody for 60 minutes in a humid environment. Finally samples were washed with PBS before being coverslipped with fluroshield including DAPI.

Adult mouse brain

Mice were perfused before the brain was dissected out of the skull before fixing in 4% paraformaldehyde in 0.12 M phosphate buffer overnight then storing overnight in 30% sucrose (or until the brain begins to sink 1-3 days). The brain was then placed in OCT on a chuck ready for sectioning on the cryostat. The brain was sectioned at 30 µm to identify the region of the anterior hypothalamus, checking the sections morphology under the microscope. Once the central hypothalamus was identified (by the expansion of the third ventricle to the ventral end of the tissue) sections were collected at 18 µm into wells with 500 µl PBS which were rocked overnight at 4°C. (Method optimisation showed labelling with antibodies was improved with

floating sections over serial section collected onto slides, data not shown). The PBS was removed and samples placed in block (PBS^{2+} 5% HINGS and 0.1% triton X) for 60 minutes at room temperature or overnight at 4°C. Primary antibody was incubated overnight on a rocker at 4°C. The following day, three ten minute PBS washes prepared the sections for incubation with 400 µl secondary antibody for 60 minutes at room temperature, DAPI stain was added at this point. Samples were then washed three times with PBS for 5 minute each, before being placed on slides utilising a small paint brush and forceps uncurling the sections individually. Once the sections were dry they were coverslipped with fluroshield without DAPI.

Adult mouse brain with antigen-retrieval

Antigen retrieval was conducted as per the previous process above. However after the brains have been sectioned, and the PBS removed, sections were place in pre-warmed citric buffer (4.1.1) at 90°C for 30 minutes. They were then allowed to cool before washing with PBS and adding the block and continuing with the remaining steps.

4.1.5 Whole mount

Neurospheres

The media was removed, under a microscope to monitor the neurospheres, from the wells of neurospheres and 4% PFA fix added for 60 minutes at 4°C. The fix was removed and the spheres washed with PBS. This was followed by the immunohistochemistry protocol (Section 4.1.6 Immunohistochemistry) beginning with blocking stage using 5% HINGS and 0.1% TritionX.

Neurospheres culture on scaffold

Random scaffold discs at a diameter of 1.3 cm were cut and placed into an ultra-low adhesion 24 well plate (Corning Costar) and they were sterilised with 70% ethanol (Sigma-aldrich) for 60 minutes. Following the ethanol removal there were three five minute PBS washes to ensure all the alcohol was removed. Samples were washed with NWS and equilibrated at 37 °C. Media was removed and then, under a microscope, neurospheres from free-floating culture were added onto the surface of the scaffold. These samples were incubated for ~20 minutes, monitoring continually not allowing the scaffolds to dry. Then 100 µl of media was added to each scaffold and incubated for a further 30 minutes before adding another 150 µl. This was to allow time for neurospheres to attach to the scaffold. The following morning, a further 150 µl was added to provide the total culture media of 400 µl. Cultures were then incubated at 37°C 5% CO_2 feeding every two/three days. Samples were fixed after 10 days culture with the media removed first and the samples then washed with PBS before fixing with 1 ml 4% PFA for 90 minutes at 4°C then stored at 4°C in 500µl PBS.

For labelling, the samples were washed with PBS before an overnight wash in PBS^{2+} (5% HINGS and 0.1% Triton X) to block against non-specific binding of the secondary antibody. Following which samples were incubated with primary antibody (150 µl) overnight at 4°C. The following day the primary antibody was removed and the samples washed with PBS followed by 48 hours in block at 4°C. Samples were then incubated with secondary antibody (150 µl) either overnight at 4°C or 60 minutes at room temperature in with DAPI stain. To be imaged, the samples were placed on a slide with forceps and a coverslip was added with fluroshield, without DAPI.

4.1.6 Immunohistochemistry

General immunohistochemistry protocol is described below and specific protocol optimisation is described within individual protocol sections. Samples were washed with PBS and then blocked for 60 minutes at room temperature or overnight in PBS^{2+} at 4°C, to reduce non-specific

binding of the secondary antibody. Differentiation and neurosphere section experiments utilised block (also referred to as PBS^{2+}) with 1% HINGS and 0.1% Trition X while whole mount neurospheres, floating sections and neurospheres on scaffold utilised block with 5% HINGS and 0.1% Trition X. Samples were then incubated overnight with the primary antibodies (Table 4.1.6 A). The following day the primary antibody was discarded and the slides washed with PBS. Following this the slides were incubated at room temperature for 60 minutes with the secondary antibody; alongside the secondary antibody DAPI stain (100 ng/ml 300 nM) could be included. This incubation was followed with PBS washes. The slides were then coverslipped with fluroshield (Sigma) either with or without DAPI dependent on whether liquid DAPI was used with the secondary antibody incubation. Images were taken on an Apotome microscope. The control slides were treated the same as other slides but replacement of a primary antibody with PBS^{2+}.

4.1.7 Image acquisition

Images were taken on a Zeiss Apotome either as snap images or Z-stacks using Zeiss software. These images were adjusted in terms of brightness/contrast in relation to their individual secondary control images in a linear fashion via Photoshop (Adobe). Each image was adjusted to the size required on Photoshop to make the figures in Illustrator (Adobe). Scale bars added using Image J.

Table 4.1.6 A: Antibodies. Included is the purpose of using this antibody along with the source and dilution used at.

Primary Antibody	**Source**	**Dilution (primary antibody)**	**Purpose**	**Secondary Antibody**	**Source**	**Dilution (secondary antibody)**
Cleaved Caspase 3	Cell Signalling technology (9661)	1:400	Apoptosis marker	Rabbit	Invitrogen 488 (A11034)	1:200
GFAP	BD Pharmingen (556329)	1:1000	An astrocyte and tanycyte sub-set marker	Mouse IgG	Invitrogen 599 (A11005)	1:200
GHRH	Abcam (ab48617)	1:200	Mature neuronal marker	Rabbit	Invitrogen 488 (A11034)	1:200
MAP2	Sigma-Aldrich (M9942)	1:1000	Neuronal differentiation marker	Mouse IgG	Invitrogen 599 (A11005)	1:200
Nestin	Abcam (ab6142)	1:500	NSPC and tanycyte marker	Mouse IgG	Invitrogen 599 (A11005)	1:200
NrCAM- 838	Martin Grumet laboratory	1:1200	Shown Tanycyte marker	Rabbit	Invitrogen 488 (A11034)	1:200
NPY	Immunostar (22940)	1:1000	Mature neuronal marker	Rabbit	Invitrogen 488 (A11034)	1:200
PH3	Upstate (06-570)	1:1000	Proliferation marker	Rabbit	Invitrogen 488 (A11034)	1:200
RIP	DSHB (AB531796)	1:20	Oligodendrocyte marker	Rabbit	Invitrogen 488 (A11034)	1:200
Six3	Placzek laboratory	1:5,000	NSPC marker	Rabbit	Invitrogen 488 (A11034)	1:200
Sox2	Abcam (ab97959)	1:200	NSPC marker	Rabbit	Invitrogen 488 (A11034)	1:200
TH	Millipore (6A2907)	1:1000	DA neuronal population marker	Rabbit	Invitrogen 488 (A11034)	1:200
Tuj1	Covenance (MMS-435P)	1:1000	Neuronal differentiation marker	Mouse IgG	Invitrogen 599 (A11005)	1:200

4.2 Electrospinning

Polymer was dissolved in solvent and stirred using magnetic follower (Fisher 12379507) until a uniform solution was produced (<3 hours) at room temperature. The solution was then placed in a syringe and pumped out through a charged needle which in turn charges the polymer. The polymer was then attracted to an earthed collector (wrapped in foil to collect the sample) forming fibres.

During the project, three different electrospinning rig systems were utilised. Firstly a custom rig (Figure 4.2 A) which includes using a Harvard apparatus PHD 2000 infuser/withdraw, with a 1 ml plastic syringe (BD plastipak) with a metallic needle (adhere). Secondly an IME rig (not shown) in collaboration with The Electrospinning Company, this rig system had temperature and humidity control which the two other rigs did not. Finally a Bioinicia rig purchased for The Dental School, Figure 4.2 B.

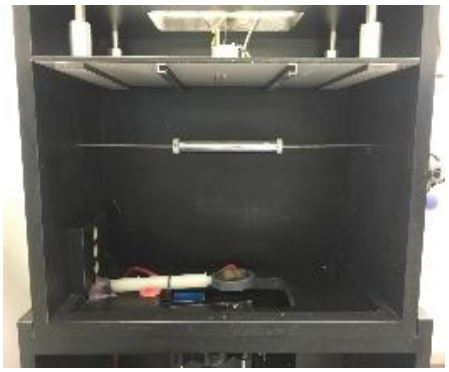

Figure 4.2 B: The original custom rig.

Figure 4.2 B: The Bioinicia rig.

4.2.1 Materials

Table 4.2.1 A lists the main materials utilised in the manufacture of scaffolds.

Table 4.2.1 B: Table of polymer and solvents utilised in the manufacture of electrospun scaffolds. Including source and product number.

Item name	**Acronym**	**Source**	**Product number**
Polycaprolactone	PCL	Sigma/Corbion	440744/ PURASORB® PC12
Dichloromethane	DCM	Fisher scientific	D/1856/17
Dimethylformamide	DMF	Fisher scientific	D/3840/17

Hexafluroisopropanol	HFIP	Sigma-aldrich/ apolloscientific	105228/29055998
Chloroform	$CHCl_3$	Sigma	372978

4.2.2 Sigma PCL in DCM/DMF

Polycaprolactone (PCL), Sigmaaldrich average Mw 80,000, (10 wt%) was dissolved in a solvent mixture of dichloromethane (DCM 92.66 wt% Fisher scientific) and dimethylformamide (DMF 7.34 wt% Fisher scientific). The solution was electrospun, utilising a custom electrospinning rig (Figure 4.2 A) onto a flat collector (stainless steel) to produce plain scaffold containing randomly orientated fibres.

Custom stainless steel (316L) templates, as shown in Figure 4.2.2 A, (made by selective laser melting (SLM)), with thanks to Alfred Sidambe, University of Sheffield, were attached to the flat collector by carbon tabs (Agar scientific) to spin scaffolds with different micro-features introduced into the scaffold.

All scaffolds were spun at an infuse rate of 2.5 at voltage 17 kV using a total of 2 ml of the solution per scaffold at a distance of 21.5 cm.

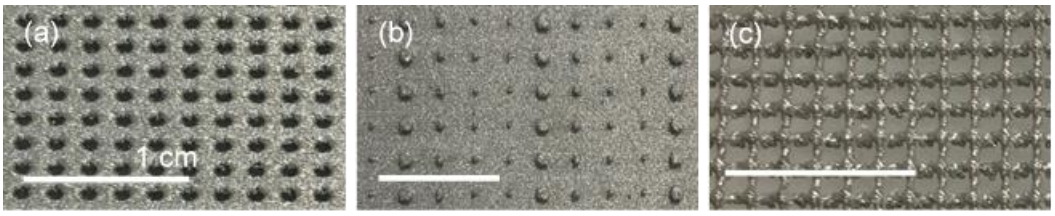

Figure 4.2.2 A: Scaffold templates. Stainless steel 316L templates (made using selective laser melting (SLM)) were utilised to generate 3D microenvironments within the electrospun scaffold (a) template 1, (b) template 2 and (c) template 3. Images of Scaffolds 1-3 are shown in Figure 6.1 B and C. Templates were made on a Renishaw SLM 125 machine by computer aided design (CAD) software (Solidworks) at the following parameters laser power 200W, speed 480mm/s, point distance 50 µm and an exposure time of 70 µs.

4.2.3 Microfeature metrology

For scaffolds 1-3, three were made of each type with two samples taken for the analysis of microfeature diameter on each scaffold, Figure 4.2.3 A.

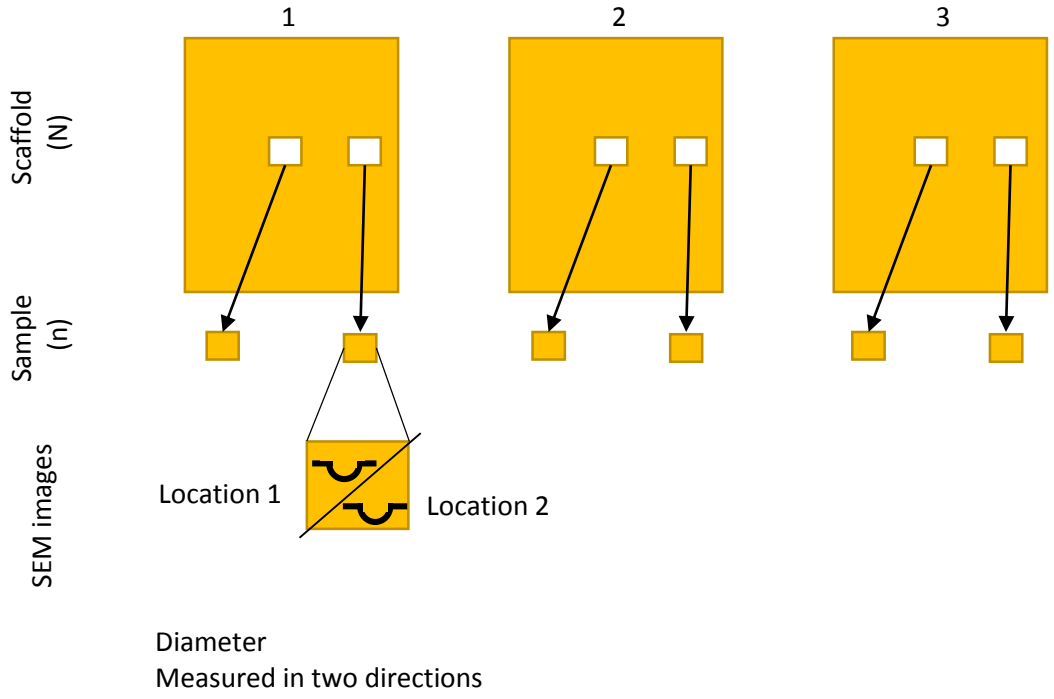

Figure 4.2.3 A: Schematic of the source of data for scaffold analysis for scaffolds 1-3 microfeature diameter.

Scanning Electron microscopy (SEM) images were taken at a magnification so that each feature filled the majority of the screen. Scaffold 1 was imaged at a magnification of X100, scaffold 2 at X25 or X50 and scaffold 3 at X50. For each scaffold type twelve microfeatures were analysed, four from each scaffold. The diameter of each microfeature was measured in two directions, as depicted in Figure 4.2.3 Figure 4.2.3 B. Statistical analysis was undertaken to identify whether the A and B lengths were significantly different using a paired t-test as it was comparing data from the same images. Analysis of the diameter between different scaffolds was done with Krustal-Wallis with Dunn's multiple comparison as the data did not show Gaussian (normal) distribution (did not pass D'Agostino & Pearson omnibus normality test).

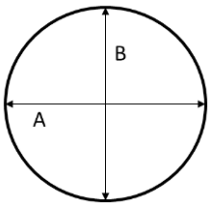

Figure 4.2.3 B: The method to measure the diameter of a microfeature. Two measurements were taken the second at a 90° angle to the first. Length A is the vertical measurement while B is the horizontal measurement.

4.3 Scaffold fibre diameter and orientation analysis

Scaffolds were characterised in terms of fibre diameter and alignment by SEM images. Figure 4.3 A provides an overview of the different stages of developing this method. There were two attempts made at data collection and the diameter was analysed by these two methods. Whereas for the analysis of alignment there were two post data collection analysis methods used in the first attempt and three separate post-collection analysis providing a total of five methods for alignment analysis.

4.3.1 Scanning Electron Microscopy

Scaffolds were imaged on a scanning electron microscope (SEM) Phillips X-L 20 BMS, with thanks to Chris Hill, with the settings working distance (WD)=9.8-10.6, Spot size=3.0 and KD=15. Then images were taken on an FEI Inspect F50, Department of Materials Science and Engineering, with thanks to the Sorby Centre, with the setting WD=10.2-11.2, Spot size=3.0 and KD=15. Images were taken at a range of magnifications described in the following sections in order to characterised fibre diameter and alignment.

First approach

Diameter and alignment on Random, Scaffold 1, Scaffold 2 larger microfeature, Scaffold 3
N=1; 1 cut out (middle); 2 locations (e.g. microenvironments) imaged per cut out;

Diameter

- Using a grid 500µm^2
- 12 squares all fibres analysed

Alignment

- Using a grid 2,000µm^2
- 3 squares all fibres analysed from entry into the square to the exit
- For each image the median value was taken away from all values to produce the angular distribution
- Converted to positive, by formula, and plotted

Second approach

Diameter on Random, Scaffold 1, Scaffold 2 all microfeatures, Scaffold 3; Alignment on Scaffold 2 larger microfeature
N=3; 2 cut outs (middle and right side); 2 locations (e.g. microenvironments) imaged per cut out;

Diameter

- Using a grid 500µm^2
- Central squares chosen
- 10 fibres analysed

Alignment

- Using a grid 2,000µm^2
- Central line used to measure the direction of 30 fibre to the right
- There was three attempts of different post analysis to produce the angular distribution (Figure 4.3.3 C)

1. Converted to positive, by formula, average value taken away from others
2. Values +90, mode taken away from all other values
3. Values +90, median taken away from all other values

Figure 4.3 A: An overview of the approaches to analyse scaffolds for fibre diameter and alignment. Including scaffold types utilised within each analysis. Further details on the analysis done for alignment in the second attempts is shown in Figure 4.3.3 C.

4.3.2 First approach

Initial analysis was undertaken on random scaffold and scaffolds 1-3, all made on the original rig system. The analysis was undertaken at N=1 and from each scaffold one sample was taken from the centre for analysis, n=1 (Figure 4.3.2 A).

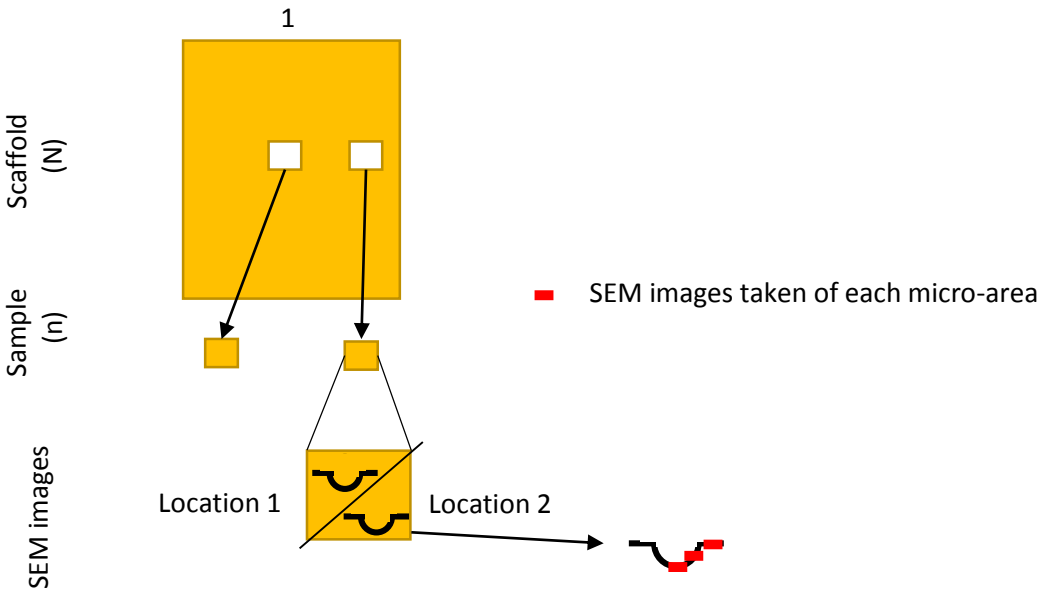

Figure 4.3.2 A: Schematic of the source of data for scaffold analysis for first approach.

The samples were placed on SEM stubs (Agar scientific) and gold coated for imaging with SEM. For each sample two locations were imaged meaning for scaffolds 1-3 there were two microenvironments analysed. For the microenvironments there are different sites of interests which will be known as areas. There were three different areas (e.g. the bottom of the well) shown in Figure 4.3.2 B. Therefore for each microfeature analysed each site was imaged. The fibres diameter and alignment was analysed using SEM images at 800X magnification with 20µm scale bar for images of random scaffold, scaffold 1, 2 (the largest microfeature) and 3.

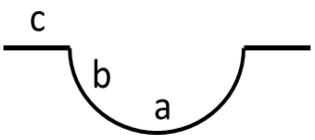

Figure 4.3.2 B: The three areas of the microenvironments analysed for the pores of scaffold 1-3. a=the bottom of the well, b=the side of the well and c= the top surface.

Fibre diameter

A grid was laid over each SEM image to provide squares with an area of 500 μm^2. The diameter of the fibres within the twelve defined squares were measured, producing per image on average 150-200 measurements. The fibre diameters were analysed by considering the frequency distribution on a histogram by inputting the data into Graphpad prism. Statistical analysis on these samples used the Krustal-Wallis with Dunn's multiple comparison, as the data did not show Gaussian (normal) distribution (did not pass D'Agostino & Pearson omnibus normality test).

Fibre orientation

A grid was laid over each SEM image providing squares with an area of 2,000 μm^2. The orientation of the fibres within three defined squares was measured, producing measurements on average of around 60 per SEM image. The median of the fibre alignments was calculated and then taken away from all other angles to provide the angular distribution from the median value. These values were then converted to their positive counter angle by the formula =IF(angle<0, 360+angle, angle). The data of both data sets (where the median value was taken away and when all values were converted to their positive counter angles) was analysed by Graphpad prism where statistical analysis was undertaken using the Kruskal-Wallis test with Dunn's multiple comparison, as the data did not show normal distribution (did not pass D'Agostino & Pearson omnibus normality test).

4.3.3 Second approach

For the second approach the scaffolds were characterised in triplicate, using scaffolds all made using the original rig. The scaffolds analysed in 4.3.2 First approach were also used in this analysis but were re-imaged by SEM following this method. For each scaffold produced two samples were taken, one from the middle and one from the right edge (Figure 4.3.3 A). Images

were taken at two locations on each sample meaning for each scaffold produced four locations were analysed for each microenvironment area. The images were analysed using Image J for fibre diameter and fibre alignment and all images were taken at a magnification of 800 X with a scale bar of 20 µm.

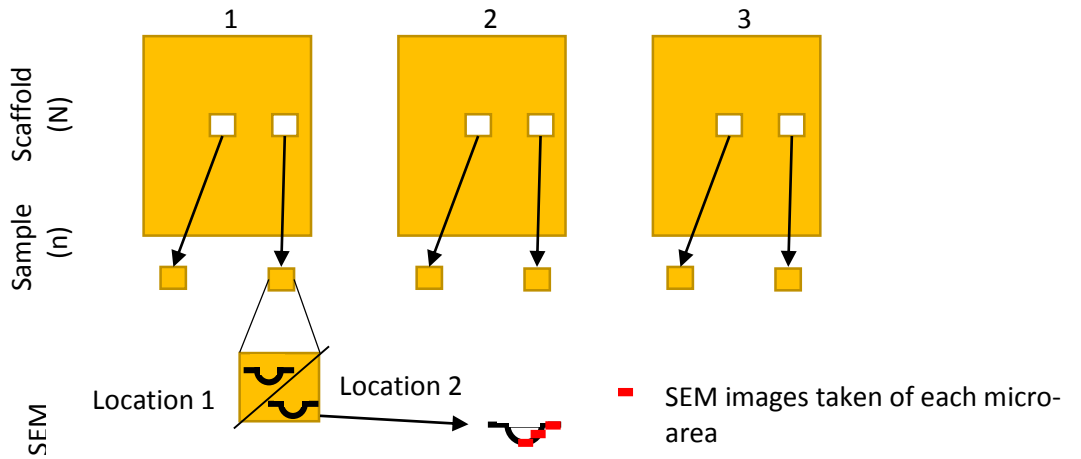

Diameter
10 fibres in a defined square measured
Alignment
30 fibres in a defined square measured
Four different methods
Final method: add 90° to each value, calculate the median and then removing this from each value

Figure 4.3.3 A: Schematic of the source of data for scaffold analysis for the second approach. Three scaffolds made and from each two samples taken from each for SEM imaging. On each sample two microfeatures were imaged.

Fibre diameter

The images taken, as described in 4.3.3 Second approach, were analysed for the average fibre diameters within the sites of the microenvironments of the different scaffolds. For each image ten fibres diameters were measured within a pre-defined square of 500 µm^2, where required the following squares were used to gain ten measurements. For each site (e.g. the bottom of the well) there were four images taken per scaffold, providing twelve images per site for analysis as there was three scaffolds. Data from images of the same scaffold type were then combined and imported into Graphpad Prism to produce a graph of the mean with standard deviation for each site of each scaffold. Statistical analysis was undertaken utilising the Krustal-Wallis with Dunn's multiple comparison test as the data did not show Gaussian distribution (did not pass D'Agostino & Pearson omnibus normality test).

Fibre orientation

For each area (bottom of the well, the side and the top surface) of the largest microfeature of scaffold 2 there were four images taken on each scaffold produced, of which there were three, Figure 4.3.3 B. This provided a total of 36 analysed images.

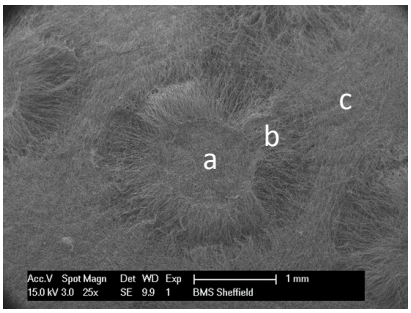

Figure 4.3.3 B: Scaffold 2 largest microfeature. An illustration of the change in fibre orientation over areas a, b and c.

The direction of 30 fibres from a vertical line (Figure 4.3.3 C) were measured and produced angles in the ranges of 0 - 90° and 0 - -90°. Figure 4.3.3 C displays the three methods which were attempted.

The third method (Figure 4.3.3 C) was the chosen method for this projects characterisation and was as follows. 90 was added to all values was utilised to ensure all angels were positive, (effectively rotating the angles by 90°). The median value of the angles of each image was taken away from all angles of that image to produce the distribution of angles for the image. The distribution from the median angle of an image was combined with other images data of the same site of the same scaffold type. The data was imported into Graphpad Prism where histograms were produced of the frequency distribution. Statistical analysis was undertaken on the results using Kruskal-Wallis test with Dunn's multiple comparisons as the data was not a Gaussian distribution (did not pass D'Agostino & Pearson omnibus normality test).

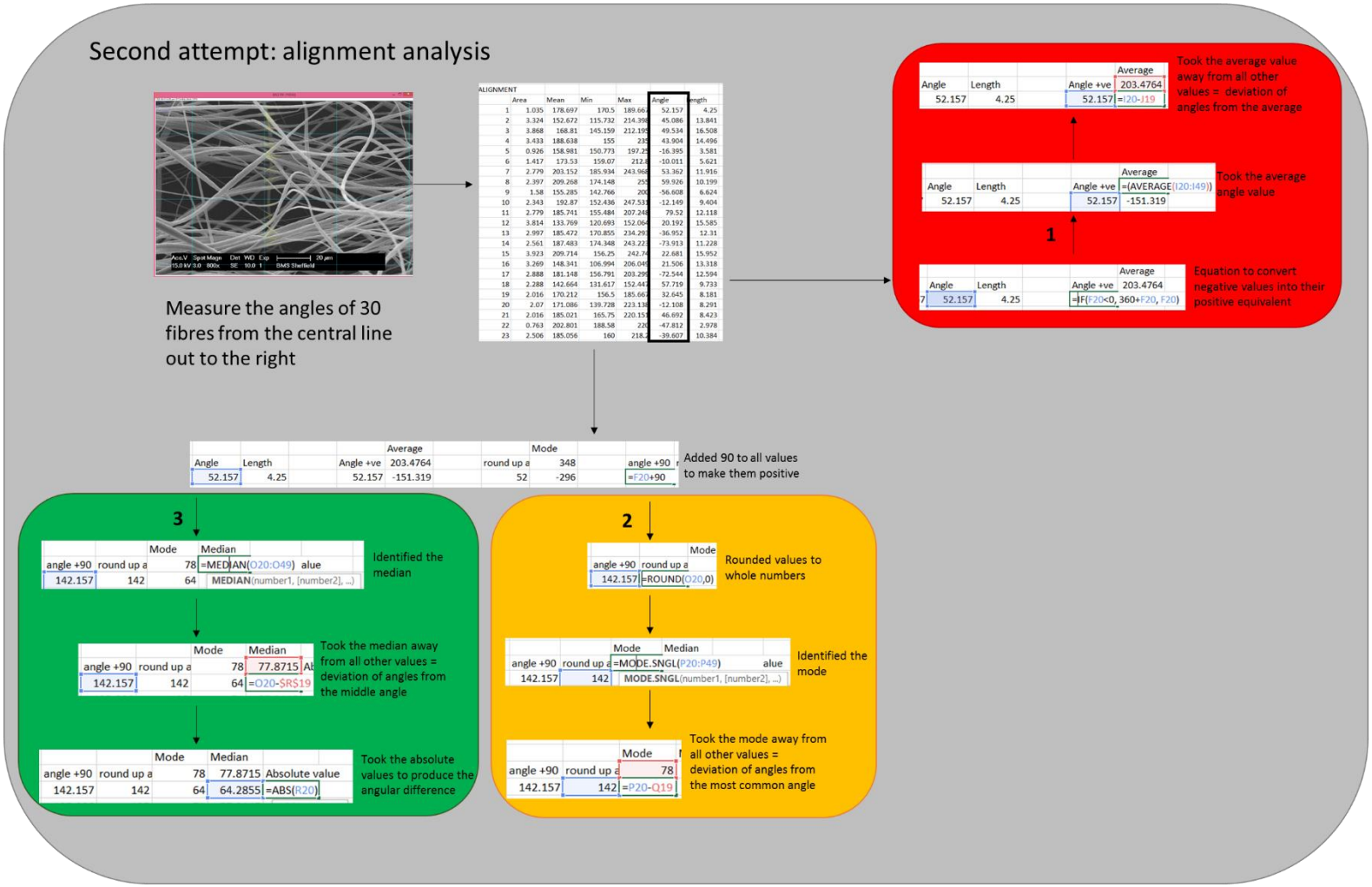

Figure 4.3.3 C: The four methods to generate a method to analysis fibre alignment. All analysis begin with counting 30 fibres to the right from the central line. 1. In which a formula was used to convert negative angles to their positive counterpart. The average of these positive angles was then taken which was then taken away from all angles. 2 and 3. Both begin with the original values measured and the addition of 90 to convert them to positive values. 2. Rounded these values to whole numbers to be able to identify the mode which was then take away from all other values. 3. Identification of the median allowed for this to be taken away from all other values. The absolute values were then taken. Results are shown in Figure 6.3.2 C.

4.3.4 Phenom SEM: Software analysis

The Phenom Desktop Pro SEM from Phenom was utilised to image samples and the fibre analyse was done utilising the Fibremetric software. For scaffold 2 the largest microfeature images were taken of scaffold one from both samples (middle and side) and from a second scaffold imaging was done on one sample (middle) by the same method discussed in 4.3.3 Second approach. The images of the three sites were then analysed in which for each microenvironment, 200 fibres were analysed for their diameter and their orientation. Diameter values were placed in graph pad for statistical analysis and presented as mean with standard deviation. For alignment analysis the values were converted from radius to degrees then were then treated by the same post-data collection analysis as described in Figure 4.2.3 C.

This software was also available at The Electrospinning Company and so scaffolds produced there were analysed utilising this software. For details on this placement see Section 4.4.2 Comparative study of polymer source and solvent system.

4.4 Aligned scaffold optimisation

Initially aligned scaffold manufacture was attempted utilising a small rotating cylinder (stainless steel 16cm by 2cm) rotated by a dremel at an estimated speed of 2,000 rpm, Figure 4.2 A. When attempting to electrospin an aligned scaffold on this system, the small cylinder vibrated and the collectable sample size was small. Therefore a new large drum was manufactured (30cm by 6cm with thanks to the Medical School workshop University of Sheffield), with the aim to reduce these issues. Figure 4.4 A explains the optimisation process to produce aligned scaffold on the original rig system. The rig was unstable at 2,000 rpm, but stabilised at around 4,000-6,000 rpm. However when attempting to stop the rotation, manual assistance was required to slow down the drum which was considered a safety hazard and so this protocol could not be maintained.

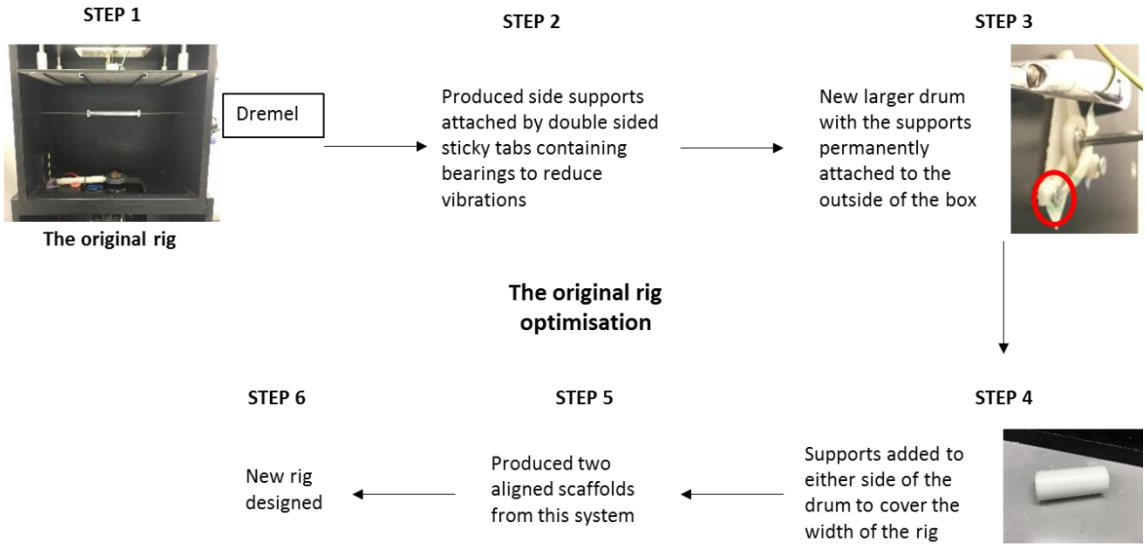

Figure 4.4 A: The optimisation process to produce aligned scaffold. Step 1 depicts the original rig in which the small drum was through a metallic rod which was through two holes in the side of the box of the rig and rotated by a dremel. Due to the vibrations from the spinning process two side supports containing bearings were manufactured (Step 2) and attached to the side of the box by sticky tabs. However, these were susceptible to falling off during the spinning process. Due to these issues, and the small sample sizes a new larger drum was manufactured, step 3 (medical workshop UoS) and the supports were attached permanently by screws to the outside of the box. As there was still vibrations, side supports were produced to cover the width of the rig as shown in Step 4. Two scaffolds were produced on this system (Step 5, Figure 6.4.1 A), however an updated rig was designed (Step 6).

4.4.1 The updated electrospinning rig

Figure 4.4.1 A: Updated custom rig. The drum was permanently attached with space below to slide a flat plate below to spin onto.

An updated version of the rig, was installed (known as the updated electrospinning rig). The updates included permanently attaching the large cylinder to the rig in order to remove the issue of vibrations, Figure 4.4.1 A. A motor was also installed to provide more accurate speed control. The distance control was improved to provide free movement instead of increments. The aim of the new rig was to improve the safety and reliability of the aligned scaffold production. Alignment production was attempted at volumes 1, 2 and 3 ml each at the rotation of 1,000 and 2,000 rpm with 17kv, 2.5 infuse rate and at a distance of 24.3cm.

4.4.2 Comparative study of polymer source and solvent system at The Electrospinning Company

Scaffolds were manufactured with either Sigma or Corbion polymer in one of the three solvents DCM/DMF, HFIP or chloroform while on placement at The Electrospinning Company. Scaffolds were manufactured three times utilising parameters in Table 4.4.2 A. Two SEM samples were taken from each scaffold and imaged by Pheomworld SEM. Fibre diameter was analysed using Fibremetricsoftware measuring 200 fibres on each SEM image. Orientation was viewed via SEM images. Two sheets of scaffolds, for both random and aligned, were manufactured with Corbion in HFIP with 3ml of solution each and for aligned scaffold 0.1 ml at 100 rpm was spun at the end to improve scaffold durability.

Table 4.4.2 A: Parameters utilised to optimise the production of aligned scaffold.

Parameters	
Voltage	+16 and -4 kV
Distance	23 cm (20 cm for original polymer comparison)

Infuse rate	1.6 ml/H (2.5 ml/H for original polymer comparison)
Rotation	Random- 100 and Aligned- 2500 rpm
Drum diameter	9 cm
Needle diameter	22.6 mm
Gas shield (for chloroform)	50 ml/min
Motion (for samples manufactured for cell culture)	10 mm/S

4.4.3 Corbion PCL scaffold optimisation at The Dental School

Once Corbion PCL was identified as the superior polymer, method parameters were optimised on the commercial electrospinning rig (Bioinicia, Spain) to manufacture these scaffolds. Initially chloroform was utilised as the solvent.

Table 4.4.3 A: Parameters for samples in Figure 6.6.1 A. Including type of scaffold, collections method, distance, rotation speed if relevant, voltage, infuse rate and volume of solvent used. For aligned samples at the end of the manufacture the drum is reduced to 200 rpm to back the sample with more randomly orientated fibres to provide structural stability to the sample, shown in Figure 6.6.1 B.

Sample	**Random/ aligned**	**Drum/Flat plate**	**Distance (cm)**	**Rotation (rpm)**	**Voltage (kV)**	**Infuse rate (ml/H)**	**Volume (ml)**
1	Aligned	Drum	22	2000->200	22.2-27.1	2-2.5	1.6
2	Random	Drum	20	200	26.2-27.8	2	0.4
3	Aligned	Drum	22	2000->200	22.5-29.8	2	0.6
4	Random	Drum	22	200	27-29	2	0.6
5	Random	Flat plate	22	N/A	24-26.9	2	0.4
6	Random	Flat plate	26	N/A	24.5-27	2	1
7	Random	Drum	22	200	24.8-27.6	2	1
8	Aligned	Drum	22	2000->200	24-27	2	1.2

A range of parameters were analysed until the optimal method was produced (Table 4.4.3 A). Three scaffold were manufactured, Table 4.4.3 B, for these settings to analyse the fibre diameter and orientation, as method in 4.3.3 second approach.

Table 4.4.3 B: Parameters utilised to manufacture random and aligned scaffold with PC12 15 wt% in chloroform.

	Drum/Flat plate	Distance (cm)	Rotation (rpm)	Voltage (kV)	Infuse rate (ml/H)	Volume (ml)
Random	Flat plate	26	N/A	26-28	2	1
Aligned	Drum	22	2000->200	20	2	1

Random samples were then manufactured at parameters shown in Table 4.4.3 C.

Table 4.4.3 C: Parameters utilised to manufacture random scaffold with PC12 15 wt% in chloroform.

Sample	Random /aligned	Drum/ Flat plate	Distance (cm)	Rotation (rpm)	Voltage (kV)	Infuse rate (ml/H)	Volume (ml)
1	Random	Flat plate	28.5	N/A	26.7	1	0.8
2	Random	Flat plate	28.5	N/A	28.7	1.8	0.2

4.4.4 Re-optimisation of Corbion PCL scaffolds

The previously optimised method (Table 4.4.3 A) failed due to a relocation of the rig and therefore the method required re-optimising which included comparing 12 and 15 wt% and solvents HFIP and chloroform. This coincided with the start of an undergraduate summer project and therefore this section of results was undertaken by Nicholas Cooper under my supervision. All samples within this section were spun with a voltage of 25.5 kV ± 1.5 kV and an infuse rate of 2 ml/H. First aligned scaffold manufacture was focused on and samples were spun at two distances 10 and 14 cm. Random samples were then manufactured comparing distances 22, 24, 26 and 28 cm. Final methods utilised were 10 and 24 cm for aligned and random respectively with 15 wt% HFIP. Scaffold analysis was done as described in as method in 4.3.3 Second approach.

4.3.6 Rheology

The solutions utilised within electrospinning were tested for their rheological properties on a rheometer (Anton Parr Physica MCR 301) by a shear sweep test using a CP-50 attachment at 20°C, Figure 4.3.6 A. The test uses a shear rate of 1-100 seconds with speeds increasing from 0.167-16.7 rotations/minute, recording the sheer stress in Pa. The solutions were made on three separate occasions, N=3, and each solution was measured in triplicate, n=3. Data was input into graph pad and presented on a log10 scale.

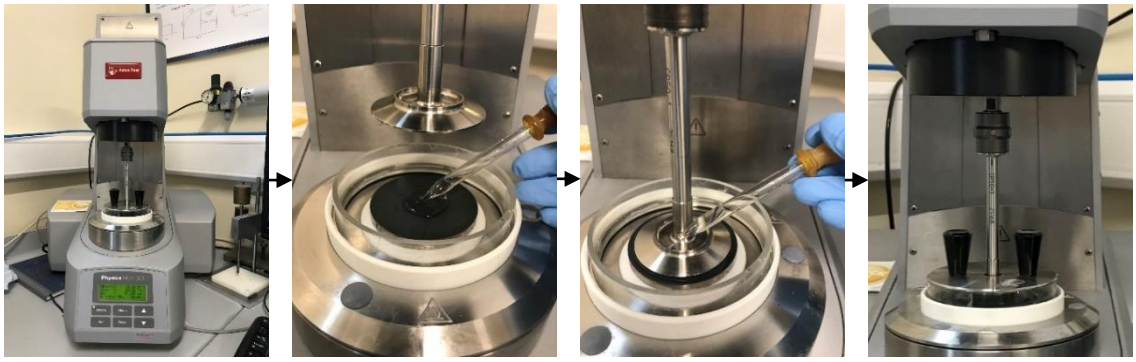

Rheometer | Add solution to test plate | Add solvent to solvent trap | Add solvent shield to enclose test area

Figure 4.3.6 A: Rheometer set up to test solution viscosity. A Rheometer from Anton Parr the Physica MCR 301 was utilised. The test solution was added (~1ml) to the test plate, at 20℃. The solution utilised within the solution was added to the solvent trap to stop the solution drying out. The solvent shield was added to enclose the test area.

4.3.7 Gel permeation chromatography

Gel permeation chromatography 0.5% w/w copolymer solutions were prepared in Tetrahydrofuran (THF) using toluene (10 µL per mL) as the flow rate marker. GPC measurements were conducted using a THF eluent containing 2.0% v/v triethylamine and 0.05% w/v butylhydroxytoluene (BHT) at a 30 °C, flow rate of 1.0 mL min^{-1}. The GPC set-up comprised of an Agilent 1260 Infinity series degasser and pump, two Agilent PLgel-MIXED C columns and a RI detector. With a series of ten near-monodisperse poly(methyl methacrylate) standards. With thanks to Dr Sebastian Spain, University of Sheffield, for running these samples.

4.3.8 Tensile testing

A uniaxial tensile tester (Bose) was used to perform a stretch experiment on scaffold samples to identify the stiffness of the sample, Figure 4.3.8 A. Samples were cut with a length of 15-20 mm that was standardised to an 8mm length between the grips and a width between 5.5-6.8 mm. The measurements of the width for each sample along with the individual thickness of the samples measured by a micrometre were used to standardise each samples results. For each scaffold from The Electrospinning Company (PC12 in HFIP), six samples were cut, n=6, in one direction and then six further samples were cut at a 90° angle, n=6. For the scaffolds from The Electrospinning Company two scaffolds were tested, N=2. For the final optimised scaffolds manufactured at The Dental School, scaffolds (PC12 in HFIP) were made on three separate occasions, N=3, n=3 samples cut in both directions.

4.3.9 General statistics

Specific statistical test for certain data sets are specified within their section. Graphs and tables of data indicate statistical differences alongside stars, **** P<0.0001, *** P=0.0002, ** P=0.0021, * P=0.0332. Data sets tested for normal distributions by D'Agostino & Pearson normality test.

Chapter 5: Tanycytes, a hypothalamic NSPC population, show variable self-renewal and differentiation under standard *ex vivo* culture conditions

In this chapter I set out to address the following objectives:

- to identify the central hypothalamus through coronal sectioning of the mouse brain labelling key cell populations by immunohistochemistry, investigating expression of NrCAM;
- to isolate and culture hypothalamic tanycytes as neurospheres;
- to confirm that hypothalamic tanycytes self-renew and differentiate *ex vivo;*
- to investigate the established *ex vivo* free-floating culture method with non-differentiation conditions for tanycyte derived neurospheres, for its impact on the self-renewal and differentiation levels of this population by immunohistochemistry;
- to investigate how passaging and culturing under non-differentiation conditions impacts on differentiation.

5.1 Characterisation of cell types in the adult hypothalamus

Previous studies have shown that central regions (also known as the tuberal region) of the adult hypothalamus harbours tanycytes, oligodendrocytes, astrocytes and mature neuronal populations. Each population is discussed in detail in Section 2.2.1. I first confirmed that I could identify the central hypothalamus and each class of cells within it.

5.1.1 Standard Immunohistochemistry is not optimal for detecting cell populations within the hypothalamus

Firstly I demonstrated that I could recognise the central region of the hypothalamus after collecting coronal sections through the eight week adult hypothalamus and staining with DAPI to label nuclei. Figure 5.1.1 A shows a typical coronal section through the central hypothalamus; the third ventricle has a characteristic shape with the median eminence (ME) ventral to the ventricle. The ARC and VMN can be identified through their characteristically organised nuclei. The ARC resides ventrally and the VMN lies just dorsal to it. A nuclei-sparse zone separates the ARC and VMN.

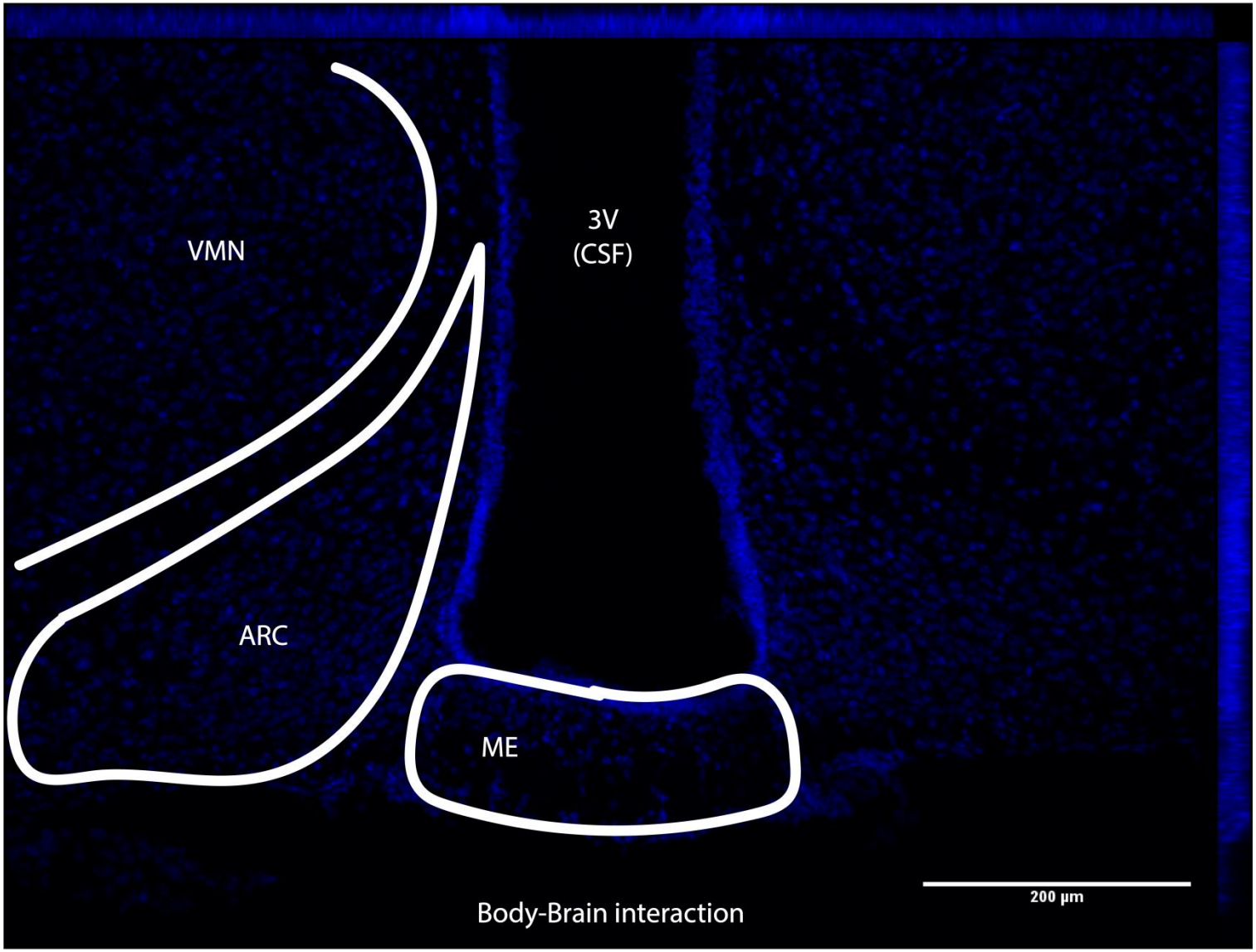

Figure 5.1.1 A: Hypothalamic nuclei around the third ventricle. Coronal section through the central hypothalamus. DAPI (blue) labels nuclei. Indicated is the third ventricle which contains CSF (cerebral spinal fluid) and two nuclei the Arcuate (ARC) and the Ventromedial (VMN). The ARC and VMN are mirror structures on both sides of the third ventricle. The Median eminence (ME) is a region of the brain lacking the blood-brain barrier to allow brain-body interactions. Scale bar 200 µm.

I then analysed a range of antibodies. Previous studies in the laboratory have shown that some antigens in the adult hypothalamus can be detected using standard immunohistochemical protocols, whereas Nestin requires an antigen-retrieval protocol [2]. I therefore compared the two methods.

Initially I used standard immunolabelling protocol, as described in 4.1.4 Sectioning in adult mouse brain. Six3 and Sox2 are two markers of NSPCs [147,148] and both can be detected in the central hypothalamus, Figure 5.1.1 B. Six3 is a transcription factor known to be involved in the induction and patterning of the developing hypothalamus, involved in particular in promoting proliferation and inducing Sonic hedgehog (Shh) expression [113,114]. Six3 labels cells lining the third ventricle. The bottom half of the third ventricle is composed of tanycytes, therefore Six3-positive cells are tanycytes. Positive cells are also detected within the ARC and VMN (as discussed in Section 2.2.1). Sox2, also known as sex determining region Y (SRY) box 2, is a transcription factor and is important for proliferation and differentiation and, like Six3, regulates Shh expression in the hypothalamus [112,113,149]. Sox2 is one of the four pluripotency markers that have been utilised to re-set differentiated cells into multipotent cells [150,151]. Sox2 is detected in low numbers of tanycytes, arranged in a 'salt and pepper' manner. Additionally, labelling is detected within the ARC and VMN nuclei. Some of this labelling appears to be non-specific as it is found outside of nuclei and in the ME. Non-specific labelling in the ME is most likely due to 'sticky' endothelial cells in this region [152]. Within Figure 5.1.1 B arrows indicate examples of positively labelled cells within the parenchyma for both Six3 and Sox2.

As previously discussed tanycytes can be sub-divided into five subsets (β1, β2, α1, dorsal α2 and ventral α2) depending on the projection of their process into the parenchyma [2]. Established tanycyte markers include Nestin and GFAP (glial fibrillary acidic protein). Nestin is a well-established NSPC marker and previous studies have described its expression in all subsets of radial glial tanycytes where it labels cell bodies and basal processes that extend into the parenchyma. Specifically Nestin labels intermediate filament protein [2,149]. GFAP is an

intermediate filament protein which labels astrocytes [120,149], dorsal α2-tanycytes and some α1-tanycytes [2]. However, I was unable to detect expression of either Nestin or GFAP, Figure 5.1.1 B. Thus, both Nestin and GFAP labelled sections were indistinguishable from control sections, which showed high levels of non-specific labelling in the ME.

NrCAM is a cell adhesion molecule (CAM) within the L1 family and is expressed within neural tissue, including the cerebellum, where it plays multiple roles in cell proliferation, differentiation and adhesion [153,154]. NrCAM labelled tanycyte cell bodies lining the ventricle wall and the long tanycyte processes. NrCAM labels β-tanycytes strongly and α-tanycytes weaker. NrCAM labelling within the hypothalamus has not previously been published. Unlike markers such as GFAP, Six3 and Sox2, NrCAM is specific to tanycytes.

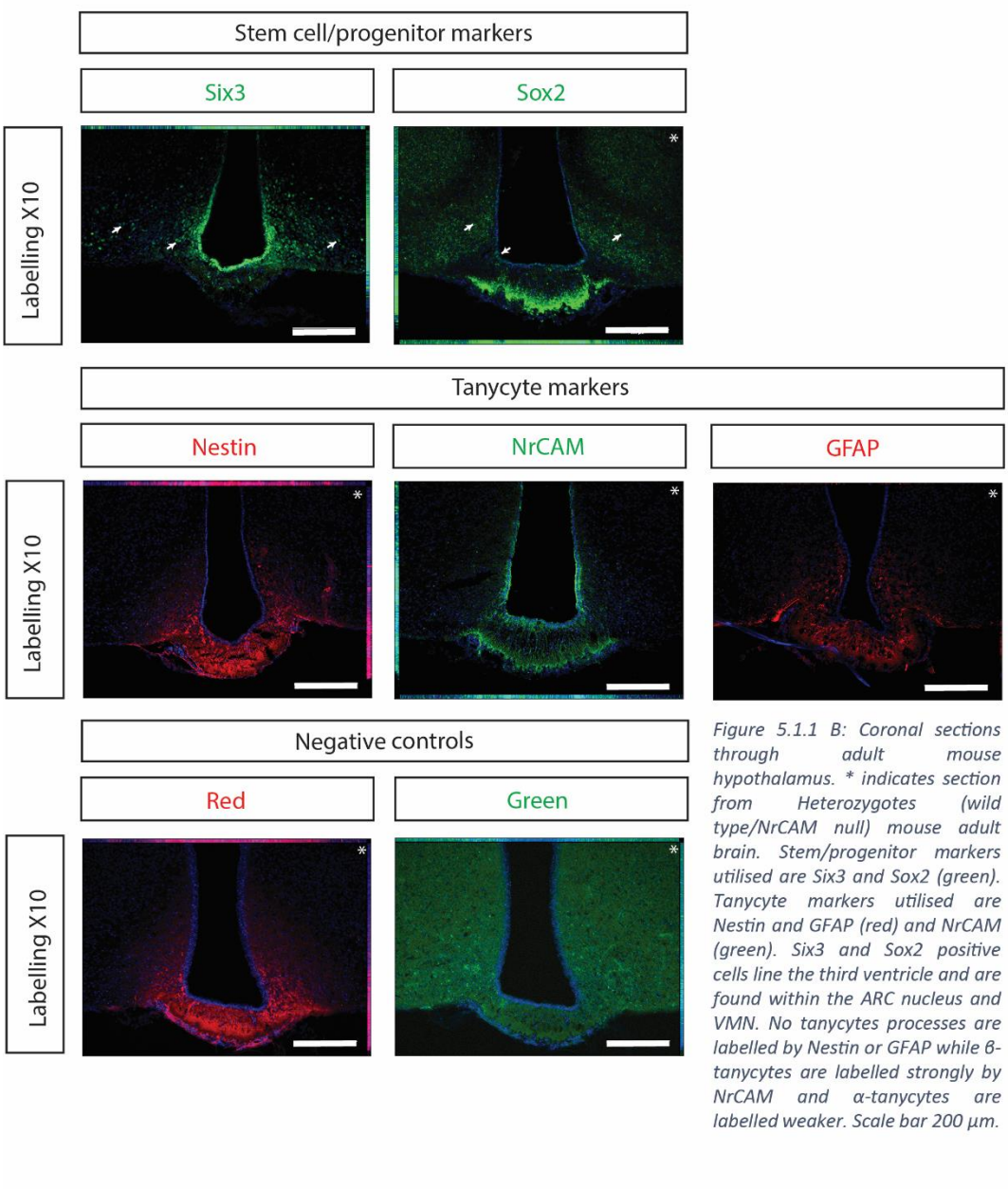

*Figure 5.1.1 B: Coronal sections through adult mouse hypothalamus. * indicates section from Heterozygotes (wild type/NrCAM null) mouse adult brain. Stem/progenitor markers utilised are Six3 and Sox2 (green). Tanycyte markers utilised are Nestin and GFAP (red) and NrCAM (green). Six3 and Sox2 positive cells line the third ventricle and are found within the ARC nucleus and VMN. No tanycytes processes are labelled by Nestin or GFAP while ß-tanycytes are labelled strongly by NrCAM and α-tanycytes are labelled weaker. Scale bar 200 µm.*

I next analysed an array of neuronal markers, Figure 5.1.1 C. Tuj1 (neuron-specific class III β-tubulin) is a marker of immature neurons, labelling dendrites [2,149,155]. Labelling of Tuj1 on adult coronal sections does not show any positive cells, perhaps not unexpected as previous research shows only low levels of neurogenesis within the unchallenged adult [2]. Microtubule-associated protein 2 (MAP2) is a neuronal differentiation marker that has low expression during the early stages of differentiation which then increases through the differentiation process [156]. It acts to assemble and stabilise microtubules and labels neuronal dendrites [157]. As expected, MAP2 labels cells in the ARC and VMN; in addition I consistently observed non-specific labelling around the ME. The ARC harbours an array of mature neuronal populations including those that express TH (tyrosine hydroxylase) known as dopaminergic neurons (DA). TH is a rate-limiting enzyme for dopamine production which acts as a neurotransmitter to inhibit prolactin secretion, promote milk synthesis and maternal behaviour [158]. Analysis of TH shows dopaminergic neurons within the ARC nucleus. Previous studies have also shown that the ARC harbours NPY (neuropeptide Y) and GHRH neurons [159]. NPY is a peptide expressed widely within the CNS including the hypothalamus where it is involved in feeding [113,116,158,159]; GHRH (growth hormone-releasing hormone) is a neuropeptide which stimulates the release of growth hormone [2,113]. However, I could not detect either NPY or GHRH neurons (not shown).

Finally I analysed markers of proliferation and oligodendrocytes. Phosphorylated histone H3 (PH3) is a mitotic marker that labels the nucleus [2] of cells in the late G2 phase/G2-M transition phase [149]. Low levels of proliferation have been reported within unchallenged mice, however I did not detect PH3+ cells. RIP antibody labels oligodendrocyte processes by labelling 2',3'-cyclic nucleotide 3-phosphodiesterase [2,160]. No RIP was detected, and high levels of non-specific labelling were observed.

In summary, these experiments suggest that standard conditions for immunolabelling were sub-optimal. I could not detect many markers, known to be expressed, and I observed consistent non-specific labelling within the ME.

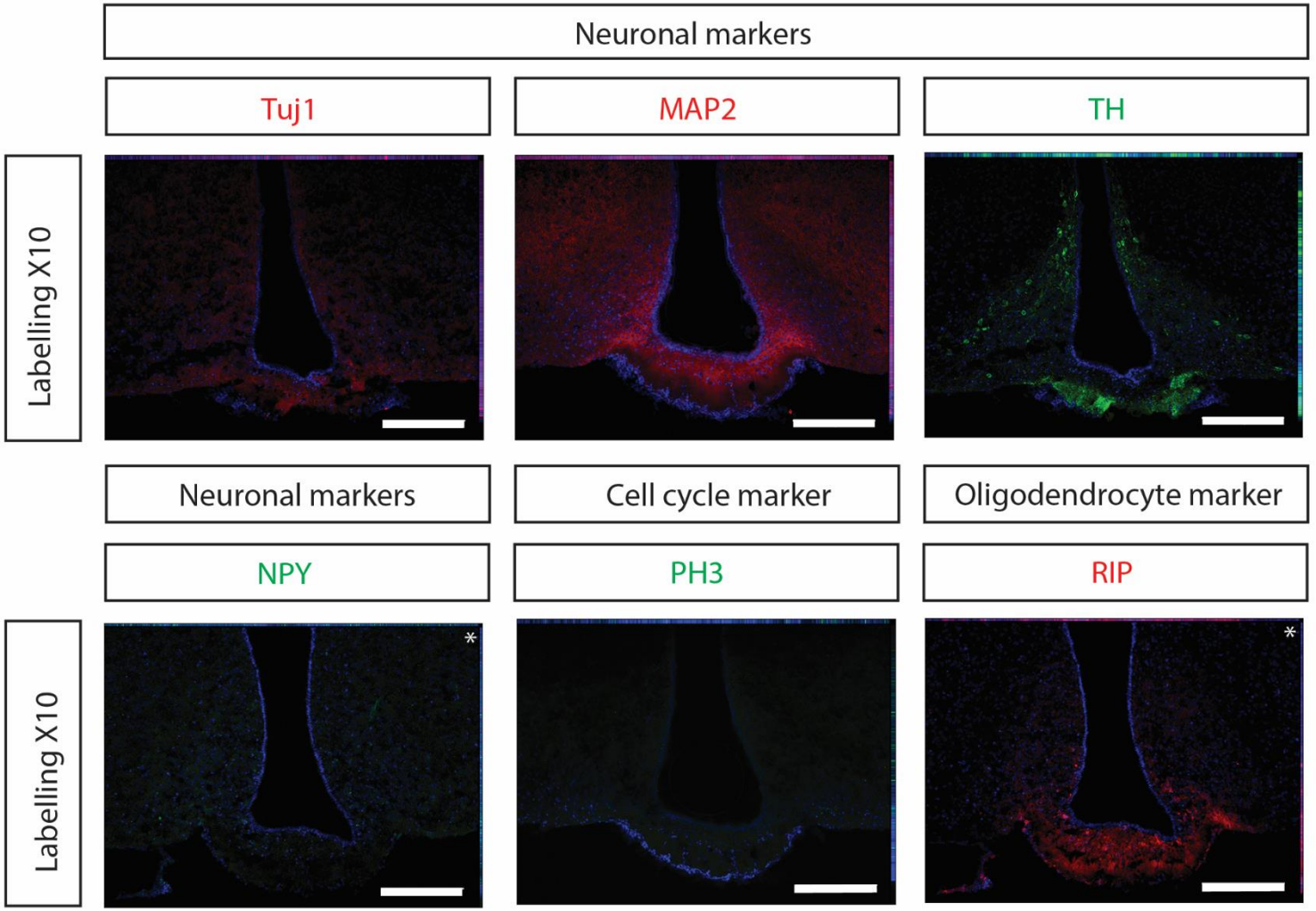

*Figure 5.1.1 C: Coronal sections through adult mouse hypothalamus. * indicates section from Heterozygotes (wild type/NrCAM null) mouse adult brain. Neuronal markers utilised are Tuj1, MAP2 (red), TH, NPY and GHRH (green). PH3 (green) is a cell cycle maker and RIP (red) is an oligodendrocyte marker. DAPI (blue) labels nuclei. There is no labelling of Tuj1 or NPY within the ARC or VMN. MAP2 positive cells are shown within the ARC and VMN along with strong non-specific labelling within the ME. TH identifies the dopaminergic neurons of the ARC nucleus. A lack of PH3 positive cells shows an absence of proliferation. RIP does not identify any oligodendrocytes surrounding the third ventricle. Control images in Figure 5.1.1 B. Scale bar 200 µm.*

5.1.2 Antigen-retrieval optimises immunolabelling in the adult hypothalamus

I next performed antigen retrieval (AR) (described in 4.1.4 Sectioning) which is a process of treating tissue to remove cross-linking bonds that form during fixation and that could potentially block antibody access to its epitope. Indeed, a previous study in the laboratory used antigen retrieval by heat-mediated treatment with citric buffer to optimally detect Nestin [2]. As shown in Figure 5.1.2 A, antigen retrieval greatly improves detection of Nestin. In the experiment shown, I barely detected Nestin in untreated samples and there was high background in the ME. By contrast after antigen retrieval, Nestin can be clearly detected on tanycyte processes, arrows indicated positive processes. As previously noted [2] Nestin labelling was highest on β-tanycytes lining the ME and weaker in α-tanycytes.

Following the improvement in Nestin labelling I investigated the impact of antigen retrieval on other markers previous utilised. As with the standard protocol, Six3 and Sox2 were detected on tanycytes that line the third ventricle and on cells within the ARC and VMN, Figure 5.1.2 B. Six3 strongly labels β-tanycytes and weakly labels some α-tanycytes, while Sox2 labels all tanycyte subsets, but in a salt and pepper manner. AR successfully removed the non-specific labelling in the ME and VMN.

Antigen retrieval likewise improved detection of NrCAM and GFAP, Figure 5.1.2 B. As with standard immunolabelling, NrCAM was detected strongly in β-tanycytes and more weakly in α-tanycytes. GFAP was now detected in alpha-tanycytes, particularly in dorsal α2-tanycytes and α1-tanycytes, as previously reported [2]. Additionally, within the parenchyma, GFAP+ astrocytes can be identified by their morphology (arrows indicate). Strong GFAP labelling can also be seen at the base of the brain, with the exception of the ME itself. This labelling is likely to be on astrocytes within the BBB. The ME is one of the regions of the brain that does not possess a BBB: here, molecules can be transported in and out of the brain [116].

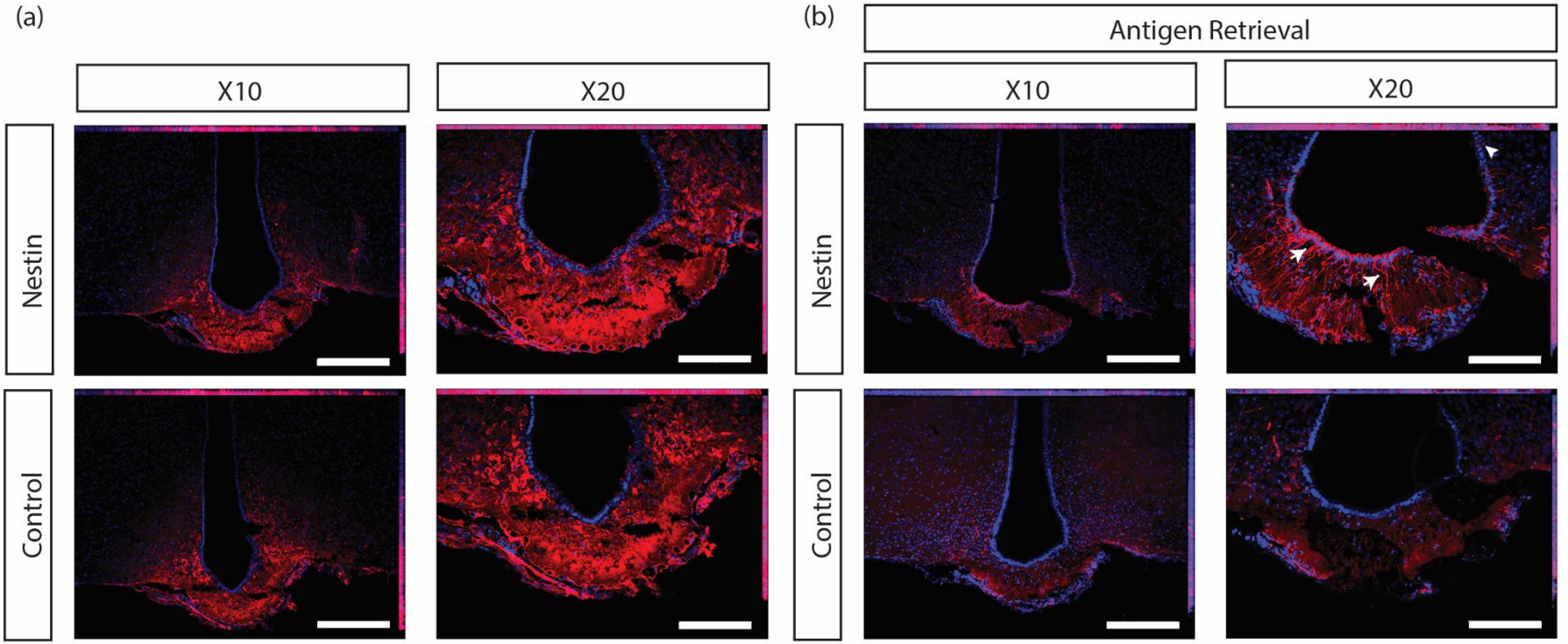

Figure 5.1.2 A: Coronal sections through adult mouse hypothalamus comparing with and without antigen retrieval. Nestin (red) and DAPI (blue) labels nuclei. (a) shows the same non-specific labelling in both Nestin labelled sections and secondary antibody control sections. While (b) with antigen retrieval with Nestin labelling show processes feeding from the third ventricle which are not present with the control section. Arrows indicate β-tanycytes and arrow heads indicate α-tanycytes, which were labelled less intensely with Nestin. Scale bar x10 images 200 µm and x20 images 100 µm.

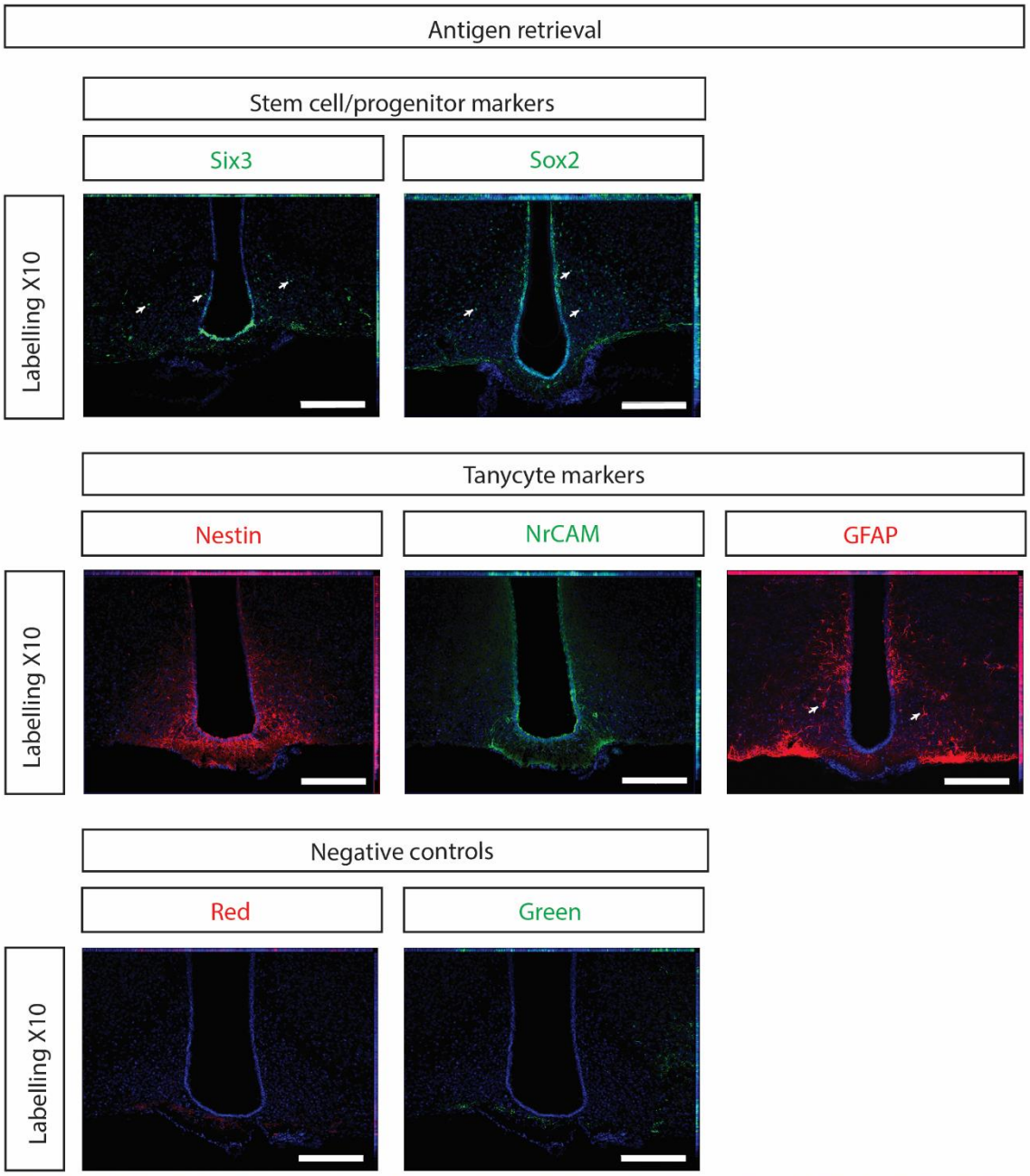

Figure 5.1.2 B: Coronal sections through adult mouse hypothalamus with antigen retrieval. Stem/progenitor markers utilised are Six3 and Sox2 (green). Tanycyte markers utilised are Nestin and GFAP (red) and NrCAM (green). DAPI (blue) labels nuclei. Nestin labels all sub-sets of tanycytes while NrCAM labels strongly in β-tanycytes and weaker in α-tanycytes. GFAP labels the subset dorsal α2 tanycytes and some α1-tanycytes. GFAP also labels astrocytes. Six3, Sox2 and GFAP+ astrocytes are indicated by arrows. N=3 for Six3 and Sox2. N=3 for Nestin and N=4 NrCAM and GFAP. Scale bar 200 µm.

Even after antigen retrieval, I detected no labelling with PH3, Figure 5.1.2 C. Under normal conditions minimal levels of proliferation have been reported in the adult hypothalamus [2,124] and PH3 labels cells in a very narrow window of the cell cycle, potentially explaining this result. However, after antigen-retrieval I detected labelling of RIP on oligodendrocyte cells present within the ARC and VMN. Consistently, antigen retrieval reduced the non-specific background labelling.

Antigen retrieval similarly improved detection of neuron-specific antibody labelling. Low numbers of weakly-positive Tuj1 cells were observed, potentially indicative of low levels of neurogenesis in the unchallenged adult [2]. MAP2 labelled many neurons within the parenchyma without the previously noted non-specific binding. The mature neuronal markers, TH, NPY and GHRH were all now detected (Figure 5.1.2 C). TH was detected in neurons within dorsal parts of the ARC, and scattered neurons within the parenchyma in more dorsal regions (higher power view shown in Figure 5.1.2 D). GHRH was clearly detected in the ARC and VMN while NPY was clearly detected in the ARC.

In summary, antigen retrieval significantly improves immunolabelling of almost every marker analysed. It enables the detection of key cell populations and reduces non-specific background to a minimum.

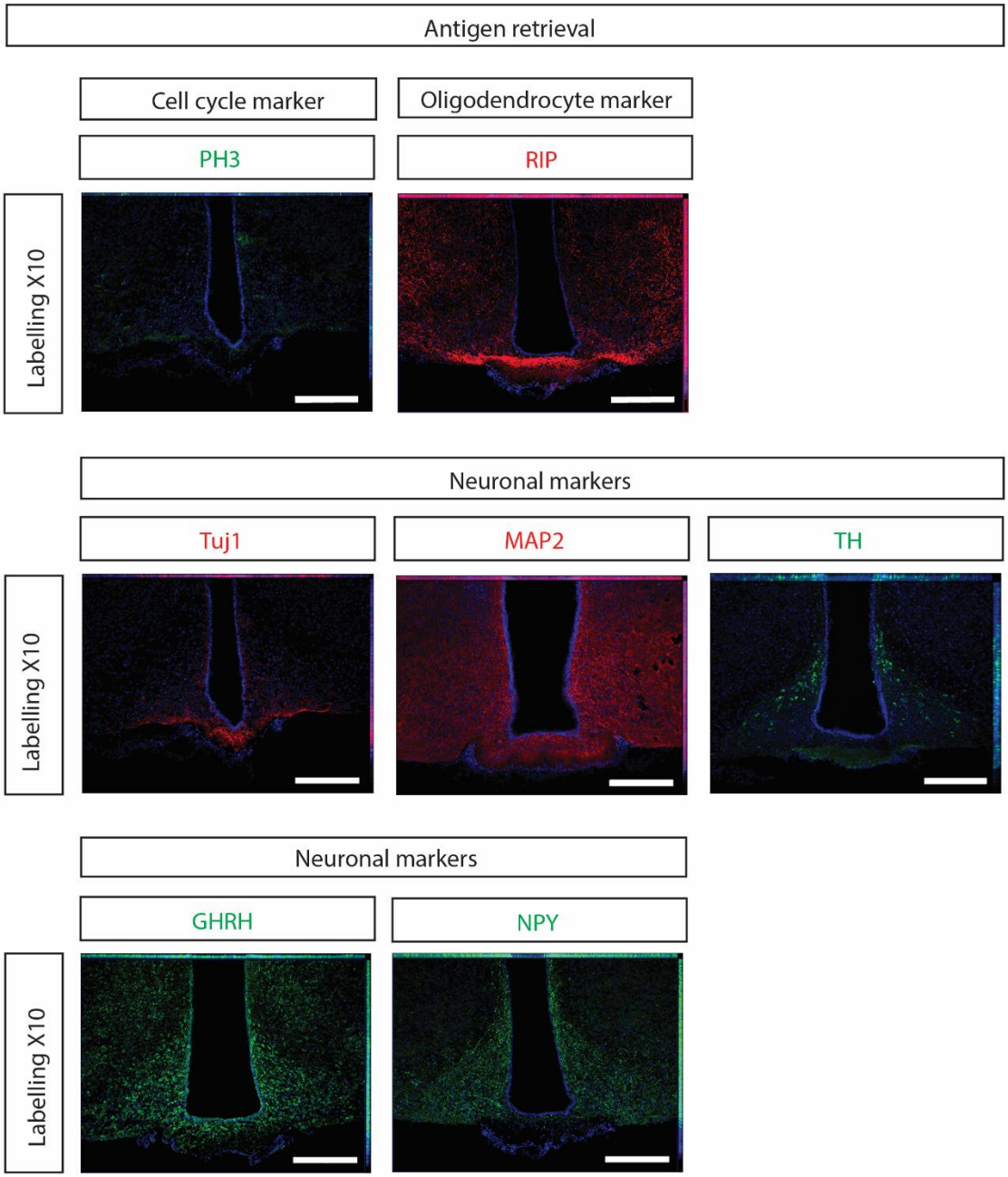

Figure 5.1.2 C: Coronal sections through adult mouse hypothalamus with antigen retrieval. PH3 (green) is a cell cycle maker and RIP (red) is an oligodendrocyte marker. Neuronal markers utilised are Tuj1, MAP2 (red), TH, NPY and GHRH (green). DAPI (blue) labels nuclei. There is an absence of PH3 positive cells so no proliferation is occurring. There is RIP labelling showing oligodendrocyte presence within the ARC and VMN. There is low levels Tuj1 a neuronal progenitor marker near the location of α-tanycytes. MAP2 and GHRH labels within both the ARC and VMN nuclei while TH and NPY labels within the ARC nuclei. N=2 PH3 and RIP. N=4 Tuj1, N=3 MAP2, N=2 TH, NPY and GHRH. Scale bar 200 µm.

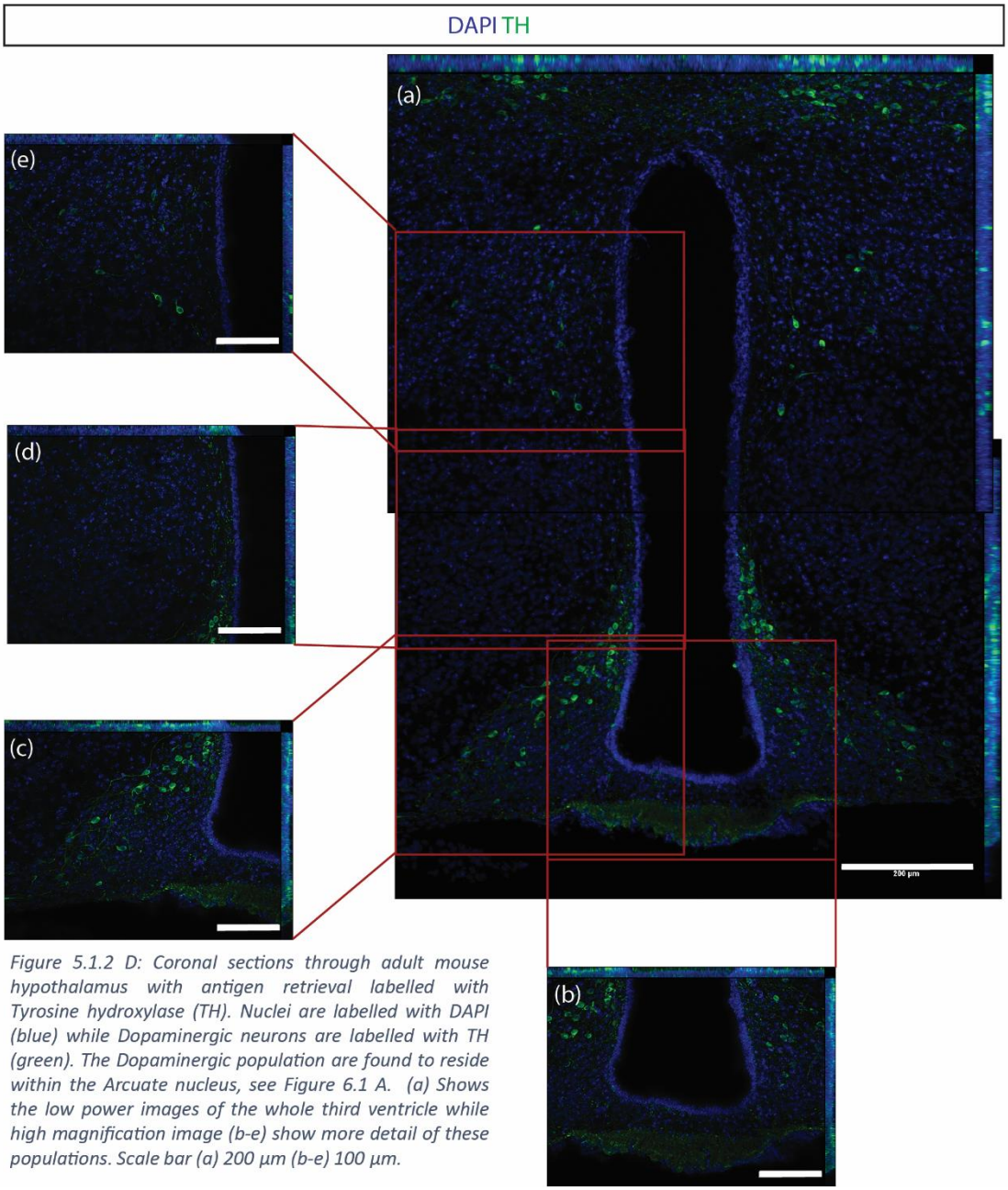

Figure 5.1.2 D: Coronal sections through adult mouse hypothalamus with antigen retrieval labelled with Tyrosine hydroxylase (TH). Nuclei are labelled with DAPI (blue) while Dopaminergic neurons are labelled with TH (green). The Dopaminergic population are found to reside within the Arcuate nucleus, see Figure 6.1 A. (a) Shows the low power images of the whole third ventricle while high magnification image (b-e) show more detail of these populations. Scale bar (a) 200 µm (b-e) 100 µm.

The improved labelling after antigen retrieval allowed me to perform double-labelling of Nestin and NrCAM to confirm NrCAM as a tanycyte marker. Co-analysis of sections with Nestin and NrCAM reveals co-labelled tanycytes (Figures 5.1.2 E and F arrows indicate processes labelled with both Nestin and NrCAM). Therefore, NrCAM is a bona fide tanycyte marker. It could prove to be a useful additional marker for the continued work to understand the different tanycyte sub-populations and their function within the adult.

Having shown that I can recognise the central hypothalamus and key resident cell populations I went on to dissect and culture tanycyte derived neurospheres from this region.

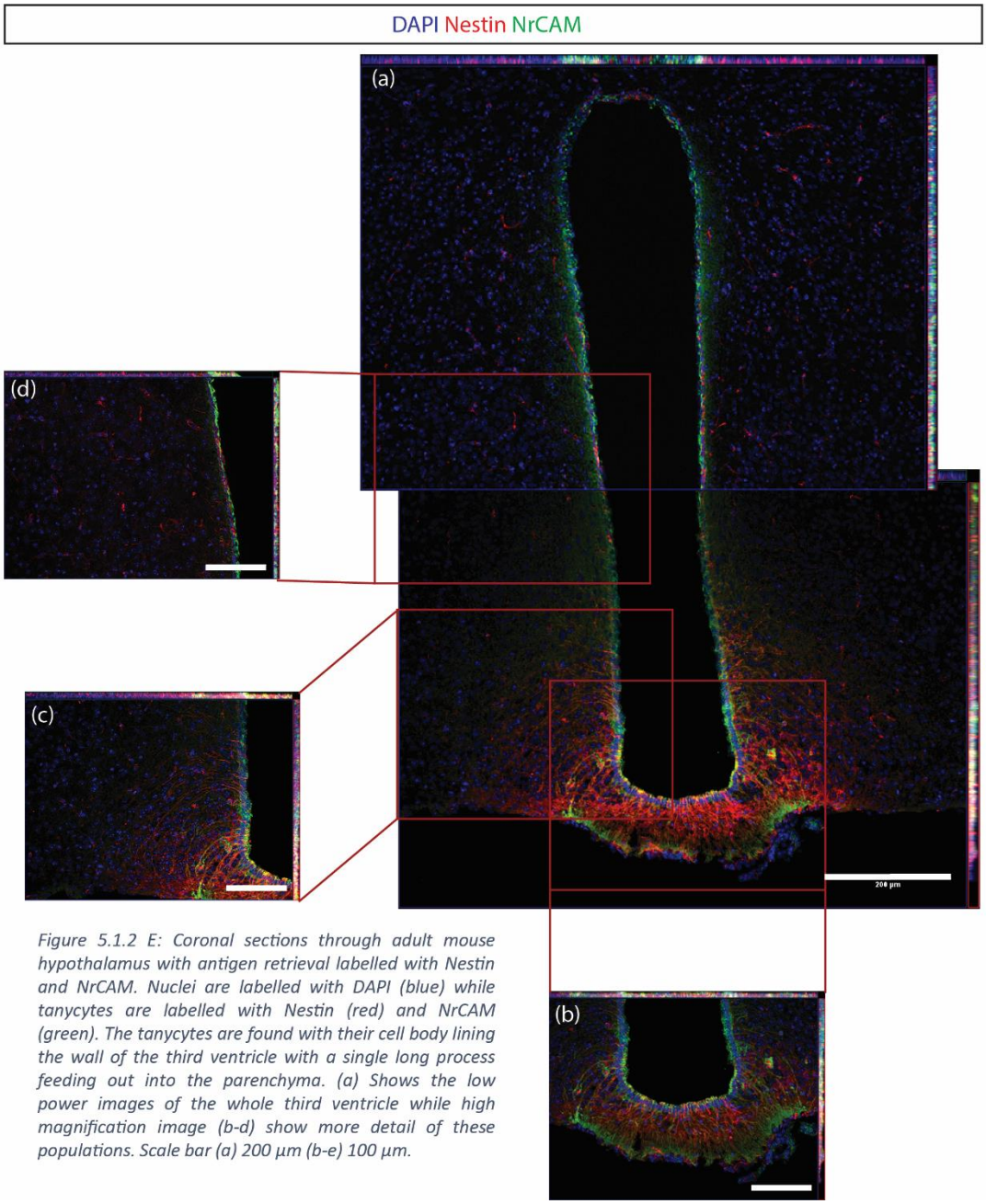

Figure 5.1.2 E: Coronal sections through adult mouse hypothalamus with antigen retrieval labelled with Nestin and NrCAM. Nuclei are labelled with DAPI (blue) while tanycytes are labelled with Nestin (red) and NrCAM (green). The tanycytes are found with their cell body lining the wall of the third ventricle with a single long process feeding out into the parenchyma. (a) Shows the low power images of the whole third ventricle while high magnification image (b-d) show more detail of these populations. Scale bar (a) 200 µm (b-e) 100 µm.

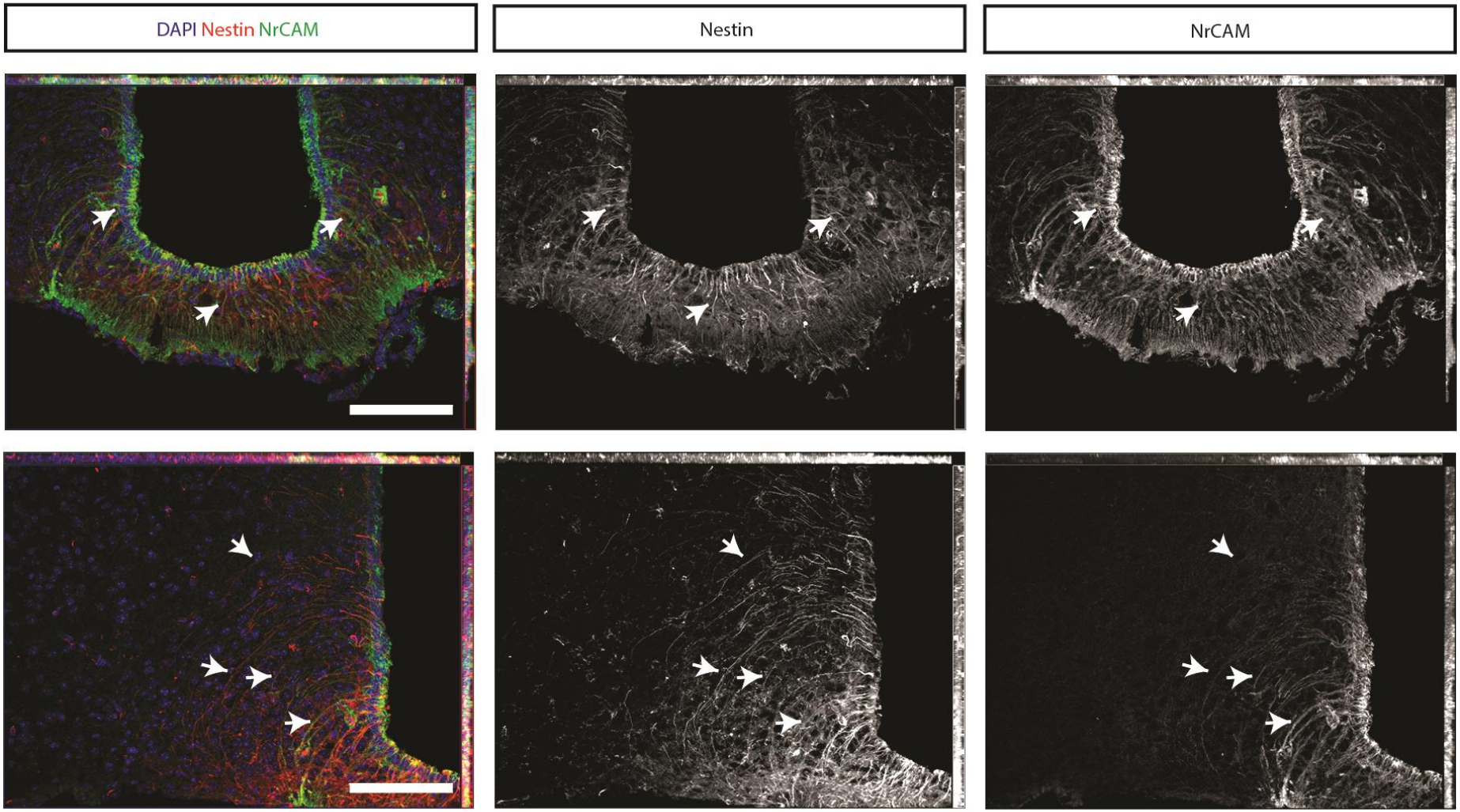

Figure 5.1.2 F: Nestin and NrCAM co-label tanycytes within the hypothalamus. Nestin (red), NrCAM (green) and DAPI (blue) labels nuclei. Coronal section through the third ventricle of the tuberal hypothalamus considering co-labelling of tanycytes with Nestin and NrCAM. The arrow heads indicate processes which are co-labelled with Nestin and NrCAM. β and α tanycytes label with both Nestin and NrCAM, however α tanycytes show weaker labelling than β tanycytes. Scale bar 100 µm.

5.2 Tanycytes are maintained when cultured under standard non-differentiation conditions but show varying low levels of differentiation

Tanycytes can be cultured *ex vivo* as neurospheres (described in 4.1.3). One of the two key features of a stem cell is its ability to self-renew in the long term. Previous studies have shown that under free-floating 'non-differentiation' conditions, tanycytes can self-renew and continue to express Nestin and Sox2 [2,134]. However, no published study has asked whether NrCAM is maintained in long-term neurospheres cultures under non-differentiation conditions. I therefore first investigated whether neurospheres maintain expression of both Nestin and NrCAM after passaging five times to P5. P5 Neurospheres were analysed both as whole mounts neurospheres and as sections in order to compare the two methods (described in 4.1.4 Sectioning in neurospheres and 4.1.5 whole mount in neurospheres respectively).

Nestin and NrCAM labelling were detected equally well in whole mounts and sections (Figure 5.2 A). This shows that, like Nestin [2], NrCAM labelling is maintained during *in vitro* culture and suggests that tanycytes continue to be present as a significant percentage of the cell population within P5 neurospheres. This implies that they are capable of self-renewal and that NrCAM is a 'stem-like' marker. To confirm that under the conditions of free-floating 'non-differentiation' culture, tanycytes proliferate, I analysed PH3. At the same time, I analysed Tuj1, a marker of differentiating neurons, to ask whether the standard free-floating non-differentiating conditions used does indeed maintain cells in an undifferentiated state and prevents spontaneous differentiation. PH3 labelling confirms that neurospheres proliferate and show that proliferating cells are found throughout the neurosphere. However, low numbers of Tuj1+ cells are detected (Figure 5.2 A arrows). In summary, this shows that neurospheres cultured under free-floating non-differentiating conditions largely self-renew but that they show small levels of differentiation. I noted that Tuj1 positive cells were more easily detected within the whole mount neurosphere and that whole mount labelling better captures the behaviour of the entire neurosphere but shows higher non-specific binding. Therefore in future experiments, I used the

whole mount method but, in an attempt to reduce the background, increase the HINGS 5-fold (Section 4.1.6).

In culturing neurospheres I noted a variability in neurosphere size. To ask whether this size difference impacted on the presence of Nestin+ NrCAM+ stem-like tanycytes, I compared tanycyte-derived P6 neurospheres of different size (Figure 5.2 B). I classified them as small (<60 micron diameter), medium (60-150 micron diameter) and large (>150 micron diameter) and then asked whether the difference in size affects expression of either Nestin or NrCAM. Figure 5.2 B shows that neurospheres express both Nestin and NrCAM and that labelling does not appear to be impacted by the size of the neurospheres. Therefore subsequent analyses considered all neurospheres as one group independent of their size.

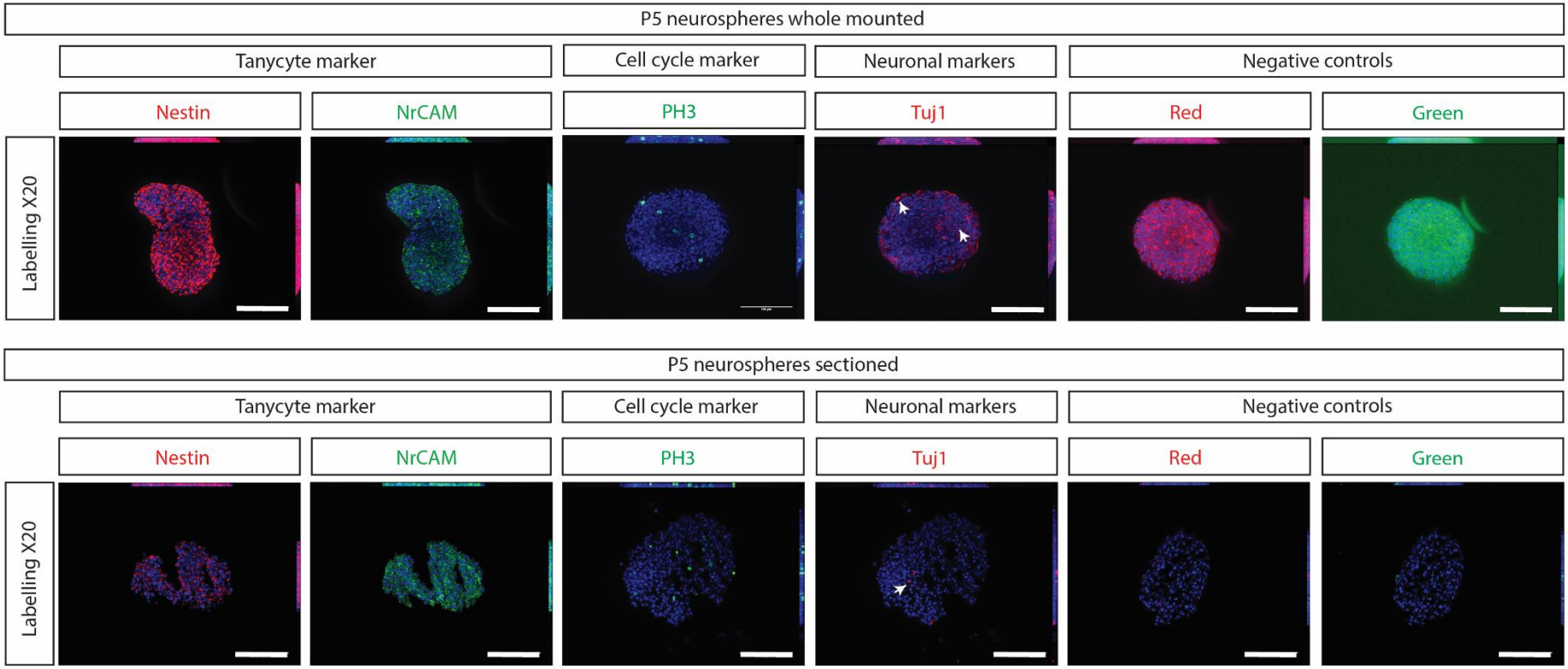

Figure 5.2 A: Passage 5 neurospheres. Whole mount and sectioned neurospheres both labelled with Nestin (red), NrCAM (green), PH3 (green) and Tuj1 (red) with DAPI (blue) labelling nuclei. Both show labelling of Nestin and NrCAM confirming presence of tanycytes and show proliferation is occurring throughout neurospheres by labelling of PH3. However, whole mounted spheres show some Tuj1 labelling at the edge of the neurosphere which is less clear in the sectioned sphere, arrows indicate positive cells. The block utilised for these experiments was 0.1% Triton X and 1% HINGS. Scale bar 100 µm.

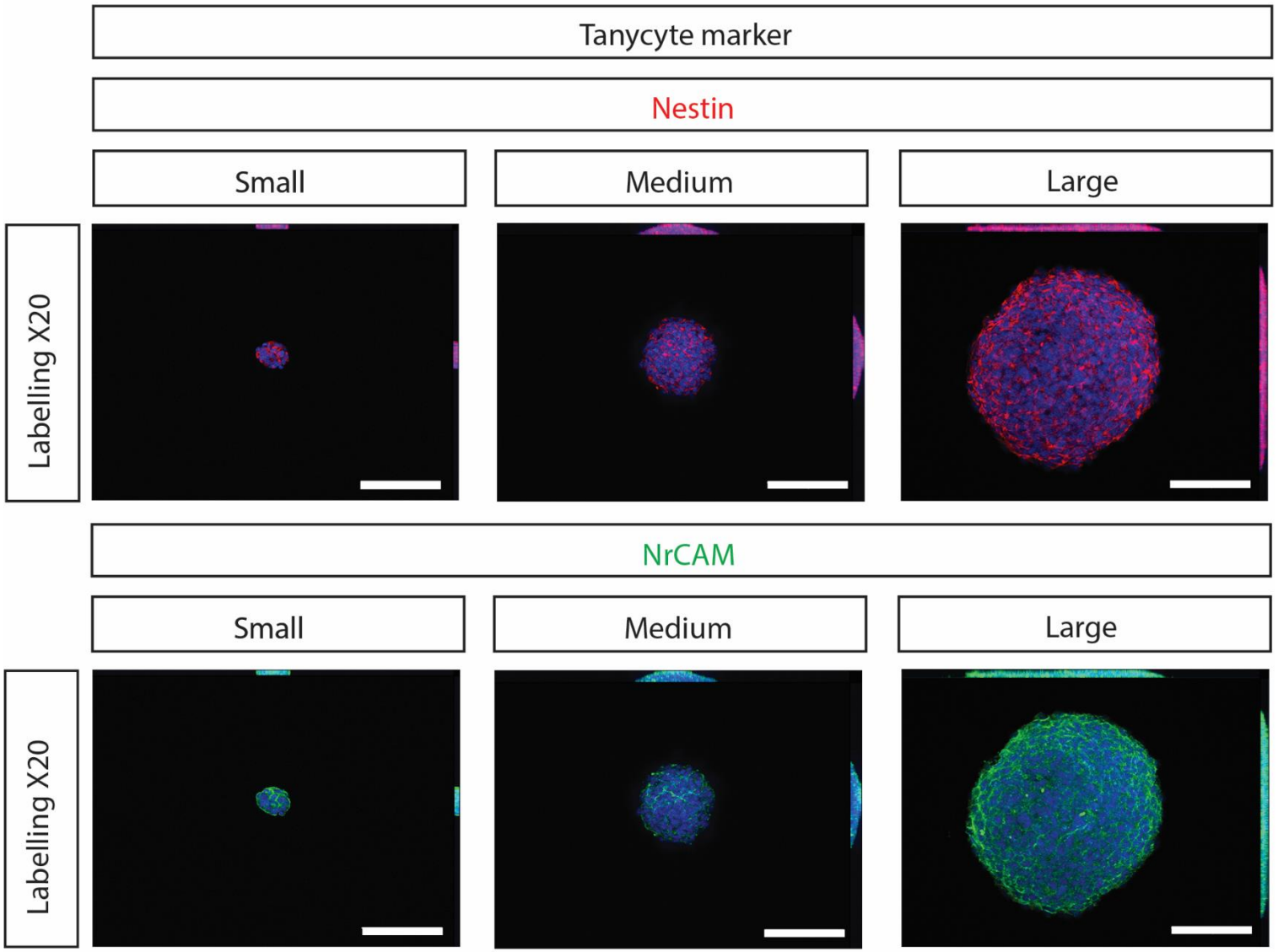

Figure 5.2 B: Passage 6 neurospheres separated based on size. Nestin (red), NrCAM (green) and DAPI (blue) labelling nuclei. Neurospheres were grouped into small, medium and large and the difference in size does not affect antibody labelling. Scale bar 100 µm.

Nestin and NrCAM appear to be expressed throughout neurospheres. However, the low levels of TujI detected indicate that some spontaneous differentiation occurs within neurospheres cultured under standard free-floating non-differentiating conditions, most marked at the periphery of the sphere. I therefore next investigated the extent of spontaneous differentiation and asked whether tanycyte-derived neurospheres from different biological replicates always show the same extent of spontaneous differentiation. To do so I cultured P6 neurospheres, sourced from three biological replicates, and labelled these with a wider range of antibodies for tanycytes, NSPCs, astrocytes, oligodendrocytes, proliferation and neuronal markers. Table 5.2 A shows the percentage of neurospheres positive for each marker within each experiment. Representative images of positive neurospheres are shown in Figure 5.2 C.

While Nestin and NrCAM are expressed in 100% neurospheres, in each replicate, other markers show more variability. Some markers, such as Tuj1 and PH3, are expressed consistently across replicates but only in a subset of neurospheres (50-60% and 85-100%, respectively). Other markers, such as Six3, show considerably more variation (20% in replicate 1 and 100% in replicate 3). This is an important finding as it suggests that the standard conditions used for current tanycyte neurosphere culture are not optimal and that from replicate to replicate, spontaneous differentiation will occur to a variable extent.

In conclusion, while neurospheres grown under standard free-floating 'non-differentiating' conditions produce many tanycytes, some differentiation occurs. This is variable between biological replicates. Such variation is important to reduce, so that these cultures can be used to draw meaningful conclusions in future studies.

Table 5.2 A: Passage 6 neurospheres with percentage of positively labelled. Three mouse pairs (utilised to isolate neurospheres as method 4.6.3 Neurosphere cell culture in cell isolation) were cultured to characterised Passage 6 neurospheres. For each experiment the n number provides how many neurospheres were analysed for each marker along with the percentage of positively labelled neurospheres. Note: mouse pair 3 is a combination of whole mount and sectioned neurospheres analysed. Mouse pair's 1 and 2 are all whole mount neurospheres.

Passage 6 neurospheres						
	Mouse pair 1		**Mouse pair 2**		**Mouse pair 3**	
	n number	**% neurospheres positively labelled**	**n number**	**% neurospheres positively labelled**	**n number**	**% neurospheres positively labelled**
Nestin	24	100	12	100	8	100
NrCAM	24	100	12	100	8	100
Tuj1	8	50	14	50	8	63
MAP2	11	92	8	63	10	100
GFAP	8	50	12	58	7	100
RIP	19	0	12	42		
Six3	20	20	8	100	7	57
Sox2	20	100	12	58	3	100
PH3	24	83	13	100	8	100
TH	16	14	14	86	10	90
Casp	10	10	12	92		

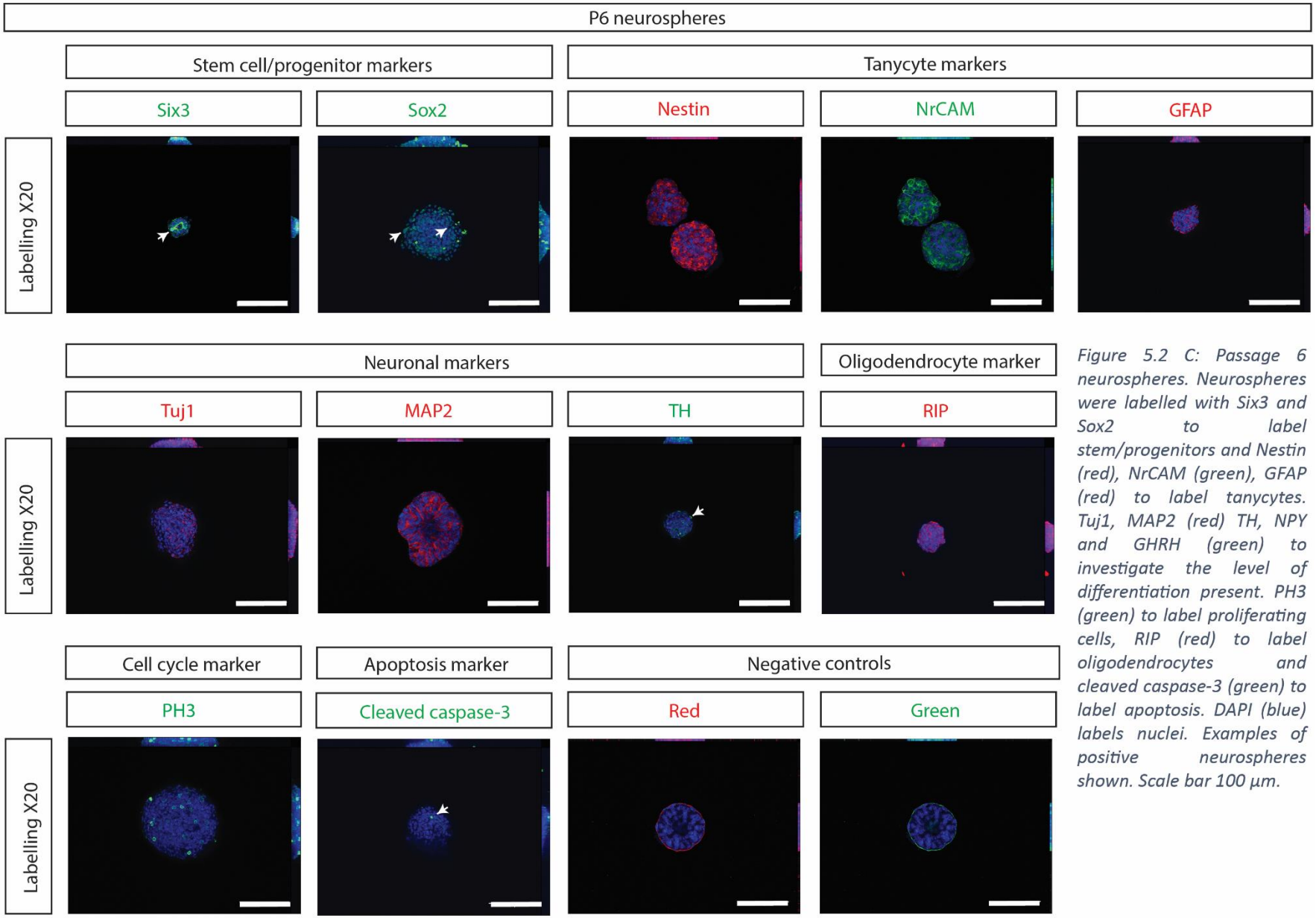

Figure 5.2 C: Passage 6 neurospheres. Neurospheres were labelled with Six3 and Sox2 to label stem/progenitors and Nestin (red), NrCAM (green), GFAP (red) to label tanycytes. Tuj1, MAP2 (red) TH, NPY and GHRH (green) to investigate the level of differentiation present. PH3 (green) to label proliferating cells, RIP (red) to label oligodendrocytes and cleaved caspase-3 (green) to label apoptosis. DAPI (blue) labels nuclei. Examples of positive neurospheres shown. Scale bar 100 µm.

5.3 Low passage neurospheres may be more potent than higher passage neurospheres

The second core feature of stem cells is their ability to differentiate into different cell lineages. A previous study has shown that P2 hypothalamic neurospheres can, under appropriate conditions, differentiate to different neuronal and glial cell types, including TH+ DA neurons [2]. I therefore set out to confirm that I could repeat the differentiation capabilities of tanycytes previously shown. At the same time I asked whether repeated passaging would affect differentiation due to the low level differentiation seen in neurospheres cultured under current free-floating non-differentiation conditions.

To begin with I differentiated P5 neurospheres for 14 days, method as stated in section 4.1.3 Neurosphere cell culture in differentiation. As shown in Fig 5.3A, Sox2+ and Six3+ cells are present alongside Nestin+ and NrCAM+ tanycytes, however NrCAM labelling appears reduced. Proliferating PH3+ cells are also still present in low numbers. Differentiation has occurred as shown by GFAP+ cells (likely to be astrocytes alongside some tanycytes) as well as Tuj1+ and MAP2+ cells (likely to be newborn neurons). Very small numbers of TH+ DA neurons were detected (arrows indicate positive cells). With the high presence of tanycyte and NSPC markers this suggests that differentiation is not 100% efficient.

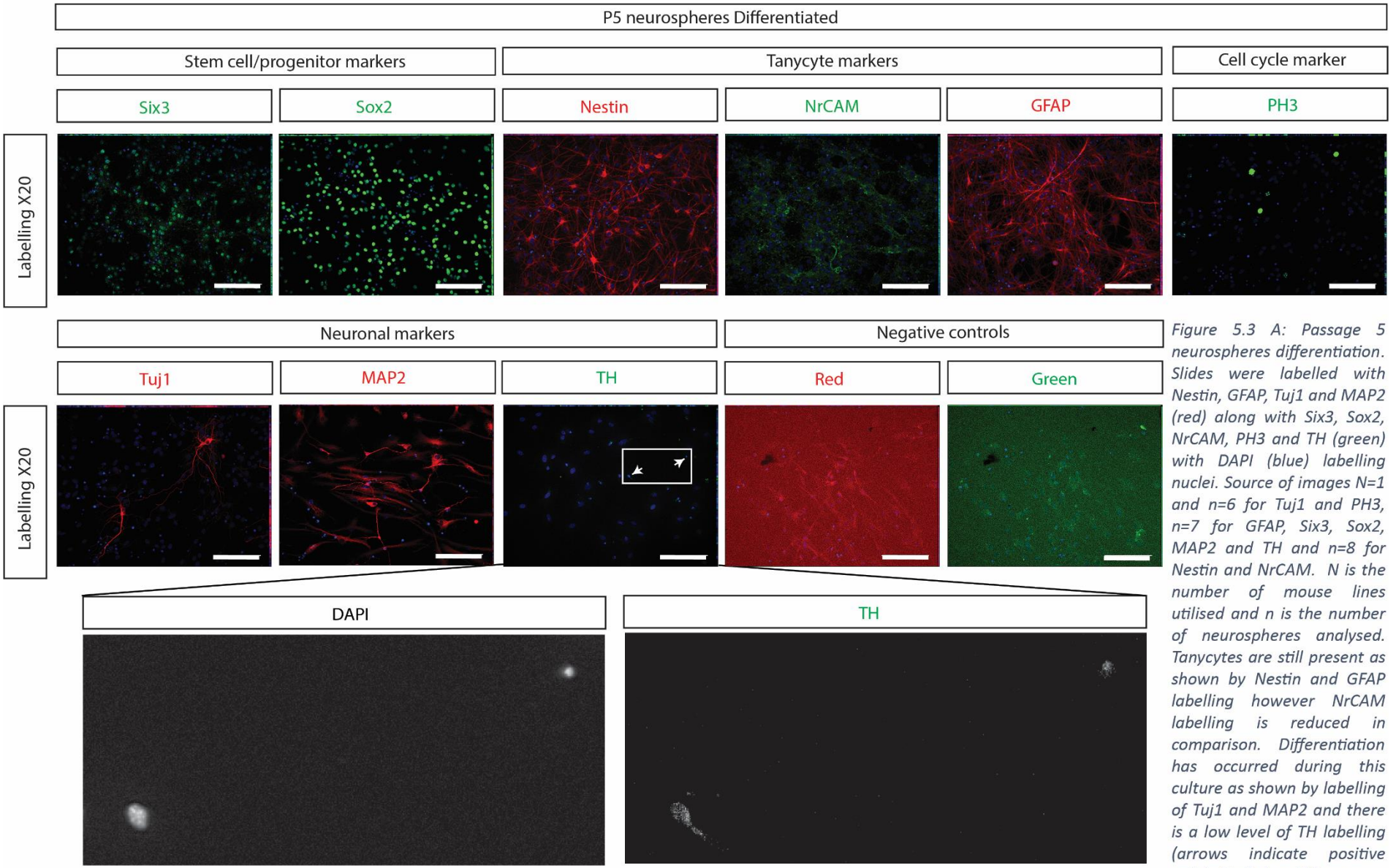

Figure 5.3 A: Passage 5 neurospheres differentiation. Slides were labelled with Nestin, GFAP, Tuj1 and MAP2 (red) along with Six3, Sox2, NrCAM, PH3 and TH (green) with DAPI (blue) labelling nuclei. Source of images N=1 and n=6 for Tuj1 and PH3, n=7 for GFAP, Six3, Sox2, MAP2 and TH and n=8 for Nestin and NrCAM. N is the number of mouse lines utilised and n is the number of neurospheres analysed. Tanycytes are still present as shown by Nestin and GFAP labelling however NrCAM labelling is reduced in comparison. Differentiation has occurred during this culture as shown by labelling of Tuj1 and MAP2 and there is a low level of TH labelling (arrows indicate positive cells). Scale bar 100 µm.

Due to the low levels of differentiation seen under non-differentiation conditions I hypothesised that over passages, differentiation capabilities is reduced within neurospheres. I tested this at two extremes, comparing P2 and P11 neurospheres after differentiation. The aim of this comparison was to identify the neurosphere population with most potential/potency.

Figure 5.3 B highlights key differences between P2 and P11 neurosphere differentiation over 8 days. Tanycytes are reduced in presence between P2 and P11 differentiated neurospheres shown by more Nestin and NrCAM labelling. GFAP labelling can be seen in sparse numbers of P11 neurospheres, while in P2 neurospheres, GFAP+ cells are found in more neurospheres but still not in all. This loss of the NSPC is confirmed by the reduction of Six3 positive cells.

Many more Tuj1+ and MAP2+ cells are detected in P2 compared to P11 neurospheres, Figure 5.3 C. TH+ cells are detected after differentiation from both P2 and P11 neurospheres however more are present from P2 neurospheres even though they are still at low numbers. Oligodendrocyte differentiation, RIP positive cells, are seen in both P2 and P11 differentiated neurospheres.

In conclusion, cell potential appears to become reduced over repeated passage and neurosphere culture. This, alongside the characterisation of neurospheres culture under non-differentiation conditions, suggests that cells do not efficiently self-renew under these free-floating conditions. In order to be able to characterise this population to better understand the tanycyte capabilities and their function within the adult hypothalamus, a culture system is required which will maintain the tanycyte population as ‘stem like’ with high unexploited potency.

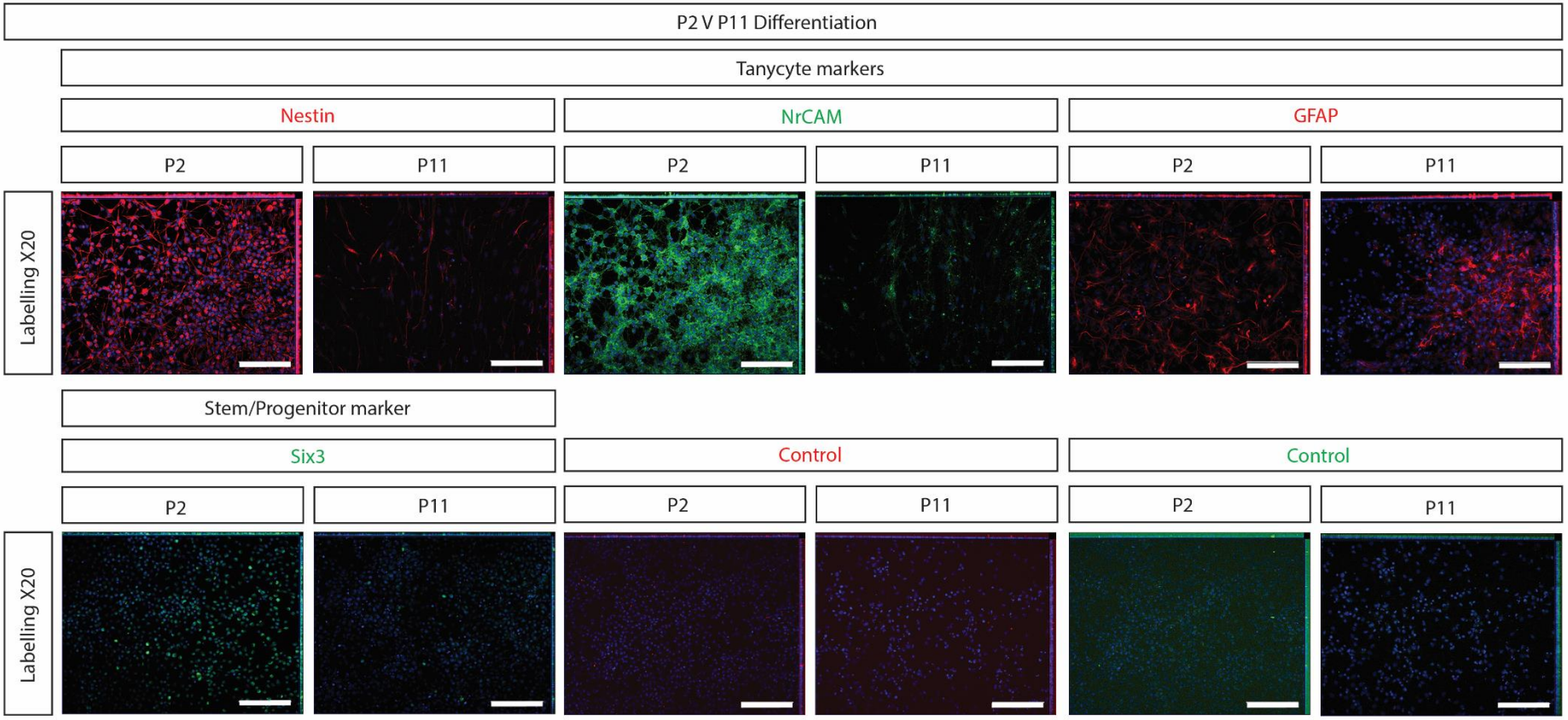

Figure 5.3 B: Differentiation of Passage 2 and Passage 11 neurospheres. Source of images for P2 N=2 and n=6 and for P11 N=1 and n=3. N is the number of mouse lines utilised and n is the number of neurospheres. Slides were labelled with Nestin and GFAP (red) along with NrCAM and Six3 (green) with DAPI (blue) labelling nuclei. Passage 2 (P2) neurospheres show higher labelling of tanycyte markers Nestin and NrCAM along with NSPC marker Six3. Both show GFAP expression. Scale bar 100 µm.

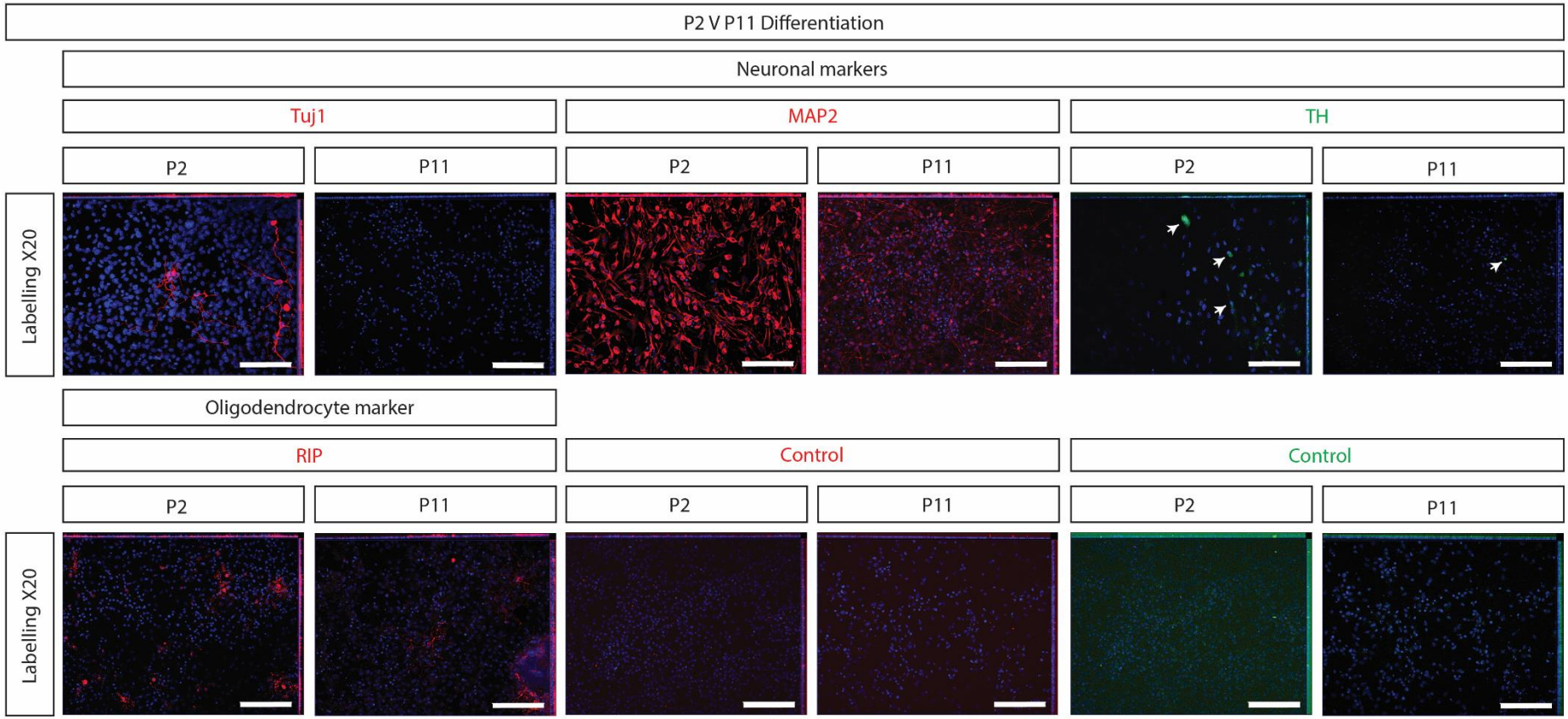

Figure 5.3 C: Differentiation of Passage 2 and Passage 11 neurospheres. Source of images for P2 N=2 and n=6 (note: 5 for MAP2 and TH due to lack of neurospheres) and for P11 N=1 and n=3. N is the number of mouse lines utilised and n is the number of neurospheres. Slides were labelled with Tuj1, MAP2 and RIP (all in red) along with TH (green) with DAPI (blue) labelling nuclei. P2 neurospheres show more labelling of differentiation markers Tuj1, MAP2, TH. Both P2 and P11 can differentiate into Oligodendrocytes (RIP). Scale bar 100 µm.

5.4 Discussion

I firstly showed I was able to recognise the central hypothalamus and identify key cell populations that reside within this region. This was done by optimising the protocol to immunolabel hypothalamic sections showing that not only does Nestin labelling improve with antigen retrieval, as previously reported [2], but I showed that all labels are improved with antigen retrieval treatment, which is an important development in the protocol for *in vivo* analysis of this region. Finally I showed that NrCAM is a marker of tanycytes co-labelling with established marker Nestin. This is another important addition as one barrier to the development of understanding for tanycytes is the lack of markers specific to tanycytes and their sub-categories. With NrCAM being another tanycyte specific marker for tanycytes this will aid in the research to understand tanycyte behaviour. I was able to isolate and culture hypothalamic tanycytes as neurospheres. While neurospheres grown under standard free-floating 'non-differentiating' conditions produce many tanycytes, some differentiation occurs. Thus self-renewal is not 100% efficient. Importantly the differentiation seen is variable between biological replicates, particularly for Six3, RIP and TH. Such variation is highly impactful on conclusions draw from studies with these types of cultures meaning this current method of culture is a barrier to expanding understand of this NSPC population. These problems, highlighted with the neurosphere assay culturing under free-floating non-differentiation conditions, was also shown to impact differentiation abilities through comparison between low and high passage neurospheres. These culture conditions not only allow for differentiation at variable levels, over time the potency of the culture is also reduced. Therefore this chapter has shown that the neurosphere culture method under free-floating non-differentiation conditions requires improvements. Therefore, I have addressed all of the objectives set out for this chapter.

In summary, ideally the culture required to investigate tanycyte characteristics and abilities is a highly potent population that is not exhibiting this potency (meaning low differentiation is seen).

One avenue is to utilise scaffold environments to support culture of cells[60,73,75], developing a system that supports the maintenance of the stem-like character of tanycytes.

Chapter 6: Electrospinning can be utilised to produce scaffolds with random or aligned fibres that have potential as a versatile tool for studying tanycyte behaviour

In this chapter I set out to address the following objectives:

- to electrospin scaffolds with random fibre orientations;
- to investigate a range of metallic templates and the impact of these structures on the fibre topology;
- to characterise the scaffolds in terms of fibre diameter and orientation, including optimisation of this method;
- to alter the electrospinning method to align fibres, thereby producing aligned scaffolds;
- to characterise the random and aligned scaffolds in terms of mechanical properties, specifically stiffness.

In order to develop a scaffold that would aid in maintaining tanycyte derived neurospheres in their 'stem-like' state the features of the scaffold that would aid in this maintenance needed to be carefully considered. Studies have shown that cell types respond differently to fibre organisation (Section 2.1.2). The response of tanycytes to mechanotransductive cues such as fibre organisation had not been published and so investigating this feature would add to the understanding of this population's behaviour. The potential of aligned fibres was of further interest for a system to maintain 'stemness' free-floating has been shown to be inefficient, Chapter 5. Aligned fibres are hypothesised to maintain tanycytes by replicating *in vivo* morphology. This morphology includes their cell body lining the ventricle with their process projecting into the parenchyma.

6.1 Metallic templates incorporate complex features into the scaffold which include different fibre organisations

Electrospinning is a manufacturing technique utilised to produce 3D fibrous scaffolds, with randomly organised fibres when collecting onto a flat plate, as shown in Figure 6.1 A. I showed that complex features, Figure 6.1 B, are introduced within the scaffold when electrospinning onto metallic templates (Figure 4.2.2 A).

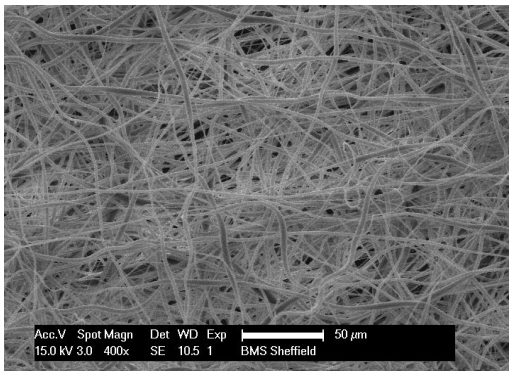

Figure 6.1 A: Random PCL scaffolds. 10% Sigma PCL in DCM/DMF. Spun at parameters stated in 4.2.2 Sigma PCL in DCM/DMF.

Scaffold 1 introduces one repeating microfeature while Scaffold 2 is comprised of four microfeatures of different sizes which repeat through the mat, Figure 6.1 C. Finally, scaffold 3 comprises of fibres orientated in several directions forming complex structures.

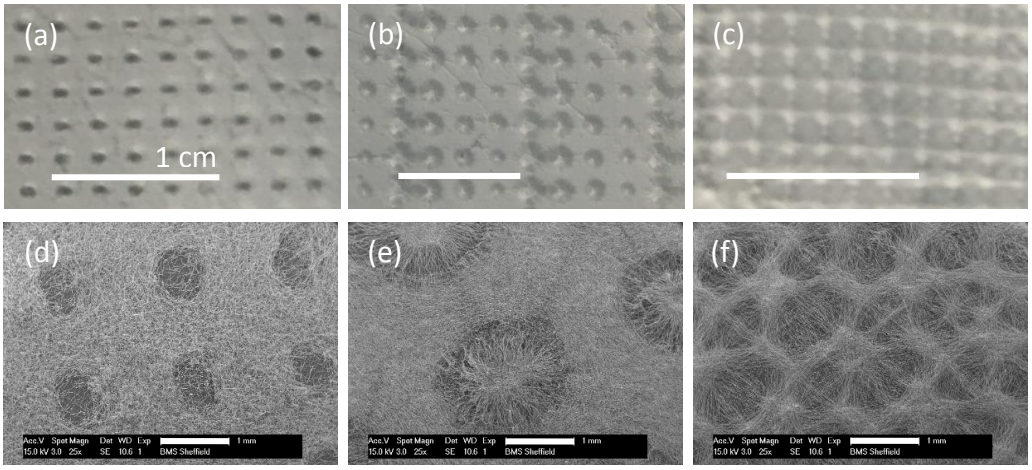

Figure 6.1 B: PCL scaffolds (a-c) optical images and (d-f) SEM images. (a and d) scaffold 1, (b and e) scaffold 2, (c and f) scaffold 3, all made using templates in Figure 4.2.2 A. 10% Sigma PCL in DCM/DMF. Spun at parameters stated in 4.2.2 Sigma PCL in DCM/DMF. Scale bar (a-c) 1 cm and (d-f) 1 mm.

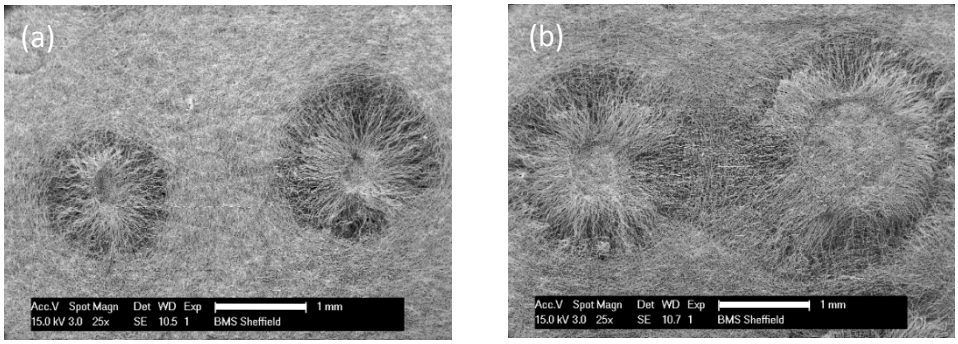

Figure 6.1 C: The four microfeatures of scaffold 2. (a) The smallest and intermediate b, (b) intermediate a and large microfeature from left to right. 10% Sigma PCL in DCM/DMF. Scale bar 1 mm.

6.2 Microfeature diameter metrology

Each template introduces differently sized and shaped microfeatures that can be seen by the eye. However, size and shape analysis was required to fully characterise these features and analyse their differences.

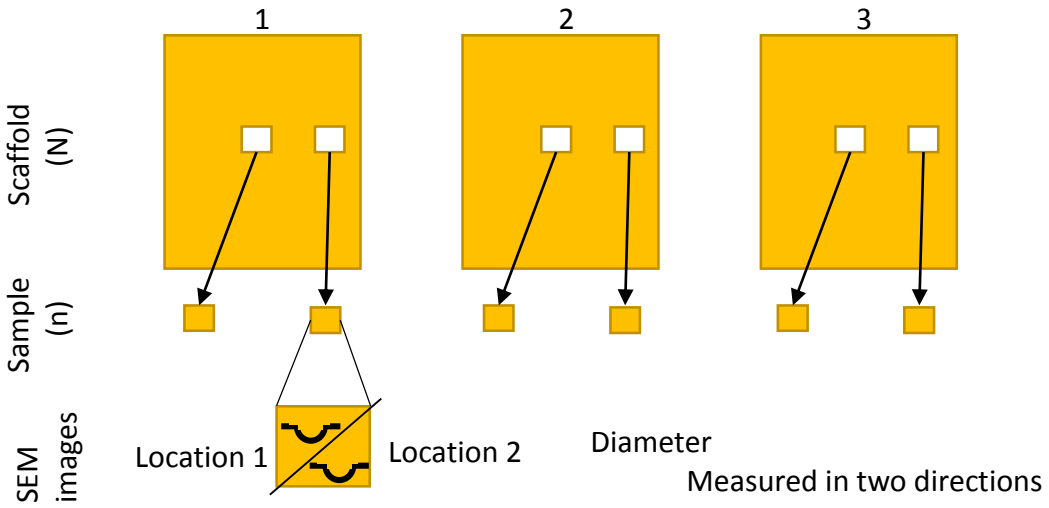

Figure 6.2 A: Schematic of the source of data for scaffold analysis of scaffolds 1-3 microfeature diameter. Scaffolds were made on three occasions (N=3) and from each scaffold, two samples were taken for SEM imaging (n=6). Two features were imaged on each sample.

For the analysis of microfeature diameter of scaffolds 1-3, scaffolds were manufactured on three occasions with two samples taken from each scaffold. On each sample two microfeatures were imaged by SEM, Figure 6.2 A. For each microfeature, two measurements were taken as described in 4.2.3. Following this the two measurements, length A and B (Figure 4.2.3 B) were compared as I wanted to identify whether the microfeature was circular. If there wasn't a significant difference between the two lengths, the two measurements were combined. If there was a significant difference between the two lengths it was considered whether combining measurements was reasonable.

The two lengths showed significant difference for scaffolds 1 and 3, while there was no significant difference between any of the four microfeatures lengths of scaffold 2, Figure 6.2 B. Therefore the lengths were combined for scaffold 2's microfeatures as well as for scaffold 1 as the difference in the two lengths was concluded to be due to an error in the templates

manufacture and this feature should be circular. Scaffold 3 however is a unique topology so the lengths were kept separate. Table 6.2 A shows the average diameter of each feature.

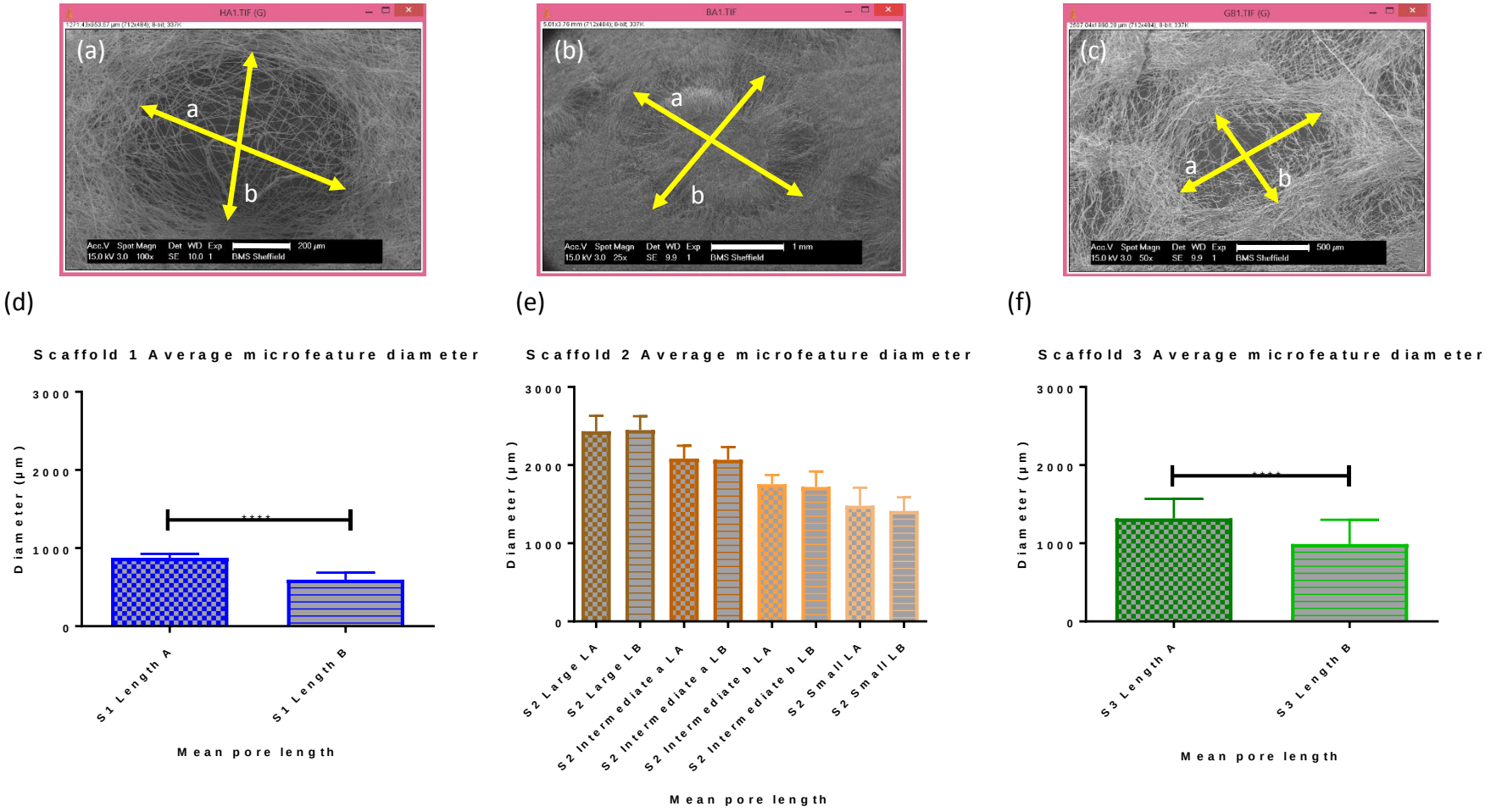

Figure 6.2 B: Microfeature diameters of scaffolds 1-3. (a-c) Screenshots of collecting measurements of microfeature diameter, arrowed lines show examples of how two measurements a and b were collected. (b) shows an example of one of the four sizes of microfeature from scaffold 2, Figure 6.1 C. (d-f) Graphs showing mean with standard deviation for each scaffold. Scale bar (a) 200 µm (b) 1 mm (c) 500 µm. The data presented is collated from the analysis of twelve images as described in Figure 6.2 A. Statistical analysis was undertaken with paired t-tests. There is no significant differences between any of the lengths of the pores on scaffold 2 while scaffold 1 and 3 have significant differences between the two lengths average diameters. 10% Sigma PCL in DCM/DMF. N=3 n=6.

Table 6.2 A: The mean and standard deviation of the microfeature sizes from scaffolds 1-3 measured in two directions. Data collated from 12 microfeatures from three scaffolds. N=3 n=6.

Scaffold	Pore name	Mean diameter (µm)	Standard deviation (µm)
1		737	±160
2	Large	2442	±184
2	Intermediate a	2077	±160
2	Intermediate b	1739	±160
2	Small	1449	±201
3		1320 by 992	±248 by ±310

I then compared each microfeature diameter with each other, Figure 6.2 C. In appendix 1 Table A1 A shows the significant differences from analysis using Krustal-Wallis statistical test with Dunn's multiple comparisons. From this analysis it was noted that not all comparisons between scaffold 2 microfeatures were significantly different and those that were significant are indicated in Figure 6.2 C. In conclusion, each template introduces a unique feature within the scaffold as shown by the significant differences between the microfeatures.

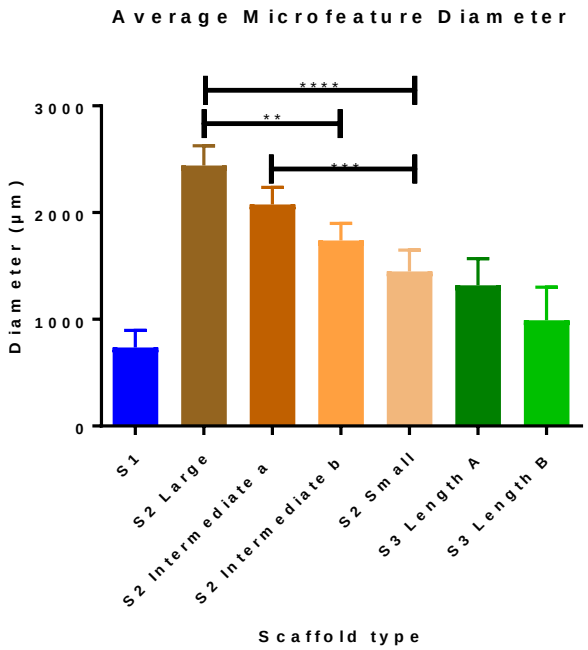

Figure 6.2 C: Comparison of the mean microfeature diameters between scaffolds 1-3. Did not pass normality test so statistical analysis has been undertaken utilising Kruskal-Wallis test where there is significant difference at P<0.0001. All significant multiple comparisons utilising Dunn's multiple comparison between the scaffold's can be found in Table A1 A.

6.3 Optimisation of method to characterise fibre properties

During the manufacture and diameter analysis of the microfeatures of scaffolds 1-3 I noted that these features contain changes in the organisation of fibres, including the level of alignment present in the different areas of the microfeatures, Figure 6.3 A (b). Therefore this raised a question of how orientation of fibres could be characterised to represent the change in the level of alignment present in different areas.

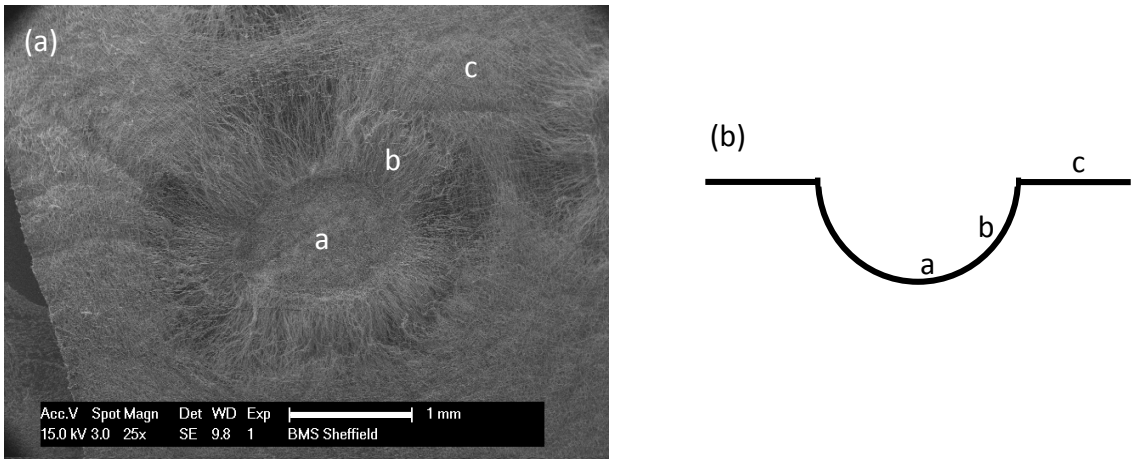

Figure 6.3 A: Scaffold 2's largest microfeature. (a) SEM image of the large microfeature (b) a schematic diagram of a section through a feature. a illustrates the region known as the bottom of the feature, b is the side of the feature and c is the top surface of the scaffold. 10% Sigma PCL in DCM/DMF. Scale bar 1 mm.

For example, scaffold 2's largest microfeature (Figure 6.3 A) was a good example of a microfeature containing three distinct areas; the bottom of the feature, side of the feature and the top surface where the level of alignment between fibres change dependent upon the area. By eye within the bottom and top surface areas fibres are both randomly organised whereas the side shows more alignment between fibres. However, while the eye is able to easily discern between levels of alignment, this is a more complex feature to analyse mathematically (Section 2.1.2). Consequently an investigation into how to characterise the level of alignment present was undertaken, utilising random scaffold and scaffolds 1-3. Within this study fibre diameters were also collated.

This optimisation can broadly be separated into two phases, the first approach was undertaken on data from a smaller data set whereas the second approach was undertaken on a wider data set (which was included in publication[161]). This analysis method utilised Image J as a tool to

measure the fibre properties[162] and will be referred to as the manual method. Details of these methods optimisation are described in 4.3.

6.3.1 First approach to characterising fibre orientation and diameter

The first analysis was done on one scaffold of each type (random and scaffolds 1, 2 and 3) from which two samples were taken from each scaffold. On each sample, two microfeatures were imaged including images of each area such as the bottom of the well, the side and top surface Figure 6.3.1 A.

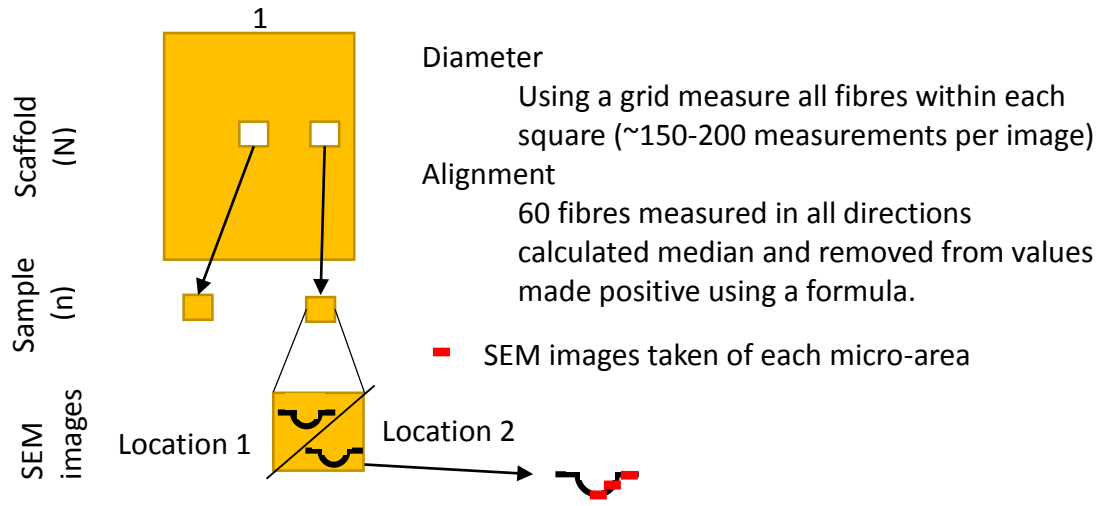

Figure 6.3.1 A: Schematic of the source of data for scaffold analysis for first approach. One scaffold for each type was manufactured (N=1) from which two samples were taken for SEM imaging (n=2). On each sample two microfeatures were imaged at all of the areas they contain.

Fibre diameter

Analysis of fibre diameters of each area showed that broadly the diameters were consistent between the areas of the microfeatures and between the different scaffolds, Figure 6.3.1 B. In appendix 1 Table A1 B shows the mean of each area along with the standard deviation and standard error of the mean. Measurements were collated as described in 4.3.2 First approach.

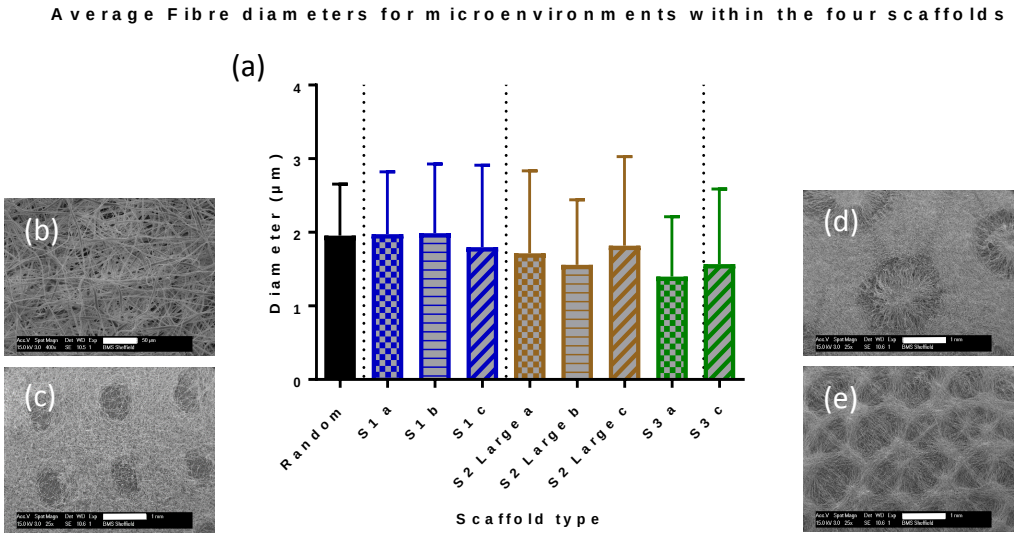

Figure 6.3.1 B: First approach to analyse fibre diameter. Showing mean with standard deviation. (a) Average fibre diameters for random scaffold and scaffolds 1-3 using the first approach for analysis. S1= scaffold 1, S2= scaffold 2 and S3= scaffold 3. a= bottom of the well b= side of the well and c=top surface. SEM images (b) random scaffold (c) scaffold 1, (d) scaffold 2 and (e) scaffold 3. Scale bar (b) 50 µm and (c-e) 1 mm. N=1 one scaffold made n=2 two samples taken from each scaffold for SEM imaging. 10% Sigma PCL in DCM/DMF.

However, the statistical analysis does identify many comparisons that are significantly different as shown in appendix 1 Table A1 C. The magnitude of these differences are unlikely to result in a different responses of cells, especially as each area shows its own standard deviation of ~1 µm. Meaning each area generally contains fibres varying in diameter from 1 to 3 µm.

Fibre orientation

Fibre orientation measurements were taken, as 4.3.2 First approach describes. This raw data then underwent post-data collection analysis. This was to make all data sets comparable as when SEM images are taken it is not easy to ensure fibres are imaged in the same direction so this variation needed to be removed from the data set. In order to do this, the median value for each image was taken away from all of the values to provide angular distribution around the median for each image. This data could then be combined for each area providing a larger pool of data to analyse. This is shown in Figure 6.3.1 C (a) where the data is presented as a box and whisker plot where the mean is presented as the middle line of the box while the two lines represent the maximum and minimum values. For graph (b) any negative values were made

positive using a formula (4.3.2 First Approach) and represented as the mean with standard deviation. However, no significant difference between the areas could be identified by this method. I was concerned by this as a difference in fibre orientation was seen by eye. I concluded that this method was not retaining the integrity of the values measured and questioned their ability to be compared to each other.

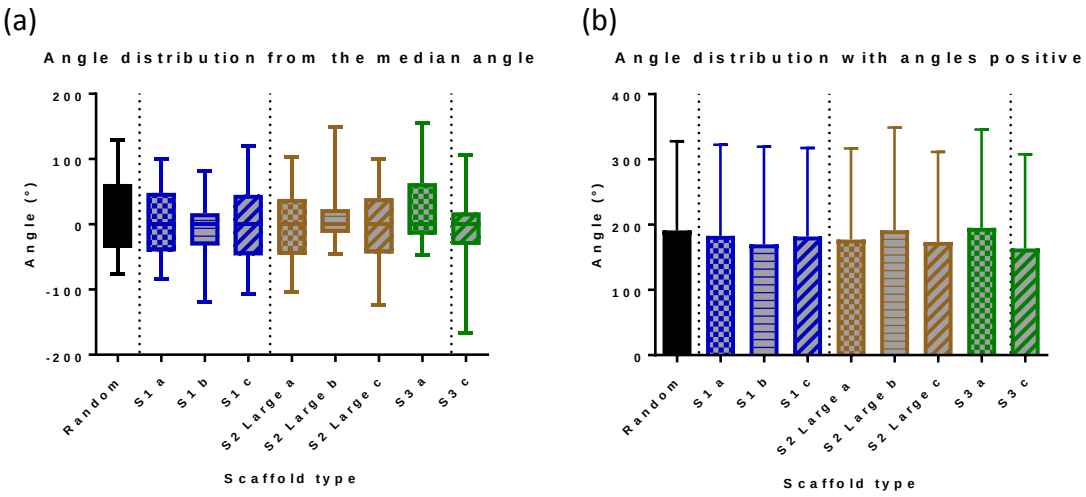

Figure 6.3.1 C: The alignment of random scaffold and scaffolds 1-3 analysed using the method discussed in 4.3.2 First approach in Fibre alignment. (a) The data analysed by taking the median and removing it from all other angles in that image and presented as a box and whisker plot. (b) The angles in (a) were converted to positive values if they were negative and plotted as mean with standard deviation. Data sets did not pass normality test. Statistical analysis with Kruskal-Wallis with Dunn's multiple comparison showed overall significant difference of P=0.05 however multiple comparison showed no significant difference between any microenvironments for either data presentation.

6.3.2 Second approach to characterising fibre orientation and diameter

Following the initial analysis, the method was re-considered as described in 4.3.3 Second approach. I suspected that measuring all of the fibres on each SEM image, and therefore measuring fibres several times, is unlikely to provide an accurate indication of the fibres present. Furthermore, this method is more demanding on the time taken to collate all of these measurements. Measuring a sample of fibres within a fixed square on a wider number of scaffolds made on separate days would provide a better indication of the fibres characteristics present in each scaffold and be more time effective. Orientation analysis was also improved from measuring fibres in all directions which were likely to be cancelling each other out in the analysis and stopping the ability to combine data from different images of the same scaffold type. To improve this a fixed point was chosen, a vertical line and angles measure from left to right as the fibres crossed this fixed line, 4.3.3 Second approach. Therefore I made three scaffolds for each type and two samples were taken from each scaffold for imaging, Figure 6.3.2 A.

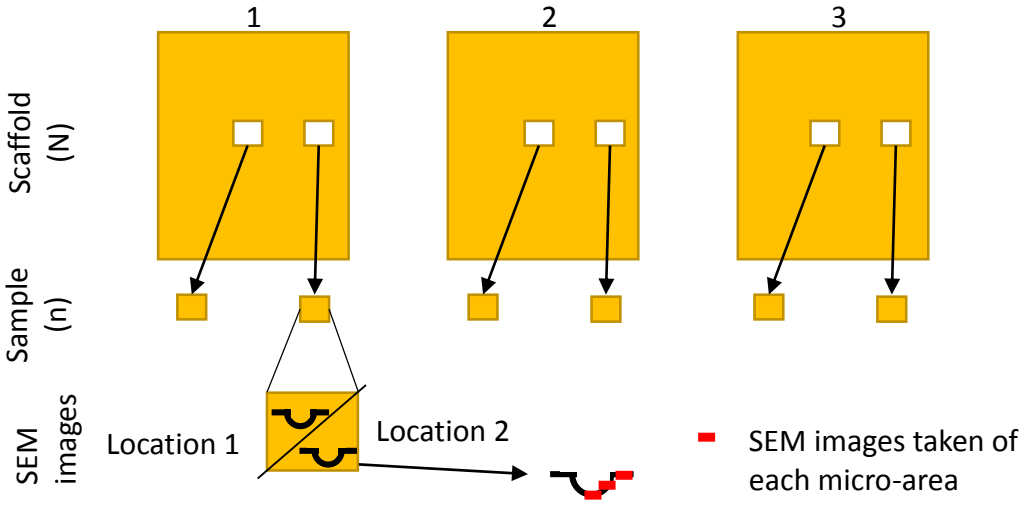

Diameter

10 fibres in a defined square measured

Alignment

Four different methods

Final method: add 90° to each value, calculate the median and then removing this from each value

Figure 6.3.2 A: Schematic of the source of data for scaffold analysis for approach 2. Three scaffolds made (N=3) and from each two samples taken from each for SEM imaging (n=6). On each sample two microfeatures were imaged.

Fibre diameter

Broadly the mean fibre diameter for each area on each scaffold type does not vary greatly, Figure 6.3.2 B, generally 2 µm ± 1 µm. In appendix 1 Table A1 D shows the mean fibre diameter for each area. Statistical analysis does identify several areas that are significantly different, Table A1 E. This analysis does identify that the bottom (a) of scaffold 1 has slightly thinner fibres to areas b and c. For scaffold 2 the side of the well (b) has thinner diameters than a or c the bottom and top surface respectively and scaffold 3 also has thinner fibres for a than c.

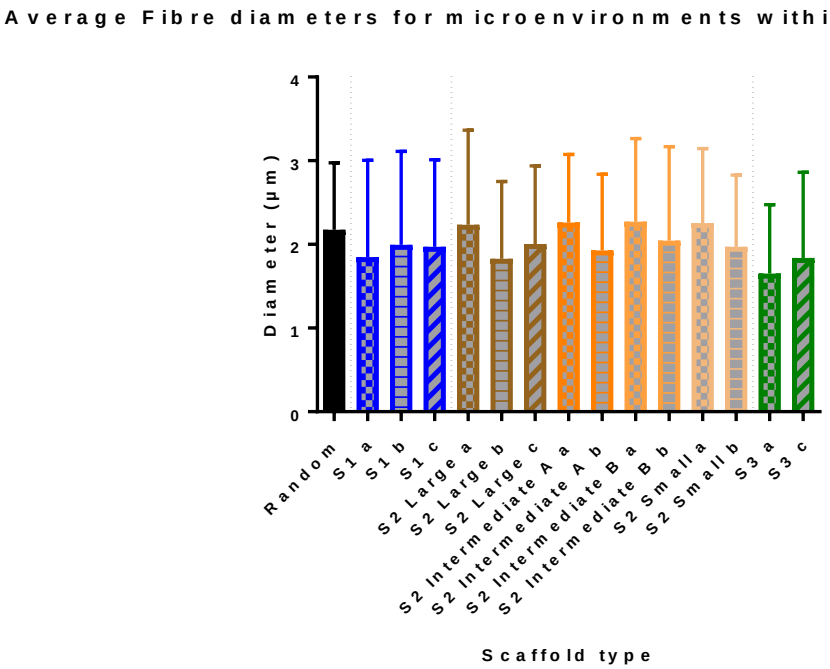

Figure 6.3.2 B: Fibre diameters for random scaffold and scaffolds 1-3 using the second approach method. Mean diameter with standard deviation shown. S1=scaffold 1, S2= scaffold 2, S3=scaffold 3. a=bottom of the well, b=side of the well, c=top surface. Not all samples pass normality test therefore statistical analysis was undertaken with Krustal-Wallis where there was significant difference at P<0.0001 and Dunn's multiple comparisons significant differences are indicated in Table A1 E. A graph of some of this date was included in a publication, Paterson et al 2017.

Fibre orientation

The first attempt at analysing fibre properties showed how complex alignment was to quantify mathematically, therefore this problem required careful consideration. As it was expected to take several revisions of the method until an appropriate and reliable method was optimised, I decided to reduce the number of samples to only use scaffold 2's largest microfeature as a test

subject for this optimisation. This microenvironment was chosen as this is the largest microfeature (Figure 6.1 C) and SEM images visibly showed a change in alignment in the three sites (Figure 4.3.3 B).

For alignment analysis three post data collection methods were tested to optimise the method to characterise fibre orientations. These values are collated from a vertical line measuring from right to left as the fibre crosses the vertical line as shown in Figure 4.3.3 C. Within this data there are negative values as the horizontal line is 0 with values below being positive while values above are negative. The first method (red) included utilising a formula to convert the angles to be positive and then taking the average from each value per image. The average was then removed from all data points to produce the distribution around the average value for each image. When considering this method using the formula to convert negative values to positive, it was potentially not the most appropriate way to handle these values. Therefore, in order to ensure all values are positive and comparable while maintaining the integrity of the data, 90 is added to all values in effect rotating the location of the 0 line. This is utilised for both the second (yellow) and third (green) methods. I also considered whether the mean was the most appropriate manner of obtaining a value to produce a distribution for each image. This was so should the majority of fibres be aligned but there were one or two fibres orientated differently than the majority this would greatly affect the mean value and therefore show higher distribution for that image. Therefore other ways of identifying a central value to calculate the distribution was required. For the yellow method the mode is taken away from the measurements per image while the green method takes the median value and then also plots the absolute values. The use of the mode as a method was rejected as not all data sets have a mode and therefore the analysis fails, whereas the median value can always be clearly identified. Therefore the green method was chosen as the most appropriate method to characterise and compare the orientations present within fibrous scaffolds.

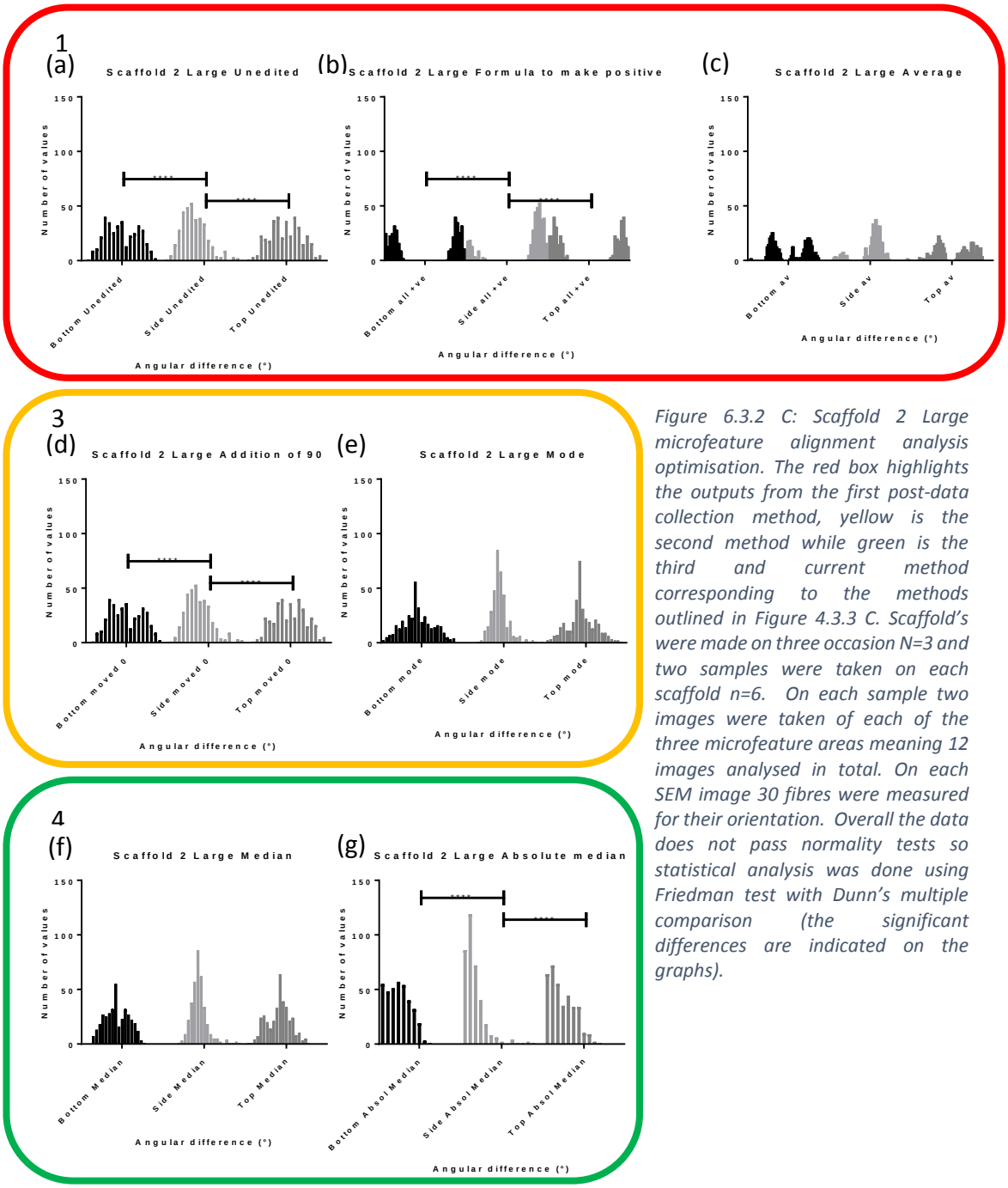

Figure 6.3.2 C: Scaffold 2 Large microfeature alignment analysis optimisation. The red box highlights the outputs from the first post-data collection method, yellow is the second method while green is the third and current method corresponding to the methods outlined in Figure 4.3.3 C. Scaffold's were made on three occasion N=3 and two samples were taken on each scaffold n=6. On each sample two images were taken of each of the three microfeature areas meaning 12 images analysed in total. On each SEM image 30 fibres were measured for their orientation. Overall the data does not pass normality tests so statistical analysis was done using Friedman test with Dunn's multiple comparison (the significant differences are indicated on the graphs).

Figure 6.3.2 C shows the histograms of each of the areas of scaffold 2 largest microfeature. From the histograms (b) the side of the well has less measurements at a larger angle difference from the median value than either (a or c) the bottom or top surface. Therefore the side of the well has more fibre alignment and the bottom and top surface are more randomly orientated. This is particularly evident in (g) which is the results utilising the chosen method (third in green). This data was finally present as absolute value to highlight the difference between the areas further. Figure 6.3.2 D shows individual graphs for each of the areas that is shown in the one graph of

Figure 6.3.2 C (g). These graphs further show the clear difference between the three areas and that the side fibres are more aligned than the bottom or top surface.

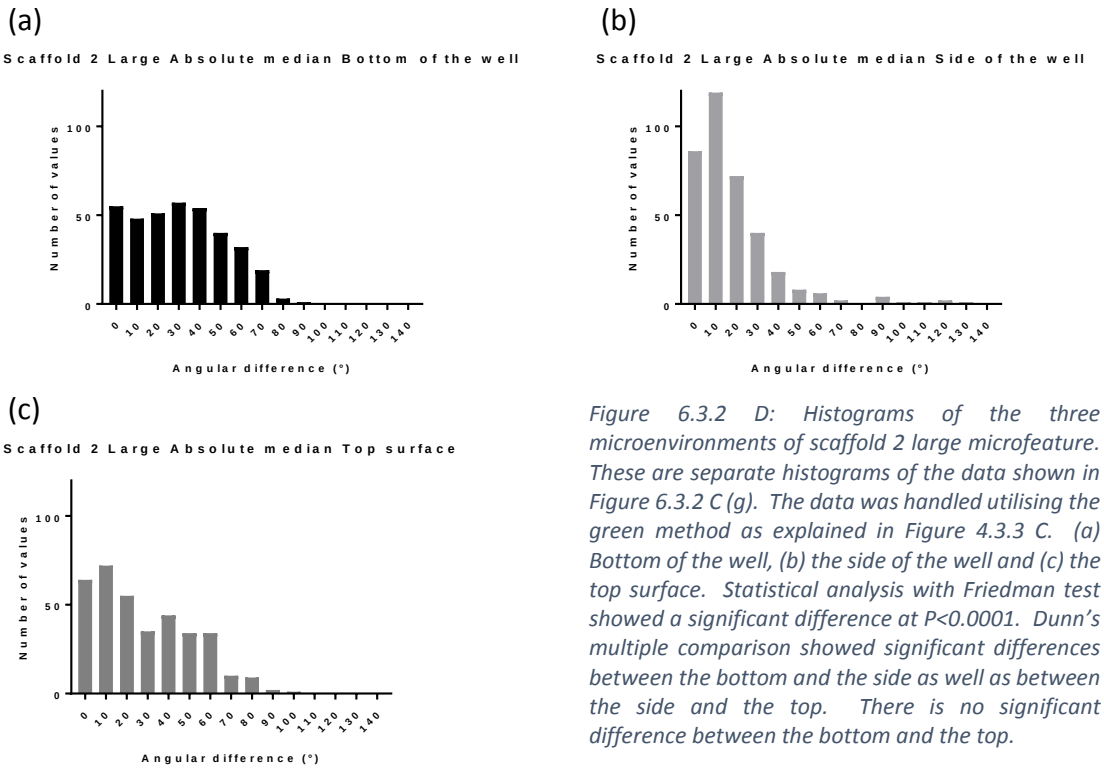

Figure 6.3.2 D: Histograms of the three microenvironments of scaffold 2 large microfeature. These are separate histograms of the data shown in Figure 6.3.2 C (g). The data was handled utilising the green method as explained in Figure 4.3.3 C. (a) Bottom of the well, (b) the side of the well and (c) the top surface. Statistical analysis with Friedman test showed a significant difference at P<0.0001. Dunn's multiple comparison showed significant differences between the bottom and the side as well as between the side and the top. There is no significant difference between the bottom and the top.

6.3.3 Comparing Manual and Software analysis of fibre properties

Once a method had been optimised to manually characterise the fibres within the electrospun scaffolds via Image J, Figure 4.3.3 C method 3 (green), I then wanted to investigate how rigorous and reliable this method was. In order to investigate this, the scaffolds were also analysed by an automatic system, Fibremetric software from Lambda, 4.3.4. With thanks to Lambda and Charlotte Worthy for providing access to their system for this trial. For this comparison two of the scaffolds were imaged on the Phenom SEM and then analysed by Fibremetric software. The same samples from two of the three scaffolds were used for both the manual and software analysis, however separate SEM images were taken for the two analyses. Two samples were imaged from the first scaffold and one sample was imaged from the second scaffold due to time constraints. On each sample two microfeatures were imaged, Figure 6.3.3 A.

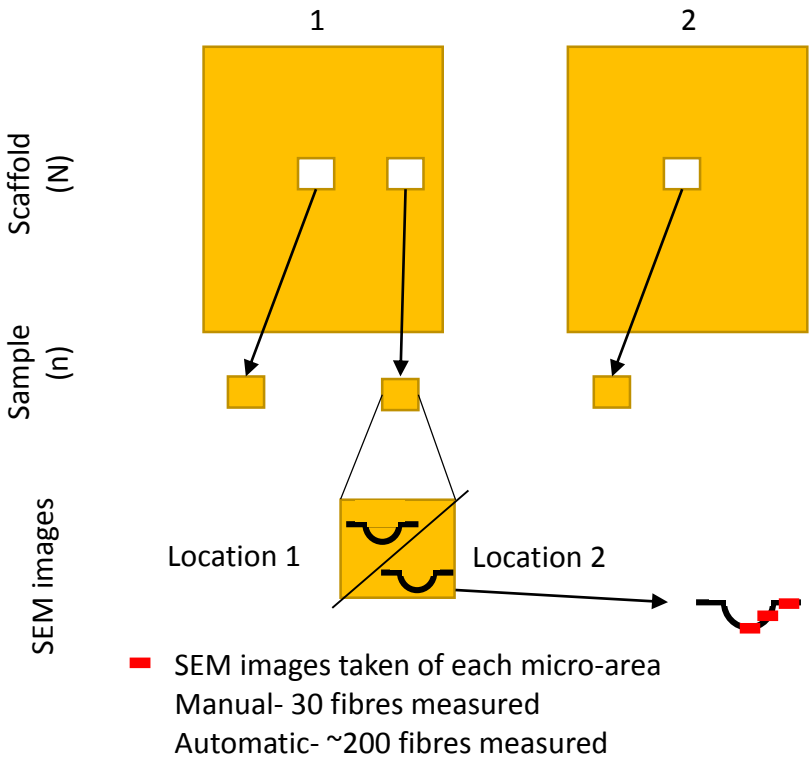

Figure 6.3.3 A: Schematic of the source of data for comparison between manual and software analysis. Two scaffolds made (N=2) with two samples taken from the first scaffold and one sample from the second scaffold (n=3). One each sample two microfeatures were imaged.

Fibre diameter

Figure 6.3.3 B compares the fibre diameter analysis (manual and software) of scaffold 2's largest microfeature. The software analysis gave a mean diameter of a= 3.5 µm, b=3.7 µm and c=3.5 µm. Whereas manual analysis gave a mean diameter of a=2.2 µm, b=1.6 µm and c=1.9 µm, Figure 6.3.3 B. The statistical analysis showed that there is only a significant difference between a and b of the manual analysis.

(a)

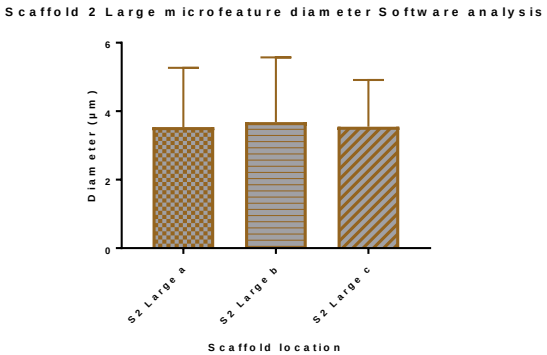

Software Diameter	S2 Large a	S2 Large b	S2 Large c
Mean	3.5	3.7	3.6
Std. Deviation	1.7	1.9	1.4
Std. Error of Mean	0.1	0.1	0.0

(b)

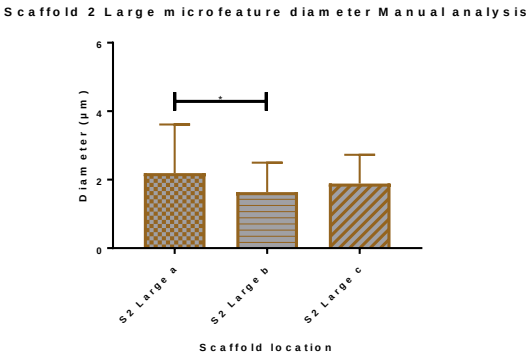

Manual Diameter	S2 Large a	S2 Large b	S2 Large c
Mean	2.2	1.6	1.9
Std. Deviation	1.4	0.9	0.8
Std. Error of Mean	0.2	0.1	0.1

Figure 6.3.3 B: Fibre diameter analysis of Scaffold 2 largest microfeature. a) Analysis by the software and b) analysis by the manual method, 4.3.3 second approach. Neither data set passed normality tests so statistical analysis was done using Kruskal-Wallis test where software analysis was not significantly different but manual analysis was at P=0.0332. Dunn's multiple comparison significant differences are indicated on the graphs.

Figure 6.3.3 C compares each areas analysis by the software and the manual method. For each area there is a significant difference between the two analysis methods. Generally, the software produces a mean diameter that is double that of the manual method.

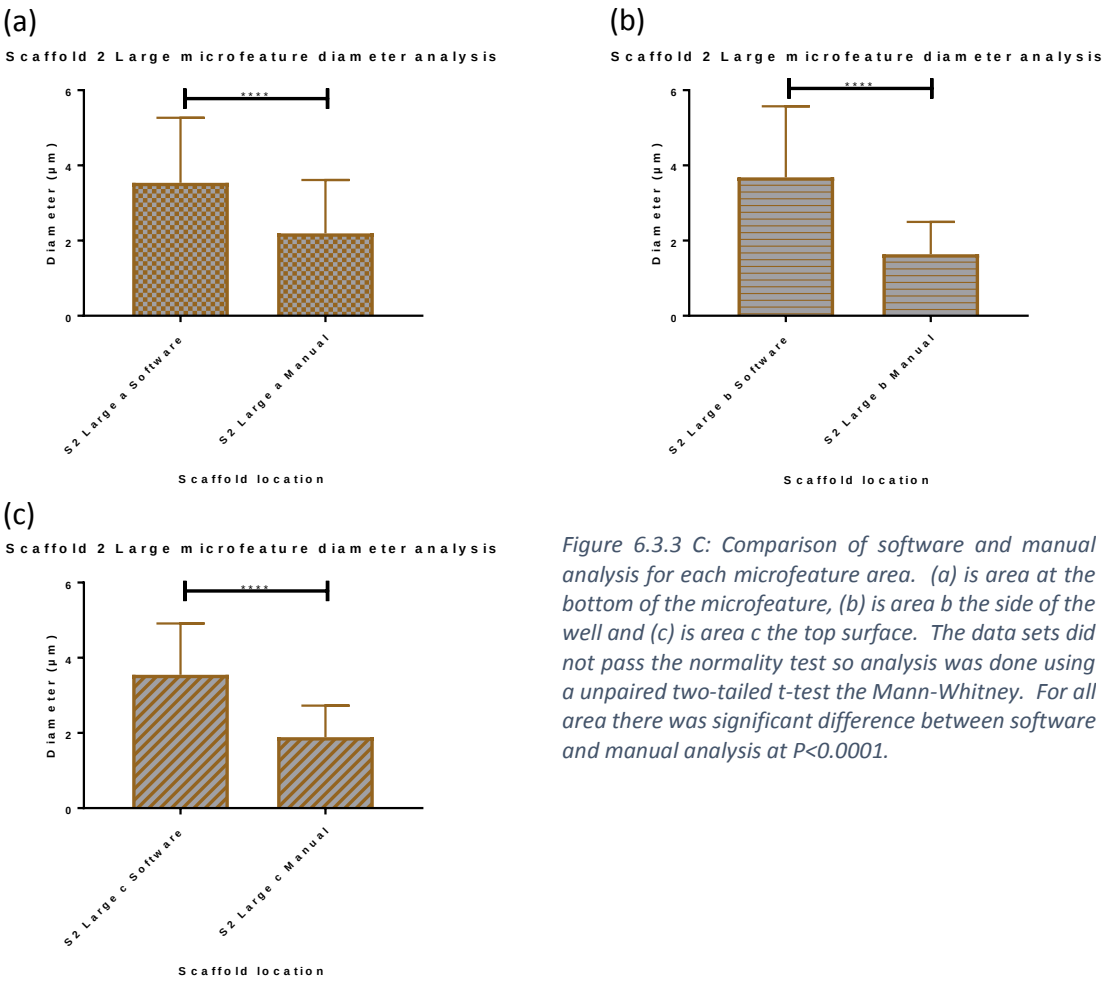

Figure 6.3.3 C: Comparison of software and manual analysis for each microfeature area. (a) is area at the bottom of the microfeature, (b) is area b the side of the well and (c) is area c the top surface. The data sets did not pass the normality test so analysis was done using a unpaired two-tailed t-test the Mann-Whitney. For all area there was significant difference between software and manual analysis at P<0.0001.

Fibre orientation

Alignment analysis is shown in Figure 6.3.3 D. The raw data as collected by the software shows no difference in the alignment present in any of the microfeature areas by eye from the histograms. Tables with mean values for each microenvironment show this is due to the data being a mixture if positive and negative values. However, with the post-data analysis Figure 4.3.3 C green method (note: this software produces orientation values in radius so they are first converted to degrees) a visible difference is identified within the graphs as b (the side of the well) had a narrower distribution from the median than either a or c so b shows more aligned. Both data sets were analysed by the Krustal Wallis test and a significant difference between both a and b and b and c was seen with or without the post-data collection method. The mean values also reflect that area b had more alignment than a or c. However software analysis produces high values than the manual analysis. For software and manual analysis areas a and c show

average angle difference from the median above 30° ±20° but software analysis producing values nearer 40° and manual analysis nearer 30°. For area b manual analysis produced 18° ±21° while software analysis produced 25° ±25°. Therefore both methods can be utilised to analyse the level or alignment but they cannot necessarily be compared to each other.

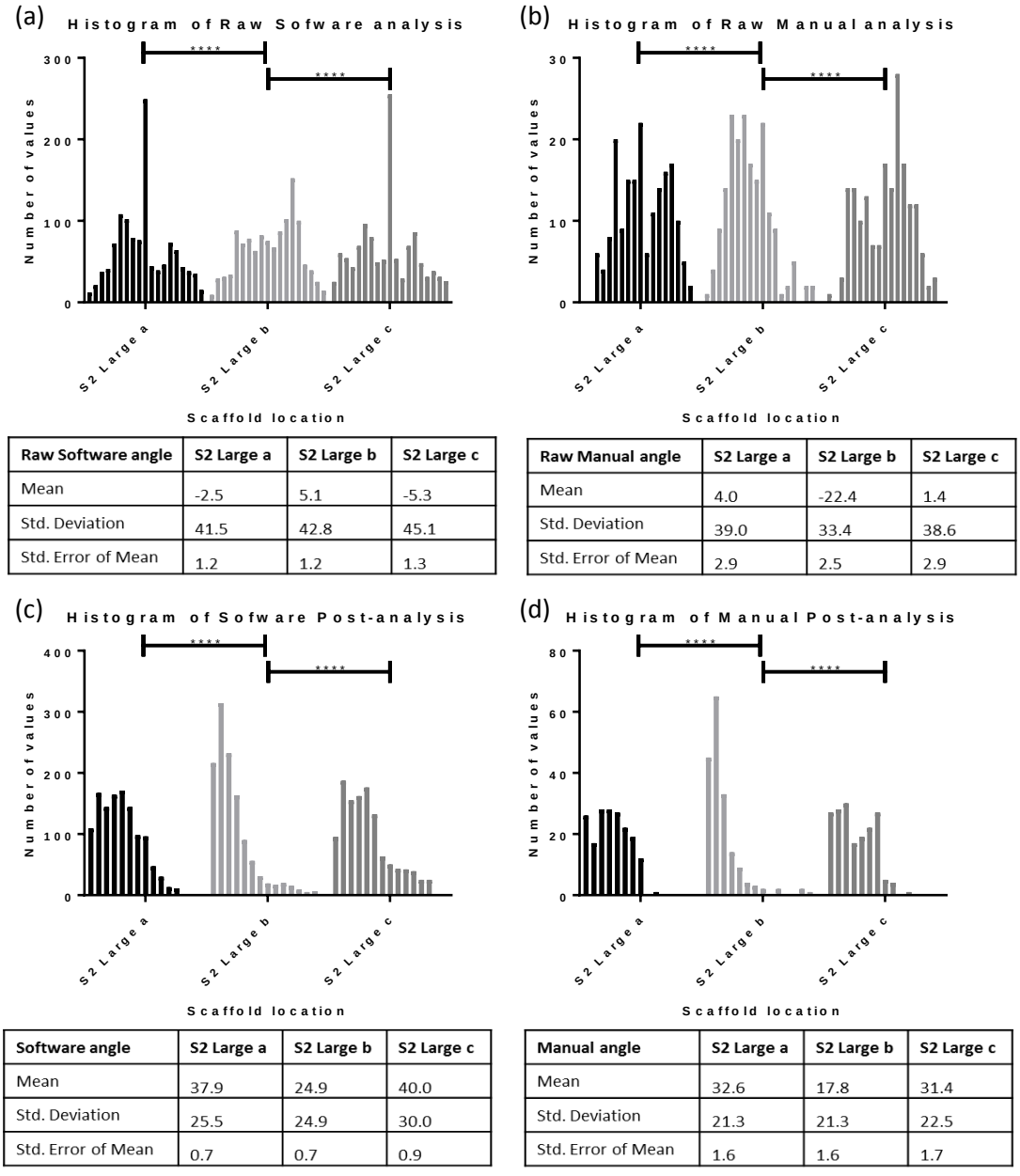

Raw Software angle	S2 Large a	S2 Large b	S2 Large c
Mean	-2.5	5.1	-5.3
Std. Deviation	41.5	42.8	45.1
Std. Error of Mean	1.2	1.2	1.3

Raw Manual angle	S2 Large a	S2 Large b	S2 Large c
Mean	4.0	-22.4	1.4
Std. Deviation	39.0	33.4	38.6
Std. Error of Mean	2.9	2.5	2.9

Software angle	S2 Large a	S2 Large b	S2 Large c
Mean	37.9	24.9	40.0
Std. Deviation	25.5	24.9	30.0
Std. Error of Mean	0.7	0.7	0.9

Manual angle	S2 Large a	S2 Large b	S2 Large c
Mean	32.6	17.8	31.4
Std. Deviation	21.3	21.3	22.5
Std. Error of Mean	1.6	1.6	1.7

Figure 6.3.3 D: Histograms of the distribution of angles from the median value for the three microenvironments. (a) Results from the software analysis unedited and (b) results from the manual method. a=bottom of the well, b=side of the well and c= the top surface. None of the data sets passes normality test so statistical analysis was done using Kruskal-Wallis where all data set were significantly different at P<0.0001. Multiple comparisons were done using Dunn's multiple comparisons and significant differences are indicated on the graphs. Showing for each analysis method the side was significantly different to the bottom and top surface. Data collated from the analysis of six images from two scaffolds. N=2 n=3.

6.4 Optimisation for aligned scaffolds using Sigma PCL and a DCM/DMF solvent system

Once the method for analysing fibre orientation had been optimised the project then turned towards investigating how cells would respond to the random and aligned fibre organisations. However, I suspected that investigating the impact of random and aligned fibres on cells utilising scaffold 2, where both of these topologies are within a small area on one scaffold, would prove problematic to separate the responses to the two topologies. Therefore, for the initial investigation it would be beneficial to have the two topologies on separate scaffolds, so I decided to manufacture separate scaffolds for random and aligned fibres.

Random scaffolds can be manufactured as shown in Figure 6.1 A. Initially the rig system had a set up for spinning aligned fibres which included a small drum rotated by a Dremel (Figure 4.4 A), however no samples could be manufactured using this set up and therefore the manufacture of aligned scaffolds required optimisation. As random scaffolds had been manufactured with diameter of 2.2 ±0.8 µm it was aimed to produce aligned scaffolds with the same fibre diameters of 2 ±1 µm.

6.4.1 Optimisation of electrospinning rig: Including a large drum

Initially a larger drum was commissioned, Figure 4.4 A. I began by introducing a larger drum as the sample size produced per spinning session would be much greater and therefore more practical for characterisation and investigating cell responses. This set up did manufacture a scaffold, Figure 6.4.1 A, which by eye had fibres more aligned than random scaffold, Figure 6.1 A. However the method was not safe to use due to the utilisation of a Dremel to rotate the drum and the instability of this rotating drum. The project also aimed for a higher degree of alignment to be able to compare the two extremes of random and aligned scaffold in this first investigation.

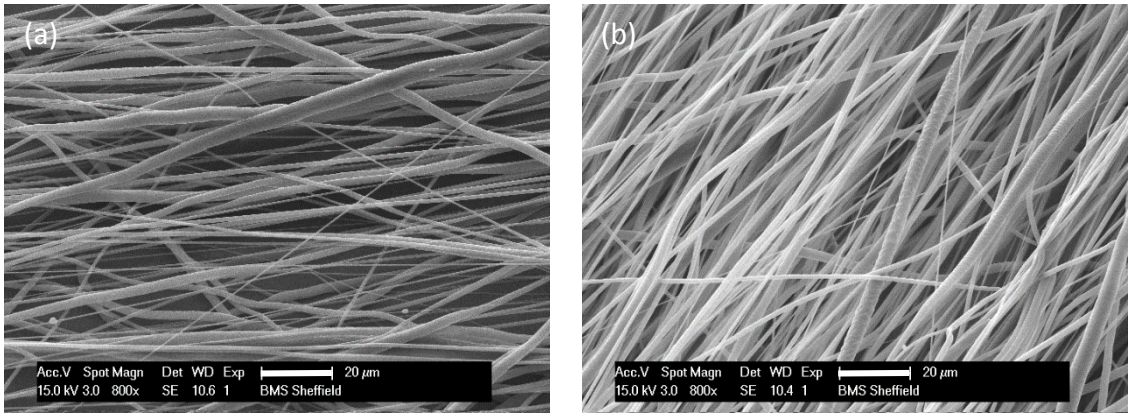

Figure 6.4.1 A: Samples of aligned fibres made on the original electrospinning rig with the large drum. (a) sample 1 made with 0.6ml 10% PCL at 25cm 17Kv, 2.5 infuse rate with a rotation speed off ~4,000rpm (b) sample 2 made with 1.5ml 10% PCL at 25cm 17Kv, 2.5 infuse rate with a rotation speed off ~4,000rpm. 10% Sigma PCL in DCM/DMF. Scale bar 20µm.

6.4.2 Optimisation of electrospinning rig: Upgraded rig

To improve the safety and longevity of the rig and manufacture of aligned scaffold a new rig was designed, (Figure 4.4.1 A). This upgraded rig included the drum being fixed within the rig and a motor to rotate the drum rather than a Dremel. Aligned scaffolds were manufactured at a range of parameters, in Section 4.4.1. However it could be easily seen by eye that the fibres were not as aligned as previous samples, Figure 6.4.1 A.

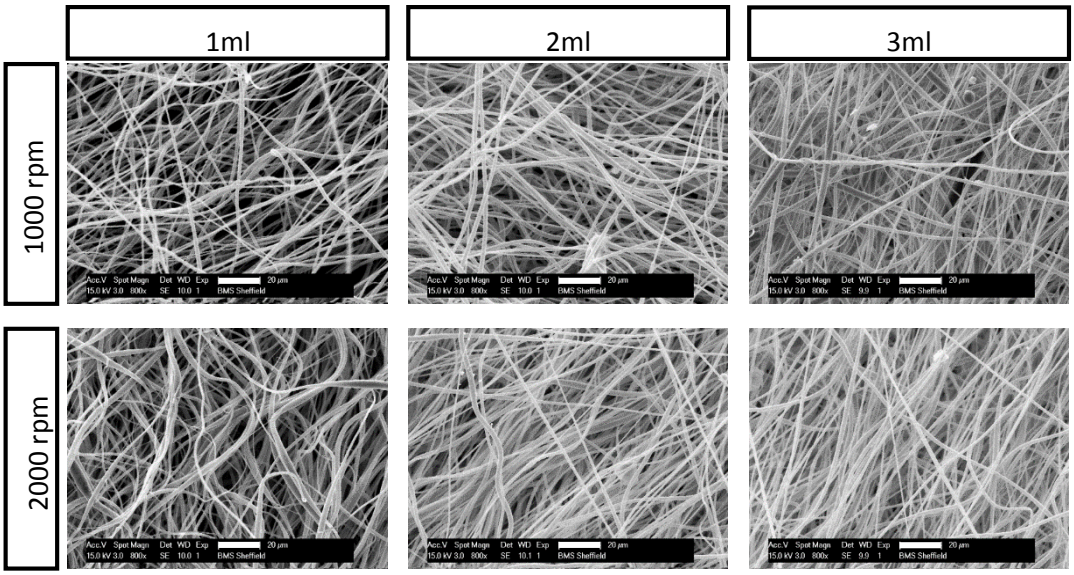

Figure 6.4.2 B: SEM images of the aligned scaffold made on the upgraded electrospinning rig. Six conditions were considered including 1, 2 and 3ml polymer solution and rotation speeds of 1,000 rpm and 2,000 rpm. All six scaffolds were made with 10% PCL at a distance of 24.5cm at 17Kv with an infuse rate of 2.6. 10% Sigma PCL in DCM/DMF. Scale bar 20µm.

6.5 Polymer Source and Solvent System impact fibre properties (Placement at The Electrospinning Company)

While the optimisation of the upgraded rig was being investigated an opportunity arose to apply for additional funding from Mede Innovation to fund a short placement of two weeks. The Electrospinning Company (TEC) is a commercial manufacturer of electrospun scaffolds and so I arranged to visit their facilities with the aim to optimise the manufacture of random and aligned PCL scaffolds.

The Electrospinning Company utilised an alternative source of PCL, Corbion PC12, due to its Good manufacturing practice (GMP) grade status. Therefore, initially a comparison between Sigma and Corbion PCL was done using the previously utilised parameters 10 wt% in DCM/DMF, Figure 6.5 A.

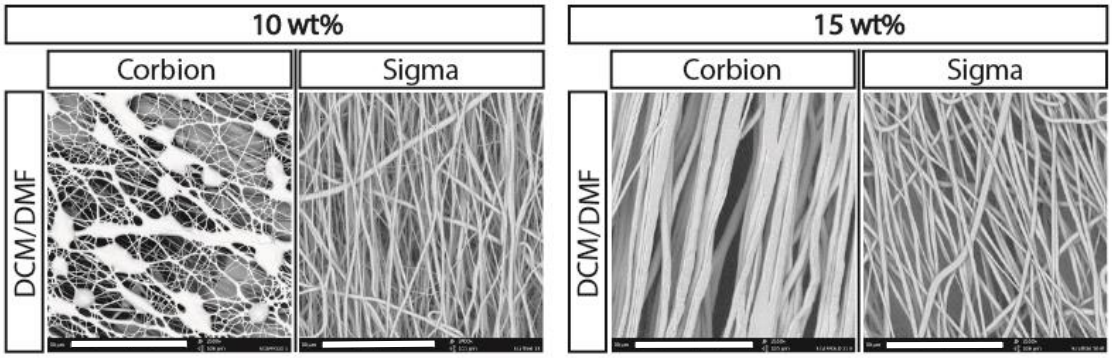

Figure 6.5 A: Comparison of Corbion and Sigma PCl. Scaffolds were made at 10 wt%, the original method, to compare the new polymer Corbion to the previously used Sigma. Then scaffold were made a 15 wt%. Samples were spun with the following parameters motion speed 10 mm/s, voltage +19 kV (needle) and -4 kV (collector), flow rate 2.5 ml/hr, 9 cm diameter drum, distance 20 cm, 2,500 rpm. Scale bar 50 µm.

Corbion PCL scaffold had beaded fibres at 10 wt% so critical entanglement concentration was not reached which is required to produce smooth fibres [163]. Scaffolds were then manufactured at 15 wt% where both polymers produced smooth fibres. Consequently moving forward scaffolds were manufactured at 15 wt%.

The placement then turned to optimising the method. I decided to compare PCL polymer sources (Sigma and Corbion), three solvent systems (DCM/DMF, HFIP and Chloroform) and collection onto a fast or slow rotation drum (random and aligned), Figure 6.5 B. This comparison was done with N=3 scaffold with two samples imaged from each, n=6, Figure 6.5 C. In order to identify which method produces the scaffolds with optimal properties for random and aligned fibre orientations, SEM images and fibre analysis were undertaken as using the method described in 4.3.3 Second approach using software collected data.

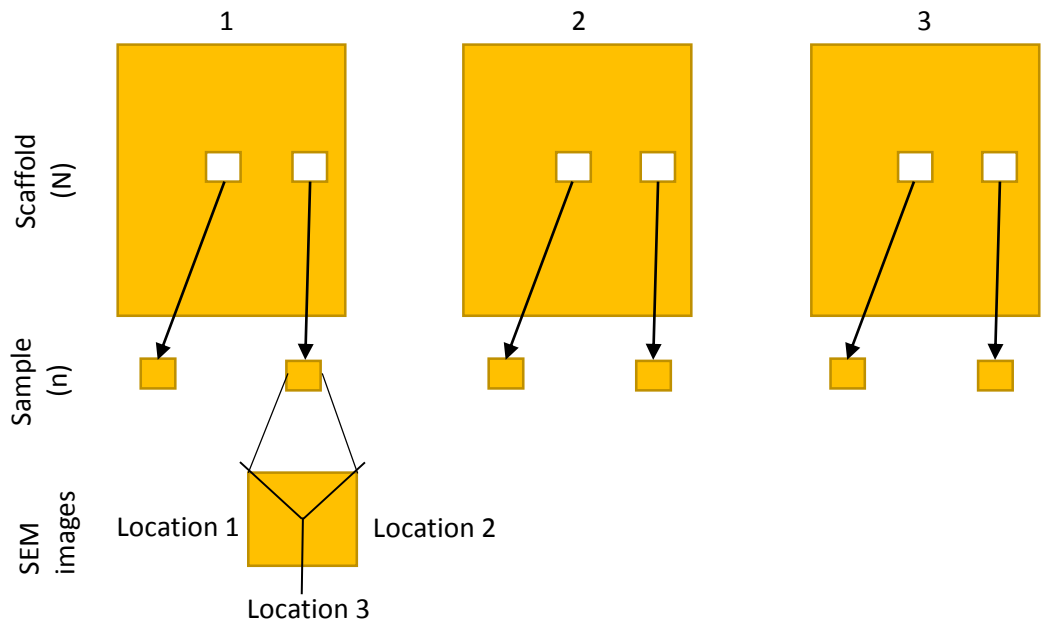

Figure 6.5 C: Schematic of the source of data for scaffold analysis of samples comparing polymer source and solvent system. Scaffolds were manufactured in triplicate (N=3) from which two samples were taken (n=6) and on each sample three SEM images were taken and provided 455 measurements for each sample.

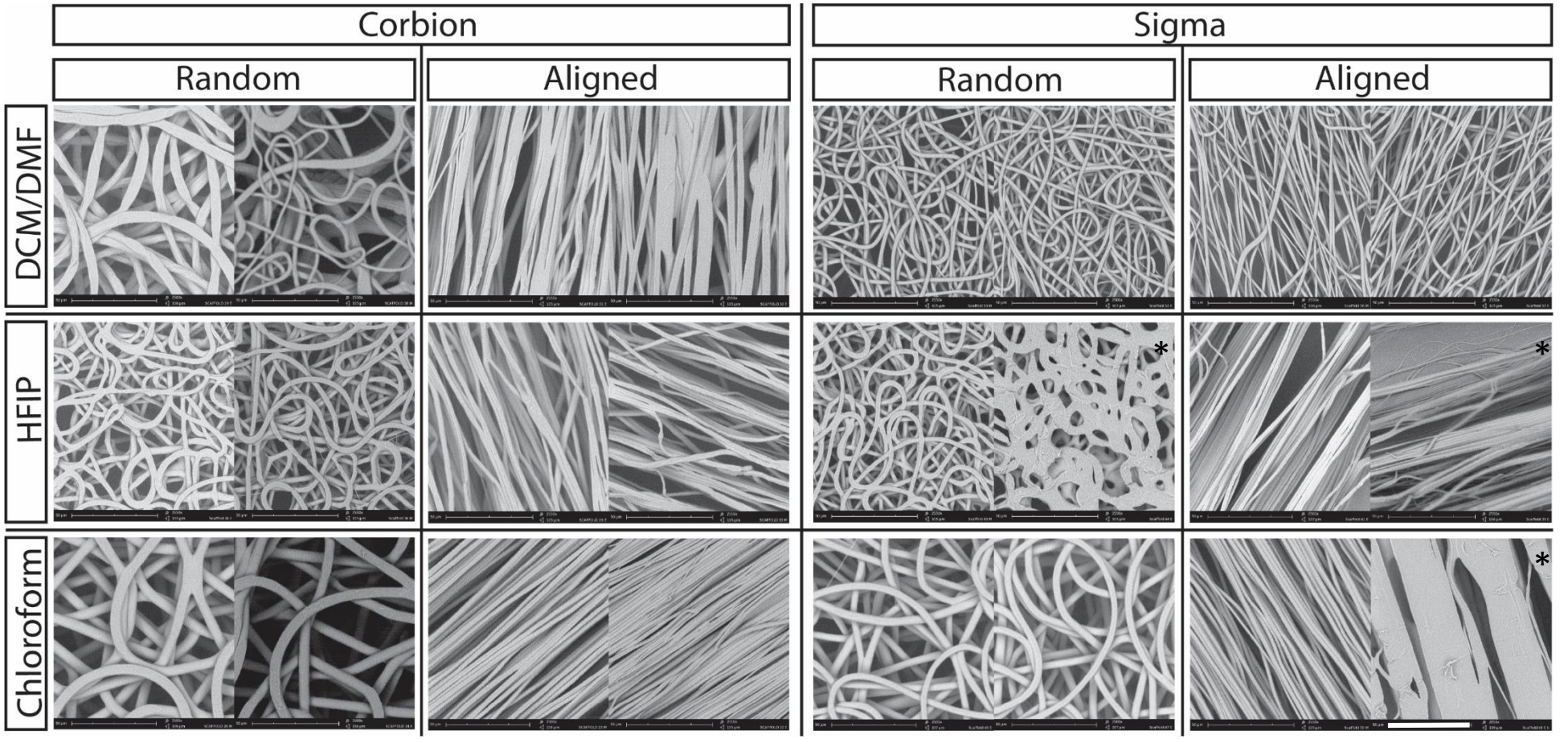

*Figure 6.5 B: Comparison of polymers Corbion and Sigma, solvents DCM/DMF, HFIP and Chloroform and collection method for producing random and aligned fibre organisations. Corbion/Sigma PCL 15 wt% in DCM/DMF, HFIP or chloroform. Scaffold were manufactured at the following parameters voltage +16 kV(needle) and -4 kV (collector), flow rate 1.6 ml/hr, 9 cm diameter drum, distance 23 cm, 2,500 rpm. For each method two scaffolds images are shown and * indicates variability between scaffolds. N=3, n=6. Scale bar 50µm.*

Fibremetric analysis of fibre diameters are shown in Figure 6.5 D and in appendix 1 details of mean diameter and standard deviations can be found in Table A1 F. When comparing these scaffolds Sigma has more variability between samples (indicated by *). The diameter is affected by polymer type, solvent system and collection method, Figure 6.5 D. When identifying the optimal method first the polymer was considered. The initial comparison at 10 wt% showed that these two polymer sources have different properties. Analysis of fibre diameters, Figure 6.5 D, showed that polymer source impacted fibres; generally Sigma produces thinner fibres than Corbion. Considering that PC12 is medical grade whilst Sigma is not, and as these two polymers have such different fibre properties, it is important to begin using medical grade as early as possible to avoid having to repeat experiments should these scaffolds be of interest for a medical directed project. This was important in this case as random and aligned scaffolds could be of use for several different situations and could be translated for use in other projects.

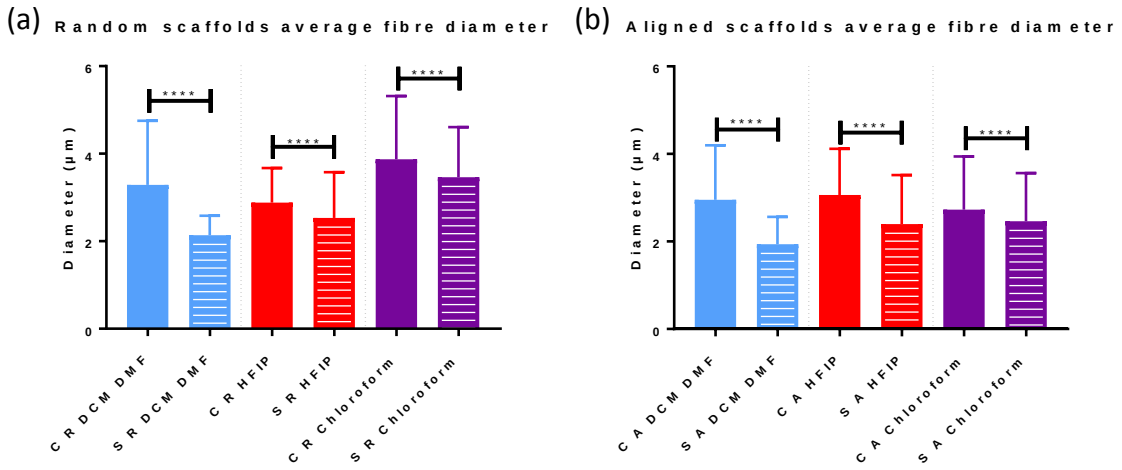

Figure 6.5 D: Fibre diameter analysis utilising Fibremetric software. Mean with standard distribution displayed. C= Corbion (PC12) S=Sigma R=Random A= Aligned. Statistical analysis done using Krustal-wallis with Dunn's multiple comparisons as all data did not pass normality test. With thanks to Dr Sebastian Spain.

To identify which solvent would produce the best set of random and aligned scaffolds, fibre diameter analysis and SEM images were considered. Both DCM/DMF and HFIP provided scaffolds with 0.3 µm and 0.2 µm difference in mean diameter between random and aligned respectively while chloroform showed a difference of 1.2 µm. Thus, for our purpose, DCM/DMF and HFIP were identified as more suitable solvent systems than chloroform as there is less difference in the mean diameter between the random and aligned scaffolds. This is important as the project aimed to have as many parameters as similar as possible between random and aligned scaffolds so only the fibre orientation was altered. Also for chloroform a gas shield had been utilised which was not available at the Dental School and may cause issues with replicating this method. DCM/DMF was discounted as it previously was not successful in producing aligned fibres on the rig at the Dental School and some variation was seen between scaffolds, Figure 6.5 B. Therefore the optimal method was chosen as 15 wt% PC12 in HFIP. Overall this comparison also showed that the collection method itself impacts fibre properties in that fast rotation thins the fibres compared to slow rotation.

6.5.1 Comparing Sigma PCL and Corbion PC12 properties

As the two polymers produced such different fibres at 10 wt% in Figure 6.5 A, the two sources of PCL were suspected to have different characteristics. Therefore, I wanted to investigate how these polymers differ so the polymers were investigated for their molecular weight by GPC, in 4.3.7. This analysis showed that the two polymers have different MWs 22 KD and 12 KD, Sigma and PC12 respectively, and different polydispersity, 1.69 and 2.03, Figure 6.5.1 A. Sigma states the Mn of the polymer as an average of 80,000 while this analysis showed the Mn as 130,982 which is higher than the stated value. Further sampling from different lots of the polymer could show how much variety is present within the product and if an average of 80,000 is produced. Corbion does not state a Mn value for its PCL source.

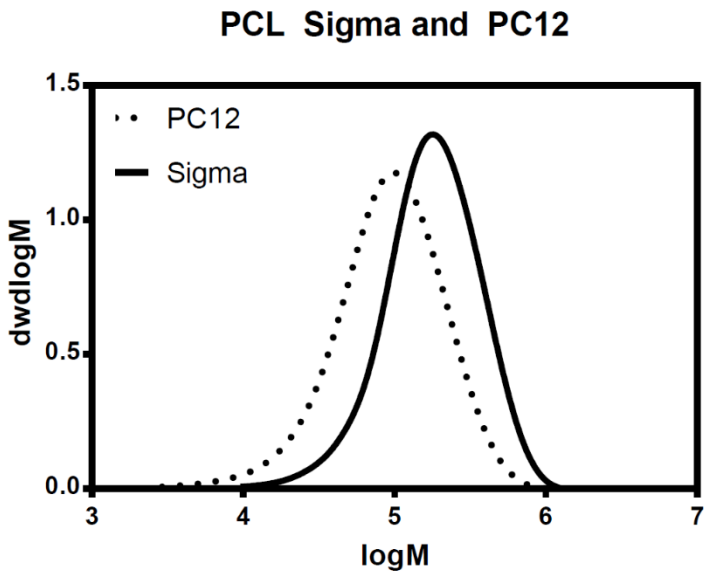

Polymer	Mn	Mw	PD
Sigma	130982	220758	1.69
PC12	61057	124007	2.03

Figure 6.5.1 A: GPC analysis of PCL from Sigma and Corbion (PC12).

While the polymer information is significant, for electrospinning the properties of the solution are more important to how the electrospinning process works and the properties of the fibres produced. The solutions were subsequently tested for their viscosity using a rheometer, method described in 4.3.6. Figure 6.5.1 B shows that changing the polymer and solvent affect the viscosity of the solution.

At 10 wt% the solutions have a lower viscosity. Corbion does not produce a smooth line indicating the solution is not at critical entanglement concertation. Corbion at 15 wt% in DCM/DMF and chloroform have very similar profiles while Sigma at 15 wt% in DCM DMF is slightly more viscous showing the impact of the different properties of the polymer sources on the electrospinning process and fibre properties. Corbion at 15 wt% in HFIP is the most viscous of the solutions.

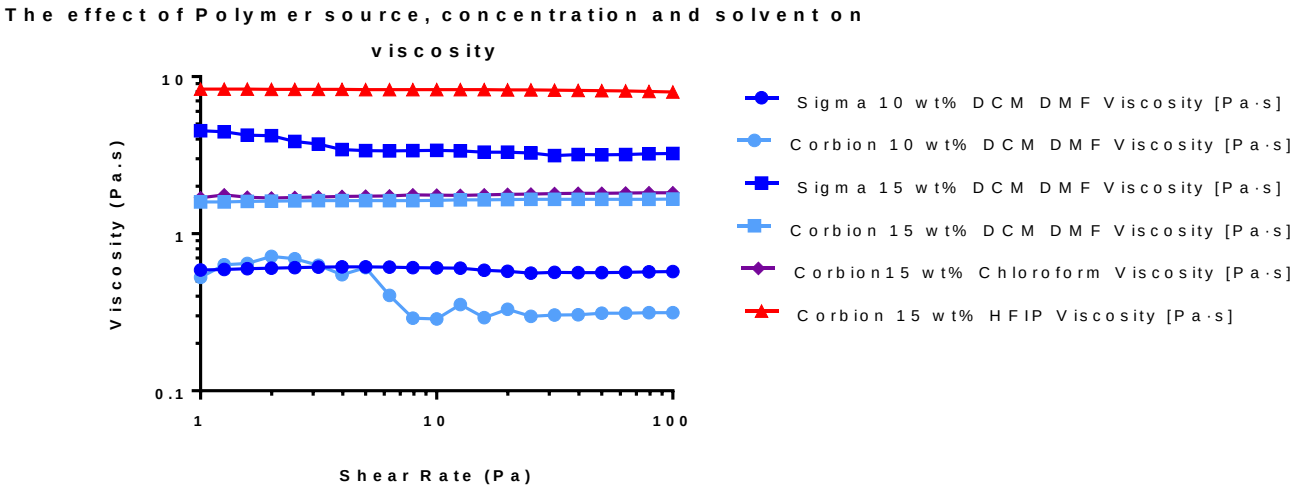

Figure 6.5.1 B: Rheology analysis of the solutions made with either Sigma or Corbion PCL at 10 or 15 wt% in DCM/DMf HFIP or chloroform. Method described in 4.3.6 Rheology.

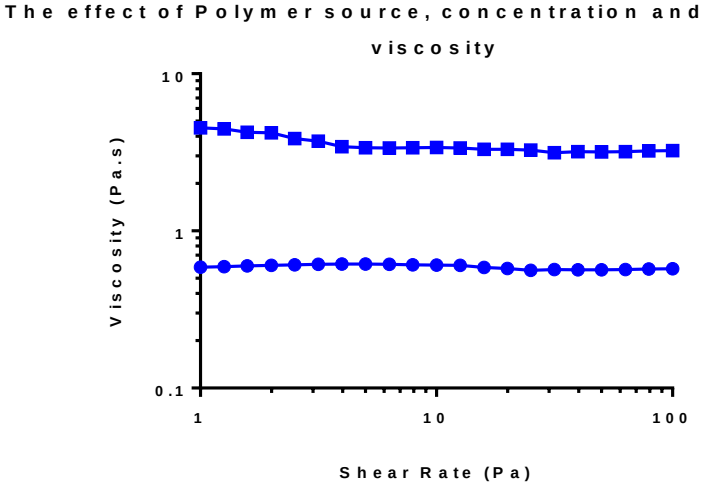

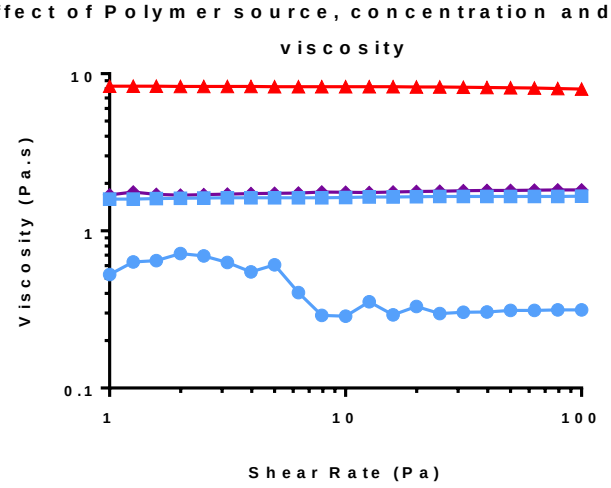

6.5.2 Random and aligned scaffolds characterisation

From the comparison, the identified method to manufacture random and aligned PCL scaffolds was Corbion (PC12) PCL in HFIP at 15 wt%. At The Electrospinning Company two sheets of both random and aligned scaffolds were manufactured for use in investigating cell responses to this topology, Figure 6.5.2 A.

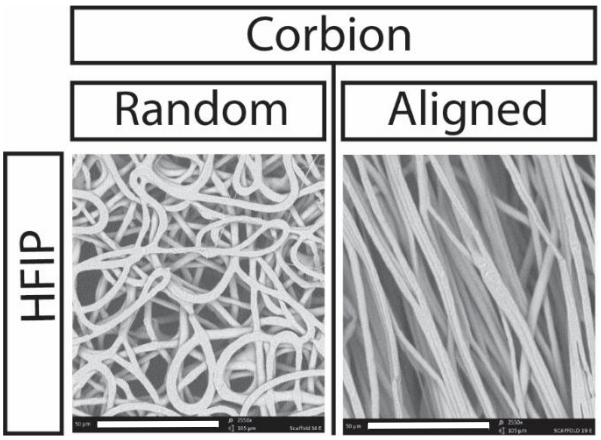

Figure 6.5.2 A: Scaffolds made with 15 wt% Corbion (PC12) in HFIP.

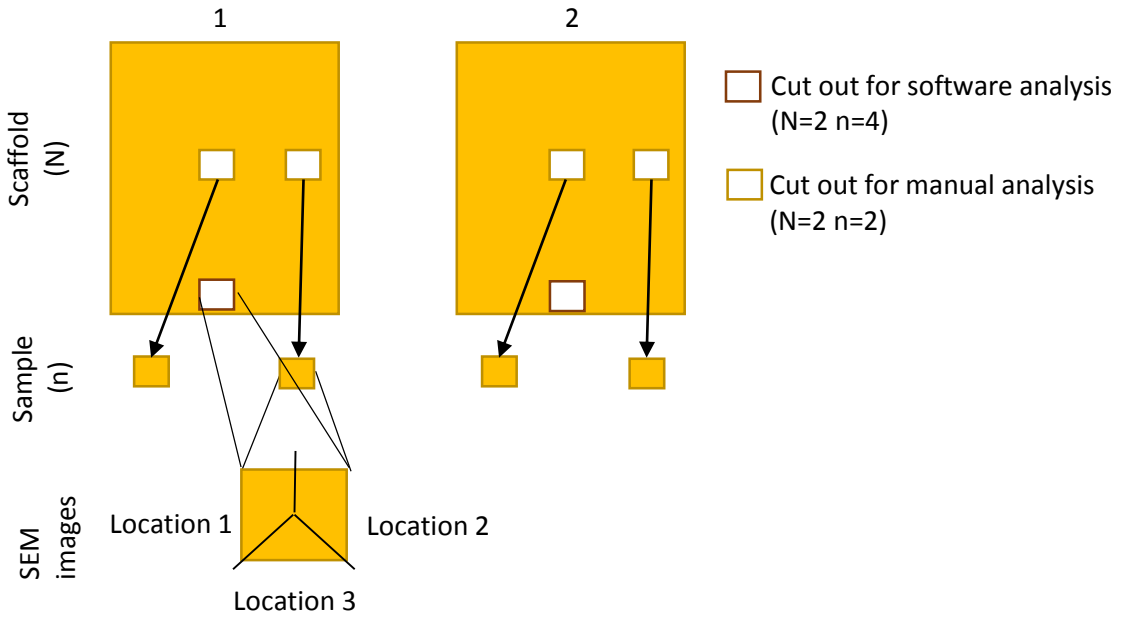

Figure 6.5.2 B: Schematic of the source of data for scaffold analysis of scaffold made at The Electrospinning Company. Comparing software and manual analysis of fibre diameter and fibre alignment. Scaffolds were manufactured twice from which one sample was taken for software analysis which included taking three SEM images which provided 449 measurements for each sample. For manual analysis two samples were taken (middle and side) on which three images were taken and 10 fibres measured for diameter and alignment. For both analysis methods alignment measurements were processes as described in 4.3.3 Second approach.

As the comparison of the manual and software analysis of scaffolds 2 largest microfeatures showed a difference in the diameter analysis, I considered it was important to compare the analysis for scaffolds made at TEC. For the two sheets of random and aligned scaffolds, one sample taken for software analysis and two samples (middle and side) were taken for SEM imaging and manual analysis, Figure 6.5.2 B.

The two analysis methods for diameter are compared in Figure 6.5.2 C. For random scaffold the manual analysis showed a range of fibres between 3.6-4 μm while software analysis showed a range of 2.8-4 μm with a mean of 3.8 and 3.4 respectively. For aligned scaffold the manual analysis showed a range of fibres between 2.4-3.6 μm and software analysis showed a range of 2-3.4 μm with a mean of 3 and 2.8 respectively. Therefore overall these two methods showed similar fibre profiles. For this comparison the two analysis methods show less inconsistency as seen previously, Figure 6.3.3 C.

Figure 6.5.2 D shows the analysis of alignment. There was a large difference in the angular distribution between manual and software data collection. For random scaffold the mean angular distribution from the median is 29.9° when analysed via the manual method and 44.2° from the software. However there is a striking difference for aligned scaffold with 5.9° from manual analysis and 30° from software analysis. This discrepancy between these two methods was not seen in the analysis of scaffold 2 large microfeature, Section 6.3.3.

(a)

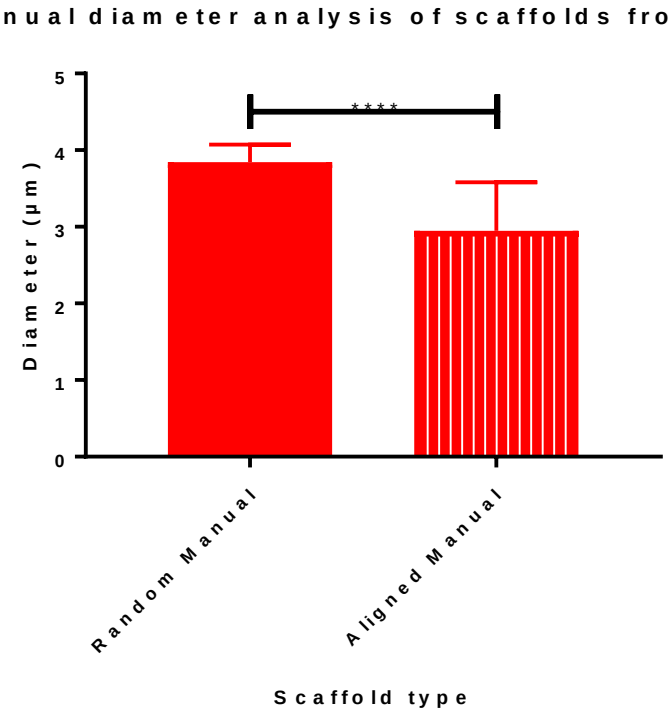

	Random Manual	Aligned Manual
Mean	3.8	3.0
Std. Deviation	0.2	0.6
Std. Error of Mean	0.0	0.1

(b)

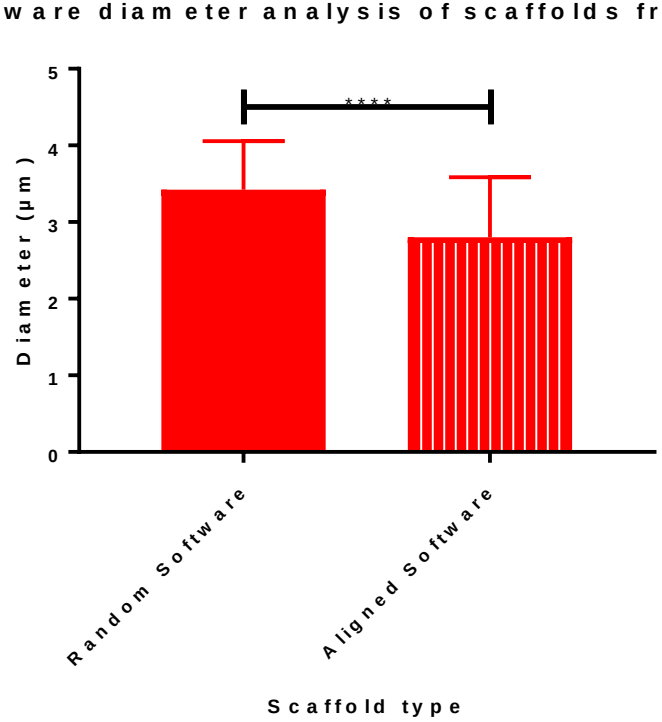

	Random Software	Aligned Software
Mean	3.4	2.8
Std. Deviation	0.6	0.8
Std. Error of Mean	0.0	0.0

Figure 6.5.2 C: Comparison of manual and software fibre diameter analysis for the two sheets of random and aligned scaffold made at The Electrospinning Company. Utilising 15 wt% PC12 with HFIP. (a) Manual analysis and (b) software analysis. Not all data sets pass normality test. Mann-Whitney analysis showed significant different between random and aligned scaffold for both manual and software analysis

(a)

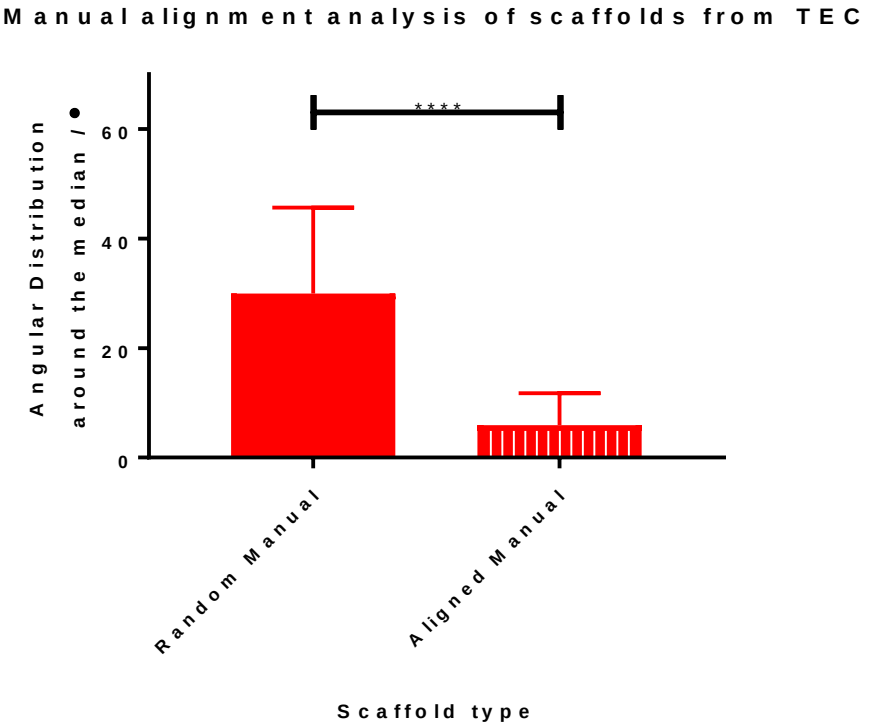

	Random Manual	Aligned Manual
Mean	29.9	5.9
Std. Deviation	15.7	5.8
Std. Error of Mean	2.0	0.8

(b)

	Random Software	Aligned Software
Mean	44.2	30.0
Std. Deviation	15.3	30.9
Std. Error of Mean	0.7	1.5

Figure 6.5.2 D: Comparison of manual and software fibre alignment analysis for the two sheets of random and aligned scaffold made at The Electrospinning Company. Utilising 15 wt% PC12 with HFIP. (a) Manual analysis and (b) software analysis. Not all data sets pass normality test. Mann-Whitney analysis showed significant different between random and aligned scaffold for both manual and software analysis

These scaffolds were then characterised in terms of their stiffness as research has shown that altering alignment alters other mechanical properties (Section 2.1.2). The stiffness of the random and aligned scaffolds made at The Electrospinning Company were investigated using a BOSE uniaxial tensile tester as described in 4.3.8. Scaffolds were measured in two directions as shown in Figure 6.5.2 E (b). Random scaffolds showed the same stiffness mean in both directions, 6.1 and 4.6 MPa. Whereas aligned scaffolds were stiffer in the parallel direction 19.8 MPa in comparison to the horizontal direction which was so weak it was not detectable.

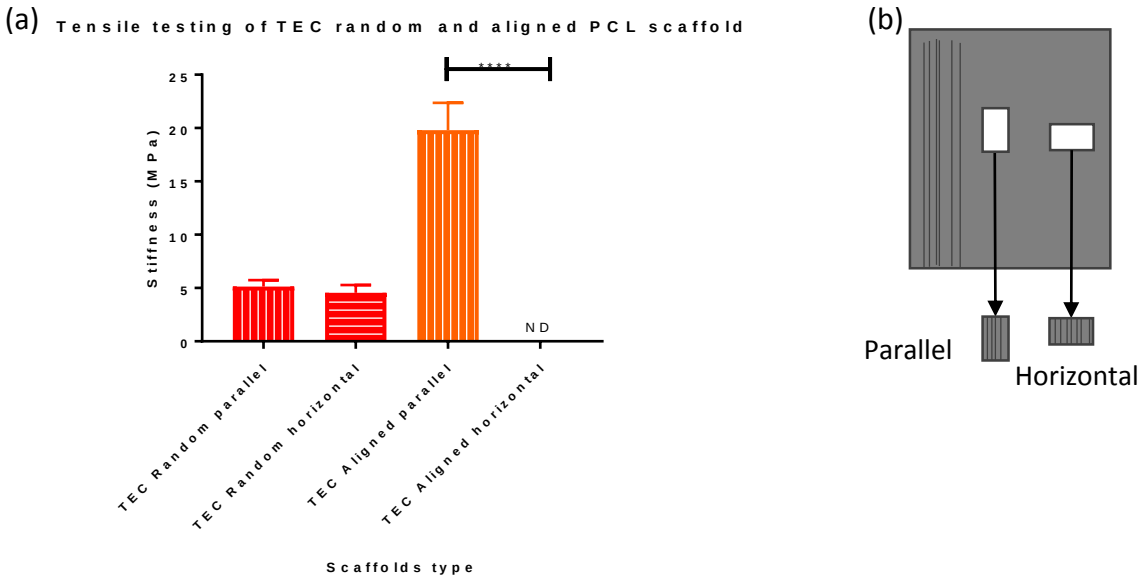

Table 6.5.2 E: Mechanical testing for the stiffness of scaffold. (a) Stiffness results from random and aligned scaffolds. Samples were taken in two orientations as shown in (b), either horizontal or parallel. Method described in 4.3.8 Tensile testing. N=2 n=12

6.6 PC12 PCL scaffold method optimised to manufacture at The Dental School

The placement at The Electrospinning Company identified the best method to manufacture random and aligned PCL scaffolds as PC12 in HFIP at 15 wt%. While HFIP had been chosen to manufacture sheets of scaffold at TEC when I returned to Sheffield it was identified that chloroform was more cost effective than HFIP and was readily available. As there was only a small difference between HFIP and chloroform scaffold fibre properties, and chloroform had previously produced highly aligned fibres, the optimisation began with chloroform to see if aligned fibres could be manufactured without the previously utilised gas shield. While also attempting to produce scaffolds with similar fibre diameters.

A commercial rig made by Bioinicia was installed at the Dental School. All scaffolds from this point were made using this rig with the aim that a commercial rig would help with scaffold reproducibility, Figure 4.2 B.

6.6.1 Optimisation: Utilising PC12 and chloroform

While scaffolds utilising the method PC12 at 15 wt% in chloroform had been manufactured at The Electrospinning Company (TEC), due to the variability of electrospinning I was aware that the method would require optimisation on the Bioinicia rig to produce viable scaffolds. Scaffolds made at TEC had fibre characteristics of mean diameter for random as 3.8 µm and aligned 3.0 µm, with mean angular distribution for random scaffold as 29.9°and 5.9° for aligned scaffold (manual analysis). Therefore scaffolds made at the Dental School were aiming to have similar properties to these TEC scaffolds. However, this project was focusing on alignments impact on cell behaviour, not on other properties such as diameter, therefore producing aligned scaffold with low degrees of angular difference from the median was the main priority. The first step was to manufacture scaffolds at a range of parameters to identify the optimal conditions to produce random and aligned fibres with PC12 at 15 wt% in chloroform on the Bioinicia rig.

Figure 6.6.1 A shows SEM images of scaffolds spun at conditions shown for each scaffold in Table 4.4.3 A. This experiment showed that spinning was possible with this solution without a gas shield.

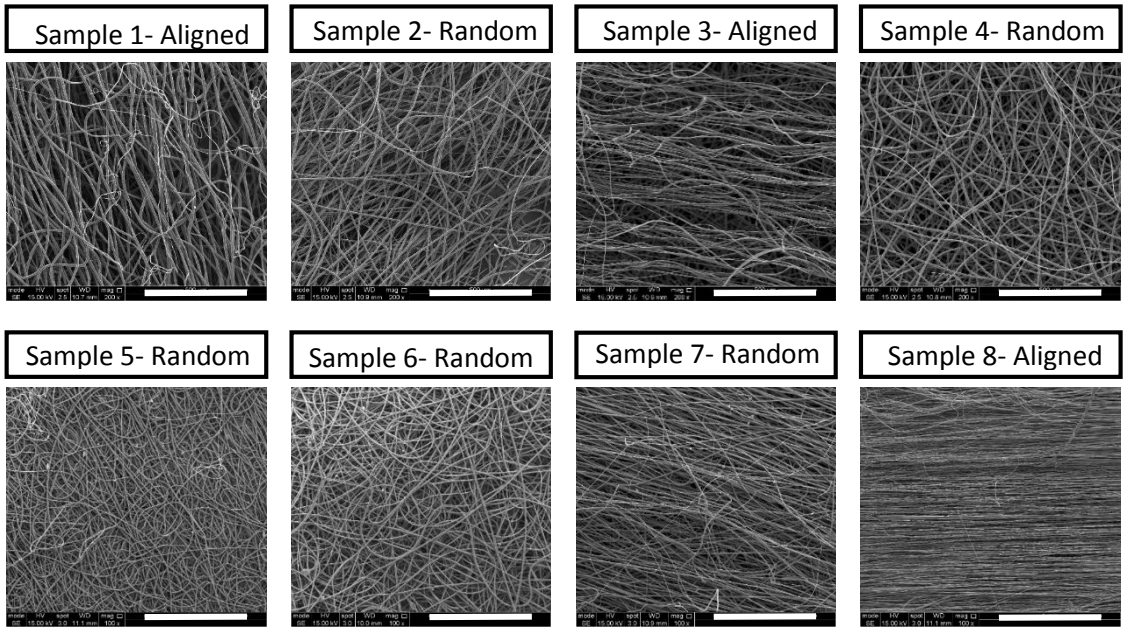

Figure 6.6.1 A: Trial of different spinning conditions for optimising method of 15 wt% PC12 in Chloroform to produce random and aligned scaffold on the Bioinicia rig. Spinning conditions for each sample shown in Table 6.6.1 A. Random samples are 2, 4, 5, 6 and 7 with 2, 4 and 7 spun on the drum and 5 and 6 spun onto a flat plate. While samples 1, 3 and 8 are aligned samples spun onto the drum at fast speed. Scale bar for samples 1-4 is 500 µm while for samples 5-8 is 1 mm.

From the SEM images the fibres that looked the best for randomly orientated fibres was sample 6 and for aligned scaffold sample 8 was identified as the most aligned. Therefore these two methods were taken forward and adapted further to produce stable methods to produce four scaffolds of both random and aligned topologies to characterise fibre properties.

During the whole optimisation process (including the placement at TEC) for the method to manufacture random and aligned PCL scaffolds I decided to back the aligned scaffold with some random fibres by reducing the speed to 200 rpm. This is shown by the SEM images in Figure 6.6.1 B. This is to provide structural stability to the aligned scaffold as the aligned fibres may fall apart without any support.

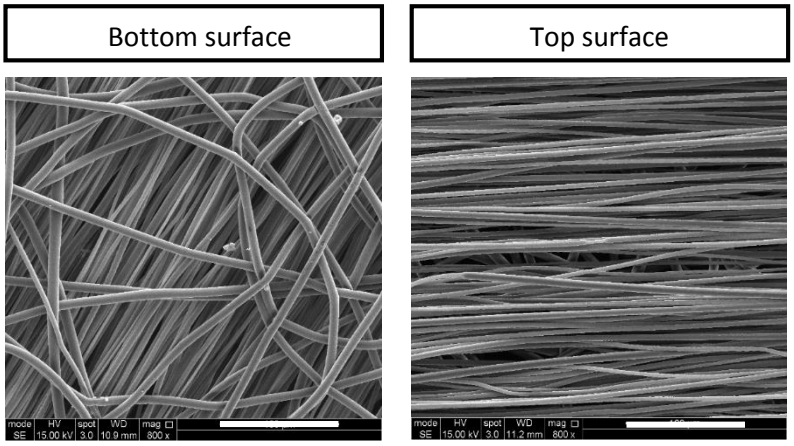

Figure 6.6.1 B: Aligned sample showing the top and bottom surface. 15 wt% PC12 in chloroform. The top surface is the first fibres to be collected on the collector and shows alignment between the fibres. The bottom surface is the last fibres collected and has been backed with random fibres to provide structural support. Scale bar 100 µm.

Once the method of manufacturing random and aligned scaffolds using 15 wt% PC12 in chloroform was optimised, the fibres for both scaffolds required analysis, as described in 4.3.3 Second approach. SEM images from examples of these scaffolds are shown in Figure 6.6.1 C.

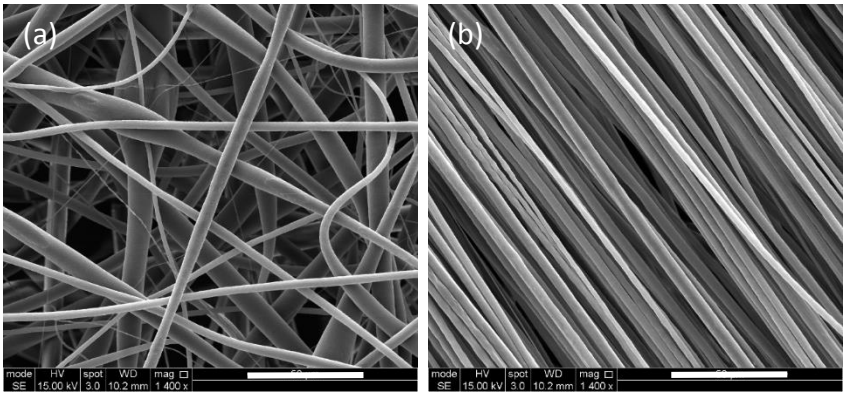

Figure 6.6.1 C: SEM of random and aligned 15 wt% PC12 in chloroform scaffolds. At parameters optimised from comparison in Table 6.6.1 A. Electrospun onto Bioinicia rig conditions spun at (a) 26 cm distance, 2 ml/H infuse rate, voltage 26-28 kV, 1 ml volume onto flat plate and (b) 22 cm distance, 2 ml/H infuse rate, voltage 20 kV, 1 ml volume, 2,000 -> 200 rpm onto drum. Scale bar for 50 µm. N=4 n=8.

For the analysis four scaffolds were made for both random and aligned. From each scaffold two samples were taken for SEM imaging, Figure 6.6.1 D. Random scaffolds had a mean diameter of 6.5 ± 2.2 µm while aligned has a mean diameter of 3.4 ± 0.5 µm, Figure 6.6.1 E (a). This analysis showed random scaffolds had a mean diameter double the mean diameter of aligned scaffold. While it is unknown whether cells cultured as neurospheres, as the tanycytes within this study will be cultured on these scaffolds, will respond or can recognised the fibre diameter or recognise this level of difference in fibre diameter I decided this was too large of a fibre

difference for this projects aims. As this research aimed to investigate the effect of alignment on this cell population it was desirable to maintain as many other parameters between the two scaffolds (random and aligned), including fibre diameter. Practically this may only be possible to within a certain range of diameter size, rather than aiming for exactly the same mean diameter and distribution, as it was shown that changing the level of alignment alters other parameters such as stiffness as shown in Figure 6.6.1 C with TEC scaffolds. The placement at TEC also showed a consistent thinning of the aligned fibres compared to the random fibres. However, as the scaffold manufactured at The Electrospinning Company has very similar fibre diameter between random and aligned, more optimisation was required for the scaffolds manufactured at The Dental School.

(a)

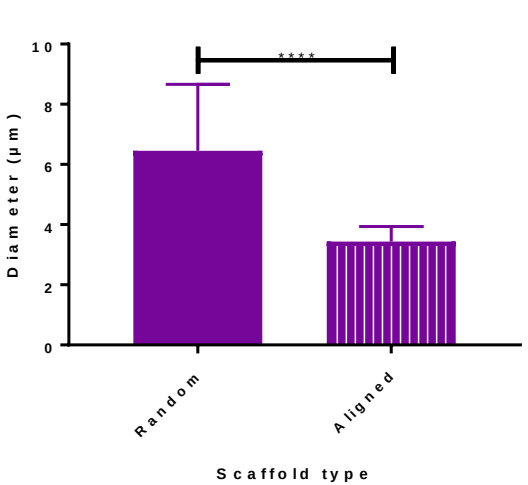

Diameter	Random	Aligned
Mean	6.5	3.4
Std. Deviation	2.2	0.5
Std. Error of Mean	0.3	0.1

(b)

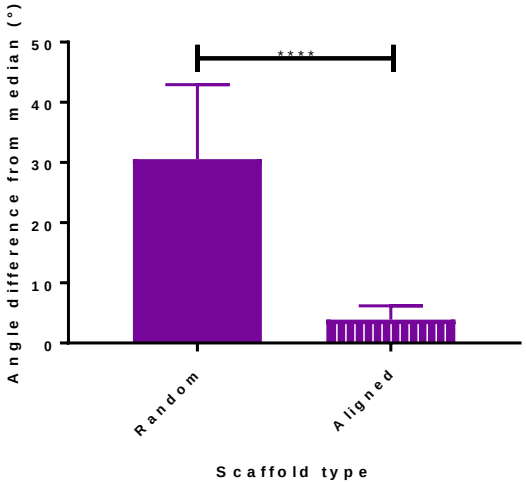

Alignment	Random	Aligned
Mean	30.6	3.9
Std. Deviation	12.4	2.3
Std. Error of Mean	1.6	0.3

Figure 6.6.1 E: Diameter and alignment analysis of optimised random and aligned scaffold manufactured with 15 wt% PC12 chloroform. Four scaffolds made on separate occasion with two samples taken for SEM and analysis, N=4 n=8, Figure 6.6.1 D. As parameters in Table 4.4.3 B. Method of analysis explained in 4.3.3 Second approach. Mean and standard deviation shown. Not all data sets pass normality test so statistical analysis was done using a two-tailed Mann-Whitney test. (a) Diameter analysis where random scaffold has a mean diameter of 6.5 µm with a standard deviation of 2.2 µm, while for aligned scaffold the mean is 3.4 µm with standard deviation of 0.5 µm. (b) Alignment analysis random has a mean angle deviation of 30.6 ° with a standard deviation of 12.4 ° and aligned has a mean of 3.9 ° with a standard deviation of 2.3 °. Random and aligned scaffold are significantly different at P<0.0001 for both diameter and alignment.

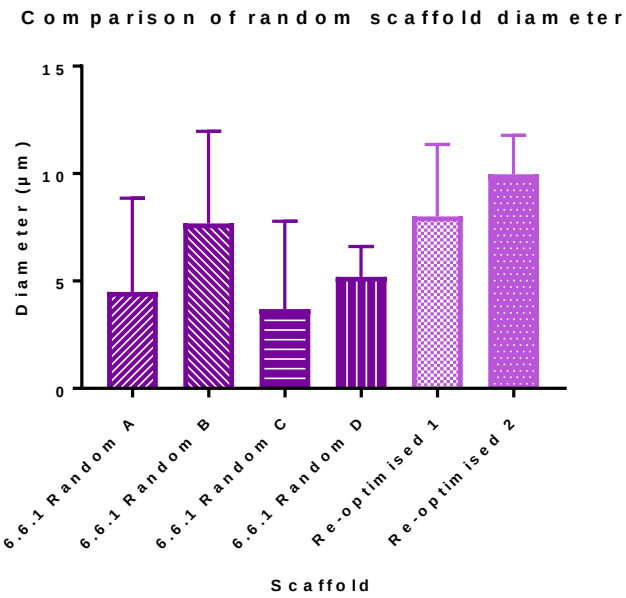

Diameter	6.6.1 Random A	6.6.1 Random B	6.6.1 Random C	6.6.1 Random D	Re-optimised 1	Re-optimised 2
Mean	4.5	7.7	3.7	6.2	8.0	10.0
Std. Deviation	4.4	4.3	4.1	1.4	3.4	1.8
Std. Error of Mean	0.8	0.8	0.8	0.3	0.6	0.3

Figure 6.6.1 F: Comparison of random scaffold 15 wt% PC12 Chloroform aiming to reduce mean diameter. The first four columns are the four separate scaffolds providing the mean data from figure 6.6.1 D where the Bioinica rig was in its original room and re-optimised 1-2 the Bioinicia rig had been re-located. The parameters these two scaffolds were spun at are shown in Table 4.4.3 B. Mean with standard deviation shown. Mean, standard deviation and standard error of mean shown. N=1 n=1 for each column.

During the characterisation of Figure 6.6.1 E scaffolds there was a laboratory reorganisation and the Bioinicia rig was moved to a different laboratory. In this new location two new random scaffolds were manufactured with the aim of reducing the diameter of the fibres. The parameters of the two new scaffolds are stated in Figure 4.4.3 B. The analysis of the diameter of these new scaffolds are shown in Figure 6.6.1 F as re-optimised 1 and 2. Within this figure is the mean diameter for each of the four scaffolds manufacture for the first optimisation characterisation shown in Figure 6.6.1 E, samples A-D. Samples A-D show the variability within the first parameters to manufacture random scaffold as the mean diameters range from 3.7-7.7 µm. The two new scaffolds have mean diameters of 8 and 10 µm. Therefore the changes that have previously been reported to reduce fibre diameter, including reducing the flow rate and increasing the distance, were ineffective[145]. As this was an unexpected result and the rig was now in a different location with different temperature and humidity known to impact

electrospinning (examples include 24°C and 27% humidity in the new location and 21°C and 54% in the old location). To test whether it was due to the different environment I decided to attempt to reproduce aligned scaffold. This manufacturing method was no longer capable of producing scaffold as fibres were not collecting on the collector but above and in front in a web, Figure 6.6.1 G. This, in part, was suspected to be due to the location of the rig. Therefore the rig was returned to the original location. However this did not allow for the previous method to be capable of producing scaffold. This highlights one of the issues with electrospinning in that the method is variable especially due to temperature and humidity.

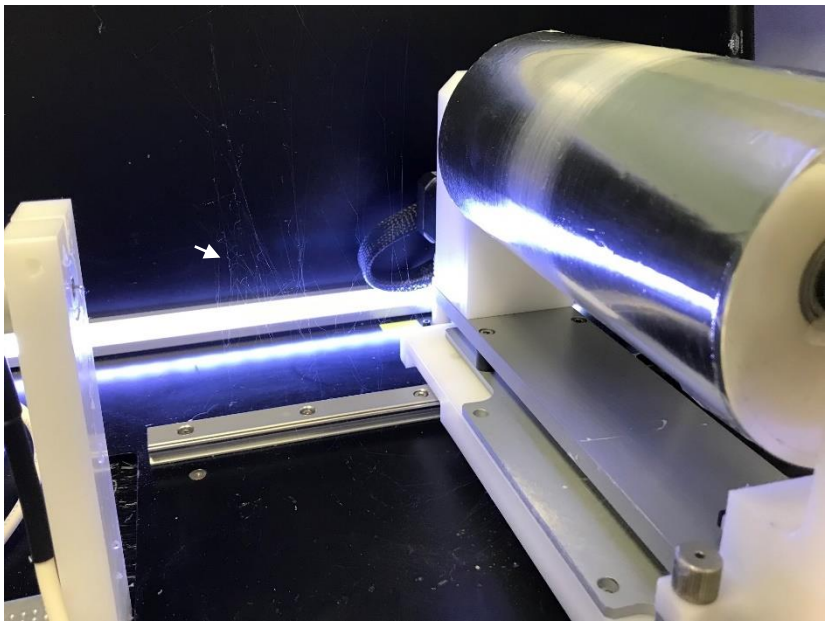

Figure 6.6.1 G: Fibres collecting in front of collector showing failure of manufacturing method. Initially fibres collect on drum before collecting in front. Even when the fibre web was cleared it would reform again reducing the amount of fibres collecting on the collector.

6.6.2 SURE Scheme project: Comparing HFIP and chloroform

The confirmation of the failure of the previously optimised method to manufacture random and aligned scaffold with 15 wt% PC12 in chloroform coincided with the start of an eight-week SURE summer project student, Nicholas Cooper. The work done within the section was undertaken by Nicholas under my supervision. Initially the aim of this project was for Nicholas to manufacture scaffolds using the previously optimised method to characterise the stiffness and biocompatibility. However, once the method was confirmed to be unable to reproduce scaffold, this project aimed to re-optimise the manufacture of random and aligned scaffold at The Dental School.

The main priority was to produce aligned scaffolds with a mean angular distribution under 10° or as close to the 5.9° produced at TEC. Random scaffold was aimed to have a value around 30°. As the previously manufactured and characterised scaffold had mean diameter for random scaffold double that of aligned scaffold (6.4 µm and 3.4 µm respectively) this opportunity was taken to attempt to reduce the difference between these diameters for these new scaffolds. Alongside this was an aim of lesser importance but a feature I was aware of in that TEC scaffold produced fibres within the range of 3-4 µm ± 0.5 µm. Therefore Nicholas aimed for diameters within this range or lower.

Optimisation of method

As the manufacture of aligned scaffold had completely failed with fibres collecting away from the collector it was important to begin by identifying what parameters would allow for fibres to collect on the collector, as aligned fibres, so the scaffold would have a thickness that was useable for cell culture experiments (i.e. able to maintain its integrity during culture in media). Initially a trial was done not collecting samples monitoring the fibre depositions with both HFIP and chloroform to investigate whether chloroform was causing the problem. The addition of a

cardboard wind-break was incorporated, Figure 6.6.2 A, which reduced the amount of polymer collecting away from the collector.

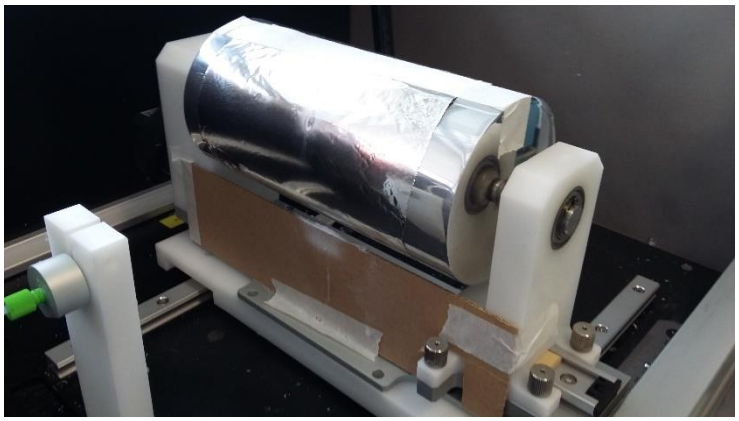

Figure 6.6.2 A: Cardboard wind-breaker for spinning aligned scaffolds. On the Bioinicia rig.

This project began by comparing 12 and 15 wt% PC12 PCL with HFIP and chloroform solvents at distances 10 and 14 cm to produced aligned fibres. SEM images of the scaffolds manufactured for this comparative study are shown in Figure 6.6.2 B.

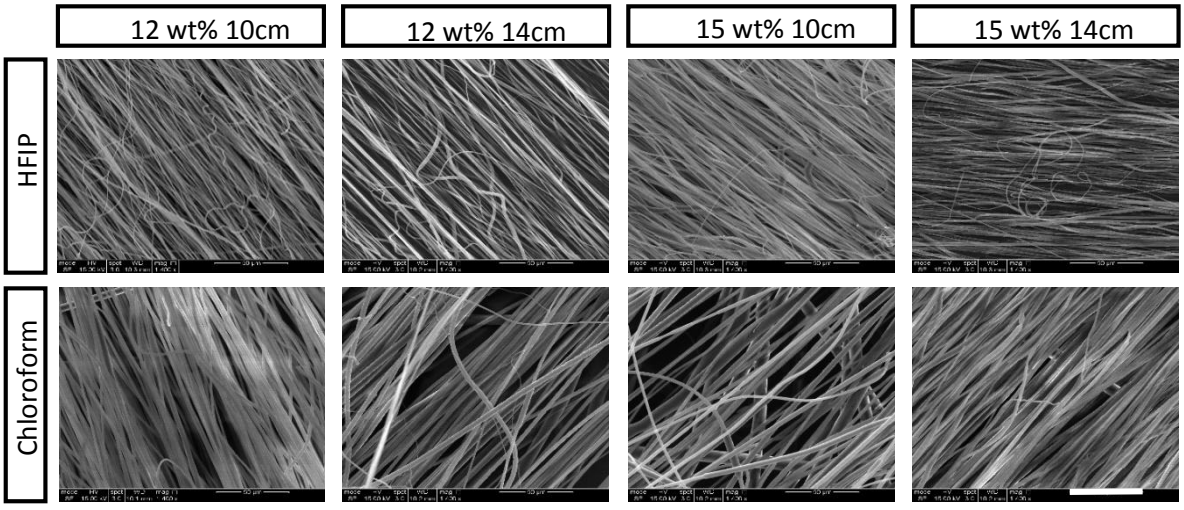

Figure 6.6.2 B: SEM images of aligned scaffold comparing 12 and 15 wt% and solvents HFIP and chloroform at distances of 10 and 14 cm. Scale bar 50 µm.

For this comparison one scaffold was manufactured for each set of conditions with one sample taken for SEM imaging, Figure 6.6.2 C, showing scaffolds could be produced with both chloroform and HFIP. The analysis of these scaffolds for fibre diameter and alignment was done

using the method in 4.3.3 Second approach. Diameters varied based on 12 or 15 wt%, solvent and distance.

At this point it was considered beneficial to have both sets of scaffold, TEC and Dental School manufactured, made with the same solution, i.e. both with HFIP. Previously HFIP had not been used due to cost and chloroform was readily available. Now HFIP was available, cost approved, and could produce scaffolds on this rig it was decided that this solution would be utilised moving forward. Also it was considered that the problem with chloroform was the inability to produce scaffolds of a thickness to be useable within cell culture. This choice was despite fibres been thinner with chloroform which were closer to the TEC scaffold, 2-4 µm versus 1.1-1.4 for HFIP, Figure 6.6.2 D. Quantitatively there were observations that the quality of the samples produced with HFIP were better than chloroform as with chloroform there were issues with removing samples from foil. In terms of alignment chloroform had higher standard deviation so fibres were more differently aligned from the median direction while HFIP had lower standard deviation and therefore was producing more consistently aligned fibres. 10 cm was identified as the better distance than 14 cm due to quantitate observations that at 10 cm the scaffolds were thicker and had better structural integrity for handling. Therefore 14 cm distance was discounted as a method option. Statistical analysis can be found in appendix 1 in Table A1 G.

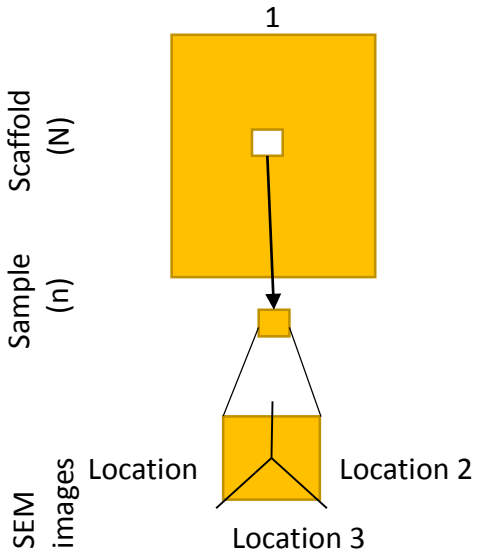

Figure 6.6.2 C: Schematic of the source of data for Aligned scaffold manufactured to compare 12 and 15 wt% and solvents chloroform and HFIP at distances of 10 and 14 cm. Scaffold were manufactured once from which one samples were taken and on each sample three SEM images were taken on which 10 fibres were measured for diameter and alignment. N=1 n=1

(a)

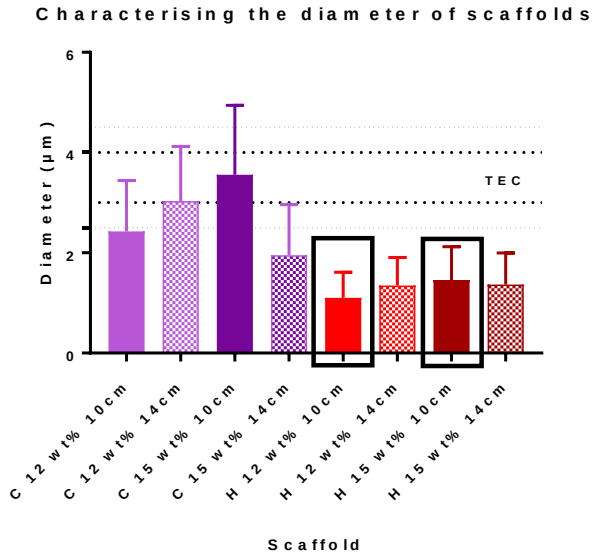

(b)

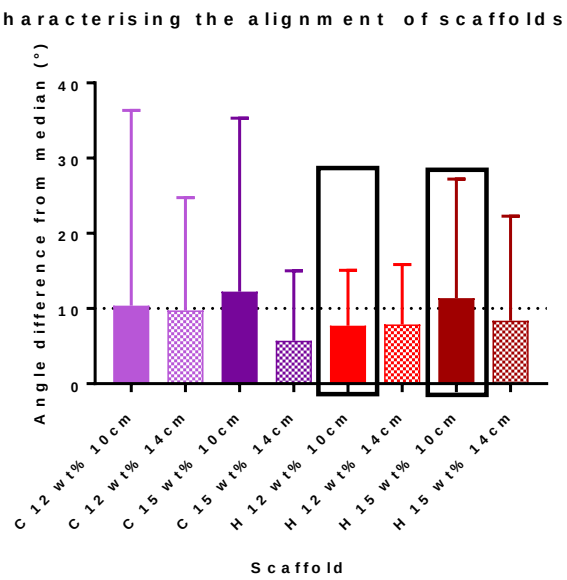

Diameter	C 12wt% 10cm	C 12wt% 14cm	C 15wt% 10cm	C 15wt% 14cm	H 12wt% 10cm	H 12wt% 14cm	H 15wt% 10cm	H 15wt% 14cm
Mean	2.4	3.0	3.6	2.0	1.1	1.4	1.4	1.4
Std. Deviation	1.0	1.1	1.4	1.0	0.5	0.6	0.7	0.6
Std. Error of Mean	0.2	0.2	0.3	0.2	0.1	0.1	0.1	0.1

Alignment	C 12wt% 10cm	C 12wt% 14cm	C 15wt% 10cm	C 15wt% 14cm	H 12wt% 10cm	H 12wt% 14cm	H 15wt% 10cm	H 15wt% 14cm
Mean	10.4	9.8	12.3	6.7	7.7	7.9	11.4	8.4
Std. Deviation	26.0	16.0	23.0	9.3	7.4	8.0	16.8	13.9
Std. Error of Mean	4.7	2.7	4.2	1.7	1.4	1.5	2.9	2.5

Figure 6.6.2 D: Aligned scaffold manufactured to compare 12 and 15 wt% and solvents chloroform and HFIP at distances of 10 and 14 cm. C= Chloroform H=HFIP. (a) Diameter analysis and (B) alignment analysis both with mean and standard deviation shown. Boxes highlight samples of interest. As method 4.3.3 Second approach. Not all samples passed normality test so statistical analysis was done using Krustal-Wallis with Dunn's multiple comparison. Table A1 G shows the significant difference between diameters while alignment had no significant differences. N=1 n=1 for each set of conditions.

To investigate which of the HFIP methods were better for producing aligned scaffolds with angle difference below 10°, the data set was expanded to produce three scaffolds. Each scaffold had one sample for SEM imaging, Figure 6.6.2 E.

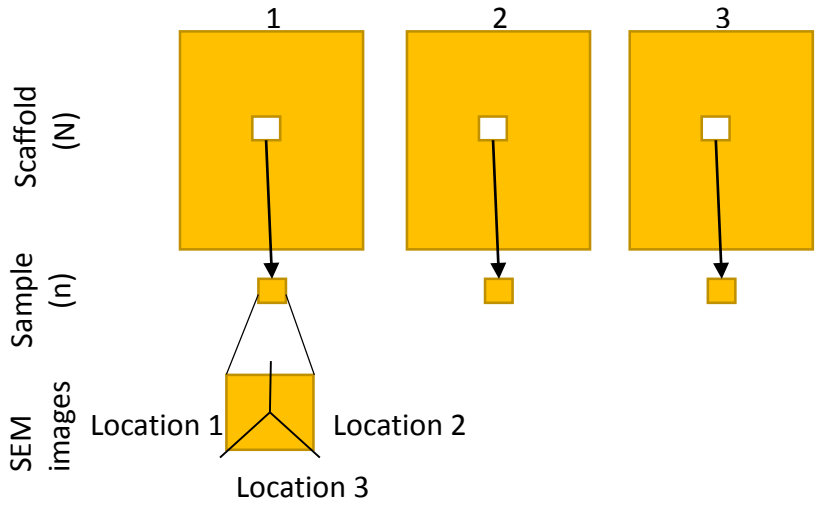

Figure 6.6.2 E: Schematic of the source of data for Aligned scaffold manufactured to compare 12 and 15 wt%. Scaffold were manufactured on three occasions and from which one sample was taken and on each sample three SEM images were taken on which 10 fibres were measured for diameter and alignment. N=3 n=3

The fibre characterisation of these scaffolds is shown in Figure 6.6.2 F. At 12 wt% the mean diameter is 1.0 µm while 15 wt% is 1.3 µm which showed a significant difference. While there is significant difference, the mean fibre diameters are not that dissimilar especially when the standard deviation is considered. For fibre orientation 12 wt% was more aligned with a mean angle difference of 8.2° while for 15 wt% the mean angle was 10.6°. When considering which was the better method for manufacturing scaffolds for 12 wt%, fibres were more aligned but had fibres that were thinner than 15 wt% that was also slightly less aligned. However with a mean angle distribution around the mean of only 0.6° above the aim of below 10°. As there was only small difference between the two methods it was difficult to identify which method, 12 or 15 wt %, would be the optimal method from this data.

(a)

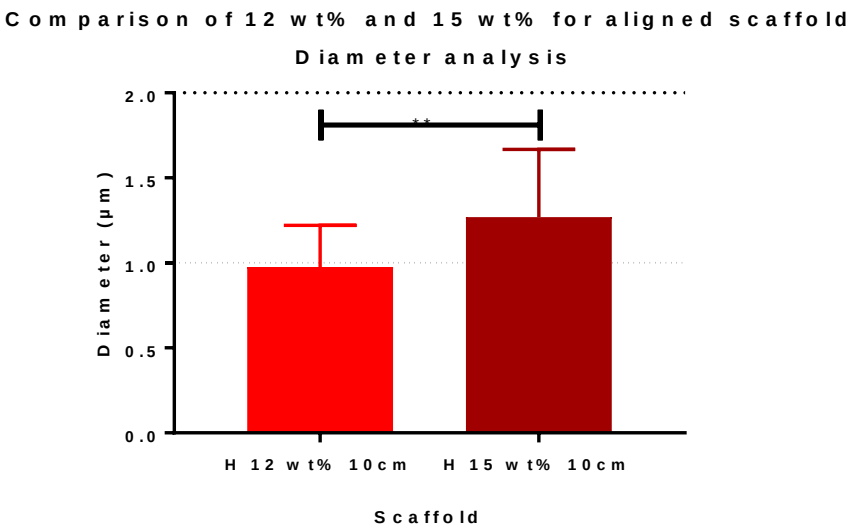

Diameter	H 12wt% 10cm	H 15wt% 10cm
Mean	1.0	1.3
Std. Deviation	0.3	0.4
Std. Error of Mean	0.1	0.1

(b)

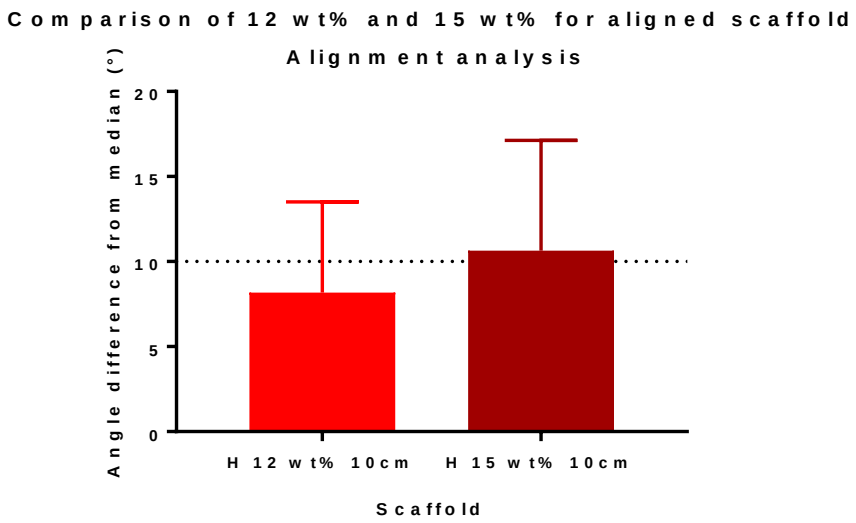

Alignment	H 12wt% 10cm	H 15wt% 10cm
Mean	8.2	10.6
Std. Deviation	5.3	6.5
Std. Error of Mean	1.0	1.2

Figure 6.6.2 F: Aligned scaffold manufactured to compare 12 and 15 wt% of PC12. H=HFIP. As method 4.3.3 Second approach. Mean and standard deviation shown. Not all samples passed normality test so statistical analysis was done using a two-tailed Mann-Whitney test. (a) Diameter analysis showed significant difference between random and aligned while (b) alignment analysis did not show significant difference. Dotted line represents aim for scaffold diameter and alignment mean angle difference from median. N=3 n=3

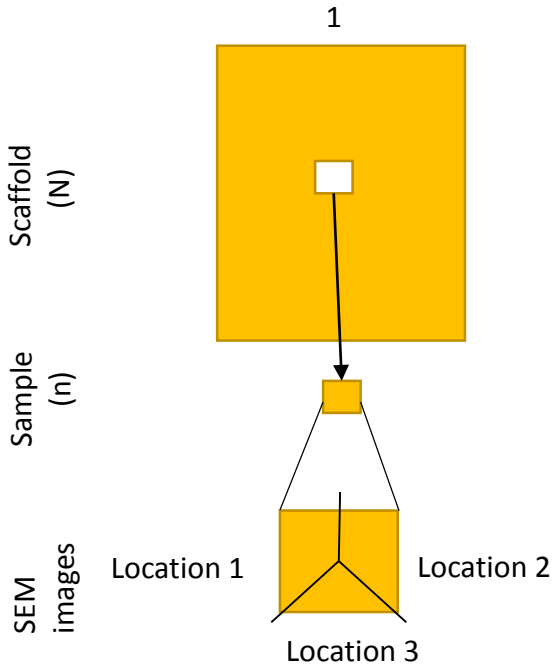

Figure 6.6.2 G: Schematic of the source of data for Random scaffold manufactured to compare 12 and 15 wt% and a range of distances. Scaffold were manufactured once from which one sample was taken and on each sample three SEM images were taken on which 10 fibres were measured for diameter and alignment. N=1 n=1

In order to assist with identifying the optimal method for random and aligned scaffold manufacture, random scaffold production was then considered. Random scaffolds were manufactured at 12 and 15 wt% at a range of distances 22, 24, 26 and 28 cm. One scaffold was made for each set of conditions and one sample taken from each for SEM imaging shown in Figure 6.6.2 G. Analysis of these samples was done using the method in 4.3.3 Second approach and shown in Figure 6.6.2 H. Aligned scaffolds produced fibres around 1 µm and while TEC has fibres 3-4 µm, however it is more important for the random and aligned scaffolds made at the Dental School to have similar fibre diameters than to be similar to TEC scaffold. Therefore samples 12 wt% 28 cm, 26 cm and 15 wt% 28 cm, 26 cm were discounted for having fibres diameters above 3 µm. For fibre orientation samples for random fibres were required to have a higher mean angle difference showing more disordered fibres within the scaffold ideally above 30°. The highest mean value was 35.8° which was shown for both 12 wt% at 22 cm and 15 wt% at 24 cm. These two samples were of most interest as they has two of the lowest fibre diameters and met the orientation aims. Statistical analysis can be found in appendix 1 in Table A1 H.

(a)

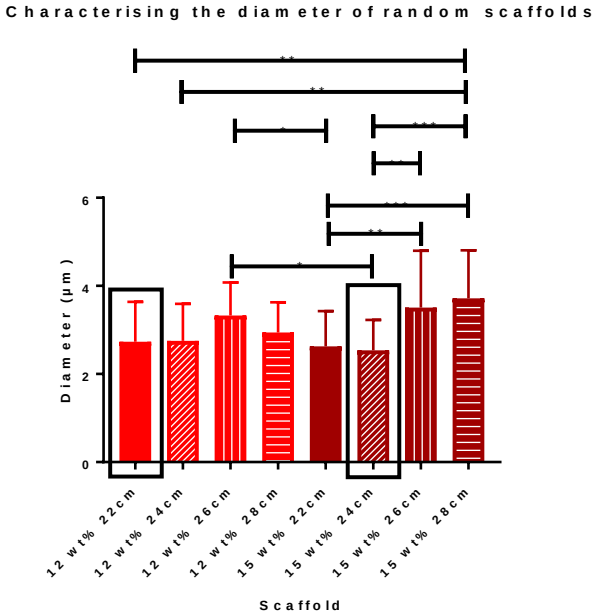

(b)

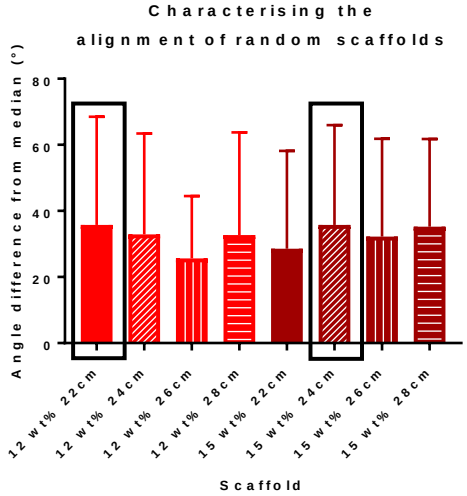

Figure 6.6.2 H: Random scaffold manufactured to compare 12 and 15 wt% and distance between needle and collector. Scaffold spun with PC12 PCL in HFIP. Distances compared were 22 cm, 24 cm, 26 cm and 28 cm. Mean and standard deviation shown. Boxes highlight samples of interest. Analysis done utilising method in 4.3.3 Second approach. Not all samples passed normality test so statistical analysis was done using Krustal-Wallis with Dunn's multiple comparison. (a) Diameter analysis showed significant difference (also shown in Table A1 H) while (b) alignment analysis did not show significant difference. N=1 n=1

Diameter	12 wt% 28cm	12 wt% 26cm	12 wt% 24cm	12 wt% 22cm	15 wt% 28cm	15 wt% 26cm	15 wt% 24cm	15 wt% 22cm
Mean	3.0	3.3	2.8	2.7	3.7	3.5	2.5	2.6
Std. Deviation	0.7	0.8	0.8	0.9	1.1	1.3	0.7	0.8
Std. Error of Mean	0.1	0.1	0.2	0.2	0.2	0.27	0.1	0.2

Alignment	12 wt% 28cm	12 wt% 26cm	12 wt% 24cm	12 wt% 22cm	15 wt% 28cm	15 wt% 26cm	15 wt% 24cm	15 wt% 22cm
Mean	32.7	25.6	32.9	35.8	35.2	32.2	35.8	28.6
Std. Deviation	31.1	18.9	30.5	32.7	26.5	29.6	30.2	29.6
Std. Error of Mean	5.7	3.5	5.6	6.0	4.9	5.4	5.5	5.4

In order to identify whether 12 or 15 wt% was better for this project, the mean diameters of the random scaffolds were compared with aligned scaffolds manufactured at 10 cm, Table 6.6.2 C. Looking at the two most interesting random scaffolds from Figure 6.6.2 H for 12 wt% comparison of aligned scaffold to random scaffolds at 22 cm, the difference was 1.6 µm. While for 15 wt% 24 cm showed a difference of 1.1 µm. The method which had the smallest mean diameter difference between random and aligned scaffolds was 15 wt% at 24 cm for random scaffold. This sample also had the highest mean angle difference so was the most randomly organised. Therefore random scaffolds manufacturing method was 15 wt% at 24 cm, while aligned scaffolds were manufactured using 15 wt% at 10 cm.

Table 6.6.2 C: Mean diameters for samples (N=1) for random and aligned scaffolds. In bold are the two random samples of most interest from Figure 6.6.2 H.

Diameter	**12 wt%**				
Random/Aligned	Random				Aligned
Distance	**22cm**	24cm	26cm	28cm	10cm
Mean	**2.7**	2.8	3.3	3.0	1.1
Std. Deviation	**0.9**	0.8	0.8	0.7	0.5

Diameter	**15 wt%**				
Random/Aligned	Random				Aligned
Distance	22cm	**24cm**	26cm	28cm	10cm
Mean	2.6	**2.5**	3.5	3.7	1.4
Std. Deviation	0.7	**0.8**	1.3	1.1	0.7

6.6.3 Characterisation of Dental School scaffolds manufactured with 15 wt% PC12 in HFIP

Scaffolds were manufactured four times (for aligned scaffold one additional scaffold was made for those analysed in Figure 6.6.2 F and three additional scaffolds for random were manufactured to the one from the comparison from Figure 6.6.2 H) with two samples for SEM images, Figure 6.6.3 A. SEM images of scaffolds random and aligned made using 15 wt% PC12 in HFIP are shown in Figure 6.6.3 B.

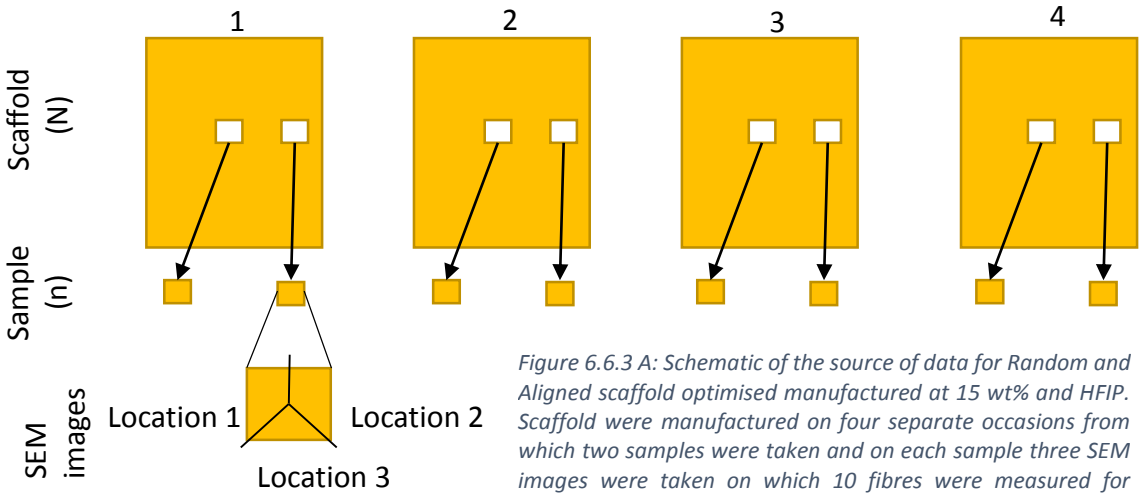

Figure 6.6.3 A: Schematic of the source of data for Random and Aligned scaffold optimised manufactured at 15 wt% and HFIP. Scaffold were manufactured on four separate occasions from which two samples were taken and on each sample three SEM images were taken on which 10 fibres were measured for diameter and alignment. N=4 n=8.

Figure 6.6.3 C shows diameter and alignment characterisation (as method 4.3.3 Second approach). Random scaffolds had a mean diameter of 3.1 ± 0.4 µm while aligned scaffold had a mean of 1.2 ± 0.3 µm. For orientation analysis, random scaffolds had a mean angle difference from the median of 30.9 ± 13.7° while aligned scaffolds showed 10.1 ± 7.6°. While there is still a mean diameter for random scaffolds double that for aligned scaffolds due to the problems manufacturing scaffold and time restraints, this was accepted for the initial investigation of cell responses to alignment in combination with the use of TEC scaffolds.

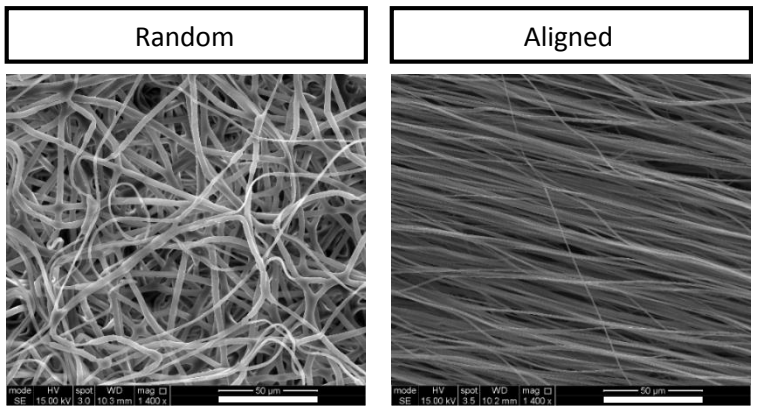

Figure 6.6.3 B: SEM Images of optimised manufacture of Random and aligned scaffold. Scaffold spun with 15 wt% PC12 PCL in HFIP. Random spun at 24 cm and aligned spun at 10 cm N=4 n=8.

(a)

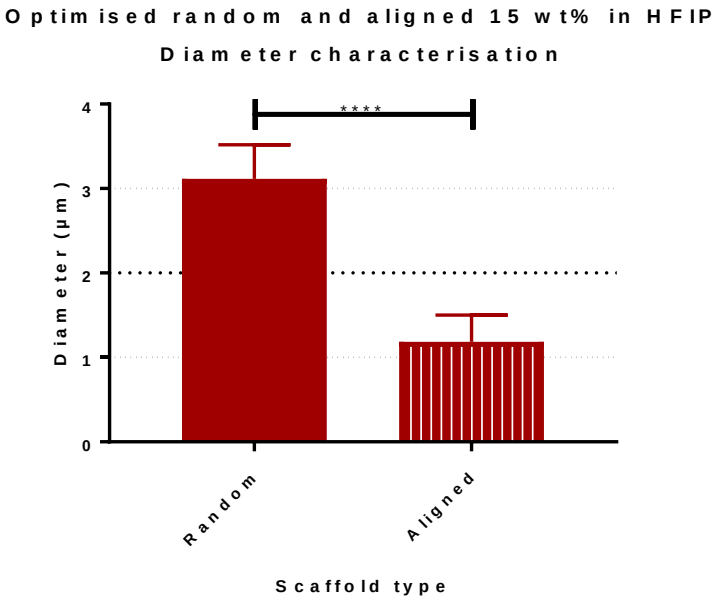

Diameter	Random	Aligned
Mean	3.1	1.2
Std. Deviation	0.4	0.3
Std. Error of Mean	0.1	0.0

(b)

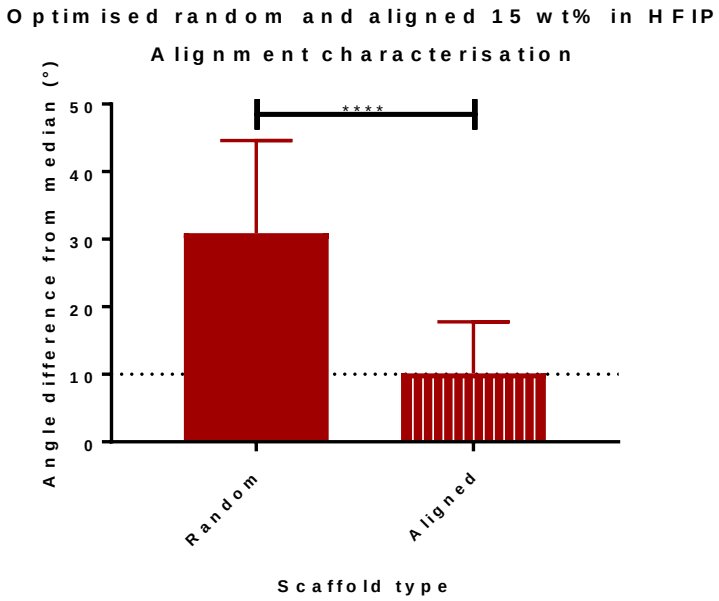

Alignment	Random	Aligned
Mean	30.9	10.1
Std. Deviation	13.7	7.6
Std. Error of Mean	1.8	1.0

Figure 6.6.3 C: Characterisation of optimised manufacture of Random and aligned scaffolds. Scaffolds spun with 15 wt% PC12 PCL in HFIP on the Bioinicia rig. Distances Random 24 cm and aligned 10 cm. As method 4.3.3 Second approach. (a) Diameter analysis and (b) alignment analysis both showing mean and standard deviation. Not all samples passed normality test so statistical analysis was done using two-tailed Mann-Whitney test. Both diameter and alignment showed significant difference between random and aligned scaffolds. Dotted line represents aim for scaffold diameter and maximum aim for mean angle difference for aligned scaffold. N=4 n=8.

These scaffolds were then characterised in terms of their stiffness, as previously for scaffold from TEC. Random scaffolds showed the same stiffness mean in both directions, 11.3 and 11.8 MPa, Figure 6.6.3 D. Whereas aligned scaffold is stiffer in the parallel direction 23 MPa in comparison to the horizontal direction which is so weak it was not detectable.

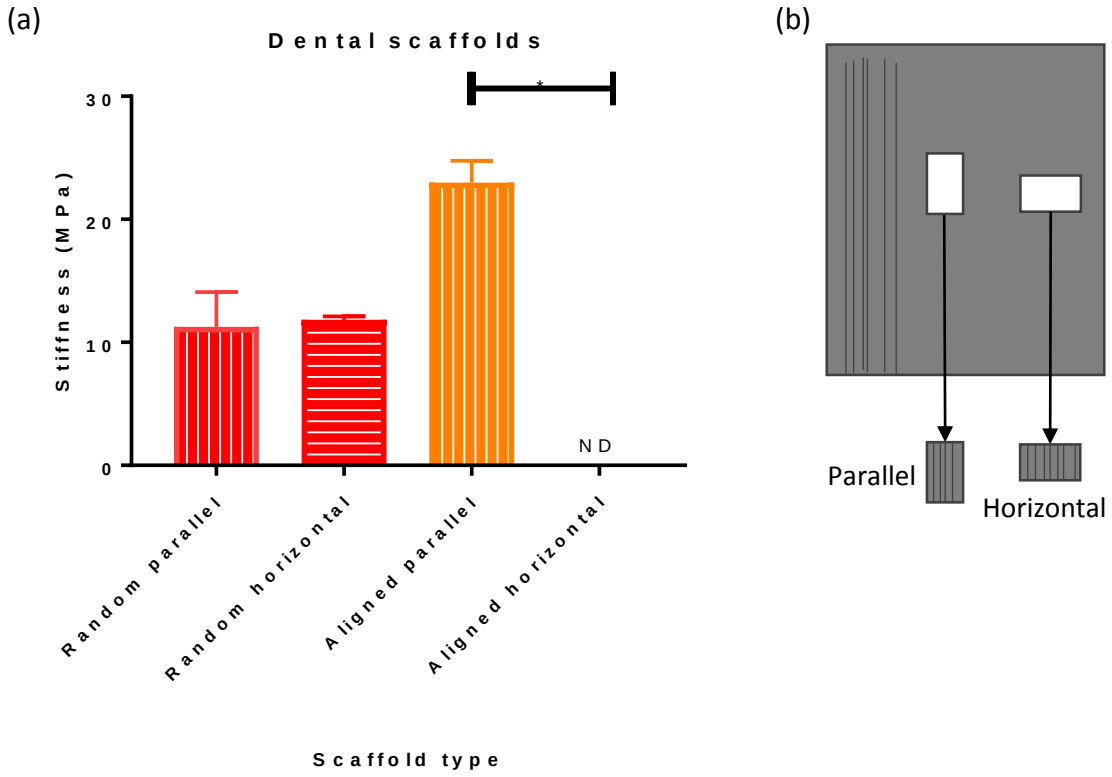

Figure 6.6.3 D: Mechanical testing for the stiffness of DS scaffold. (a) Stiffness results from random and aligned scaffolds. Samples were taken in two orientations as shown in b, either horizontal or parallel. N=3 n=9 for each sample orientation.

6.7 Discussion

6.7.1 Introduction of microfeatures within the electrospun mat

Electrospinning onto patterned metallic templates introduces microfeatures into the scaffold, the shape of the microfeature formed is dependent upon the structure of the template. Template 1 introduces one repeating feature into the surface of scaffold 1 which is formed by the fibres interacting and covering the hole within template 1. Figure 6.3.2 B and Table A1 D shows that the bottom area (a) has slightly thinner fibres than the side of the well (b) and the top surface (c). This is due to the fibres having to transverse the hole within the template therefore being slight stretched as they fall to cover this distance. During the analysis of the microfeatures of scaffold 1 it was identified that these microfeatures were not circular as their two lengths were significantly different, Figure 6.2 B, and when closely inspected a bean shape can be seen, Figure 6.7.1 A. This is suspected to be due to a problem in the manufacture of template 1 as the template was fabricated (3D- printed) at an angle during selective laser melting (SLM) which introduced an error in the hole of the template leading to this being shaped feature rather than a circular feature. This template could be re-made by manufacturing on a flat plane to remove this error.

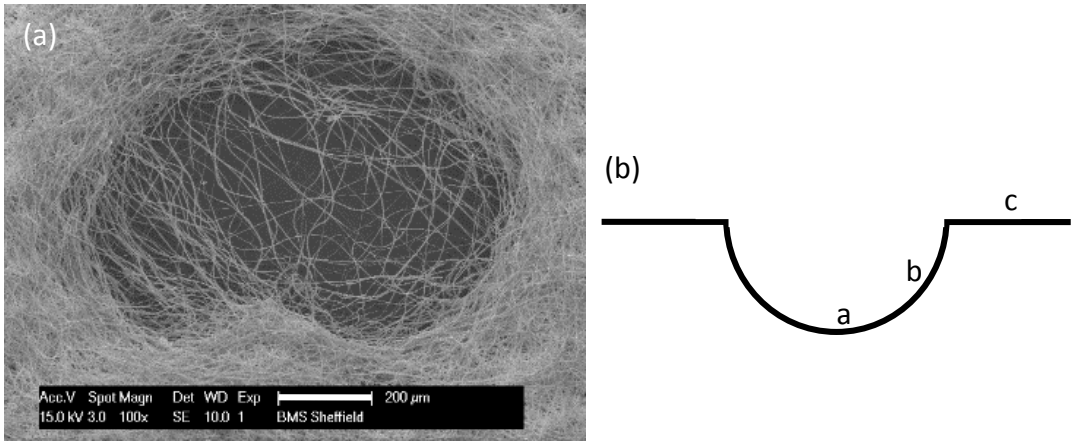

Figure 6.7.1 A: Scaffold 1 microfeature. (a) A microfeature from scaffold 1. Displaying the microfeature is not circular but contains an irregularity. Scale bar 200 µm. (b) diagram illustrating the areas of the microfeatures a= bottom of the well, b= side of the well and c= top surface.

Scaffold 2 has four differently sized repeating features that mirror the protrusions on template 2. These features form with random fibres at the base of the feature where the fibres interacted with the top of the metallic protrusion on the template. The top surface of the electrospun

scaffold also has random fibre organisation as this is where the fibres interact with the flat base of the template. The sides of the features show alignment as the fibres are required to transverse the top of the protrusion on the template to the bottom surface of the template. This also results in the stretching of the fibres leading to the slightly narrower fibres seen for the side of the microfeature in all four microfeatures, Figure 6.3.2 B and Table A1 D.

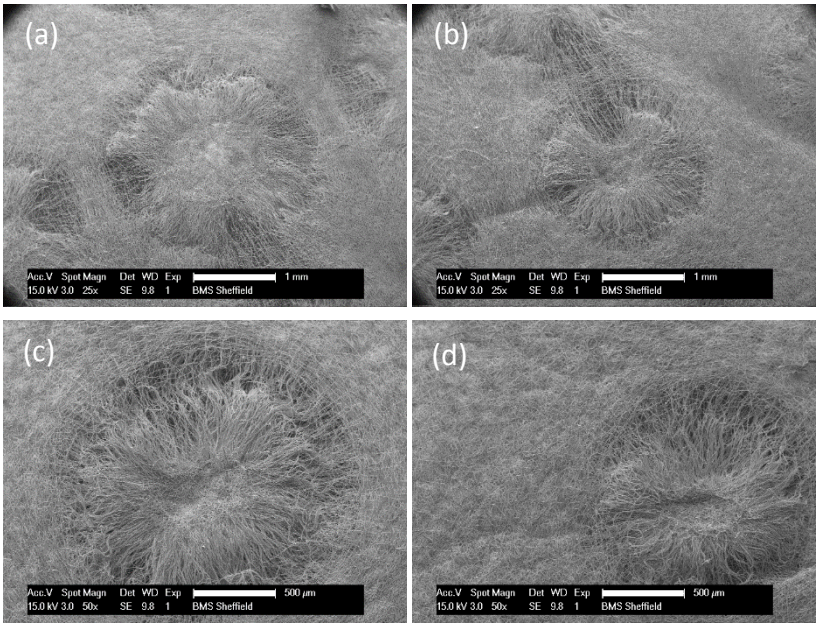

Figure 6.7.1 B: The four microfeatures of scaffold 2. (a) The largest, (b) intermediate a, (c) intermediate b and (d) small microfeature. Scale bar 1 mm (a and b) and 500 µm (c and d).

Scaffold 3 is a complex structure with different planes of alignment, Figure 6.7.1 C. This is because the template is a grid and therefore the denser regions of fibres are where the metallic grid cross and the lines of the grid can be seen linking these dense regions. The feature of this template is square, not circular unlike scaffolds 1 and 2, and is formed by fibres traversing the

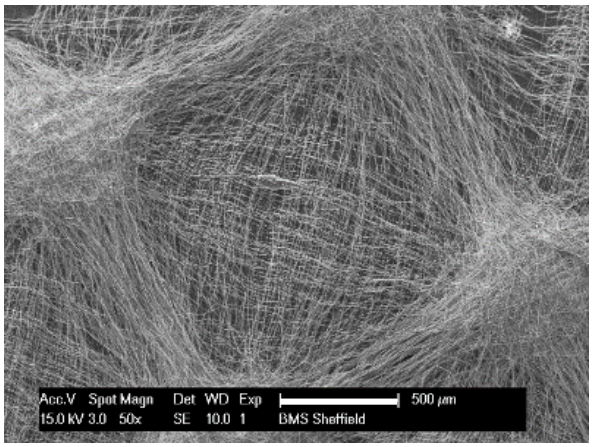

Figure 6.7.1 C: The complex structure formed by template 3. Scale bar 500µm.

square space between the metallic lines of the template. Alignment is formed between opposite dense regions which are where the metal lines cross on the template. Similarly, the fibres are slightly thinner in the bottom region (a) than the top surface (c), Figure 6.3.2 B and Table A1 D. Previous research into alignment has shown that short distances between parallel lines fibres will align between these two parallel lines which explains why there is alignment present at the bottom of the well but in several directions [164].

While statistical analysis identified slightly thinner fibres in certain areas of these microfeatures the change is very small and therefore unlikely to cause a change in cell behaviour, especially as all areas have similar standard deviations meaning all areas have a range of diameters present.

This project moved away from these microfeatures to separate scaffolds of random and aligned fibres. However, these microfeatures have the potential to be a useful tool for other research aims or in the future to expand on the responses of tanycytes. They also could be characterised further for the depth of the microfeature and the density of fibres within each area.

6.7.2 Fibre analysis

The investigation of these microfeatures highlighted that different areas contain different fibre orientations. This led to the question of how alignment would impact cell behaviour. Due to the complexity of the microfeatures having both random and aligned fibre regions within one scaffold it was expected to make investigating any different responses difficult as they could not be isolated easily. Therefore it was decided to simplify the scaffold by producing separate sheets of random and aligned fibre orientated scaffolds for initial investigations into tanycytes responses to random and aligned fibre orientations. Before this could be investigated, the fibre properties required characterisation and the method for this needed optimisation. While the manufacture of aligned scaffold was being investigated, random scaffolds and scaffolds 1-3, manufactured using Sigma PCL in DCM/DMF, were utilised as samples for optimising the fibre characterisation method.

The analysis of fibre properties, including diameter and orientation, initially seemed to be straight forward as the eye easily discerns between these features. In practice however, this method required much more consideration in terms of the size of the sample and how the measurements were collated. Thus two approaches were considered to develop the method.

In the method of the First approach (4.3.2) the areas all broadly had a diameter of 2 ±1 µm, despite significant difference being identified. This method measures all fibres within the SEM image meaning that single fibres are measured potentially several times, which is good to identify how variable each fibres diameter is along its length. On the other hand, the measuring of several fibres many times may be skewing the data and is much more time consuming. Another concern with this method is that alignment analysis shows no significant differences which does not correlate with the visible change in alignment between these areas. This method collates measurements in all directions meaning the angles are not comparable or capable of being combined, i.e. some are positive while others are negative. This method for orientation analysis was considered to not be appropriate data collection.

Consequently, for orientation analysis Second approach (4.3.3) it was decided to use a vertical line and measure the angles at which fibres were crossing this line from left to right. This then standardises the type of angle measurements being collected ensuring they are all comparable. Once the data collection method was optimised, the post-data collection method was considered in three ways, Figure 4.3.3 C. As for the Second approach, alignment analysis first method, I decided not to utilise the formula because I was not confident it was handling the angles appropriately to maintain them to be compared. I did not use the mode from the second method as occasionally there is not a mode present within a data set meaning analysis is halted for that image while the median is more representative of the most common direct fibres are facing which assists with the investigation into how much alignment is present. As a result, method three (green) is the optimised method and shows that the side of the microfeature had more fibre alignment than either the bottom or top surface.

The Second approach also attempted to improve diameter analysis by choosing one square in a consistent grid and measure a set number of fibres as this reduces the amount of time taken to collate the data. This analysis showed the same trend as the First approach of 2 ±1 µm for fibre diameter. Therefore this sampling method introduced in the Second approach was shown to be appropriate along with showing that measuring fibres several times in the First approach was not skewing the data. Again significant differences between different areas were identified. However it is not expected that cells would respond differently due to the fibre diameters as broadly each contains fibre with diameters ranging from 1-3 µm. With any differences being around 0.3 µm there is a range of diameters found in each area so these subtle differences are unlikely to be detected. This project is also investigating the impact of tanycytes behaviour which are cultured as 3D spheres and so an interesting point to consider is whether culture as 3D is more likely to be impacted by fibre diameter than single cells. Potentially a spherical culture will detect more subtle fibre differences as the cell to cell communication is stronger and so these cultures may be more sensitive to the topology. Alternatively the culture of cells as 3D spheres may be less likely to sense these small changes than single cells. Further research is required on these small differences to identify if cells do response these small margins of difference in diameter.

In order to investigate how reliable the orientation analysis of the manual method was, the results were compared with the results from the Fibremetric software. Diameter analysis was also available from the software analysis so this was compared to the manual method devised as well. Comparison between manual and automatic analysis showed there is a difference between the mean fibre diameters with the software analysis showing mean diameters almost double that produced by the manual method, Figure 6.3.3 B and C. The difference between the two methods is suspected to be due to the automatic method not being fully reliable as there is false measurements taken particularly at the larger end of fibre diameters, Figure 6.7.2 A. It is possible to edit the data collected but this requires access to the system to check the data points

removed are not true measurements. Access to this system was not readily available making this post-data collection adjustment impossible in this instance.

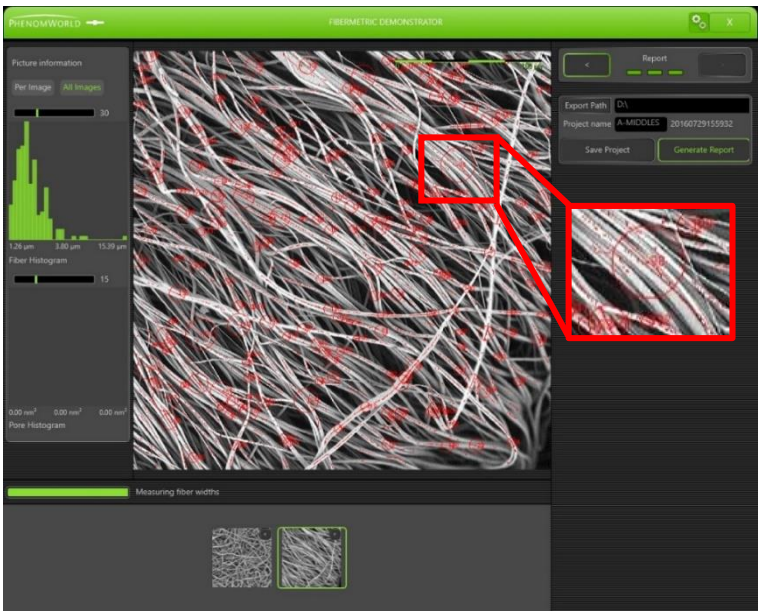

Figure 6.7.2 A: An example of fibremetric analysis with an example of a false positive measurement. This point measured a diameter at 16.4 µm.

For the orientation analysis comparing manual and automatic fibre analysis methods, considering the raw data, Figure 6.3.3 D (a) and (b), while there are statistical differences it is not visibly clear whereas once the post-data collection is applied, (c) and (d), the difference between the three areas becomes visibly clearer. This comparison shows the same trend as the manual method in that the side of the feature showed more alignment than the bottom or top surface. However the two methods produced different values of angular difference for each area. This may be due to the larger number of measurements taken by the software method (200 per image) compared to the sampling method of the manual approach (30 per image). I therefore concluded the manual method was suitable for electrospun scaffold characterisation.

In continuing the investigation into developing a rigorous method to analyse fibre orientations I also had an undergraduate mathematical student working on a project with SEM images and data collected from the large microfeature of scaffold 2 utilised in the second attempt of manual analysis. This student's aim was to identify a rigorous method for analysing orientation particularly to be used when producing scaffold with varying levels of alignment. However due

to personal circumstance this project was not completed, but further investigations may produce interesting results in the future.

6.7.3 Random and aligned scaffold manufacture

Random scaffolds had already been shown to be producible on the original rig system with Sigma PCL in DCM/DMF, however the aligned scaffold attempt with the original rig set up of a small drum rotated by a Dremel did not produce aligned fibres. The updates to the rig, including a larger drum and having this permanently fixed with a motor for rotation, was not able to produce aligned fibres safely and with the level of alignment required.

6.7.4 Optimisation of the method to produce random and aligned PCL scaffolds

Optimisation attempts to manufacture random and aligned scaffolds with Sigma PCL in DCM/DMF were unsuccessful. The placement at The Electrospinning Company introduced me to Corbion (PC12) PCL polymer and solvents HFIP and chloroform. This led to the comparison of polymer (Sigma and PC12) and solvent systems (DCM/DMF, HFIP and Chloroform).

The different MW and polydispersity of two sources of polymer shows that they have different properties and rheological analysis explains why they spun differently. For the samples I concluded the higher the viscosity the better the electrospinning of the solution as shown by the final method 15 wt% Corbion PC12 in HFIP, Figure 6.5.1 B. PC12 produced beaded fibres at 10 wt% (Figure 6.5 A) as the critical entanglement concentration was not being reached meaning smooth fibres could not be produced. Smooth fibres were manufactured at 15 wt% for Corbion while Sigma produced smooth fibres at 10 and 15 wt%. This is due to Corbion having a lower MW, 22 KD and 12.4 KD, Sigma and PC12 respectively. Corbion is better as a source of PCL in comparison to Sigma as it is medical grade and this comparison shows changes between sources of polymer can greatly affect fibre properties which could therefore potentially impact upon cell

responses. From this study I concluded that projects should work with medical grade products as early as possible to avoid repeating work and potentially having to re-optimise methods and repeat experiments. I also showed that solvent system and collection method impacts fibre properties. For the collection method the fibres were consistently thinner for aligned scaffold where the drum was rotating at high speeds than for random scaffolds where the drum was rotating slowly. This is due to the fibres being pulled more for aligned scaffolds and therefore becoming thinner.

Analysis of fibre diameter and SEM images showed that Corbion PCL was better than Sigma PCL as there was more variability between Sigma scaffolds, Figure 6.5 B. Comparison of solvents discounted DCM/DMF as it was previously utilised unsuccessfully and when considering SEM images variation was seen between fibres produced. There was minimal difference between HFIP and chloroform, however HFIP was chosen due to the more similar fibre diameters between random and aligned scaffolds despite chloroform showing better alignment.

For the scaffolds made at TEC for use in cell culture experiments, these scaffolds were analysed both by the software and the manual method providing another opportunity to test how comparable the two methods are. In this case the fibre diameters are very similar as reported by the software and the manual method, showing that the latter is a very appropriate sampling method. However alignment analysis was different for random scaffold, manual analysis provided a mean of 29.9 ±15.7° whereas software produced a mean of 44.2 ±15.3°. The main issue was alignment analysis manual provided a mean of 5.9 ±5.8° whereas software 30.0 ±30.9°. The software measure for fibre orientation (30.0°) is considered to be incorrect as the manual method provides a much smaller mean distribution of fibres around the mean (5.9°) which correlates to what can be visible seen on SEM images of these scaffolds where fibres are aligned. This issue was not seen to this extent when the automatic method was utilised for comparison of scaffold 2 largest microfeature. This is a concerning result leading to questions of the viability of the software to analyse fibre orientations under these conditions and is

potentially due to the user settings within the system. Another potential issue with the software method is that while the manual method takes one measurement from a set point, the software takes continual measurements along a fibre collecting data points when the values are significantly different to previous collected measurements. Further investigation into the programming of data collection is required to understand how this has occurred. While both methods are capable of characterising fibre alignment (in the case of scaffold 2 analysis for the software method) and comparing between random and aligned scaffold, they are not compatible methods to directly compare to each other.

HFIP was utilised to manufacture scaffolds both at The Electrospinning Company and at The Dental School (after optimisation where chloroform was not able to produce repeatable scaffolds with a thickness for use in cell culture) so comparisons of cell response between these two pairs is based on similar manufacturing processes. Any changes in cell responses identified between the two set of random and aligned scaffolds can therefore not be due to solvent utilised to manufacture the scaffolds.

When considering the properties of the random and aligned scaffolds manufactured at TEC and the DS they do have differences in their mechanical properties. Firstly their fibre diameters differ with TEC scaffolds which had a mean diameter of 3.8 and 3.0 µm for random and aligned respectively while scaffolds made at the DS had mean diameters of 3.1 and 1.2 µm for random and aligned scaffolds respectively. The thinner fibres of the aligned scaffold made at the DS potentially could have an impact on differing cell responses, particularly as the standard deviation for these scaffolds are much narrower than scaffolds 1-3 microfeatures. As previously stated, a difference in fibre diameter of 1-3 µm could to be large enough to produce differing cell responses (Section 2.1.2). However a previous study with neuronal cells on fibres with diameters of 2.4 and 3.7 µm showed little difference in behaviour [87]. Most studies for cell responses utilise fibres within the nanometre range, so potentially micrometre fibres either do not impact cells differently or further research is required for this area. Therefore the difference

in fibre diameters between the pairs of random and aligned scaffolds allow an opportunity to investigate whether this will have an impact on tanycyte responses, particularly as I will be investigating how a 3D spherical culture responds to these fibres. However these previous studies consider single cell responses to fibre diameter whereas this study will study neurosphere culture where cells maintain a 3D culture in close contact with other cells, thereby potentially altering the impact of the topology on the whole sphere.

Secondly characterisation of these two pairs of scaffolds by tensile testing in both cases showed that random and aligned scaffolds have different stiffness's. This replicated what is reported in the literature, that fibre orientation is closely linked to other mechanical properties including stiffness [39,165]. In both cases, aligned scaffolds were also shown to be anisotropic as in one orientation they are much stronger than random scaffold while samples cut at 90° difference the aligned scaffold easily falls apart. The process of backing aligned scaffolds with random fibres was to provide some stability for the scaffolds when cultured without the forces used within stiffness testing. The aligned scaffolds from TEC and the DS had similar stiffness's however the random scaffold made at the DS was stiffer than the random scaffold made at TEC. In summary fibre orientation is directly linked to fibre diameter and scaffold stiffness properties. This provides a degree of difficulty in isolating any one of these features to study properties in isolation. Also noted is the difference in scaffold properties produced at TEC and the DS highlighting the importance of a controlled environment, including temperature, on the scaffold manufacturing process particularly as the DS scaffold was much more challenging to manufacture than TEC scaffolds.

In conclusion, this chapter has reached the three objectives I set. Electrospinning onto metallic templates each with their own structure introduced complex microfeatures into the electrospun scaffold. The features morphology is representative of the structure of the metallic template meaning they are all unique in structure. One element that is consistent between each of these microfeatures is the incorporation of different fibre orientations. The fibres in some areas of

these features are aligned while other areas remained randomly organised. A manual method was optimised in order to characterise the orientation of fibres along with fibre diameter and this was then compared to automatic software to investigate its rigour, showing both methods are capable of analysing fibre features but are not necessarily comparable to each other.

For investigating how tanycytes of the adult hypothalamus would respond to fibre orientation, a method to manufacture random and aligned scaffolds was optimised with collaboration with The Electrospinning Company, considering polymer source and solvent systems. Therefore random and aligned fibrous scaffolds manufactured at The Electrospinning Company and the Dental School with 15 wt% PC12 in HFIP are now characterised in preparation for studying tanycyte responses. An overview of these two sets of random and aligned scaffolds properties is shown in Figure 6.7.4 A.

Scaffold manufacture overview

Mede/TEC placement

The Electrospinning Company

	Random	Aligned
Manual diameter (µm)	3.8 ± 0.2	3.0 ± 0.6
Manual alignment (°)	29.9 ± 15.7	5.9 ± 5.8
Software diameter (µm)	3.4 ± 0.6	2.8 ± 0.8
Software alignment (°)	44.2 ± 15.5	30.0 ± 30.9

Random

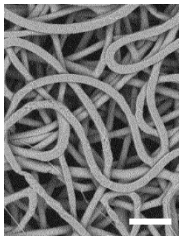

Aligned

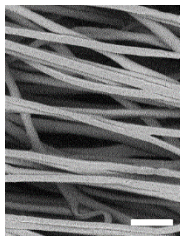

	Random		Aligned	
	Parallel	Horizontal	Parallel	Horizontal
Stiffness (MPa)	6.1	4.6	19.8	N/A

The Dental School

	Random	Aligned
Manual diameter (µm)	3.1 ± 0.4	1.2 ± 0.3
Manual alignment (°)	30.9 ± 30.9	10.1 ± 10.1

Random

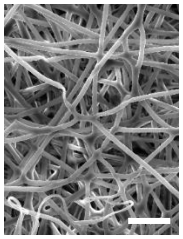

Aligned

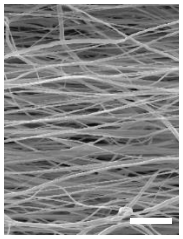

	Random		Aligned	
	Parallel	Horizontal	Parallel	Horizontal
Stiffness (MPa)	11.3	11.8	23.0	N/A

SURE Scheme

Post-SURE

Figure 6.7.4 A: An overview of the two set of random and aligned scaffolds manufactured within this project. Including fibre analysis, SEM images and stiffness properties. Scale bar 25 µm.

Chapter 7: The Electrospinning Company aligned PCL scaffolds are capable of maintaining tanycytes whereas aligned Dental School scaffolds are not

In this chapter I set out to address the following objectives:

- to characterise P3 neurospheres under free-floating 'non-differentiation' culture conditions;
- to investigate whether neurospheres could be cultured on electrospun PCL scaffolds with both random and aligned topologies;
- to investigate the morphology of neurospheres cultured on random and aligned scaffolds;
- to investigate the expression of markers of tanycytes and differentiating neurons on neurospheres cultured on both random and aligned scaffolds.

Chapter 5 highlighted the inefficiency of the free-floating neurosphere assay in maintaining a stem-like tanycyte population and the need to develop a system to improve the *ex vivo* culture of these cells. Chapter 6 then investigated the manufacture and characterisation of random and aligned scaffolds. In this chapter I aimed to culture tanycyte-derived neurospheres on random and aligned scaffold pairs, manufactured at either The Electrospinning Company or The Dental School, Figure 6.7.4 A, (hereafter referred to as TEC scaffolds and DS scaffolds, respectively), to investigate the impact of random and aligned fibres on the maintenance of stem-like tanycytes. *In vivo*, tanycytes form the ventricular layer that lines the third ventricle of the brain (Figure 5.1.1 B) where they show a high degree of organisation (tightly-packed in a neuroepithelial-like arrangement and displaying apico-basal polarity). I hypothesise that aligned scaffolds may encourage neurospheres to become organised within such an arrangement and that this could maintain tanycyte stem-like cells, reducing spontaneous differentiation. I therefore firstly set out to examine the morphology of neurospheres cultured on each scaffold type and secondly, the expression of several markers.

I analysed six of the previously utilised markers including the tanycyte markers Nestin, NrCAM and GFAP and the neuronal differentiation markers TH and Tuj1. Other differentiation markers

such as those for oligodendrocytes were not included to simplify this initial study. Finally I also analysed expression of cleaved Caspase-3 to determine whether culture on the scaffolds led to cell death, specifically apoptosis levels.

Within chapter 5 I characterised Passage 5 and Passage 6 (P5/6) neurospheres cultured in a free-floating neurosphere assay under 'non-differentiation' conditions and concluded that spontaneous differentiation occurs under these conditions. I also investigated P2 and P11 neurosphere differentiation and demonstrated that these extreme passage numbers have very different differentiation capabilities. Based on these findings, I concluded that it was important to culture low passage neurospheres for the investigation into the impact of fibre orientation. I chose to work with P3 neurospheres as a balance between the requirement for low passage neurospheres and having a sufficiently large number of neurospheres within each culture to be able to draw meaningful conclusions.

7.1 Passage 3 free-floating neurospheres show some spontaneous differentiation

Before testing the impact of random and aligned scaffolds on neurosphere behaviour (morphology and marker expression), P3 neurospheres were characterised after culture in a free-floating neurospheres assay in standard non-differentiation conditions to investigate the level of spontaneous differentiation occurrence at P3.

Similar to P6 neurospheres (Figure 5.2 B), I noted a variation in neurosphere size in P3 neurospheres (Figure 7.1 A). I could categorise P3 neurospheres as small, medium and large as previously documented. However, no difference in labelling was noted with respect to size, although in large neurospheres there was some limitation in penetration of both DAPI stain and antibody labelling in the centre of the neurosphere, most likely due to the dense culture. However this was minimal, thus all neurospheres were analysed as one group irrespective of size.

P3 neurospheres were fixed as whole spheres and labelled with Nestin, NrCAM, Tuj1, TH, GFAP and cleaved Caspase-3 (Method as 4.1.5). Figure 7.1 B shows examples of positively labelled neurospheres, while Table 7.1 A shows the percentages of positively labelled neurospheres in each of the three repeats. All neurospheres were positive for Nestin and NrCAM with the exception of one neurosphere which was positive for Nestin whilst negative for NrCAM. However, all neurospheres showed spontaneous differentiation although there were variations in the different repeats. Thus the percentage of positively labelled neurospheres for Tuj1 and TH ranged from 35-70% and 45-80% respectively, while GFAP ranged from 0-70%. Tuj1 and TH positive labelling was primarily seen at the periphery of the neurosphere. Caspase-3 positive labelling occurred at low levels in 20-70% of neurospheres. Therefore P3 neurospheres showed variable differentiation at similar levels to those seen in P6 neurospheres. In summary this characterisation has shown that neurospheres derived from the hypothalamus were capable of self-renewal (Nestin and NrCAM positive) but that culture under the free-floating neurosphere assay in non-differentiation conditions is not 100% efficient as spontaneous differentiation was present at variable levels (Tuj1 and TH positive). This supports the data from P5 and P6 neurospheres which led to the same conclusion but also showed this also occurred at lower passage numbers.

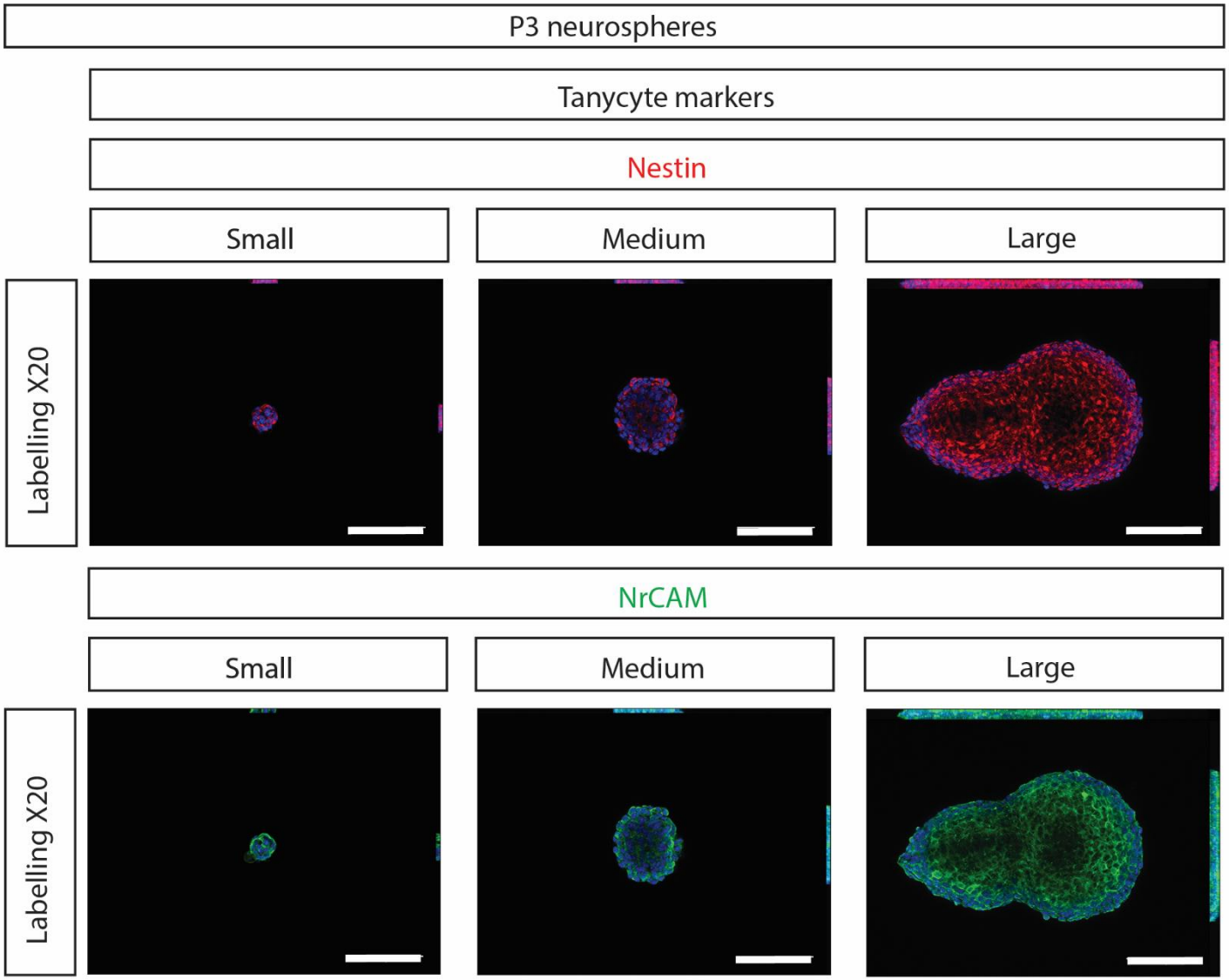

Figure 7.1 A: Passage 3 neurospheres separated based on size. Method as 4.1.5 whole mount in neurospheres. Nestin (red), NrCAM (green) and DAPI (blue) labelling nuclei. Neurospheres were grouped into small, medium and large and the difference in size does not affect antibody labelling, except in large neurosphere there is a limitation in neurosphere penetration to the centre of the sphere. Scale bar 100 µm.

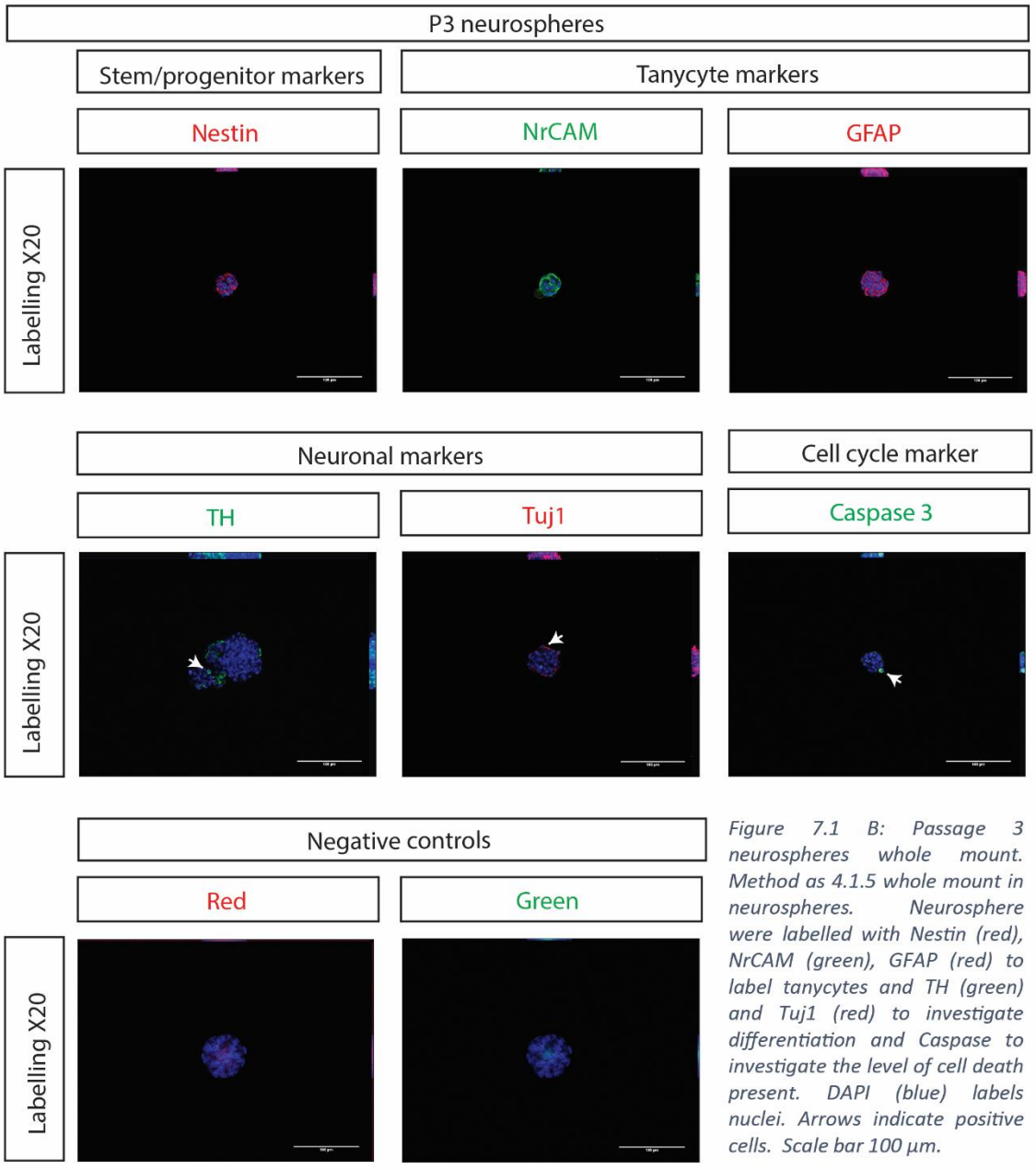

Figure 7.1 B: Passage 3 neurospheres whole mount. Method as 4.1.5 whole mount in neurospheres. Neurosphere were labelled with Nestin (red), NrCAM (green), GFAP (red) to label tanycytes and TH (green) and Tuj1 (red) to investigate differentiation and Caspase to investigate the level of cell death present. DAPI (blue) labels nuclei. Arrows indicate positive cells. Scale bar 100 µm.

Table 7.1 A: Passage 3 neurospheres antibody labelling. For each mouse pair utilised to isolate neurospheres (as method 4.6.3 Neurosphere cell culture in cell isolation) the percentage of neurospheres positively labelled with the antibody are indicated.

Passage 3 neurospheres						
	Mouse pair 1		**Mouse pair 2**		**Mouse pair 4**	
	n number	**% neurospheres positively labelled**	**n number**	**% neurospheres positively labelled**	**n number**	**% neurospheres positively labelled**
Nestin	8/8	100	25/25	100	10/10	100
NrCAM	8/8	100	25/25	100	9/10	90
Tuj1	11/16	68.8	12/28	42.9	3/9	33.3
TH	13/16	81.3	17/28	60.7	4/9	44.4
GFAP	0/17	0	19/27	70.4	1/10	10
Casp	4/17	23.5	18/27	66.7	7/10	70

7.2 Tanycyte-derived neurospheres show changes in morphology in response to fibre orientation

I next set out to determine whether I could limit spontaneous differentiation by culturing on specific electrospun scaffolds. Initially I aimed to establish that tanycyte derived neurospheres were able to attach to electrospun surfaces and then could be cultured. Neurospheres were cultured on scaffolds for 10 days (method as 4.1.5) and then observed with DAPI, a nuclear stain. DAPI positive nuclei were consistently found on all scaffolds (Figure 7.2 A).

When tanycyte-derived neurospheres were cultured in the free-floating assay under non-differentiation conditions, the neurospheres had spherical morphology (Figure 7.1 B). However, when the neurospheres attached to the scaffold, their morphology changed showing a distinct shape unique to random or aligned scaffolds. On random scaffolds, neurospheres remained circular in their morphology but flattened, while on aligned scaffolds the neurospheres elongated along the scaffold fibres. The higher the alignment between the fibres of the scaffold, the more elongated the neurosphere; thus The Electrospinning Company (TEC) aligned scaffold showed more fibre alignment (5.9 ±5.8°) than the Dental School (DS) scaffold (10.1 ±7.6°) and this was reflected in the level of elongation and the width of the neurosphere (Figure 7.2A).

Individual nuclei could be seen to align along the fibres (Figure 7.2 A arrows) and showed organisation; nuclei were aligned on aligned scaffold. On random scaffolds nuclei are clustered together and appeared less organised overall.

In summary, tanycyte derived neurospheres could be cultured on TEC and DS scaffold and showed morphological change alongside changes to nuclear organisation.

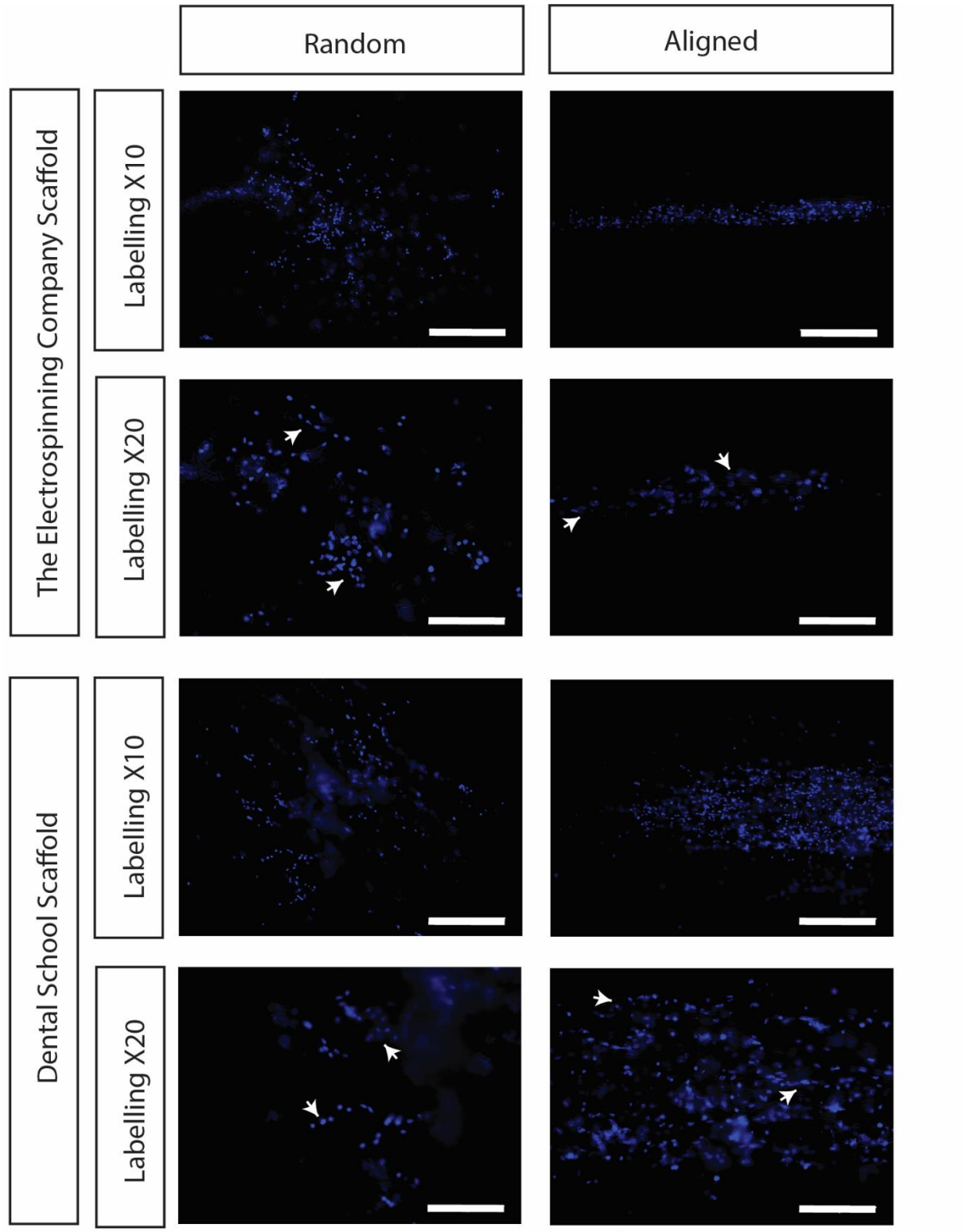

Figure 7.2 A: Culture of neurospheres on random and aligned scaffolds leads to a morphological change. DAPI (blue) labels nuclei. On both TEC and Dental scaffold neurospheres remain spherical on random scaffold while on aligned neurospheres are elongated. When individual nuclei are considered on aligned they are lined on the fibres whereas on random scaffold nuclei are more disordered as the fibres are disordered. Scale bar for 200 µm X10 images and 100 µm for X20 images.

7.2.1 The Electrospinning Company aligned scaffolds better support tanycytes, but do not reduce spontaneous differentiation

Next I went on to determine whether the changes in neurosphere morphology and nuclear organisation impacted on spontaneous differentiation by analysing the expression of key markers. First I considered the random and aligned scaffold made at TEC (Table 7.2.1 A and Figure 7.2.1 A). For this study four mouse pair-derived P3 neurosphere cultures were analysed, N=4.

The P3 neurospheres cultured on aligned TEC scaffolds showed consistent and high levels of expression of the tanycyte markers Nestin, NrCAM and GFAP, (Figure 7.2.1 A). Similar to neurospheres cultured under non-differentiation conditions in the free-floating assay, intense expression of Nestin and NrCAM was detected on all neurospheres cultured on TEC aligned scaffolds. However, TEC-aligned scaffolds better-supported GFAP-expression. GFAP expression was detected on 96% neurospheres on aligned TEC scaffold, compared to detection on 27% of free-floating neurospheres.

P3 neurospheres cultured on random TEC scaffolds showed less intense expression of Nestin, NrCAM and GFAP (Figure 7.2.1 A) in comparison to those cultured on aligned TEC scaffolds. Nestin showed 100% of positively labelled neurospheres in all three culture conditions (free-floating, random TEC scaffold and aligned TEC scaffold) but as stated the neurospheres on random scaffold had less intense labelling. NrCAM showed 96% positive neurospheres on random TEC scaffold and 97% in free-floating culture alongside neurospheres on random scaffold having less intense expression than either culture on aligned TEC or free-floating. Therefore in free floating culture and on random TEC scaffold some neurospheres appear to be downregulating Nestin and NrCAM expression, but expression is maintained more consistently for all neurospheres when cultured on aligned TEC scaffold. Also when comparing neurosphere cultured on random and aligned TEC scaffold it was noted that the cells within the neurospheres

have different shapes. On aligned scaffolds these cells are elongated along the fibres with long processes whereas on random the cells have a shorter process, (Figure 7.2.1 B).

For GFAP expression showed a similar trend to Nestin and NrCAM, notably there was less intense expression of GFAP on random TEC scaffold compare to aligned TEC scaffold. Moreover, there was also few positive neurospheres on random TEC scaffold (74%) compared to aligned TEC scaffold (96%). For GFAP cultured under free-floating culture conditions there are less GFAP positive neurospheres with an average of 31%. Therefore culture on TEC scaffold better supports the maintenance of GFAP expression particularly on aligned TEC scaffold. Together, these results suggests that aligned, but not random TEC scaffolds, were better at maintaining tanycytes than free-floating cultures (more GFAP and NRCAM+ neurospheres).

To test this further, I analysed the differentiation markers Tuj1 and TH. Each was detected on neurospheres cultured on both random and aligned TEC scaffolds and was detected on a similar proportion of neurospheres to those cultured under free floating non-differentiation conditions. On both random and aligned TEC scaffolds, Tuj1 was detected on around 50% neurospheres and stronger labelling was seen on the cells cultured on aligned scaffolds (Figure 7.2.1 A) under free-floating conditions where Tuj1 was detected on 48% of neurospheres. On average TH was detected in 62% of neurospheres when cultured in the free-floating assay, however TH was detected in 90% of neurospheres cultured on both random and aligned TEC scaffolds. The low levels of Caspase 3 positive cells shows that cells are able to be cultured on these scaffolds without high levels of cell death.

As with free-floating cultures, neurospheres ranged in size when cultured on random and aligned TEC scaffolds. I therefore investigated if tanycyte maintenance or spontaneous differentiation were affected by the neurosphere size. This analysis demonstrated that both large and small neurospheres showed similar levels of stem/progenitor tanycytes versus differentiated cells. Figure 7.2.1 B shows examples of large and a small neurospheres cultured on either random or aligned TEC scaffolds. I detected labelling by Nestin and NrCAM under all

conditions, although again aligned TECs scaffolds support a higher intensity of expression for these markers when compared to random scaffolds, regardless of neurosphere size. Analysis of Tuj1, TH and cleaved Caspase-3 also revealed no difference in expression between the small or large neurospheres, Figure 7.2.1 C.

In summary, aligned TEC scaffold, while not been capable of preventing spontaneous differentiation, this scaffold is better able to support tanycyte maintenance than random TEC scaffold or free-floating.

Table 7.2.1 A: Number of neurospheres positively labelled cultured on TEC scaffolds. Shown is the number of positively labelled neurospheres over the four experiments and the average percentage of positively labelled neurospheres. Also shown is the average of positive neurospheres labelled from free-floating culture from Table 7.1 A for comparison.

TEC Scaffold					**Free-floating culture**	
	Random		Aligned			
Nestin	27/27	100%	28/28	100%	43/43	100%
NrCAM	27/28	96%	28/28	100%	42/43	97%
Tuj1	18/33	55%	16/30	53%	26/53	48%
TH	32/33	97%	27/30	90%	34/53	62%
GFAP	17/23	74%	26/27	96%	20/54	27%
Casp3	7/23	30%	15/27	56%	29/54	53%

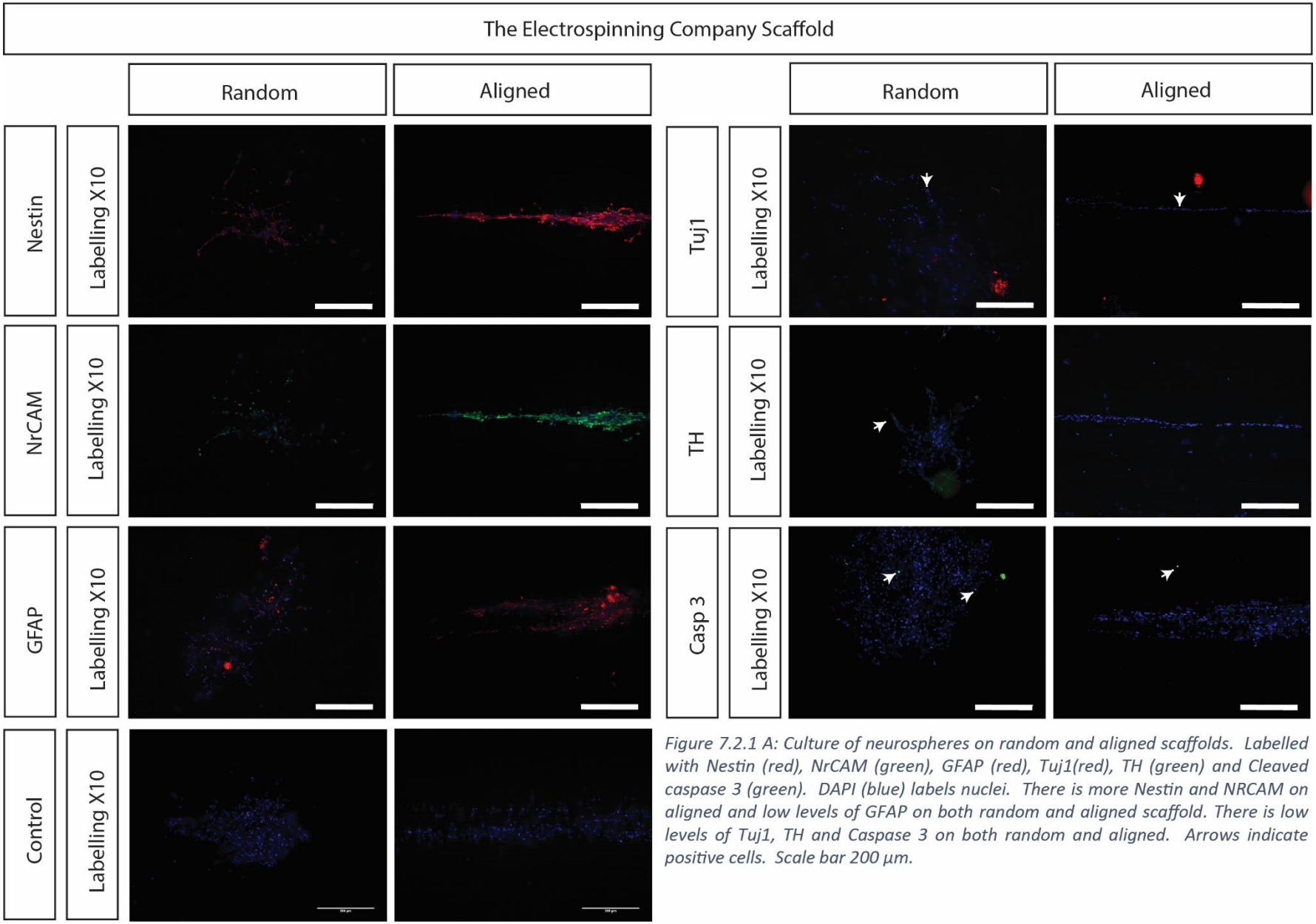

Figure 7.2.1 A: Culture of neurospheres on random and aligned scaffolds. Labelled with Nestin (red), NrCAM (green), GFAP (red), Tuj1(red), TH (green) and Cleaved caspase 3 (green). DAPI (blue) labels nuclei. There is more Nestin and NRCAM on aligned and low levels of GFAP on both random and aligned scaffold. There is low levels of Tuj1, TH and Caspase 3 on both random and aligned. Arrows indicate positive cells. Scale bar 200 µm.

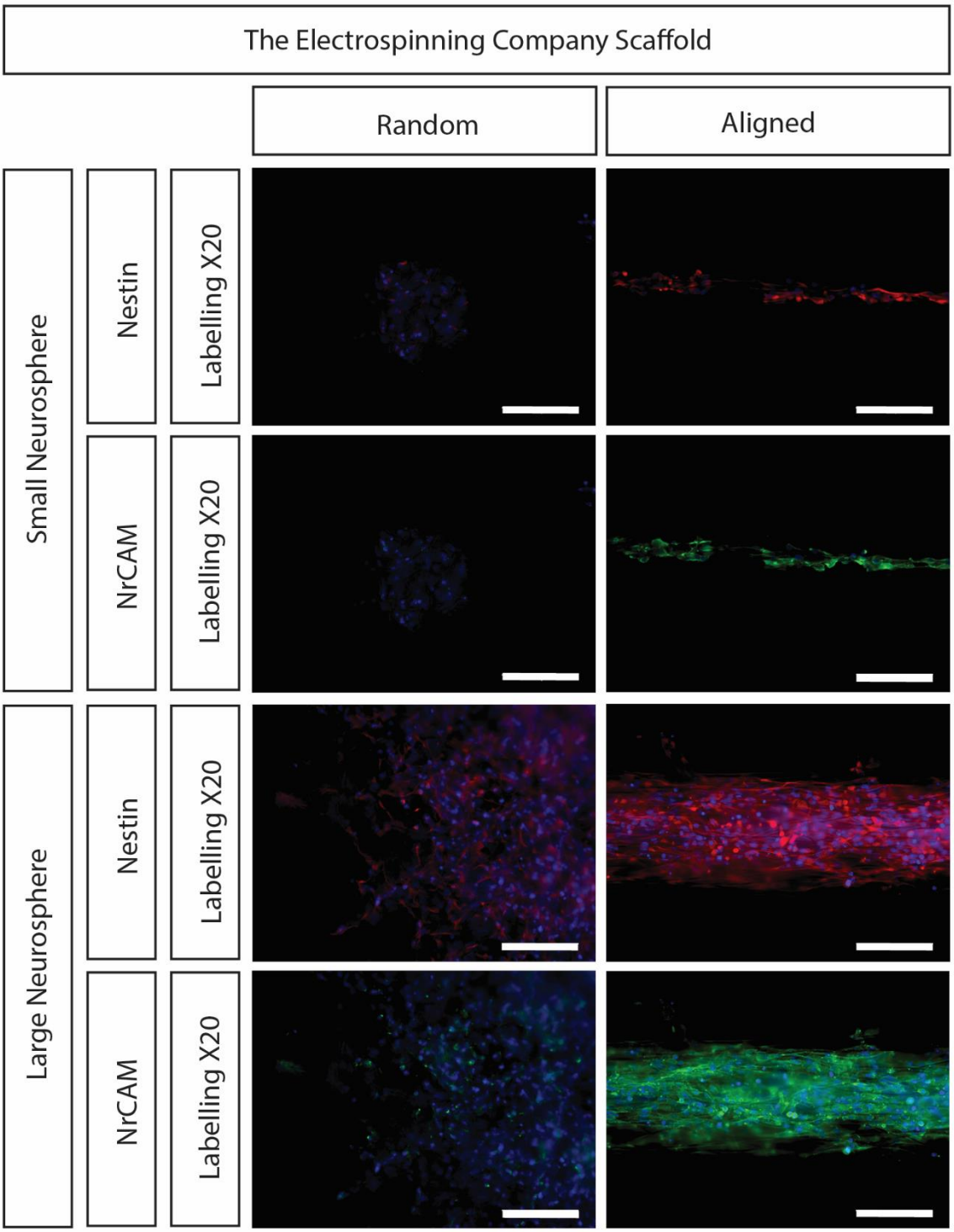

Figure 7.2.1 B: Small and large neurospheres cultured on TEC scaffolds labelled with Nestin (red) and NrCAM (green). DAPI (blue) labels nuclei. Scale bar 100 µm.

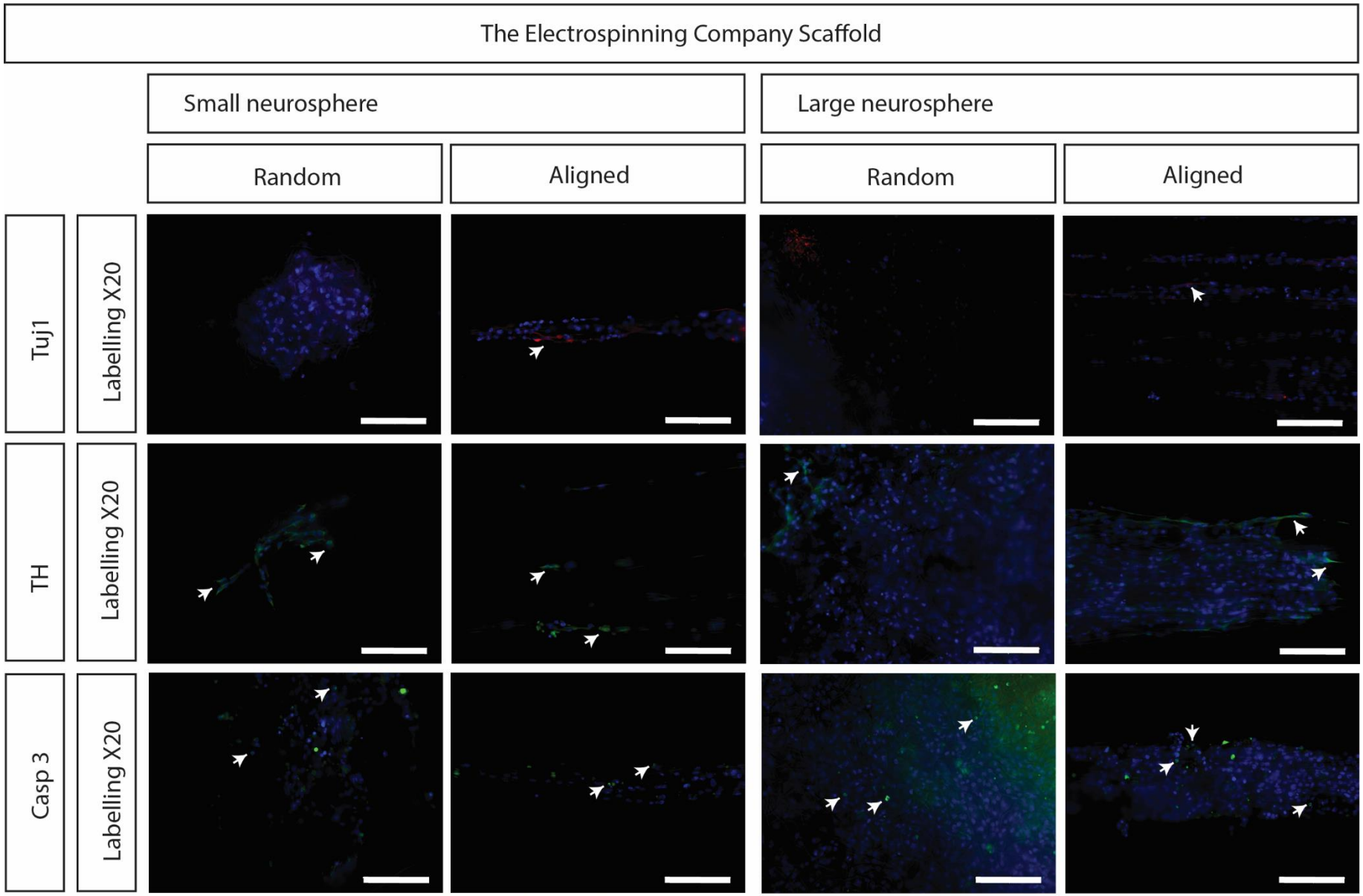

Figure 7.2.1 C: Culture of neurospheres on random and aligned scaffolds labelled with Tuj1 (red), TH (green) and Cleaved Caspase 3 (green). DAPI (blue) labels nuclei. There is low levels of Tuj1, TH and Caspase 3 on both random and aligned scaffolds. Arrows indicated positive cells. Scale bar 100 µm.

7.2.2 Dental School aligned scaffolds do not support either tanycytes, or reduce spontaneous differentiation

In parallel to culturing neurospheres on TEC scaffolds, neurospheres were cultured on random and aligned scaffolds made at the DS (Figure 7.2.2 A N=3 as there was three parallel experiments with TEC scaffolds). Nestin and NrCAM were detected on all neurospheres cultured on random and aligned DS scaffolds. Nestin was detected at the same intensity on random and aligned DS scaffolds; however NrCAM expression was more intense on random DS scaffolds, compared to aligned DS scaffolds. It was difficult to determine whether fibre orientation of the DS scaffolds affected Nestin and NrCAM expression as there was a great deal of variation between neurospheres which was not evident when neurospheres were cultured on TEC scaffolds (Figure 7.2.2 B). The variation of marker intensity was of particular note for Nestin labelling of neurospheres cultured on random scaffolds.

GFAP expression was detected on a higher proportion of neurospheres cultured on aligned DS scaffolds than on random DS scaffolds, (77% and 35% respectively); in comparison neurospheres cultured under free-floating condition 27% were positive neurospheres for GFAP labelling. This does not concur with the results of Nestin and NrCAM labelling which suggests that tanycytes are less-well supported on aligned DS scaffolds than on random DS scaffolds. However, since GFAP marks astrocytic glia cells, as well as tanycytes, it is possible that this shows that aligned DS scaffolds support tanycyte differentiation rather than maintenance.

I then considered the other differentiation markers to identify whether aligned DS scaffold were more capable of maintain these markers. Tuj1 labelling was detected on a higher proportion of neurospheres cultured on aligned versus random DS scaffolds (86% versus 50% respectively) suggesting that aligned DS scaffolds encouraged differentiation, in comparison to free-floating conditions (in the latter, 48% of neurospheres were Tuj1 positive). TH labelling likewise suggested that aligned DS scaffolds encourage differentiation. TH was detected on 75% of neurospheres cultured on random scaffolds, but on 100% of neurospheres cultured on aligned

DS scaffolds. For free-floating neurospheres, 62% were positively labelled for TH again showing more differentiation when cultured on either DS scaffolds. However it is important to note that for Tuj1 and TH this data comes from one experiment and not three as for all other investigated markers. This was due to infections on either the random or aligned scaffolds in two of the three replicates.

Cleaved Caspase-3 positive cells were found at low consistent levels on both random and aligned scaffold (75% and 62% respectively).

In summary aligned DS scaffolds were not able to maintain tanycytes in contrast to aligned TEC scaffold, but did maintain increased GFAP expression alongside differentiation markers, Tuj1 and TH, in comparison to random DS scaffold and free-floating culture.

Table 7.2.2 A: Number of neurospheres positively labelled cultured on Dental School scaffolds. Shown is the number of positively labelled neurospheres over the three experiments and the average percentage of positively labelled neurospheres. Also shown is the average of positive neurospheres labelled from free-floating culture from Table 7.1 A for comparison.

DS Scaffold					**Free-floating culture**	
	Random		Aligned			
Nestin	17/17	100%	13/13	100%	43/43	100%
NrCAM	17/17	100%	13/13	100%	42/43	97%
Tuj1	2/4	50%	6/7	86%	26/53	48%
TH	3/4	75%	7/7	100%	34/53	62%
GFAP	6/17	35%	10/13	77%	20/54	27%
Casp3	9/12	75%	8/13	62%	29/54	53%

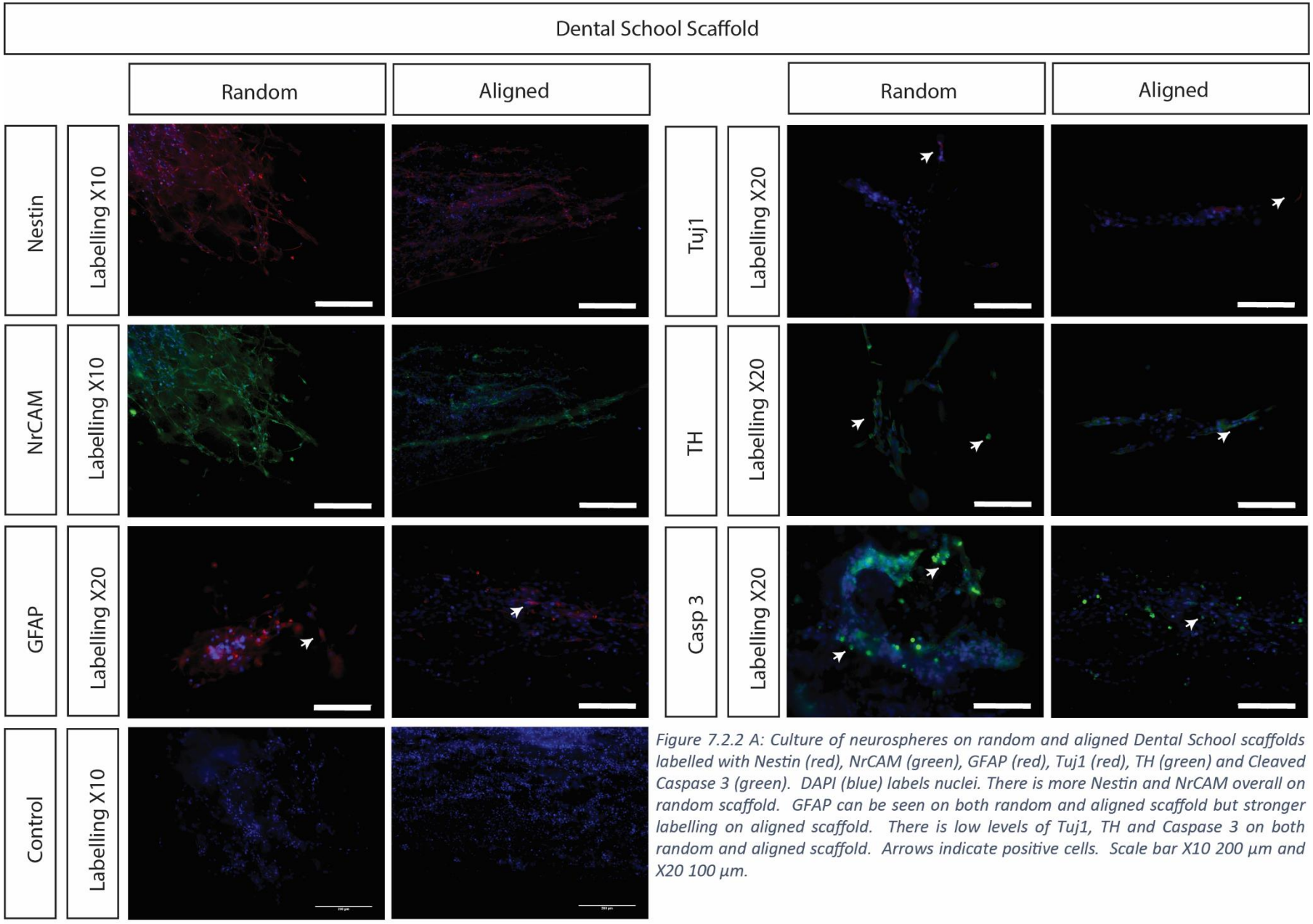

Figure 7.2.2 A: Culture of neurospheres on random and aligned Dental School scaffolds labelled with Nestin (red), NrCAM (green), GFAP (red), Tuj1 (red), TH (green) and Cleaved Caspase 3 (green). DAPI (blue) labels nuclei. There is more Nestin and NrCAM overall on random scaffold. GFAP can be seen on both random and aligned scaffold but stronger labelling on aligned scaffold. There is low levels of Tuj1, TH and Caspase 3 on both random and aligned scaffold. Arrows indicate positive cells. Scale bar X10 200 µm and X20 100 µm.

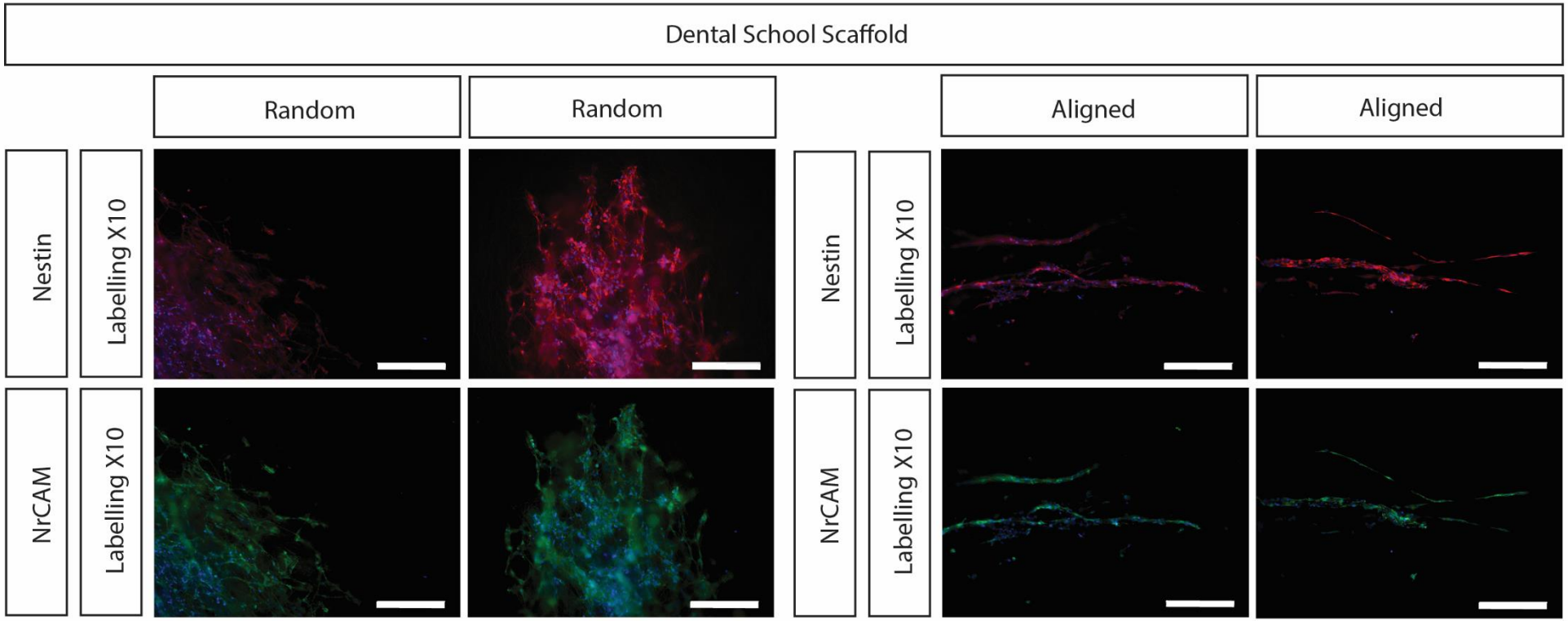

Figure 7.2.2 B: Culture of neurospheres on random and aligned Dental School scaffolds show variation in labelling. Labelled with Nestin (red) and NrCAM (green). DAPI (blue) labels nuclei. There was variation between expression of Nestin and NrCAM particularly on random scaffold and particularly for Nestin. Scale bar 100 µm.

7.3 Discussion

Characterisation of P3 neurospheres solidified the conclusion within chapter 5 that the neurosphere assay was not 100% efficient in maintaining tanycyte cells as low levels of differentiation occurs even at low passage numbers. In P3 free-floating neurosphere characterisation, a single neurosphere was negative for NrCAM (Table 7.1 A) which is either indicative of a small number of neurospheres being NrCAM negative or poor antibody labelling. In order to identify how frequently neurospheres are NrCAM negative at P3, further characterisation of P3 free-floating neurospheres would be required. In order to develop the understanding of this brain stem-like population, improvements to this culture system are required to maintain the 'stemness' of this population whilst removing spontaneous differentiation.

I have shown that neurospheres can be cultured on PCL electrospun scaffolds and that on random and aligned fibre organisations neurospheres showed strong morphological responses to this fibre orientation. On random scaffolds, the neurospheres remain generally spherical but are flattened, while on aligned scaffolds the cells appear to follow the aligned fibres elongating the neurospheres in comparison to the spherical morphology when cultured in free-floating conditions. This morphology change is represented also at a nuclei level where the nuclei align along the fibres. Thus nuclei are more organised on aligned scaffolds whilst being clustered on random scaffolds where the fibres are more disordered.

I then investigated the effect of this culture on a variety of markers and showed that random and aligned topologies impact upon the level of expression of these markers. Thereby showing that fibre morphology is an important cue to tanycyte behaviour. TEC aligned scaffolds, whilst unable to prevent spontaneous differentiation, maintained tanycytes as shown by the higher intensity of tanycyte markers (Nestin and NrCAM) when compared to neurospheres cultured on random scaffold. However, analysis on DS scaffolds did not show this same trend. Aligned DS scaffold better maintained differentiation markers (Tuj1 and TH) as well as GFAP, while Nestin

and NrCAM were more variable in terms of the intensity of expression between random or aligned DS scaffolds. The differences between the expression intensities of these markers when neurospheres were cultured on the two pairs of scaffolds are most likely due to the differences between their mechanical properties. As the properties vary between all four scaffolds (Figure 6.7.4 A) more research is required to draw final conclusions. However this preliminary work can provide insight to guide the project forward. Therefore I have addressed all of the objectives set out for this chapter.

Firstly I will consider the differences between random and aligned TEC scaffold. Aligned TEC scaffolds better maintained tanycytes than random TEC scaffolds but were not able to eliminate spontaneous differentiation. While the hypothesis that aligned fibres will better maintain tanycytes has been shown by the higher intensity of tanycyte markers along with more positive neurospheres on aligned scaffolds for GFAP and NRCAM, in comparison to random scaffold, this data is not sufficient to conclude whether this is due to the replication of *in vivo* morphology of highly organised and elongated tanycytes. Further research to investigate whether the aligned TEC scaffold is replicating *in vivo* organisation could be done by studying apico-basal polarity of the cells on this substrate.

The fibre orientation is thought to be the cause of the maintenance of tanycytes on aligned TEC scaffold however, random and aligned TEC scaffolds, alongside the different fibre organisations, have other different properties including the mean fibre diameter 3.8 ±0.2 µm and 3.0 ±0.6 µm respectively. TEC scaffolds show a difference in fibre diameter of 0.8 µm, which is reduced further when the standard differentiations are considered and so is unlikely to be influencing cell behaviour. Research into the impacts of fibre diameters is an ongoing area of research (Section 2.1.2). For tanycytes further research is required focusing on the impact of fibre diameter to understand the impact of this cue on tanycyte behavioural responses. Another difference between random and aligned TEC scaffold is the stiffness with 6.1 and 4.6 MPa for random TEC scaffold and 19.8 and N/A MPa for aligned. These stiffness measurements were

collected by the scaffold samples being under stress via tensile testing, as the samples are pulled apart to produce these stiffness values. While this is an important result in terms of scaffold characterisation to show that fibre orientation is linked to other mechanical properties as the stiffness value changes as a result of changing fibre orientation, it is a macro-stiffness value as it measures stiffness of the whole scaffold (many fibres within the sample). In terms of the influences the cells experience this value is not as relevant as the cells have not been cultured under scaffold stress condition. The tanycytes are cultured in 3D neurospheres and therefore are in contact with several fibres over the neurosphere meaning the individual fibre stiffness is more influential on cell behaviour, known as a micro-stiffness value. AFM is an alternative method for calculating the stiffness of fibres, the micro-stiffness value. Therefore the macro-stiffness values calculated for these scaffolds are more difficult to utilise in concluding differencing cell responses, but as macro and micro properties are linked the macro values can be utilised as indicatory. Therefore the differing stiffness of these scaffolds may also be involved in behavioural responses and further investigation of this property, i.e. with other properties such as alignment maintained at a consistent value, is required. This however is a challenge as fibre orientation changes are known to alter stiffness as previously discussed (Section 2.1.2).

Differentiation markers Tuj1 and TH are comparable between random and aligned TEC scaffolds in terms of the percentage of positive neurospheres, but the intensity was higher on aligned scaffold. Therefore the differences between these scaffolds properties influence these markers. Overall this corresponds with other research which has shown that higher levels of neuronal differentiation is seen on aligned substrates [86]. Therefore fibre alignment is potentially an important cue to maintain tanycytes and also promote neuronal differentiation with other properties such as diameter or stiffness being important to separate these two outcomes (maintenance or differentiation).

On DS scaffolds, tanycytes were not better maintained on aligned scaffold when compared to random scaffold and there was more variation between neurospheres in terms of the intensity

of expression. However, markers Tuj1, TH and GFAP all showed more positive neurospheres on aligned DS scaffold. For random DS scaffold the mean fibre orientation was 30.9 ±30.9° compared to 10.1 ±10.1° for aligned. Random DS scaffolds had a mean diameter of 3.1 ±0.4 µm while aligned DS scaffold had a mean of 1.2 ±0.3 µm. When comparing DS scaffolds fibre diameter differs to a greater extent than TEC scaffolds and therefore could be having a greater influence in the different cell behavioural responses as there is a two-fold difference. As previously discussed in Sections 2.1.2 and 6.7.4 this range of fibre diameter difference potentially could impact cell behaviour however limited literature has looked at these specific diameters, highlighting a need to further investigate these specific diameters for tanycytes.

As the behavioural responses of neurospheres cultured on TEC and DS scaffolds varied along with their differing mechanical properties, I compared results from the TEC and DS scaffold together in order to begin to draw final conclusions about which factors have influenced each of the behavioural responses.

The key difference between these two aligned scaffolds is the level of alignment present. TEC aligned scaffold showed more alignment (5.9 ±5.8°) than DS aligned scaffold (10.1 ±10.1°), therefore TEC aligned scaffold is potentially more efficient in organising and elongating tanycytes. This observation is also supported by images labelled with DAPI where morphology was considered and neurospheres on TEC aligned scaffold elongated more than neurospheres on DS aligned scaffold. However, other properties also differ between TEC aligned scaffold and DS aligned scaffold including fibre diameters 3.0 ±0.6 µm versus 1.2 ±0.3 µm. As with the difference between DS random and aligned scaffolds, the aligned scaffolds of TEC and DS also show more than a twofold difference and therefore this feature is potentially involved in behavioural differences. In conclusion, fibres of around 3 µm may be able to maintain tanycytes in combination with alignment while 1 µm is not able to maintain tanycytes as well.

As previously discussed, due to the issues with the infections incurred when culturing DS samples, two of these samples for Tuj1 and TH were not included in the final analysis. In order

to be able to draw any representative conclusions for comparison of these two markers between the two sets of scaffolds, further repeat experiments of the DS scaffolds neurosphere cultures are required. These issues with infections of the DS scaffold were not experienced with TEC produced scaffolds, thus alternative sterilisation techniques may be required for future DS scaffold utilisation. It is therefore difficult to draw conclusions of which scaffold better supported differentiation other than the highest percentage of positive neurospheres were found on aligned DS scaffold where thinner fibre and the highest macro-stiffness was present. However, other studies with neuronal cells showed higher neurite growth on thicker fibres as discussed in 2.1.2 [87]. Therefore future work could investigate whether thin aligned scaffold promote differentiation of neuronal cells.

Both TEC and the DS scaffolds showed a low level of Caspase-3 in the majority of neurospheres demonstrating that the scaffolds are able to support neurosphere culture without resulting in high levels of cell death.

When comparing the two aligned scaffolds, TEC aligned scaffold maintained tanycyte markers whereas DS aligned scaffolds did not, highlighting the importance of controlling the parameters during electrospinning to produce scaffolds as was the case for the manufacture of TEC scaffold. Whereas for DS scaffolds manufactured in a laboratory setting some parameters were not controlled, such as temperature, which impacted the scaffolds fibre properties and in turn impacted cell behaviour. High quality scaffolds with reproducible properties are essential for investigating cell responses.

In summary this project has shown that tanycyte derived neurosphere respond to mechanical cues of fibre orientation and potentially diameter which influence behavioural responses. These scaffolds provide an initial study for the basis of continuing to investigate how tanycyte NSPC respond to fibre diameter, orientation and substrate stiffness. Aligned TEC scaffold provides a good starting substrate to develop a system for the controlled maintenance of tanycyte cells,

providing progress towards a culture system where this novel and very important NSPC population can be studied further.

Chapter 8: Conclusions and future work

8.1 Conclusion

The original hypothesis of this project was that aligned electrospun scaffolds would both maintain stem-like tanycytes and reduce spontaneous differentiation. In summary, I have shown that tanycytes appear to be better maintained on aligned TEC scaffold, however the properties of this scaffold were not sufficient to prevent spontaneous differentiation. The scaffolds manufactured at TEC and the DS present varying mechanical properties including fibre dimeter and orientations alongside macro-stiffness values. Comparison of neurospheres cultured on these scaffolds showed that tanycytes respond to these properties. However, as these three properties vary between each of the four scaffolds it was not always possible to understand the impact of individual properties on behavioural responses. Despite attempting to manufacture scaffolds at the DS with the same properties as scaffolds produced at TEC, differences in fibre diameter and orientation were still present. Although highly reproducible in a controlled environment, electrospinning can be prone to erratic reproducibility and it was not possible to control all environmental factors to replicate TEC properties for DS scaffolds. Therefore, in the future it is important to produce scaffolds where only one of these scaffold properties is changed while the other two are maintained as controls to study each factor individually. However, the variance in these scaffolds has provided the insight into tanycytes responding to fibre diameter and stiffness which are therefore other scaffold properties of interest for future work.

I will now consider the objectives I set out for this project. I was able to address all of these objectives, however some will require further investigation as discussed in section 8.2.

Firstly I identified the central hypothalamus by key markers. Through this *in vivo* hypothalamic characterisation I identified NrCAM as a novel marker of tanycytes specific to this population, which is particularly important as other tanycyte markers such as GFAP labels both tanycytes as well as astrocytes. This became an issue when analysing neurospheres cultured on scaffolds as it led to the question of which population was being labelled by GFAP, tanycytes or early

astrocyte progenitors. I was also able to isolate and culture tanycyte derived neurospheres and show that the standard culture method of free-floating neurospheres via the neurosphere assay, while capable of maintaining a tanycyte population, was not 100% efficient and spontaneous differentiation was occurring. I then showed that culture via these conditions greatly affected the differentiation capabilities of the neurospheres, thus highlighting the need for improvements to this culture system to be able to maintain tanycytes for their continued study. Literature has shown the potential of artificial/synthetic substrates for *in vitro* study of cell behaviour in response to mechanical properties, including the influence of orientation. This evidence, alongside the preliminary data, showed indications that tanycyte derived neurospheres would respond to orientation leading to the hypothesis that aligned fibres would maintain a tanycyte population. The maintenance of tanycytes on aligned fibres was hypothesised to be due to alignment replicating the highly organised, elongated morphology of tanycytes that are part of the ventricular layer epithelium and also show apico-basal polarity *in vivo* of the adult hypothalamus.

I then progressed to the objective to manufacture electrospun scaffolds in order to be able to test my hypothesis. I was able to produce random scaffolds and introduce features, via metallic templates, which contained areas of random and aligned fibre orientations. These scaffolds, Scaffolds 1-3, were utilised to investigate alignment as a property to be measured mathematically, thereby developing a method to characterise fibre properties including fibre diameter. This process highlighted again the complexity of characterising a feature such as fibre orientation and therefore the importance of clarity for the method used when reporting scaffold properties. The manual method produced is suitable to compare fibre properties between scaffolds.

In order to simplify the comparison of random and aligned topologies, the project progressed to manufacturing separate scaffolds for random and aligned fibre orientations. Previously random scaffolds had been manufactured, however optimisation was required to develop a method to

manufacture aligned scaffolds. This included comparing polymer source, (Sigma and Corbion), and solvents, (DCM/DMF, HFIP and chloroform), to identify the final method 15 wt% PC12 PCL in HFIP. This comparison highlighted the impact that different polymer sources had on fibre properties, including diameter, as while they are both PCL they have different molecular properties. My studies demonstrated that the solvents utilised also influenced the fibre properties. Finally collecting fibres on a rotating drum at high speed, aligned scaffold, showed a consistent thinning of the fibres in comparison to when collecting on a slowly rotating drum or a flat plate, random scaffold. This provides the reason for the continued problem with having different fibre diameters between random and aligned scaffolds and shows that maintaining all properties, and only changing one, is difficult as they are all inter-related.

The method, 15 wt% PC12 in HFIP, was then utilised to manufacture random and aligned scaffolds at the DS, which did require further optimisation for this setting. Therefore there were two sets of random and aligned scaffold pairs, TEC and DS, to investigate tanycyte behaviour in response to fibre orientation. These scaffolds were characterised for fibre diameter and alignment, along with their macro-stiffness, to provide a more complete view of the mechanical properties of these scaffolds. This indicated that macro-stiffness is altered in line with fibre orientation changes. Aligned scaffolds were anisotropic and were much stiffer than random scaffolds when tested in the direction of alignment, but much weaker against the alignment. As previously discussed the two pair of scaffolds, TEC and DS, produced different mechanical properties with the DS scaffold being more variable than TEC. Therefore when utilising electrospun scaffolds it is very important to have a system where as many environmental conditions, such as temperature and humidity, can be controlled as for TEC scaffolds manufacture. This control then allows for the manufacture of reproducible scaffolds, which is essential to fully investigate cell responses as scaffold properties are consistent.

Finally I have been able to show that tanycyte derived neurospheres were able to be cultured on these PCL electrospun scaffolds and that they show strong morphological changes to fibre

orientation. Neurospheres remain circular on random scaffolds but elongate on aligned fibres. Importantly, marker expression is altered on these scaffolds. As previously stated the main conclusion was that aligned TEC scaffold appeared to be able to better support tanycyte self-renewal, (more intense expression of Nestin+ NrCAM+ tanycytes in comparison to other conditions), but was not capable of stopping spontaneous differentiation. Percentages of positively labelled neurospheres for Tuj1 and TH were consistent between random and aligned TEC scaffolds. DS scaffolds did not show this same trend, mainly this difference in tanycyte response to TEC and DS scaffold is hypothesised to be due to TEC aligned scaffolds having more fibre alignment than DS aligned scaffolds and the different fibre diameters, (DS scaffolds fibres are thinner than TEC scaffolds). This project was not able to address in full the mechanism of why more tanycytes are maintained on TEC aligned scaffolds and therefore the part of the hypothesis of this being due to a replication of *in vivo* morphology is still to be addressed.

8.2 Future work

I will now consider the main areas of interest for continuing this research to expand the knowledge gained from this thesis further. For this I have identified two main avenues of interest. Firstly the investigation of the mechanism behind the maintenance of tanycytes on TEC aligned scaffold and secondly investigations into how the different biomechanical cues impact this cell population's behaviour.

Before addressing these two main avenues I will firstly discuss how the method of scaffold characterisation could be improved further. The first aspect that requires examination is why comparisons between manual and software analysis varied greatly for orientation characterisation of TEC aligned scaffolds. This highlights some of the problems associated with the use of software. The manual method could also potentially be improved further in line with producing a range of fibre orientations rather than only considering the two ends of the scale,

(random and highly aligned). The collaboration with the Mathematic and Statistics Department could provide this development.

To explore why more tanycytes are maintained on aligned TEC scaffolds in comparison to random TEC scaffolds, this would firstly involve manufacturing more scaffolds via TEC and characterising these scaffolds ensuring that the properties are consistent with the scaffolds utilised within this project. Then in order to fully identify whether tanycytes are maintained due to the replication of *in vivo* morphology, apico-basal markers should be investigated to see whether polarity is induced on aligned TEC scaffold. Also the changes to interactions with the fibres on random versus aligned TEC scaffolds could also be studied, such as by integrin markers. The different expression intensities of tanycyte markers on random and aligned scaffolds could also be investigated by quantification. This could be done by quantifying fluorescent images or the level of protein present by western blot.

Alternatively, further research could focus on investigating individual mechanical properties to identify which properties influence behavioural responses. This could include focusing on considering the impact of fibre diameter or stiffness on tanycyte behaviour. The aim of focusing on the impact of fibre diameter would be to identify whether on aligned fibres the fibre diameter is capable of influencing the level of differentiation occurring. Focusing on 1 and 3 µm diameters as on DS aligned scaffold (~1 µm) there was over 90% positive neurospheres for neural differentiation markers whereas on TEC aligned scaffold (~3 µm) they were few positive neurospheres. Also between these two scaffolds there was a slight difference in the level of alignment, with TEC scaffold being more aligned. This thesis has concluded that high level of alignment is important for the maintenance of the tanycytes and in the future a variety of degrees of alignment could be explored as to how this property impacts upon tanycyte maintenance. Importantly the diameter cannot be ignored as a potential factor for tanycytes maintenance on TEC aligned scaffold. Therefore it would be very important to separate these

two properties and identify which one influences which behaviours, or alternatively identify that both are required to be at specific levels.

Otherwise, as macro-stiffness values varied between random and aligned scaffolds and between manufacturers, the stiffness at the micro-level could also be changed as these values are connected. The utilisation of AFM as a method to measure the micro-stiffness of the scaffold would show whether adjusting the fibre orientation affects this property, for TEC and DS scaffolds. In order to adjust these stiffness values alternative substrates options may be required. This could include other polymers with different stiffness properties to PCL or even a combination of fibres with hydrogels. In the literature the majority of other studied with NSC populations have used softer substrates than PCL fibres, such as hydrogels (section 2.1.2).

Increasing evidence shows that SCs will be exposed to one combination of factors at times of normal activity, however they will receive different cues – for instance, different concentrations of signals or cues at different time intervals, when there is damage. It will therefore take a great deal of research with combined efforts from different disciplines, (including biologists, physicists, engineers and mathematicians), to understand the cues and their effects on the SCs. Therefore understanding each cues influence in isolation is important, but the effect of different cues combined is also essential for full understanding of tanycytes *in vivo* behaviour.

While this project focused on neuronal differentiation, in the future the inclusion of markers for oligodendrocyte and astrocyte differentiation would also be of particular interest. Other papers have shown that when stem cells are exposed to different substrate stiffnesses, different differentiation lineages are induced (section 2.1.2). An astrocyte specific marker would be required, as the GFAP marker led to some confusion over whether the higher GFAP intensity on aligned TEC and aligned DS scaffold was due to tanycytes or astrocytes.

References

1. Saper, C. B. & Lowell, B. B. The hypothalamus. *Current Biology* **24**, R111–R1116 (2014).

2. Robins, S. C. *et al.* α-Tanycytes of the adult hypothalamic third ventricle include distinct populations of FGF-responsive neural progenitors. *Nature communications* **4**, 2049 (2013).

3. Van Pham, P., Vu, B. T., Lu-Chinh Phan, N., Le, H. T. & Phan, N. K. In vitro spontaneous differentiation of human breast cancer stem cells and methods to control this process. *Biomedical Research and Therapy* **2**, 14 (2015).

4. Saha, K., Pollock, J. F., Schaffer, D. V & Healy, K. E. Designing synthetic materials to control stem cell phenotype. *Current Opinion in Chemical Biology* **11**, 381–387 (2007).

5. Ramalho-Santos, M., Yoon, S., Matsuzaki, Y., Mulligan, R. C. & Melton, D. a. Transcriptional Profiling of Embryonic and Adult Stem Cells. *Science* **302298**, 597–600 (2002).

6. Mitalipov, S. & Wolf, D. Totipotency, Pluripotency and Nuclear Reprogramming. *Advances in biochemical engineering/biotechnology* **114**, 185–199 (2009).

7. Gattazzo, F., Urciuolo, A. & Bonaldo, P. Extracellular matrix: A dynamic microenvironment for stem cell niche. *Biochimica et Biophysica Acta - General Subjects* **1840**, 2506–2519 (2014).

8. Condic, M. L. Totipotency: What It Is and What It Is Not. *STEM CELLS AND DEVELOPMENT* **23**, 796–812 (2014).

9. Lesch, B. J. & Page, D. C. Genetics of germ cell development. *Nat Rev Genet* **13**, 781–794 (2012).

10. Seydoux, G. & Braun, R. E. Pathway to Totipotency: Lessons from Germ Cells. *Cell* **127**, 891–904 (2006).

11. Yeom, Y. I. *et al.* Germline regulatory element of Oct-4 specific for the totipotent cycle of embryonal cells. *Development* **122**, 881–894 (1996).

12. Reubinoff, B. E. *et al.* Embryonic stem cell lines from human blastocysts: somatic differentiation in vitro. *Nat. Biotechnol.* **18**, 399–404 (2000).

13. Li, D. *et al.* Role of mechanical factors in fate decisions of stem cells. *Regen Med.* **6**, 229–240 (2011).

14. Watt, F. M. & Huck, W. T. S. Role of the extracellular matrix in regulating stem cell fate. *Nature reviews. Molecular cell biology* **14**, 467–73 (2013).

15. Meilhac, S. M. *et al.* Active cell movements coupled to positional induction are involved in lineage segregation in the mouse blastocyst. *Developmental Biology* **331**, 210–221 (2009).

16. Fuchs, E. Cell biology: More than skin deep. *The Journal of Cell Biology* **209**, 629–632 (2015).

17. Fuchs, E., Tumbar, T. & Guasch, G. Socializing with the neighbors: Stem cells and their niche. *Cell* **116**, 769–778 (2004).

18. Morrison, S. J. & Spradling, A. C. Stem Cells and Niches: Mechanisms That Promote Stem Cell Maintenance throughout Life. *Cell* **132**, 598–611 (2008).

19. Molofsky, A. V, Pardal, R. & Morrison, S. J. Diverse mechanisms regulate stem cell self-renewal. *Curr Opin Cell Biol* **16**, 700–707 (2004).

20. Fuchs, E. & Cédric, B. Epidermal Stem Cells of the Skin. *Annu Rev Cell Dev Biol.* **22**, 339–373 (2006).

21. Takahashi, K. & Yamanaka, S. Induction of Pluripotent Stem Cells from Mouse Embryonic and Adult Fibroblast Cultures by Defined Factors. *Cell* **126**, 663–676 (2006).

22. Van der Sanden, B., Dhobb, M., Berger, F. & Wion, D. Optimizing Stem Cell Culture. *Journal of Cellular Biochemistry* **111**, 801–807 (2010).

23. Mckee, C. & Chaudhry, G. R. Advances and challenges in stem cell culture. *Colloids and Surfaces B: Biointerfaces* **159**, 62–77 (2017).

24. Schofield, R. The relationship between the spleen colony-forming cell and the haemopoietic stem cell. *Blood cells* **4**, 7–25 (1978).

25. Xie, T. & Spradling, A. C. A Niche Maintaining Germ Line Stem Cells in the Drosophila Ovary. *Science* **290**, 328–330 (2000).

26. Kiger, A. A. Stem Cell Self-Renewal Specified by JAK-STAT Activation in Response to a Support Cell Cue. *Science* **294**, 2542–2545 (2001).

27. Tulina, N. & Matunis, E. Control of stem cell self-renewal in Drosophila spermatogenesis by JAK-STAT signaling. *Science (New York, N.Y.)* **294**, 2546–9 (2001).

28. Hsu, Y.-C., Li, L. & Fuchs, E. Emerging interactions between skin stem cells and their niches. *Nature medicine* **20**, 847–56 (2014).

29. Hsu, Y.-C. & Fuchs, E. A family business: stem cell progeny join the niche to regulate homeostasis. *Nature Reviews Molecular Cell Biology* **13**, 103–114 (2012).

30. Donnelly, H., Salmeron-sanchez, M. & Dalby, M. J. Designing stem cell niches for differentiation and self-renewal. *The Royal Society* **20180388**, 1–18 (2018).

31. Mousavi, S. J. & Hamdy Doweidar, M. Role of mechanical cues in cell differentiation and proliferation: A 3D numerical model. *PLoS ONE* **10**, 1–23 (2015).

32. Guilak, F. *et al.* Control of Stem Cell Fate by Physical Interactions with the Extracellular Matrix. *Cell Stem Cell* **5**, 17–26 (2009).

33. Lee, D. A., Knight, M. M., Campbell, J. J. & Bader, D. L. Stem cell mechanobiology. *Journal of Cellular Biochemistry* **112**, 1–9 (2011).

34. Greco, V. & Guo, S. Compartmentalized organization: a common and required feature of stem cell niches? *Development (Cambridge, England)* **137**, 1586–94 (2010).

35. Nowak, J. A., Polak, L., Pasolli, H. A. & Fuchs, E. Hair Follicle Stem Cells Are Specified and Function in Early Skin Morphogenesis. *Cell Stem Cell* **3**, 33–43 (2008).

36. Wong, V. W., Levi, B., Rajadas, J., Longaker, M. T. & Gurtner, G. C. Stem cell niches for skin regeneration. *International journal of biomaterials* **2012**, 926059 (2012).

37. Goldstein, J. & Horsley, V. Home sweet home: skin stem cell niches. *Cellular and Molecular Life Sciences* **69**, 2573–2582 (2012).

38. Shimizu, H. *et al.* Distinct expression patterns of Notch ligands, Dll1 and Dll4, in normal and inflamed mice intestine. *PeerJ* **2**, e370 (2014).

39. Saha, K. *et al.* Substrate modulus directs neural stem cell behavior. *Biophysical journal* **95**, 4426–38 (2008).

40. Doetsch, F., Caillé, I., Lim, D. A., García-Verdugo, J. M. & Alvarez-Buylla, A. Subventricular Zone Astrocytes Are Neural Stem Cells in the Adult Mammalian Brain. *Cell* **97**, 703–716 (1999).

41. Paredes, M. F., Sorrells, S. F., Garcia-Verdugo, J. M. & Alvarez-Buylla, A. Brain size and limits to adult neurogenesis. *Journal of Comparative Neurology* **524**, 646–664 (2016).

42. Lois, C., García-Verdugo, J. M. & Alvarez-Buylla, a. Chain migration of neuronal precursors. *Science (New York, N.Y.)* **271**, 978–981 (1996).

43. Alvarez-Buylla, A. & García-Verdugo, J. M. Neurogenesis in adult subventricular zone. *The Journal of neuroscience* **22**, 629–634 (2002).

44. Zhang, C.-L., Zou, Y., He, W., Gage, F. H. & Evans, R. M. A role for adult TLX-positive neural stem cells in learning and behaviour. *Nature* **451**, 1004–7 (2008).

45. Kléber, M. & Sommer, L. Wnt signaling and the regulation of stem cell function. *Current opinion in cell biology* **16**, 681–7 (2004).

46. Blanpain, C., Lowry, W. E., Geoghegan, A., Polak, L. & Fuchs, E. Self-renewal, multipotency, and the existence of two cell populations within an epithelial stem cell niche. *Cell* **118**, 635–648 (2004).

47. Chiba, S. Notch signaling in stem cell systems. *Stem cells* **24**, 2437–2447 (2006).

48. Kular, J. K., Basu, S. & Sharma, R. I. The extracellular matrix : Structure , composition , age-related differences , tools for analysis and applications for tissue engineering. *Journal of Tissue Engineering* **5**, 1–17 (2014).

49. Jayadev, R. & Sherwood, D. R. Basement membranes Ranjay. *Current Biology* **27**, R207–R211 (2017).

50. Frantz, C., Stewart, K. M. & Weaver, V. M. The extracellular matrix at a glance. *Journal of cell science* **123**, 4195–4200 (2010).

51. Chan, C. K. F. *et al.* Endochondral ossification is required for haematopoietic stem-cell niche formation. *Nature* **457**, 490–4 (2009).

52. Conway, A. & Schaffer, D. V. Biophysical regulation of stem cell behavior within the niche. *Stem cell research & therapy* **3**, 50 (2012).

53. Stevens, M. M. & George, J. H. Exploring and Engineering the Cell Surface Interface. *Science* **310**, 1135–1139 (2005).

54. Donnelly, H., Dalby, M. J., Salmeron-sanchez, M. & Sweeten, P. E. Current approaches for modulation of the nanoscale interface in the regulation of cell behavior. **14**, 2455–2464 (2018).

55. Nava, M. M., Raimondi, M. T. & Pietrabissa, R. Controlling Self-Renewal and Differentiation of Stem Cells via Mechanical Cues. *Journal of Biomedicine and Biotechnology* **2012**, 1–12 (2012).

56. Trappmann, B. *et al.* Extracellular-matrix tethering regulates stem-cell fate. *Nature Materials* **11**, 742–742 (2012).

57. Yim, E. K. F., Darling, E. M., Kulangara, K., Guilak, F. & Leong, K. W. Nanotopography-

induced changes in focal adhesions , cytoskeletal organization , and mechanical properties of human mesenchymal stem cells. *Biomaterials* **31**, 1299–1306 (2010).

58. Kim, S., Turnbull, J. & Guimond, S. Extracellular matrix and cell signalling : the dynamic cooperation of integrin , proteoglycan and growth factor receptor. *Journal of endocrinology* **209**, 139–151 (2002).

59. Fletcher, D. A. & Mullins, R. D. Cell mechanics and the cytoskeleton. *Nature* **463**, 485–492 (2010).

60. Maul, T. M., Chew, D. W., Nieponice, A. & Vorp, D. A. Mechanical stimuli differentially control stem cell behavior: Morphology, proliferation, and differentiation. *Biomechanics and Modeling in Mechanobiology* **10**, 939–953 (2011).

61. Tan, S. & Barker, N. Engineering the niche for stem cells. *Growth factors (Chur, Switzerland)* **31**, 175–84 (2013).

62. Fisher, O. Z., Khademhosseini, A., Langer, R. & Peppas, N. A. Bioinspired Materials for Controlling Stem Cell Fate. *Accounts of Chemical Research* **43**, 419–428 (2010).

63. Ortega, Í., Deshpande, P., Gill, A. a, MacNeil, S. & Claeyssens, F. Development of a microfabricated artificial limbus with micropockets for cell delivery to the cornea. *Biofabrication* **5**, 025008 (2013).

64. Kothapalli, C. R. & Kamm, R. D. Biomaterials 3D matrix microenvironment for targeted differentiation of embryonic stem cells into neural and glial lineages. *Biomaterials* **34**, 5995–6007 (2013).

65. Wheeldon, I., Ahari, A. F. & Khademhosseini, A. Microengineering Hydrogels for Stem Cell Bioengineering and Tissue Regeneration. *Journal of the Association for Laboratory Automation* **15**, 440–448 (2010).

66. Truckenmüller, R. *et al.* Fabrication of cell container arrays with overlaid surface topographies. *Biomedical Microdevices* **14**, 95–107 (2012).

67. Gobaa, S. *et al.* Artificial niche microarrays for probing single stem cell fate in high throughput. *Nature Methods* **8**, 949–955 (2011).

68. Moeller, H.-C., Mian, M. K., Shrivastava, S., Chung, B. G. & Khademhosseini, A. A microwell array system for stem cell culture. *Biomaterials* **29**, 752–763 (2008).

69. Raimondi, M. T. *et al.* Three-dimensional structural niches engineered via two-photon laser polymerization promote stem cell homing. *Acta Biomaterialia* **9**, 4579–4584 (2013).

70. Nam, J., Perera, P., Rath, B. & Agarwal, S. Dynamic regulation of bone morphogenetic proteins in engineered osteochondral constructs by biomechanical stimulation. *Tissue engineering. Part A* **19**, 783–92 (2013).

71. Liu, C. *et al.* The effect of the fibre orientation of electrospun scaffolds on the matrix production of rabbit annulus fibrosus-derived stem cells. *Bone Research* **3**, (2015).

72. Christopherson, G. T., Song, H. & Mao, H. Q. The influence of fiber diameter of electrospun substrates on neural stem cell differentiation and proliferation. *Biomaterials* **30**, 556–564 (2009).

73. Matthews, J. A., Wnek, G. E., Simpson, D. G. & Bowlin, G. L. Electrospinning of collagen nanofibers. *Biomacromolecules* **3**, 232–238 (2002).

74. Zussman, E., Theron, A. & Yarin, A. L. Formation of nanofiber crossbars in electrospinning. *Applied Physics Letters* **82**, 973–975 (2003).

75. Ortega, Í., Ryan, A. J., Deshpande, P., MacNeil, S. & Claeyssens, F. Combined microfabrication and electrospinning to produce 3-D architectures for corneal repair. *Acta Biomaterialia* **9**, 5511–5520 (2013).

76. Vaquette, C. & Cooper-White, J. J. Increasing electrospun scaffold pore size with tailored collectors for improved cell penetration. *Acta Biomaterialia* **7**, 2544–2557 (2011).

77. Engler, A. J., Sen, S., Sweeney, H. L. & Discher, D. E. Matrix Elasticity Directs Stem Cell Lineage Specification. *Cell* **126**, 677–689 (2006).

78. Maldonado, M. *et al.* The effects of electrospun substrate-mediated cell colony morphology on the self-renewal of human induced pluripotent stem cells. *Biomaterials* **50**, 10–19 (2015).

79. Gilbert, P. M. *et al.* Substrate elasticity regulates skeletal muscle stem cell self-renewal in culture. *Science* **329**, 1078–81 (2010).

80. Lutolf, M. Designing materials to direct stem cell fate. *European Cells and Materials* **22**, 25 (2011).

81. Mas-moruno, C., Su, B. & Dalby, M. J. Multifunctional Coatings and Nanotopographies : Toward Cell Instructive and Antibacterial Implants. *Advanced healthcare materials* **1801103**, 1–26 (2019).

82. Elosegui-artola, A., Trepat, X. & Roca-cusachs, P. Control of Mechanotransduction by Molecular Clutch Dynamics. *Trends in Cell Biology* **28**, 356–367 (2018).

83. Kuo, Y.-C., Hung, S.-C. & Hsu, S. The effect of elastic biodegradable polyurethane electrospun nanofibers on the differentiation of mesenchymal stem cells. *Colloids and surfaces. B, Biointerfaces* **122**, 414–22 (2014).

84. Yan, J. *et al.* Effect of fiber alignment in electrospun scaffolds on keratocytes and corneal epithelial cells behavior. *Journal of Biomedical Materials Research Part A* **100A**, 527–535 (2012).

85. Shang, S., Yang, F., Cheng, X., Walboomers, X. F. & Jansen, J. A. The effect of electrospun fibre alignment on the behaviour of rat periodontal ligament cells. *European cells and Materi* **19**, 180–192 (2010).

86. Yim, E. K., Pang, S. W. & Leong, K. W. Synthetic Nanostructures Inducing Differentiation of Human Mesenchymal Stem Cells into Neuronal Lineage. *Experimental cell research* **313**, 1820–1829 (2007).

87. Valderrama, L. R. L. *et al.* Unidirectional neuronal cell growth and differentiation on aligned polyhydroxyalkanoate blend microfibres with varying diameters. 1–14 (2019). doi:10.1002/term.2911

88. Pham, Q. P., Sharma, U. & Mikos, A. G. Electrospinning of polymeric nanofibers for tissue engineering applications: a review. *Tissue engineering* **12**, 1197–211 (2006).

89. Courtney, T., Sacks, M. S., Stankus, J., Guan, J. & Wagner, W. R. Design and analysis of tissue engineering scaffolds that mimic soft tissue mechanical anisotropy. *Biomaterials* **27**, 3631–3638 (2006).

90. Baker, B. M. *et al.* Cell-mediated fiber recruitment drives extracellular matrix mechanosensing in engineered fibrillar microenvironments Brendon. *Nature Materials* **14**, 1262–1268 (2015).

91. Oh, S. *et al.* Stem cell fate dictated solely by altered nanotube dimension. *Proceedings of the National Academy of Sciences of the United States of America* **106**, 2130–2135 (2009).

92. Chaudhuri, B. B., Kundu, P. & Sarkar, N. Detection and gradation of oriented texture. *Pattern Recognition Letters* **14**, 147–153 (1993).

93. Karlon, W. J., Covell, J. W., Mcculloch, A. D., Hunter, J. J. & Omens, J. H. Automated measurement of myofiber disarray in transgenic mice with ventricular expression of ras. *Anatomical Record* **252**, 612–625 (1998).

94. Ortega, I., McKean, R., Ryan, A. J., MacNeil, S. & Claeyssens, F. Characterisation and evaluation of the impact of microfabricated pockets on the performance of limbal epithelial stem cells in biodegradable PLGA membranes for corneal regeneration. *Biomater. Sci.* **2**, 723–734 (2014).

95. Amore, A. D. *et al.* From single fiber to macro-level mechanics: A structural finite-element model for elastomeric fibrous biomaterials. *J Mech Behav Biomed Mater* **39**, 146–161 (2015).

96. Castellano, D. *et al.* A Comparison of Electrospun Polymers Reveals Poly(3-hydroxybutyrate) Fiber as a Superior Scaffold for Cardiac Repair. *Stem cells and development* **00**, 1–12 (2014).

97. Rolandi, M. & Rolandi, R. Self-assembled chitin nanofibers and applications. *Advances in colloid and interface science* **207**, 216–22 (2014).

98. Place, E. S., George, J. H., Williams, K., Stevens, M. M. & George, J. H. Synthetic polymer scaffolds for tissue engineering and the life sciences toward the development of biological. *Royal Society of Chemistry* **38**, 1139–1151 (2009).

99. Ramachandran, C. *et al.* Synthetic biodegradable alternatives to the use of the amniotic membrane for corneal regeneration: assessment of local and systemic toxicity in rabbits. *British Journal of Ophthalmology* **103**, 286–292 (2019).

100. Gonzalez-Perez, O. Neural stem cells in the adult human brain. *Biol Biomed Rep* **2**, 59–69 (2012).

101. Sanai, N. *et al.* Unique astrocyte ribbon in adult human brain contains neural stem cells but lacks chain migration. *Nature* **427**, 740–744 (2004).

102. Fiorelli, R., Azim, K., Fischer, B. & Raineteau, O. Adding a spatial dimension to postnatal ventricular-subventricular zone neurogenesis. 2109–2120 (2015). doi:10.1242/dev.119966

103. Gonzalez-perez, O. *et al.* Stress by noise produces differential effects on the proliferation rate of radial astrocytes and survival of neuroblasts in the adult subgranular zone. *Neuroscience Research* **70**, 243–250 (2011).

104. Seri, B., Garcı, J. M., Mcewen, B. S. & Alvarez-buylla, A. Astrocytes Give Rise to New Neurons in the Adult Mammalian Hippocampus. **21**, 7153–7160 (2001).

105. Zhao, C., Deng, W. & Gage, F. H. Review Mechanisms and Functional Implications of Adult Neurogenesis. 645–660 (2008). doi:10.1016/j.cell.2008.01.033

106. Bond, A. M., Ming, G. & Song, H. Review Adult Mammalian Neural Stem Cells and Neurogenesis : Five Decades Later. *Stem Cell* **17**, 385–395 (2015).

107. Mizrak, D. *et al.* Single-Cell Analysis of Regional Differences in Adult V-SVZ Neural Stem Cell Lineages Article Single-Cell Analysis of Regional Differences in Adult V-SVZ Neural Stem Cell Lineages. *CellReports* **26**, 394-406.e5 (2019).

108. Garci, M., Seri, B., Collado-morente, L. & Ewen, B. S. M. C. Cell Types , Lineage , and Architecture of Adult Dentate Gyrus. **378**, 359–378 (2004).

109. Pierce, A. a & Xu, A. W. Compensatory Mechanism To Regulate Energy Balance. **30**, 723–730 (2011).

110. Wang, X. *et al.* Wnt Signaling Regulates Postembryonic Hypothalamic Progenitor Differentiation. *Developmental Cell* **23**, 624–636 (2012).

111. Migaud, M. *et al.* Emerging new sites for adult neurogenesis in the mammalian brain: A comparative study between the hypothalamus and the classical neurogenic zones. *European Journal of Neuroscience* **32**, 2042–2052 (2010).

112. Xie, Y. & Dorsky, R. I. Development of the hypothalamus: conservation, modification and innovation. *Development* **144**, 1588–1599 (2017).

113. Burbridge, S., Stewart, I. & Placzek, M. Development of the Neuroendocrine Hypothalamus. *Comprehensive Physiology* **6**, 623–643 (2016).

114. Bedont, J. L., Newman, E. A. & Blackshaw, S. Patterning, specification, and differentiation in the developing hypothalamus. *Wiley Interdisciplinary Reviews: Developmental Biology* **4**, 445–468 (2015).

115. Fu, T., Towers, M. & Placzek, M. A. Fgf10 + progenitors give rise to the chick hypothalamus by rostral and caudal growth and differentiation. *The Company of Biologists* **144**, 3278–3288 (2017).

116. Campbell, J. N. *et al.* A molecular census of arcuate hypothalamus and median eminence cell types. *Nature Neuroscience* **20**, 484–496 (2017).

117. Valério-Gomes, B., Guimarães, D. M., Szczupak, D. & Lent, R. The Absolute Number of Oligodendrocytes in the Adult Mouse Brain. *Frontiers in Neuroanatomy* **12**, 1–19 (2018).

118. Kim, J. G. *et al.* Leptin signaling in astrocytes regulates hypothalamic neuronal circuits and feeding. *Nature Neuroscience* **17**, 908–910 (2014).

119. Camandola, S. Astrocytes, emerging stars of energy homeostasis. *Cell Stress* **2**, 246–252 (2018).

120. Chowen, J. A. *et al.* The role of astrocytes in the hypothalamic response and adaptation to metabolic signals. *Progress in Neurobiology* **144**, 68–87 (2016).

121. Cabezas, R. *et al.* Astrocytic modulation of blood brain barrier: perspectives on Parkinson's disease. *Frontiers in Cellular Neuroscience* **8**, 1–11 (2014).

122. Sousa-Ferreira, L., Almeida, L. P. de & Cavadas, C. Role of hypothalamic neurogenesis in feeding regulation. *Trends in Endocrinology and Metabolism* **25**, 80–88 (2014).

123. Mirzadeh, Z., Merkle, F. T., Soriano-navarro, M. & Garcia-verdugo, J. M. Neural Stem Cells Confer Unique Pinwheel Architecture to the Ventricular Surface in Neurogenic Regions of the Adult Brain. *Cell Stem Cell* **3**, 265–278 (2008).

124. Pérez-Martín, M. *et al.* IGF-I stimulates neurogenesis in the hypothalamus of adult rats. *European Journal of Neuroscience* **31**, 1533–1548 (2010).

125. Haan, N. *et al.* Fgf10-expressing tanycytes add new neurons to the appetite / energy-balance regulating centres of the postnatal and adult hypothalamus. *Journal of Neuroscience* **33**, 6170–6180 (2013).

126. Elizondo-Vega, R. *et al.* The role of tanycytes in hypothalamic glucosensing. *Journal of Cellular and Molecular Medicine* **19**, 1471–1482 (2015).

127. Mullier, A., Bouret, S. G., Prevot, V. & Dehouck, B. Differential distribution of tight junction proteins suggests a role for tanycytes in blood-hypothalamus barrier regulation in the adult mouse brain. *Journal of Comparative Neurology* **518**, 943–962 (2010).

128. Xu, Y. *et al.* Neurogenesis in the ependymal layer of the adult rat 3rd ventricle. *Experimental Neurology* **192**, 251–264 (2005).

129. Cariboni, A. *et al.* Establishment of a radial glia-like mouse fetal hypothalamic neural stem cell line (AC1) able to differentiate into neuroendocrine cells. **2133**, 1–6 (2014).

130. Cavallucci, V., Fidaleo, M. & Pani, G. Neural Stem Cells and Nutrients: Poised Between Quiescence and Exhaustion. *Trends in Endocrinology and Metabolism* **27**, 756–769 (2016).

131. Park, D. *et al.* Nestin is required for the proper self-renewal of neural stem cells. *Stem Cells* **28**, 2162–2171 (2010).

132. Robins, S. Neural Stem/ Progenitor cells in the Adult Mouse Hypothalamus. (2009). doi:uk.bl.ethos.557423

133. Livesey, F. J. A potential link between obesity and neural stem cell dysfunction. *Nature Cell Biology* **14**, 987–989 (2012).

134. Li, J., Tang, Y. & Cai, D. IKKβ/NF-κB disrupts adult hypothalamic neural stem cells to mediate a neurodegenerative mechanism of dietary obesity and pre-diabetes. *Nature Cell Biology* **14**, 999–1012 (2012).

135. Lee, D. A. *et al.* Tanycytes of the Hypothalamic Median Eminence Form a Diet-Responsive Neurogenic Niche. *Nature neuroscience* **15**, 700–702 (2012).

136. Gao, Y., Tschöp, M. H. & Luquet, S. Hypothalamic tanycytes: Gatekeepers to metabolic control. *Cell Metabolism* **19**, 173–175 (2014).

137. Langlet, F. *et al.* Tanycytic VEGF-A boosts blood-hypothalamus barrier plasticity and access of metabolic signals to the arcuate nucleus in response to fasting. *Cell Metabolism* **17**, 607–617 (2013).

138. Langlet, F., Mullier, A., Bouret, S. G., Prevot, V. & Dehouck, B. Tanycyte-like cells form a blood-cerebrospinal fluid barrier in the circumventricular organs of the mouse brain. *Journal of Comparative Neurology* **521**, 3389–3405 (2013).

139. Khajavi, R. & Abbasipour, M. Electrospinning as a versatile method for fabricating coreshell, hollow and porous nanofibers. *Scientia Iranica* **19**, 2029–2034 (2012).

140. Vasita, R. & Katti, D. S. Nanofibers and their applications in tissue engineering. *International Journal of Nanomedicine* **1**, 15–30 (2006).

141. A, F. PROCESS AND APPARATUS FOR PREPARING ARTIFICIAL THREADS. (1934).

142. A, F. METHOD AND APPARATUS FOR SPINNING. (1939).

143. Subbiah, T., Bhat, G. S., Tock, R. W., Parameswaran, S. & Ramkumar, S. S. Electrospinning of nanofibers. *Journal of Applied Polymer Science* **96**, 557–569 (2005).

144. Hayati, I., Bailey, a & Tadros, T. . Investigations into the mechanism of electrohydrodynamic spraying of liquids. *Journal of Colloid and Interface Science* **117**, 222–230 (1987).

145. Li, Z. & Wang, C. Effects of Working Parameters on Electrospinning. in *Archives of Hellenic Medicine* **32**, 15–28 (2013).

146. Ulery, B. D., Nair, L. S. & Laurencin, C. T. Biomedical Applications of Biodegradable Polymers. *J Polym Sci B Polym Phys* **49**, 832–864 (2011).

147. Thiel, G. How Sox2 maintains neural stem cell identity. **2**, 10–11 (2013).

148. Appolloni, I. *et al.* Six3 Controls the Neural Progenitor Status in the Murine CNS. *Cereb Cortex* **3**, 553–562 (2008).

149. Zhang, J. & Jiao, J. Molecular Biomarkers for Embryonic and Adult Neural Stem Cell and Neurogenesis. *Biomed Res Int* **2015**, 727542 (2015).

150. Goetzke, R., Sechi, A., de Laporte, L., Neuss, S. & Wagner, W. Why the impact of mechanical stimuli on stem cells remains a challenge. *Cellular and Molecular Life Sciences* **75**, 1–16 (2018).

151. Olynik, B. M. & Rastegar, M. The genetic and epigenetic journey of embryonic stem cells into mature neural cells. *Frontiers in Genetics* **3**, 1–16 (2012).

152. Daneshtalab, N., Doré, J. J. E. & Smeda, J. S. Journal of Pharmacological and Toxicological Methods Troubleshooting tissue speci fi city and antibody selection : Procedures in immunohistochemical studies. *Journal of Pharmacological and Toxicological Methods* **61**, 127–135 (2010).

153. Sakurai, T. *et al.* Overlapping functions of the cell adhesion molecules Nr-CAM and L1 in cerebellar granule cell development. *Journal of Cell Biology* **154**, 1259–1273 (2001).

154. Grumet, M., Mauro, V., Burgoon, M. P., Edelman, G. M. & Cunningham, B. A. Structure of a new nervous system glycoprotein, Nr-CAM, and its relationship to subgroups of neural cell adhesion molecules. *The Journal of cell biology* **113**, 1399–412 (1991).

155. Von Bohlen Und Halbach, O. Immunohistological markers for staging neurogenesis in adult hippocampus. *Cell and Tissue Research* **329**, 409–420 (2007).

156. Mohammad, M. H., Al-Shammari, A. M., Al-Juboory, A. A. & Yaseen, N. Y. Characterization of neural stemness status through the neurogenesis process for bone marrow mesenchymal stem cells. *Stem Cells and Cloning: Advances and Applications* **9**, 1–15 (2016).

157. Lim, R. W. L. & Halpain, S. Regulated association of microtubule-associated protein 2 (MAP2) with Src and Grb2: Evidence for MAP2 as a scaffolding protein. *Journal of Biological Chemistry* **275**, 20578–20587 (2000).

158. Zhang, X. & van den Pol, A. N. Dopamine/Tyrosine Hydroxylase Neurons of the Hypothalamic Arcuate Nucleus Release GABA, Communicate with Dopaminergic and Other Arcuate Neurons, and Respond to Dynorphin, Met-Enkephalin, and Oxytocin. *The Journal of neuroscience : the official journal of the Society for Neuroscience* **35**, 14966–

82 (2015).

159. Mano-Otagiri, A. *et al.* Growth hormone-releasing hormone (GHRH) neurons in the arcuate nucleus (Arc) of the hypothalamus are decreased in transgenic rats whose expression of ghrelin receptor is attenuated: Evidence that ghrelin receptor is involved in the up-regulation of GHRH e. *Endocrinology* **147**, 4093–4103 (2006).

160. Watanabe, M. *et al.* Monoclonal Antibody Rip Specifically 3 0 -Phosphodiesterase in Oligodendrocytes. **533**, 525–533 (2006).

161. Paterson, T. E. *et al.* Selective laser melting – enabled electrospinning : Introducing complexity within electrospun membranes. *Journal of Engineering in Medicine* **231**, 565–574 (2017).

162. Schindelin, J. *et al.* Fiji: An open source platform for biological image analysis. *Nature Methods* **9**, 676–682 (2012).

163. Li, Z. & Wang, C. *One-dimensional nanostructures electrospinning technique and unique nanofibers*. *Springer* (2013). doi:0.1007/978-3-642-36427-3

164. Teo, W. E. & Ramakrishna, S. A review on electrospinning design and nanofibre assemblies. *Nanotechnology* **17**, R89–R106 (2006).

165. Wen, J. H. *et al.* Interplay of matrix stiffness and protein tethering in stem cell differentiation. *Nature Materials* **13**, 979–987 (2014).

166. Taylor, G. Electrically Driven Jets. *Proceedings of the Royal Society A: Mathematical, Physical and Engineering Sciences* **313**, 453–475 (1969).

Appendix

Appendix 1: Appendix for Chapter 6

Table A1 A: Statistical summary of microfeature diameter comparison of scaffolds 1-3 by Krustal-Wallis test with Dunn's multiple comparison. Graph shown in Figure 6.2 C.

Dunn's multiple comparisons test	Summary
S2 Large vs. S2 Intermediate b	**
S2 Large vs. S2 Small	****
S2 Large vs. S1	****
S2 Large vs. S3 Length A	****
S2 Large vs. S3 Length B	****
S2 Intermediate a vs. S2 Small	***
S2 Intermediate a vs. S1	****
S2 Intermediate a vs. S3 Length A	**
S2 Intermediate a vs. S3 Length B	****
S2 Intermediate b vs. S1	****
S2 Intermediate b vs. S3 Length B	**
S2 Small vs. S1	*

Table A1 B: First approach to analyse fibre diameter mean for each area and scaffold type. S1= scaffold 1, S2= scaffold 2 and S3= scaffold 3. a= bottom of the well b= side of the well and c=top surface.

	Random	S1 a	S1 b	S1 c	S2 Large a	S2 Large b	S2 Large c	S3 a	S3 c
Mean	2.0	2.0	2.0	1.8	1.7	1.6	1.8	1.4	1.6
Std. Deviation	0.7	0.9	0.9	1.1	1.1	0.9	1.2	0.8	1.0
Std. Error of Mean	0.0	0.1	0.1	0.1	0.1	0.1	0.1	0.1	0.1

Table A1 C: Statistic analysis of the first approach diameter analysis. The Kruskal-Wallis test showed overall significant difference at P<0.0001 and Dunn's multiple comparison analysis show significant difference between pairs. Graph shown in Figure 6.2.1 B.

Microfeature area	Significance
Plain vs. S2 Large a	****
Plain vs. S2 Large b	****
Plain vs. S2 Large c	**
Plain vs. S3 a	****
Plain vs. S3 c	****
S2 Large a vs. S1 a	**
S2 Large a vs. S1 b	***
S2 Large a vs. S3 a	*
S2 Large b vs. S1 a	***
S2 Large b vs. S1 b	****
S2 Large c vs. S1 b	*
S2 Large c vs. S3 a	**
S1 a vs. S3 a	****
S1 a vs. S3 c	****
S1 b vs. S3 a	****
S1 b vs. S3 c	****
S1 c vs. S3 a	****
S1 c vs. S3 c	**

Table A1 D: Average diameters of the sites of the random scaffolds and scaffolds 1-3 from the second approach to fibre analysis. Including details of the standard deviation and standard error of the mean.

Scaffold site	**Average diameter (µm)**	**Standard deviation**	**Standard error of the mean**
Plain	2.2	0.8	0.1
S1 a	1.9	1.2	0.1
S1 b	2.0	1.1	0.1
S1 c	2.0	1.0	0.1
S2 Large a	2.2	1.1	0.1
S2 Large b	1.8	0.9	0.1
S2 Large c	2.0	0.9	0.1
S2 Intermediate A a	2.3	0.8	0.1
S2 Intermediate A b	1.9	0.9	0.1
S2 Intermediate B a	2.3	1.0	0.1
S2 Intermediate B b	2.0	1.1	0.1
S2 Small a	2.3	0.9	0.1
S2 Small b	2.0	0.9	0.1
S3 a	1.7	0.8	0.1
S3 c	1.8	1.0	0.1

Table A1 E: Statistical analysis of second fibre analysis of random scaffolds and scaffolds 1-3. Using Krustal-Wallis with Dunn's multiple comparison of Figure 6.3.2 B.

Dunn's multiple comparisons test	Summary
Plain vs. S3 a	***
Plain vs. S3 c	*
S1 a vs. S2 Large a	*
S1 a vs. S2 Intermediate A a	**
S1 a vs. S2 Intermediate B a	*
S1 a vs. S2 Small a	*
S2 Large a vs. S3 a	***
S2 Large a vs. S3 c	*
S2 Large b vs. S2 Intermediate A a	*
S2 Intermediate A a vs. S3 a	****
S2 Intermediate A a vs. S3 c	**
S2 Intermediate B a vs. S3 a	***
S2 Intermediate B a vs. S3 c	*
S2 Small a vs. S3 a	****
S2 Small a vs. S3 c	**

Table A1 F: Mean fibre diameters for polymer and solvent comparison. All data in µm. C= Corbion (PC12) S=Sigma R=Random A= Aligned. For all scaffolds the standard error of the mean was 0.0.

Diameter (µm)	Mean	Std. Deviation
C R DCM DMF	3.3	1.5
C R HFIP	2.9	0.8
C R Chloroform	3.9	1.5
C A DCM DMF	3	1.3
C A HFIP	3.1	1.1
C A Chloroform	2.7	1.2
S R DCM DMF	2.1	0.5
S R HFIP	2.5	1.1
S R Chloroform	3.5	1.2
S A DCM DMF	2	0.6
S A HFIP	2.4	1.1
S A Chloroform	2.5	1.1

Table A1 G: Statistical analysis using Krustal-Wallis with Dunn's multiple comparison of diameter analysis of samples comparing 12 and 15 wt% and solvents chloroform and HFIP at distances of 10 and 14 cm.

Dunn's multiple comparisons test	Summary
C 12 wt% 10cm vs. H 12 wt% 10cm	****
C 12 wt% 10cm vs. H 12 wt% 14cm	***
C 12 wt% 10cm vs. H 15 wt% 10cm	**
C 12 wt% 10cm vs. H 15 wt% 14cm	***
C 12 wt% 14cm vs. C 15 wt% 14cm	*
C 12 wt% 14cm vs. H 12 wt% 10cm	****
C 12 wt% 14cm vs. H 12 wt% 14cm	****
C 12 wt% 14cm vs. H 15 wt% 10cm	****
C 12 wt% 14cm vs. H 15 wt% 14cm	****
C 15 wt% 10cm vs. C 15 wt% 14cm	***
C 15 wt% 10cm vs. H 12 wt% 10cm	****
C 15 wt% 10cm vs. H 12 wt% 14cm	****
C 15 wt% 10cm vs. H 15 wt% 10cm	****
C 15 wt% 10cm vs. H 15 wt% 14cm	****
C 15 wt% 14cm vs. H 12 wt% 10cm	**

Table A1 H: Statistical analysis using Krustal-Wallis with Dunn's multiple comparison of Random scaffold diameter analysis of samples comparing 12 and 15 wt% and distances.

Dunn's multiple comparisons test	Summary
12 wt% 26cm vs. 15 wt% 24cm	*
12 wt% 26cm vs. 15 wt% 22cm	*
12 wt% 24cm vs. 15 wt% 28cm	**
12 wt% 22cm vs. 15 wt% 28cm	**
15 wt% 28cm vs. 15 wt% 24cm	***
15 wt% 28cm vs. 15 wt% 22cm	***
15 wt% 26cm vs. 15 wt% 24cm	**
15 wt% 26cm vs. 15 wt% 22cm	**